Cardiac Stem Cell Therapy for Heart Failure

Lien-Cheng Hsiao

St Catherine College

Department of Physiology, Anatomy and Genetics

University of Oxford

Trinity Term 2012

Supervisors:

Prof. Kieran Clarke, Prof. Zhanfeng Cui and Dr. Carolyn A. Carr

Acknowledgments

I would like to express my deepest appreciation to Professor Kieran Clarke for the great opportunity of working in her group towards my DPhil. With her continuous support and advice, I was able to work steadily towards the completion of my project. I would like to express my sincere gratitude towards Professor Zhanfeng Cui for welcoming me into his lab for tissue engineering and for his concern following my recent bike accident. I must thank all of the group members for helping me with the techniques and expertise in the area. I am truly grateful for Dr. Carolyn Carr; she was remarkably patient and understanding throughout my DPhil study. Her scientific expertise and guidance has helped me to grasp the essence of the work and to develop my ideas coherently. Working in the Cardiac Metabolism Research group has been an inspiring experience and here, I would like to thank everyone in the group who has encouraged me through many obstacles. Most importantly, many thanks must go to the stem cell group members – Dr. Daniel James Stuckey, Dr. Jun Jie Tan, Dr. Suat Cheng Tan, Dr. Renata Gomes, Khadijeh Pakzad, Lucy Ambrose, Arne bruyneel, Filippo Perbellini. I have a special thank to Dr. Jilong Liu and Dr. Jing Yu for the technical and social support. I would also like to take this opportunity to thank Dr. Tim Horder and Dr. Jane Green for their kindness in having my family with them when we could not sort out accommodation for the first week and special thanks to Sally Harte for solving the crisis. I also give my huge thanks to my parents and all of my friends, particularly to Gary, Sherry, Arthur, Yu-Hsuan, Nina, Tao's family, John's family, Scott's family, Cat Boaz and Dr. Hsu's family for the greatest love and support. Last but not the least, I am indebted to my beloved wife, Su-Ching Lai who looks after my family with all her heart and tolerates the stress when I was depressed. Kevin, my son, has always been responsible for his school work: I am so proud of him. Moreover, my sweet daughter, Chelsea, has constantly cheered me up with countless jokes and incredible consideration whenever she realized I am melancholic. My thesis will not be completed without the continuous support from my lovely and sweet family.

Abstract

Cardiovascular disease is a leading cause of death worldwide and becomes increasingly prevalent in the elderly population. Independent of etiopathogenesis, heart failure (HF) is the final common stage of numerous heart diseases. Cardiac stem cell (CSC) therapy has emerged as a promising cell-based strategy for treatment of HF. However, cell replacement is not able to fully restore a structurally damaged myocardium in advanced and end-stage HF. The objective of this project was to test the following hypotheses: that a bioengineered heart extracellular matrix (ECM) with preserved intact geometric structure could be generated using decellularization by coronary perfusion; and that autologous CSCs, to repopulate this ECM, could be isolated and expanded from the adult heart, with the caveat that autologous CSCs are depleted and impaired by both aging and chronic dilated cardiomyopathy. This will help to develop a possible therapeutic approach for advanced HF, using a combination of CSCs and engineering technique. Resident CSCs were isolated from explant-derived cells (EDCs) and expanded into cardiosphere-derived cells (CDCs) *via* cardiosphere formation. The CDCs expressed CSC markers (c-kit and Sca-1), pluripotent markers (Oct3/4 and Sox2), and the cardiac lineage-committed marker (Nkx2.5), and showed clonal expansion, self-renewal, and cardiomyogenic potential *in vitro*. In tissue engineering experiments, CDCs survived and proliferated within biomaterial alginate scaffolds for up to 7 weeks. An engineered bioartificial ECM scaffold was successfully produced from a whole rat heart using retrograde coronary perfusion and possessed an intact 3D architecture with functionally perfusable vascular network. Compared with ventricles, cultures derived from atria produced significantly higher number of c-kit$^+$ and Sca-1$^+$ CSCs (c-kit: 13% vs. 3.4%; Sca-1: 82% vs. 53%, respectively) and exhibited greater clonogenic and proliferative capacity. CDCs could be grown from young and aged mice, but the yield of CSCs significantly declined with age, as did cell migration and differentiation potential. In comparison to wild-type mice, atrial-CDCs from dystrophic mice showed no significant differences in CSC subpopulations and characteristics, despite confirmation of cardiac dysfunction using MRI. In conclusion, CDCs could be considered to be a viable cell candidate for cardiac therapy and may be used to treat HF at various stages, in combination with myocardial tissue engineering.

Contents

Abbreviations

ACEI	Angiotensin-converting enzyme inhibitor
AMI	Acute myocardial infarction
ARB	Angiotensin-receptor blocker
CDC	Cardiosphere-derived cell
CEM	Complete explant medium
CGM	Cardiosphere growth medium
CM-DiI	Chloromethyl-benzamidodialkylcarbocyanine
CO	Cardiac output
CSC	Cardiac stem cell
cTnI	Cardiac troponin I
cTnT	Cardiac troponin T
CVD	Cardiovascular disease
DAPI	4', 6-diamidino-2-phenylindole
DMD	Duchenne muscular dystrophy
DMEM	Dulbecco's modified eagle medium
DMSO	Dimethyl sulfoxide
ECG	Electrocardiogram
ECM	Extracellular matrix
EDC	Explant-derived cell
EDV	End diastolic volume
EPC	Endothelial progenitor cell
ESV	End systolic volume
5-aza	5-azacytidine
H&E	Hematoxylin and eosin
HF	Heart failure
HSC	Hematopoietic stem cell
IHD	Ischemic heart disease
IGF-1	Insulin-like growth factor-1
IMDM	Iscove's modified Dulbecco's medium
HSC	Haematopoietic stem cell
iPSC	Induced pluripotent stem cell
LVAD	Left ventricular assist device
LVEF	Left ventricular ejection fraction
MLC	Myosin light chain

MRI	Magnetic resonance imaging
MRS	Magnetic resonance spectroscopy
MSC	Mesenchymal stem cell
PBS	Phosphate buffered salineRpm
QRS	Q wave, R wave and S wave
RT-PCR	Reverse transcriptase polymerase chain reaction
Sca-1	Stem cell antigen-1
SCG	Single copy gene
SEM	Standard error of mean
SV	Stroke volume
T	Tesla
3D	Three-dimensional
VEGF	Vascular endothelial growth factor

Chapter 1

Introduction

1.1 Heart failure

According to the World Health Organization (WHO), cardiovascular diseases (CVDs) are the major cause of death globally (Figure 1.1), leading to an estimated 17.3 million deaths in 2008 [1]. Furthermore, despite modern advances in therapy and management, the number of annual deaths due to CVDs worldwide continues to increase; by 2030, it is expected that nearly 23.6 million people will die from heart diseases including heart failure (HF) [2, 3].

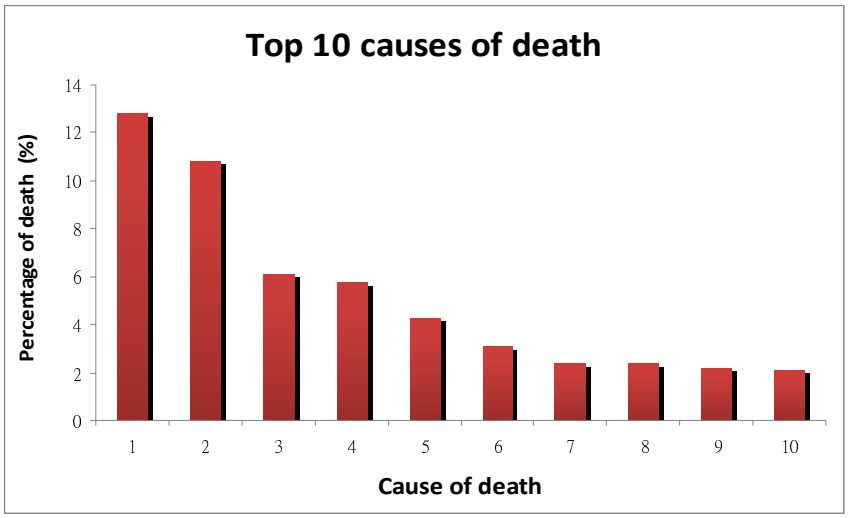

Figure 1.X Ten leading causes of death globally, based on updated data 2011 published by the World Health Organization. *Number on the abscissa indicates diseases as follows:* ***1****. Coronary heart disease,* ***2****. Cerebrovascular disease,* ***3****. Low respiratory infections,* ***4****. Chronic obstructive pulmonary disease,* ***5****. Diarrhoeal disease,* ***6****. HIV/AIDS,* ***7****. Trachea, bronchus, lung cancers,* ***8****. Tuberculosis,* ***9****. Diabetes mellitus,* ***10****. Road traffic accidents. Abbreviations: HIV = Human Immunodeficiency Virus and AIDS = Acquired Immune Deficiency Syndrome [1].*

The majority of cardiovascular disease is composed of cardiac diseases. On the basis of the aetiology, heart diseases can be broadly divided into either ischemic (e.g., coronary artery disease and myocardial infarction) or non-ischemic heart disease (e.g., valvular heart disease and hereditary cardiomyopathy). Regardless of the underlying cause, however, HF is the final common stage of many diseases associated with the heart [4]. Based on recent statistics, more than 900,000 people are living with HF in the UK, which represents about 5% of medical hospitalizations [5]. Approximately 5.8 million people are affected with HF in the USA and over 23 million worldwide [6]. Under medical treatment, 20-30% of HF patients die in the first year of diagnosis and 45-60% after 5 years, respectively [2, 7]. Thus, HF has become a major public

health issue in terms of high mortality rate and enormous healthcare expenditure [8].

1.2 Current therapies for heart failure

1.2.1 Medical therapy

Standard pharmacological agents for HF include diuretics, angiotensin-converting-enzyme inhibitors (ACEIs), beta-blockers, angiotensin-receptor blockers (ARBs), and aldosterone antagonists [9]. The actions of these drugs are mainly through the modification of ventricular remodeling and the systemic responses (i.e., sympathetic and rennin-angiotensin-aldosterone systems) [9]. Diuretics are useful in the management of fluid retention to relieve symptoms such as dyspnea [10, 11]. As the first-line therapy, ACEIs have been shown to improve symptoms, reduce ventricular size and increase the ejection fraction (EF) modestly [10, 11]. Like ACEIs, beta-blockers are also in the list of first-line drugs in patients with HF, which can increase the EF and relieve symptoms if tolerated. ARBs are similar in action to ACEIs in patients with chronic HF [12, 13]. The use of the aldosterone antagonist (spironolactone) showed further reduction in symptoms, hospitalization and mortality in severe HF patients receiving a diuretic, an ACEI and a beta-blocker [14]. Other drugs, such as hydralazine/isosorbide dinitrate and digoxin, can be prescribed to ameliorate symptoms and improve quality of life depending on patients' needs [9].

1.2.2 Interventional therapy

Interventional therapy, which is less invasive than surgery, includes percutaneous transluminal coronary angioplasty (PTCA), implantable cardioverter-defibrillator (ICD) and biventricular cardiac pacing (cardiac resynchronization therapy; CRT), which could benefit patients with HF under certain circumstances. Elective PTCA improves symptoms and heart function in patients with ischemic HF and viable myocardium by coronary revascularization with or without the use of stents. ICDs were shown to reduce mortality in HF patients with a high risk of sudden cardiac death in a systemic review of randomized controlled trials [15]. Moreover, as many as one third of patients with severe HF developed intra-ventricular conduction delays, which are associated with dyssynchronized contraction of the left ventricle, resulting in inefficient pumping work [16-

18]. Based on clinical randomized trials, CRT was shown to reduce symptoms, improve heart function and increase survival rate in selected patients, when added to optimal medical therapy [16-19]. Importantly, CRT did not lead to a reduction in mortality rate in patients with a relatively low risk of death [9]. As a result, the use of CRT is recommended in subjects with severe HF, an EF less than 35%, sinus rhythm and a wide QRS complex (>120 msec; QRS complex stands for the combination of Q, R, and S waves in electrocardiograms, indicating electrical activation of the ventricle, which occurs before ventriclular contraction.) [10, 11].

1.2.3 Surgical therapy

Coronary artery bypass graft (CABG) is an effective treatment in patients with chronic ischemic cardiomyopathy, still suffering from angina or reversible myocardial ischemia, and leads to better outcomes than medical therapy [20]. The gold standard therapy for end-stage HF remains heart transplantation, which improves patients' symptoms (95% symptom-free rate) and extends their life span with about 90% 1-year survival and 60% 10-year survival [21, 22]. Nevertheless, patients receiving heart transplantation require lifelong immunosuppression and face the possibilities of severe post-operative complications, such as primary graft failure (PGF) and transplant vasculopathy [23]. Furthermore, only 5,000 heart transplants are carried out annually in more than 300 countries; unfortunately 10% of terminal HF patients on the waiting list for transplantation die every year because of limited organ supply and long waiting times [24, 25]. Its impact is therefore epidemiologically trivial in light of a global population in need [26]. Mechanical circulatory support (MCS) with the left ventricular assist device (LVAD) has been used as bridge-to-transplant (BTT) or bridge-to-recovery (BTR) therapies over the past decade [22]. In addition, because of its efficacy in BTT and BTR, the long-term use for end-stage HF patients who are ineligible for transplantation (i.e., destination therapy; DT) has been investigated and suggested after the development of newer LVADs with continuous-flow pumps [27-29]. LVAD resulted in 1-year survival of nearly 80% and improvements in symptoms and quality of life in patients with advanced or end-stage HF [30]. However, the use of LVAD still causes around 5-10% peri-operative mortality and is linked to frequent short- and long-term

complications such as infection, bleeding and device failure [30].

1.2.4 Limitations of current therapy for heart failure

Pathophysiologically, HF is characterized by an irreversible loss of cardiac myocytes and residual fibrotic scar tissue, which results in progressive deterioration of cardiac function [31]. Over the past decade, great advances in pharmaceuticals, device technology and surgery have alleviated symptoms, improved quality of life and reduced mortality in patients with cardiovascular disease [9]. However, apart from transplantation, the treatments available to date are unable to reverse the state of HF or prevent the progression to end-stage HF as the lost functional myocardium is not replaced by these approaches. Unfortunately, furthermore, the definitive therapy - cardiac transplantation is significantly restricted by the number of available donor organs [28]. Accordingly, it is hoped to develop a novel therapeutic method that can efficiently repair and regenerate the damaged myocardium, eventually structurally and functionally restoring the heart.

1.3 Stem cell-based therapy for heart disease

Stem cell-based therapy aims to replenish lost myocardial cells, restore blood flow, modulate remodeling, and improve contractility by delivering stem or progenitor cells to the injured region of the heart [32]. In general, there are two strategies for the treatment of CVDs using a cell-based approach: cellular cardiomyoplasty (cell transplantation) and cardiac tissue or organ engineering.

1.3.1 Cellular cardiomyoplasty

Over recent years, repair and regeneration of the damaged myocardium in patients with acute myocardial infarction (AMI) and post-infarct HF has been investigated with cellular cardiomyoplasty involving the implantation of cells *via* either direct intra-myocardial (IM) (transepicardial or transendocardial) injection or coronary infusion by intracoronary (IC), retrograde coronary sinus (RCS) or systemic intravenous (IV) administration [33-35]. Coronary administration is a less invasive procedure compared with intramyocardial injection, but

microvascular occlusion and microinfarction have been reported after cell transplantation of large cells, such as mesenchymal stem cells, without special precautions [47]. Each of these cell delivery methods aimed to transfer sufficient numbers of cells to the target site in the injured heart and to maximize cell retention, thereby achieving robust therapeutic effects [34]. In landmark human trials of intracoronary and intramyocardial stem cell therapy, the number of cells transplanted ranged from roughly 2 x 10^7 to 5 x 10^9 [118]. A meta-analysis found that left ventricular EF may be significantly improved only when more than 10^8 stem cells were delivered into patients with myocardial infarction [153]. However, regardless of the cell type and the route of cell delivery, low retention and engraftment occurred and this remains one of the key issues limiting the therapeutic outcome after cell transplantation into the heart [36]. It has been reported that, within the myocardium, less than 10% of the cells were retained one hour after 10^7 of PBMNC (peripheral blood mononuclear cell) administration by either IC or RCS (IM: 11±3%, IC: 2.6±0.3%, and RCS: 3.2±1%, respectively) [33]. The greatest proportion of cells was found in the lungs, the liver and the kidneys [388]. Acute loss of delivered cells from the heart occurs because they are often washed out *via* coronary blood flow or mechanically ejected at the injection site shortly following transplantation [37]. Terrovitis *et al.* reported that cell retention rates in beating hearts are significantly lower than in non-beating hearts after intramyocardial cell delivery [36]. Additionally, the pathological heart (e.g., post-infarction) is a hostile milieu, which results in poor survival when cells are transplanted into the damaged myocardium because of localized hypoxia, acidosis, lack of nutrients and accumulation of toxic waste [38]. It was suggested that the survival rate of transplanted cells was estimated at between 0.1% and 10% following intra-myocardial injection [39, 40]. A variety of pre-treatments, including up-regulation of AKT [41], over-expression of Bcl-2 [42], statins [43], eNOS-enhancing substances [44] and hypoxic-preconditioning [45] have been shown to improve the survival of transplanted cells through activating anti-apoptotic and/or NO-related signaling pathways [38, 46].

Importantly, the underlying mechanism by which stem or progenitor cells could improve cardiac function has not been fully ascertained. However, it has been widely suggested that the major mechanism for the beneficial effects of transplanted cells, including, skeletal myoblasts, bone

marrow-derived cells and heart-derived cells, may be largely due to paracrine effects rather than to the generation of new myocardium [49, 50]. Paracrine effects are, of course, also dependent on cell retention. In other words, the observed beneficial effects to date resulted from the secretion of growth factors, cytokines and other local signaling molecules, which lead to angiogenesis, anti-remodeling, anti-inflammation, anti-apoptosis, and possibly to activation of resident CSCs [51] and increased survival of residual cardiomyocytes, all eventually improving cardiac function [31, 35, 37, 52].

Taken collectively, cellular cardiomyoplasty, especially *via* intracoronary infusion for the treatment of heart disease, is an exceptionally attractive approach as it is minimally invasive and widely available worldwide [47]. Furthermore, in the past 10 years, this method has been used in a large number of clinical trials, which have demonstrated safety, feasibility and efficacy in patients. However, in addition to the limitations of low retention and poor survival, there are still many questions and issues that need to be addressed, such as patient selection, ideal cell type, sufficient cell dosage, route of cell delivery and optimal timing for cell administration [38, 48].

1.3.2 Cardiac tissue engineering

Various approaches have been proposed to fabricate engineered tissue constructs for the treatment of CVDs through the use of different biomaterials and assembling technologies. Overall, these approaches can be classified into two main forms: *in vitro* tissue engineering, such as biomaterial-based constructs (porous scaffolds or extracellular matrix-based hydrogels), scaffoldless systems (cell sheets), and biological patches (decellularized matrix), generally designed to replace fibrous scar tissue after attachment to an injured part of the myocardium, and *in situ* tissue engineering (injectable alginate or self-assembling peptide nanofibers) [48, 49, 53].

1.3.2.1 *In vitro* tissue engineering

In vitro tissue engineering can produce artificial tissue constructs, typically known as scaffolds, which involve the combination of cells and biomaterials. A scaffold can act as a vehicle which provides cells with a suitable environment to populate and grow before implantation to the

injured area and integration into the host tissue. Cardiac tissue engineering has been considered as a potential alternative to repair and regenerate the diseased heart, especially for post-infarct HF [48]. In contrast to cell transplantation, even though the application of bioengineered cardiac tissue for reconstruction of injured myocardium involves surgical intervention, it could also be applied to repair of congenital and acquired heart defects and even radical regeneration of the end-stage failing heart in the future [32].

A variety of biodegradable and biocompatible materials have been employed to develop three-dimensional biomaterial constructs. Natural and synthetic polymeric biomaterials, and combinations thereof, have been suggested for use in cardiac tissue engineering, including alginate, collagen, gelatin, poly-lactic acid (PLA), and poly-glycolic acid (PGA) [54]. An ideal biomaterial is required to enhance cell attachment, proliferation and differentiation, and therefore may solve the problems of low retention and poor engraftment following cell implantation [48, 53]. Zimmermann *et al.* developed an engineered heart tissue (EHT), a heart muscle model system, by combining neonatal cardiomyocytes and collagen type I under mechanical strain [55]. Furthermore, the EHT was reported to improve heart function and increase systolic wall thickness of infarction after implantation [56]. Leor *et al.* prepared 3D porous alginate scaffolds seeded with foetal rat cardiac cells using a freeze-drying technique. After the scaffolds were implanted onto the injured myocardium as a pericardial patch in a rat model of MI, the biografts enhanced neovascularization, attenuated left ventricular dilation and improved heart function [57]. However, although scaffolds are biocompatible and biodegradable, inflammation and immunogenicity may occur in the process of degradation in the body [54].

The production of decellularized patches involves the removal of cellular materials from tissue using detergent, which gets rid of any potentially immunogenic components, but retains the underlying extracellular matrix (ECM). Various decellularized cardiovascular tissues, such as pericardium, vascular wall, and valve leaflets, have been engineered using immersion decellularization [58-60]. An acellular ECM, prepared from porcine small intestine submucosa, was seeded with rabbit MSCs and implanted onto the infarcted region of the rabbit heart. In

addition to an improvement in heart function, differentiation of MSCs into cardiac and vascular cells was observed in the injured region [61].

In 2002, cell sheet engineering was first proposed by Shimizu *et al.* [62]. Unlike other *in vitro* engineering techniques, the cell sheet engineering is a scaffoldless system. Briefly, this technology involves the use of novel cell culture surfaces, coated with a specific polymer, called poly (N-isopropylacrylamide), or PIPAAm, which is temperature-responsive. Importantly, the polymer is slightly hydrophobic and cell adhesive at 37^{o}C, but becomes very hydrophilic and non-cell adhesive below 32^{o}C, so cells can be harvested simply by reducing the temperature. Furthermore, without the necessity for trypsinization, the confluent monolayered cells with the underlying ECM are harvested together as a cell sheet, which can be directly attached to other cell sheets or naturally implanted onto tissue surfaces in the body [62, 63]. In 2006, the monolayered MSCs sheet was reported to reverse wall thinning in the scar area and improved heart function after transplantation onto the infarcted area of the rat heart, suggesting that transplantation of monolayered MSCs sheet may be a potential therapeutic means for cardiac regeneration [64].

One of the major challenges of *in vitro* engineering is to overcome the limited thickness of the construct, as the maximum oxygen diffusion is limited to approximately 200 μm [65, 66]. Channelled cardiac extracellular matrix scaffolds, oxygen carriers and stacked cell sheets have been employed to increase the construct thickness by improving oxygen supply [67, 68].

1.3.2.2 *In situ* tissue engineering

In contrast to the *in vitro* approach, *in situ* tissue engineering, characterized by a scaffold-free approach, involves the direct injection of the biomaterial mixed with cells into the injured site [48]. The major advantage of this strategy is that there is no need for open surgery for implantation of engineered scaffolds. A variety of biomaterials have been employed for *in situ* engineering, including fibrin glue 69], collagen [70], alginate [71] and self-assembling peptides [72, 73]. For example, Davis *et al*. employed self-assembling peptides, which naturally form nanofibers when injected with cells into the myocardium, to produce a microenvironment of

scaffold *in situ*, which is advantageous for cell growth and vessel development [72]. Leor *et al.* demonstrated that intracoronary injection of alginate hydrogel formed *in situ* could reverse ventricular remodelling in a swine model of AMI, which resulted from increased scar thickness and physical support by the injectable implant [74].

Finally, it is probable that different therapeutic strategies should be adopted depending on the extent of damaged vasculature and myocardium in the ischemic heart. For example, cardiac organ engineering might be a better therapy for advanced HF than single cell transplantation or myocardial patches because of relatively generalized pathological lesions in severe heart failure. In the regenerative medicine field, therefore, generating a replacement organ is the ultimate goal to treat the patient in the end-stage of disease. However, this is a big challenge, as the heart is a complex anisotropic helix in architecture composed of collagen-based extracellular matrix, with intercalated cardiac myocytes and fibroblasts, and dense supporting vascular network [53, 75]. Myocardial patches hold promise to replace focal non-contractile fibrous scar tissue for post-infarct HF, but are not adequate for replacement of the whole organ in terminal HF. In 2008, Taylor and co-workers developed a perfusable rat heart matrix with preserved vascular network, competent valves and intact chamber geometry using a perfusion decellularization method. After reseeding with neonatal rat cardiomycytes and endothelial cells, the recellularized heart construct generated pumping work consistent with about 2% of adult and 25% of fetal heart function under electrical and mechanical stimulation [76]. The next steps are to repopulate the decellularized matrix with autologous cells from either stem cells or stem cell-derived differentiating cells and optimize construct growth at different stage of maturity [49].

1.4 Types of stem cells

By definition, stem cells are undifferentiated cells that are clonogenic, self-renewing, and pluripotent or multipotent, capable of giving rise to all or multiple cell types in the body [77]. Typically, stem cells can be divided into three broad categories: embryonic stem cells, derived from the inner cell mass of blastocysts, induced pluripotent stem cells, derived from adult

differentiated cells through reprogramming by the introduction of pluripotent transcription factors, and adult stem cells, such as skeletal myoblasts, haematopoietic stem cells, mesenchymal stem cells, endothelial stem cells and cardiac stem cells present in adult tissues.

Since 2000, a number of different cell types have been used to treat patients with AMI or chronic ischemic cardiomyopathy in clinical trials, including skeletal myoblasts, bone marrow mononuclear cells, circulating progenitor cells and mesenchymal stem cells [31, 52, 77, 78]. However, these cells of various sources have presented mixed results and no cell type has been proved to be the best candidate for cardiac therapy in clinical trials conducted to date [52, 78]. On the other hand, it is important to note that autologous CSCs, including c-kit$^+$ cells and cardiosphere-derived cells, are already being investigated in phase I clinical trials. Encouragingly, the results of two clinical trials were recently released in Lancet, reporting the safety and efficacy of the use of endogenous CSCs in patients with ischemic heart failure [79, 80]. This indicates that CSCs have a potential to become the ideal cell population for the stem-cell based therapy. With better understanding of resident CSCs and advances in engineering technology, it is hoped that the combination of CSCs and cardiac tissue/ organ engineering could play a crucial role in the future of cardiovascular regenerative medicine. Each of these stem cells described above has its own advantages and disadvantages, which are briefly summarized in Appendix Table 7, and will be discussed below in more detail.

1.4.1 Embryonic stem cells

Embryonic stem cells (ESCs), the prototypical stem cell, can develop into all cell types in the body, including pancreatic β-cells, neural cells and cardiomyocytes [83, 84]. The isolation of mouse embryonic stem cells was first reported in 1981 [85]. Mouse ESCs (mESCs) were originally used to investigate embryonic development and establish genetically modified mice [68]. Over time, researchers expanded their interest to the field of regenerative therapy involving a stem cell-based approach [68]. In 1998, the first human ESCs (hESCs) were isolated by Thomson *et al*. [86] and have subsequently been attracting significant interest as a potential cell source for regenerative medicine due to their pluripotent capability and proliferation potential.

A number of studies showed that mESC- and hESC-derived cardiomyocytes can survive and improve heart function when injected into infarcted myocardium in murine models [87-90]. However, there are several undesirable limitations with the practical application of hESCs, such as ethical problems, teratoma formation and immunological rejection, which have hampered the initiation of clinical trials in patients with cardiovascular disease [91, 92]. It is clear that a better understanding of molecular and genetic pathways for ESC differentiation and cardiac development could prevent contamination with undifferentiated ESCs, preventing teratoma formation when transplanted into the body [52, 93]. Alternatively, to overcome the ethical issues and immune rejection, induced pluripotent stem cells might present a prospectively attractive alternate, as they are of autologous origin (patient-specific) [84].

1.4.2 Induced pluripotent stem cells

Induced pluripotent stem cells (iPSCs) have been generated using a process which involves the retroviral introduction of transcription factors related to pluripotency into adult terminally differentiated cells, such as dermal fibroblasts, causing them to revert to an embryonic stem cell-like stage [94]. Takahashi *et al*. established that over-expression of four transcription factors (Sox2, Oct4, c-Myc, and Klf4) could convert adult mouse and human skin fibroblasts into pluripotent stem cells [94, 95]. Furthermore, differentiation of iPSCs into functional murine cardiomyocytes has been demonstrated [96, 97]. In 2007, Yu *et al.* successfully reprogrammed human somatic cells to iPSCs using four genes including Sox2, Oct4, Nanog and Lin28 [98]; these human iPSCs have the potential to differentiate into functional cardiomyocytes [99, 100].

Importantly, despite subtle epigenetic differences associated with reprogramming, iPSCs strongly resemble ESCs in terms of morphology, differentiation capacity, gene expression profile and teratoma formation [101]. The use of iPSCs avoids the ethical dilemmas and immunological problems of ESCs, as they are derived from an autologous source, however there remain concerns for clinical application because their generation employs viruses and oncogenes, associated with tumorigenesis [93]. Thus, for safety reason, the development of approaches using

nonvector pluripotent induction [102-104] without the need for oncogenes [105] might pave the way for clinical applications in the future [35, 84]. Nevertheless, it should also be noted that tetratoma formation, low efficiency of cardiomyocyte differentiation, genetic abnormalities and high cost are other roadblocks to routine clinical use [37].

1.4.3 Adult stem cells

In contrast to pluripotent stem cells (ESCs and iPSCs), adult stem cells are undifferentiated, multipotent cells, which exist among differentiated cells within tissues or organs throughout the body [35]. In general, these cells are able to self-renew and differentiate into tissue-specific mature cells in order to maintain homeostasis within their host tissue. However, it has been reported that adult stem cells have the potential to transdifferentiate into different cell types (i.e., developmentally unrelated cells), termed plasticity [106, 107]. To date, a variety of adult stem cells have been investigated for their therapeutic potential for treatment of cardiovascular disease, including skeletal myoblasts, bone marrow mononuclear cells, hematopoietic stem cells, mesenchymal stem cells, endothelial progenitor cells and endogenous cardiac stem cells.

1.4.3.1 Skeletal myoblasts

Skeletal myoblasts or satellite cells, which give rise to skeletal muscle, were extensively studied in animal models of MI before entering the clinical arena, due to the advantages of their contractile phenotype, high expansion capacity in culture, good resistance to ischemia and autologous origin [31, 37, 93, 108]. Reports from experimental studies have shown that implanted myoblasts resulted in ventricular wall thickening and increased contractility, thereby improving function in the infarcted myocardium [109-112]. Based on the positive results, skeletal myoblasts were the first cell type to be examined in a human trial for cardiac repair [113]. After beneficial effects were shown in several pilot studies, further randomized controlled trials (RCT) using autologous skeletal myoblasts were conducted including MAGIC, MARVEL-1 and SEISMIC. The MAGIC study by Menasche *et al*. was terminated early because of a failure to reveal clinical efficacy in patients undergoing coronary artery bypass grafting (CABG) for

ischemic cardiomyopathy [114]. Recently, the SEISMIC trial by Duckers *et al*. reported that injection of autologous skeletal myoblasts in patients with HF is safe and relieves symptoms based on a trend towards improved exercise tolerance in the cell-treated group despite no significant effect in LVEF [115]. However, despite improving cardiac function when transplanted into ischemic myocardium, these cells were unable to transdifferentiate into cardiomyocytes and integrate electromechanically with the host myocardium, thereby increasing the risk of sustained ventricular tachycardia, a life-threatening arrhythmia [93]. Collectively, in the light of no cardiomyocyte regeneration, failure to integrate with host myocardium, potential lethal arrhythmia and mixed results, further research is required prior to future clinical applicability.

1.4.3.2 Bone marrow-derived stem cells

The bone marrow is an heterogeneous tissue, consisting of different subpopulations, including hematopoietic stem cells (HSCs) and endothelial progenitor cells (around 2-4%), very rare mesenchymal stem cells (MSCs) (0.001 to 0.01% of the nucleated cells) and large proportions of committed progenitor cells and their specifically differentiated progeny [117]. Bone marrow-derived cells have the capacity to proliferate, migrate, and differentiate into various cell types [118]. Technically, bone marrow-derived cells are easily accessible either by bone marrow aspiration or by isolation from peripheral blood after mobilization with cytokines such as stem cell factor (SCF) and/or granulocyte colony-stimulating factor (G-CSF) [35]. These cells have attracted great attention as candidates for cell-based therapy because of their autologous origin, safety, ease of isolation and reduced immunogenicity (MSCs) [119, 120]. The use of bone marrow mononuclear cells (BMMNCs), endothelial progenitor cells (EPCs), purified progenitor cells ($CD34^+$ or $CD133^+$), HSCs and, MSCs in experimental and clinical studies has provided informative data related to human CVDs [121].

(I) Hematopoietic stem cells (HSCs)

HSCs, identified by the expression of cell surface antigens such as CD34, CD133, c-kit (CD117), and stem cell antigen-1 (Sca-1), are lineage negative (Lin-) [32, 122]. These cells can be obtained from the bone marrow, umbilical cord and the peripheral blood, giving rise to all blood cell types

[122]. HSCs have been extensively studied and used to treat a variety of hematological disorders in the clinic, such as anemia, leukemia and lymphoma [35]. Orlic *et al.* showed that Lin-/c-kit+ bone marrow cells injected into infarcted myocardium of mice were able to generate new cardiomyocytes [123]. However, other studies have been unable to demonstrate cardiomyocyte transdifferentiation of HSCs and cardiac function improvement in animal models of MI [124, 125]. Furthermore, over the past years, several clinical trials of human HSCs have shown insignificant or no benefits in terms of EF [52, 122]. Although EF has been used as a surrogate for evaluation of heart function in animal and clinical studies, it has been suggested that accurate mesurements of regional LV wall motion might potentially offer a valuable assessment of the true efficacy of stem cell therapy as the exact mechanisms of global LVEF improvement in patients remain largely unidentified [389].

(II) Mesenchymal stem cells (MSCs)

MSCs, identified by the surface marker expression of CD90, CD105 and CD73, but negative for CD14, CD34, CD45, CD11b, CD19, CD79 and HLA-DR, are precursors of non-hematopoietic tissues, such as bone marrow, muscle, cartilage, adipose tissue and heart, and have the capacity to give rise to fibroblasts, osteoblasts, chondroblasts and adipocytes *in vitro* [126, 127]. MSCs injected into infarcted myocardium could increase regional blood vessel density, prevent scar expansion, promote regional wall motion and prevent ventricular remodelling [128, 129]. Experimental results suggested that MSCs were able to transdifferentiate into cardiomyocyte-like cells under special culture conditions (such as coculture with cardiomyocytes or exposure to 5-azacytidine) and in normal or injured myocardium in animals [130-132]. In addition, MSCs can differentiate into an endothelial phenotype when treated with vascular endothelial growth factors in a chronic ischemic model [133, 134]. Intriguingly, Hatzistergos *et al*. demonstrated that allogeneic bone marrow MSCs stimulated the proliferation and differentiation of c-kit$^+$ CSCs when injected into a swine model of MI [51]. Two clinical trials conducted in the past years have demonstrated safety and feasibility and displayed improvement in LV function; however these benefits are inconsistent [135, 136]. So far, it remains controversial whether MSCs have the

potential to transdifferentiate into cardiomyocytes [78, 137].

(III) Endothelial progenitor cells (EPCs)

EPCs, identified by CD34, CD133 and KDR, are a specialized subset of hematopoietic cells, which can be isolated from bone marrow, peripheral blood or umbilical cord blood [138]. During the development of the blood system, endothelial progenitor cells and hematopoietic stem cells originate from a common primitive cell, namely the hemangioblast [139]. Asahara *et al.* demonstrated that a fraction of $CD34^+$ population from peripheral blood circulation is characterized by the expression of antigens related to hematopoietic stem cells, including CD34, CD133, c-kit, VEGFR-2, CD144, and Sca-1 [140]. Upon differentiation, endothelial progenitor cells are found to lose the CD133 antigen and begin to express VE-cadherin and vWF [141]. It has been shown that *in vitro* expanded EPCs transplanted into ischemic animal model home to the injured site of the heart to modulate remodelling and induce angiogenesis/neovascularisation through anti-apoptotic and angiogenic effects, eventually leading to functional improvement [142-144]. Additionally, there has been some evidence showing that EPCs could transdifferentiate into myocardial lineages including cardiomyocytes, endothelial cells and smooth muscle cells both *in vitro* and *in vivo* [145, 146]. However, like HSCs and MSCs, no general consensus has been reached concerning the transdifferentiation of EPCs into cardiac myocytes, as other investigators have failed to repeat the findings [147, 148].

(IV) Bone marrow mononuclear cells (BMNNCs)

BMMNCs, isolated by density centrifugation following bone marrow aspiration, have been intensively studied as potential therapy for ischemic heart disease [37]. They are therefore the most common bone marrow cell type used in clinical trials for patients with AMI and chronic ischemic cardiomyopathy over the last decade [38]. In the early cohort and randomized pilot studies, BMMNCs resulted in a modest increase, of between 1% and 5%, in LVEF at short-term follow up (3 to 6 months) [52, 121]. However, some clinical trials have not demonstrated consistent results at long-term follow up (longer than 12 months) [149]. For example, the REPAIR-AMI trial, a RCT including 204 patients, showed that intracoronary delivery of

BMMNCs following AMI increased EF by 2.5% (p = 0.01) compared with the control group at 4 months follow-up. The significant effect on EF was lost at 12 months follow-up, although decreased mortality was observed in the treatment group [150]. Importantly, there are two recent clinical trials: BALANCE for AMI and STAR-heart for ischemic cardiomyopathy using BMMNCs, both showing a significant improvement in EF and survival rate in the treated group receiving BMMNC transplantation at 5 years follow-up, suggesting that BMMNC therapy results in significant and long-standing improvements in LV function and mortality in patients with AMI and chronic IHD [151, 152]. Meta-analyses of randomized controlled trials concluded that functional improvement can be achieved in patients with AMI by BMMNC treatment over conventional therapy [153, 154]. There are clinical trials using BMMNCs still in progress in the world, such as TIME and FOCUS in the USA and REGENERATE-AMI, REGENERATE-IHD and REGENERATE-DCM in the UK, assessing the safety, feasibility and efficacy of administration of BMMNCs in patients with different clinical situations such as acute myocardial infarction, chronic ischemic cardiomyopathy or dilated cardiomyopathy [155-157]. It is hoped that more clinical studies will provide further insights into the therapeutic efficacy and help solve unanswered issues regarding bone marrow-derived cell transplantation in patients with cardiovascular disease, including optimal cell type, cell dosing, and timing and route of delivery.

1.4.4 Endogenous cardiac stem cells

The heart has traditionally been regarded as a terminally differentiated, post-mitotic organ without the ability to regenerate itself. Recently, this dogma has been challenged by the discovery of resident cardiac stem/progenitor cells in the heart of several species including mouse [158, 159], rat [160, 161], dog [162], pig [47, 163] and human [164, 165]. Furthermore, a study by Hsieh *et al*. using a genetic fate-mapping approach, demonstrated that cardiac stem cells replenished adult mammalian cardiomyocytes lost after injury due to myocardial infarction or pressure overload [166]. These different subpopulations of cardiac stem cells have been identified and classified based on their properties and various surface markers such as c-kit and Sca-1.

1.4.4.1 Cardiac c-kit$^+$ stem cells

C-kit (CD117), the tyrosine kinase receptor for the stem cell factor, was initially reported to be expressed on the surface of hematopoietic stem cells [167]. In 2003, Beltrami and colleagues described for the first time the discovery of a subpopulation of Lin$^-$ and c-kit$^+$ cardiac stem cells (CSCs) in the rat heart, which are clonogenic, multipotent and capable of self-renewal [160]. Some cells of this population were found to co-express cardiac specific transcription factors such as Gata4, Gata5, Nkx2.5 and MEF2C, suggesting that they were at the early stage of differentiation committed to myocardial lineages. These c-kit$^+$ cells showed remarkable potential to differentiate into all cardiac lineages and regenerated the damaged myocardium in a rat model of MI [160]. Subsequently, Bearzi *et al*. developed methods for isolation and expansion of c-kit$^+$ human CSCs (hCSCs) from small myocardial specimens. Furthermore, when injected into immunocompromised rats and mice, these cells differentiated into cardiomyocytes and improved the LV performance of infarcted hearts [168]. Some studies have shown that c-kit$^+$ cells are triggered and regenerate new cardiomyocytes in response to pathological lesions [169, 170]. In addition, endogenous c-kit$^+$ cells can be activated to promote myocardial repair through the mediation of insulin-like growth factor-1 (IGF-1) and hepatocyte growth factor (HGF) [163, 171]. Endogenous Lin$^-$ c-kit$^+$ cells are very rare within the myocardium (on average, 1 in every 10^4 myocytes), which makes it imperative to isolate and expand c-kit$^+$ cells for a certain period to generate clinically-relevant numbers [160]. Nevertheless, it was reported that c-kit$^+$ CSCs can be expanded through growth in culture beyond the population doubling limit of somatic cells (>40) and long-term *in vitro* culture up-regulated Gata4 expression, resulting in enhanced cardiomyogenic differentiation [172]. Moreover, intracoronary transplantation of c-kit$^+$ CSCs has been shown to reverse adverse remodelling, improve heart function (EF) and stimulate endogenous cardiac stem cells in infarcted rat hearts [173].

Because of the inspiring evidence in pre-clinical animal studies, the first phase I human clinical trial using endogenous c-kit$^+$ stem cells in patients with ischemic heart disease has been initiated. The SCIPIO trial by Bolli *et al*. was designed to examine the safety and efficacy of intracoronary delivery of autologous CSCs, which are expanded c-kit-expressing cells from right atrial

appendages, in patients with ischemic cardiomyopathy. The initial results, published in the November 2011 issue of Lancet, are encouraging, confirming the safety and feasibility, and providing the evidence which shows intracoronary infusion of autologous c-kit$^+$ CSCs leads to a significant improvement in LV systolic function and a substantial reduction in scar size at one year follow up [79].

1.4.4.2 Cardiac sca-1$^+$ stem cells

Sca-1 (stem cell antigen-1), a member of the Ly-6 family, was first described as one of the cell surface antigens expressed on hematopoietic stem cells [174]. Multipotent stem cells derived from bone marrow and skeletal muscles express Sca-1 [175-177]. Thereafter, several groups identified various heterogeneous subpopulations of Sca-1$^+$ cells on the basis of different subsets of markers co-expressed with Sca-1 [178]. In 2003, Oh *et al.* were the first to isolate Sca-1$^+$/CD31$^+$ stem cells in the adult mouse heart, which are negative for blood cell lineage markers, c-kit, flt-1, flk-1, CD34, and CD45, but express cardiac transcription factors such as Gata4, MEF2C and TEF-1. These cells could differentiate into cardiomyocytes with expression of cardiac-specific genes (Nkx2.5, cTnI, and MHC) upon stimulation with the demethylation agent 5-azacytidine [179]. In addition, Matsuura *et al.* reported that a population of Sca-1$^+$, c-kit$^+$, CD34$^+$ and CD45$^+$ cells gave rise to spontaneous beating cardiomyocytes and the differentiated cells showed expression of cardiac transcription factors and contractile proteins when treated with oxytocin [180]. On the other hand, transplantation of Sca-1$^+$/CD31$^-$ cells resulted in improved LVEF following MI by cardiomyocyte regeneration and myocardial neovascularisation through paracrine effects, suggesting an *in vivo* therapeutic potential [181].

Accumulating evidence in many studies has suggested that cardiac Sca-1$^+$ stem cells from mouse heart are self-renewing, clonogenic, and multipotent, and have the potential to differentiate into cardiomyocytes both *in vitro* and *in vivo* [179, 180, 182, 183]. In contrast to c-kit$^+$ CSCs, the equivalent of murine cardiac stem cells expressing Sca-1 has not yet been identified in humans. Recently, Smits *et al.* isolated and expanded a population of cardiac-derived Sca-1-like cells (human cardiomyocyte progenitor cells) from fetal and adult human hearts by clonal expansion

or MACS isolation using the antibody targeted at mouse Sca-1. Furthermore, they demonstrated that these cells could be differentiated into beating cardiomyocytes with high efficiency (80-90%) after treatment with 5-azacytidine and vitamin C/transforming growth factor-β in a chronological order [184]. However, little is known whether these human cells represent a suitable stem cell type for cardiac repair and regeneration in the treatment of cardiovascular diseases.

1.4.4.3 Cardiac side population cells

The side population (SP) cells, characterized by their ability to efflux Hoechst 33342 (a DNA-binding dye) *via* the transporter, ATP-binding cassette sub-family G member 2 (ABCG2; CDw338), have been identified in several adult tissues such as bone marrow and skeletal muscle [185]. Hierlihy *et al.* were the first to report the existence of a cardiac SP cell population with stem cell-like activity and the potential of cardiomyogenic differentiation in the postnatal murine myocardium [186]. It has been shown that adult cardiac side population cells are heterogeneous in nature, consisting of distinct subpopulations of cells expressing c-kit, Sca-1, CD31, CD34, VE-cadherin, mesenchymal progenitors, vascular endothelial cells and cardiomyogenic precursors [187]. Several studies have reported that cardiac side population cells found in rodents are able to give rise to three major cardiac lineage cardiomyocytes, endothelial cells and smooth muscle cells *in vitro* [188-190]. *In vivo*, it was shown that these cells homed to the damaged myocardium and differentiated into three cardiac lineages when infused into adult rats [Oyama 2007]. Furthermore, Liang *et al.* demonstrated that a subset of cardiac SP cells ($Sca\text{-}1^{+}/CD31^{-}$) migrated to the injured site and gave rise to cardiomyocytes or endothelial cells through the SDF-1/CXCR4 system in a murine model of myocardial ischemia [191]. Cardiac SP cells have shown the potential for the commitment of cardiovascular lineages both *in vitro* and *in vivo*, however, more research is required to investigate their therapeutic effects on cardiac function upon transplantation into a myocardial ischemic model.

1.4.4.4 Cardiospheres and cardiosphere-derived cells

Messina *et al*. described a method to culture cardiac stem cells *via* the formation of multicellular clusters, termed cardiospheres, from mouse heart explants and human ventricular biopsies. These

cardiospheres were clonogenic and expressed c-kit, Sca-1, and CD31, CD34, and Flk-1 based on immunophenotypic and flow cytometric analyses [158]. Mouse cardiospheres spontaneously contracted after their generation, but human cardiospheres were seen to beat only after coculture with rat cardiomyocytes, nevertheless, both indicated that these CSC populations have the potential to differentiate into cardiomyocytes. Furthermore, murine cardiospheres were shown to differentiate into cardiomyocytes with contractility as well as vascular cells when transplanted into the ischemic heart of immunodeficient mice [158].

Subsequently, Smith *et al.* modified the protocol described by Messina's group to substantially expand cardiosphere-derived cells (CDCs) *in vitro* and showed myocardial regeneration and functional improvement when these cells were injected into the infarcted mouse heart [165]. Intracoronary delivery of autologous CDCs led to the formation of new tissue, reduction in infarct size and improvement of haemodynamics in a pig model of ischemic cardiomyopathy [47]. In contrast to other populations of CSCs, cardiospheres and CDCs have been reported to contain a mixed population consisting of c-kit$^+$ and Sca-1$^+$ cardiac progenitor cells, and cells expressing CD90 (cardiac mesenchymal-related) and CD31/CD34 (endothelial progenitor-related) markers [158, 165, 192, 193]. It is possible that the cardiac progenitor cells could readily engraft, differentiate and function when transplanted into the injured myocardium in the presence of cardiac mesenchymal stem cells and endothelial progenitor cells *via* synergistic paracrine effects [193, 194]. In short, so far, cardiospheres and CDCs have been isolated and used for treatment of ischemic heart disease in various animal models, including mouse [158, 192], rat [36, 161], and pig [47, 195], and shown evidence of new cardiomyocyte formation or beneficial effects on cardiac function.

After the accumulation of promising results, the CADUCEUS trial, led by Marban *et al*., aimed to investigate the effects of autologous CDC transplantation *via* the intracoronary route in patients with a recent MI and ischemic left ventricular dysfunction. The results, published in Lancet early in 2012, were that intracoronary infusion of autologous CDC contributed to significant increases in viable myocardium, regional contractility and regional systolic wall

thickening despite no significant change in LVEF, which might be explained by the fact that EF at baseline was only moderately impaired (39%), leaving little room for improvement by 6 months [80]. Because of the positive findings, further research with longer follow-up and larger, phase 2 studies are required to confirm the true and persistent clinical benefits.

1.4.4.5 Islet-1$^+$ cardiovascular progenitors

Laugwitz *et al.* reported the identification of a subpopulation of cardiovascular progenitor cells in postnatal mouse, rat and human myocardium, which express an embryonic marker of LIM-homeodomain transcription factor Islet-1 (Isl1) [196]. During cardiac development, Isl1$^+$ progenitor cells, derived from the second heart field, contribute to the right ventricle, outflow tract and partial atria [197]. The number of these cells is very low at postnatal ages with between 500 and 600 cells per heart [198]. Isl1$^+$ progenitors are negative for c-kit, Sca-1 and CD31, but co-express the cardiac specific transcription factors Nkx2.5 and Gata4; importantly they have the potential to differentiate into smooth muscle cells, endothelial cells and fully functional cardiomyocytes [196, 199]. Although Isl1$^+$ progenitor cells may represent an attractive cell source for cardiac repair and regeneration, the fact that the Isl1$^+$ progenitor population rapidly declines shortly after birth limits their clinical application in the adult patient [198, 200, 201].

1.4.4.6 Epicardium-derived stem cells

Another source of endogenous resident cardiac progenitor cells with regenerative potential for the adult heart is the epicardium, with several groups reporting the discovery of epicardium-derived myocardial and vascular progenitors in embryonic mouse and adult human heart [202-206]. During heart development, a subset of epicardial cells, known as epicardium-derived cells (EPDCs), delaminate from the epicardium and subepicardium and migrate into the myocardium through a process of epithelial-to-mesenchymal transition (EMT) prior to differentiation into specialized cells [207]. EPDCs are multipotent in both embryonic and adult hearts, capable of giving rise to adventitial fibroblasts, coronary smooth muscle cells, endothelial cells and cardiomyocytes [178, 201, 208].

Adult human EPDCs were found to reduce remodelling and increase ejection fraction when transplanted into an immunodeficient mouse model of myocardial infarction [209]. Moreover, Smart *et al.* reported that the activation of quiescent EPDCs in the adult mouse heart can be enhanced using a naturally occurring protein called thymosin beta 4 (Tβ4; a small actin-binding protein that activates integrin-linked kinase); this stimulating factor releases the EPDCs from a dormant state and restores their pluripotent potential with differentiation into cardiomyocytes after their migration to the damaged site of the heart [202, 210]. Although the induction of cardiomyocyte differentiation by Tβ4 is not efficient at present, this strategy also provides another prospective means of stem cell-based cardiac therapy through *in situ* activation of resident cardiac progenitor cells by specific factors without additional complications of isolation and expansion *ex vivo* and possible problems like low retention and engraftment, relative to cell transplantation [201, 211].

1.5 Aging and cardiac stem cells

Increaing age is a major risk factor for CVD [212, 213]. As demographic statistics show that the average age of many countries has been rising rapidly, CVD is becoming more prevalent among the general population. Although stem cell-based therapy has attracted a great deal of attention for potential treatment in heart diseases, for example, in AMI, dilated cardiomyopathy and chronic HF [118], it has been shown that there is a reduction in number and migratory activity of circulating EPCs ($CD34^+/KDR^+$) or bone marrow-derived HSCs ($CD133^+$) with age in healthy subjects and patients with ischemic heart disease [214-216]. Umbilical cord blood-derived HSCs possess higher potential of proliferation and expansion than HSCs from adult bone marrow or peripheral blood and their self-renewing capacity is also superior to that of adult cells [217]. Nishino *et al.* showed that aged neural stem cells increased $P16^{Ink4a}$ and $P19^{Arf}$ expression (markers of cellular senescence), which led to a reduction in self-renewal capacity [218]. Normally, stem cells experience replicative senescence with loss of self-renewal potential, commitment and differentiation [219]. Fan *et al.* revealed that cell growth and colony forming-unit fibroblasts (CFU-F) were markedly reduced in human MSCs from old patients. Additionally,

when transplanted into the infarcted myocardium of rats, young human MSCs exhibited significant improvement in heart function compared to old human MSCs [220]. Collectively, it has been suggested that aging could change the intrinsic characteristics of adult tissue-specific stem cells, including proliferation, clonogenic potential, migration and survival, which are critically associated with their regenerative efficacy in therapies.

Presently, among various CSCs, c-kit-positive CSCs and cardiosphere-derived cells (CDCs) are the only two types of resident cardiac stem cells entering a phase I clinical trial following positive evidence in pre-clinical studies. Some studies have displayed that, similar to other stem cells, c-kit$^+$ CSCs decline in number and function with increasing age [213, 221, 222]. However, little is known about the effects of chronological age on the cell pool and biological characteristics of CDCs. Importantly, as elderly people (aged 65 or older) have the highest incidence of cardiovascular disease in the stage of heart failure (HF), to use CDCs as an autologous cell source for the treatment of HF, it is essential to understand the impact of aging on these cells, especially number and properties in terms of isolation, expansion, clonogenicity, migration and differentiation.

1.6 Cardiac stem cells in nonischemic cardiomyopathy

Nonischemic cardiomyopathy, including hereditary cardiomyopathy and viral myocarditis, accounts for approximately one third of cases of HF [9]. Recently, in the era of stem cell-based therapy, a variety of stem cell types have been studied in AMI and chronic ischemic HF and used to treat these patients. Unfortunately, the investigation of stem cells, especially CSCs, in nonischaemic heart diseases is still in its infancy. Our lab has investigated the deterioration of cardiac function, energy metabolism and pathophysiology in Duchenne muscular dystrophy (DMD, dystrophin-deficient cardiomyopathy) using an mdx mouse model and is in collaboration with other researchers for the pursuit of possible treatments. We have demonstrated progressive cardiac disfunction with age in the MDX mouse heart, and therefore this was selected as a model system to investigate the effect of nonischemic cardiomyopathy on the CSC population.

DMD, an X-linked recessive disease, is characterized by a systemic lack of dystrophin protein in the sarcolemma, affecting skeletal and cardiac muscles [223] and is the most common and severe form of human muscular dystrophy, occuring in 1 in 3,500 live newborn males [224-226]. Patients used to die in their late teens or early twenties, mainly from pulmonary problems, such as respiratory infection and failure [227]. Recent advances in respiratory care have decreased mortality from lung complications in patients with DMD, who now can live to their late twenties to mid thirties and may even survive into their forties [227]. Currently available therapies have increased life span in DMD patients, but this has led to the majority of surviving patients eventually developing HF due to dilated cardiomyopathy (DCM), which is now the major cause of death. Approximately 90% of DMD patients will suffer from DCM, which gradually progresses to HF [225] and is responsible for the death of 10-50% of all cases [227, 229, 326-328].

Over the past decades, tremendous progress has been made in understanding the molecular mechanisms of DMD, however, there is still no cure to date [226]. Nevertheless, there are several different therapeutic approaches being investigated, such as gene therapy, cell-based therapy and mutation-specific treatments [229]. In 1995, Koh *et al.* explored the therapeutic potential of fetal cardiomyocytes when transplanted into the hearts of dystrophic mice and dogs, and found no significant effect as the dystrophin expression was limited to the engrafted cells [230]. A number of stem cell sources have been investigated to treat DMD, including skeletal myoblasts, bone marrow-derived and blood-derived cells [231]. As in gene therapy, initial cell-based therapy focused on the restoration of dystrophin to the heart, however, multiple studies revealed limited or no expression [232]. Additionally, the immune response still raises a concern [226]. However, little is known about the properties and functions of endogenous CSCs present in the diseased heart of DMD. Finally, the better understanding of resident CSCs (cardiosphere-derived cells) in an animal model of DMD may pave the way for the treatment of DMD using an autologous, endogenous heart-committed stem cell in the future.

1.7 Objectives

The objectives of the work in this thesis were to prove both the hypothesis that a bioartificial whole rat heart ECM, which retained integral 3D architecture with perfusable coronary vasculature, could be engineered using a decellularization method by detergent perfusion and the hypothesis that aging and disease adversely affect the number and characteristics of endogenous cardiac stem cells. High-resolution cine-MRI was utilized for the first time to characterize an accellular rat heart matrix made using the published protocol but with fine modifications. The effects of age and non-ischemic cardiomyopathy on the cardiosphere-derived cell population were investigated for the first time. Furthermore, to optimise cardiomyogenic differentiation of cardiosphere-derived cells for use within a 3D system, differentiation was induced *in vitro* using chemical agents (i.e., 5-azacytidine, DMSO, and ascorbic acid) instead of by co-culture.

Specifically, the aims were to:

- Develop the decellularized heart matrix combined with cardiac stem cells as a novel therapy for heart failure and establish an *in vitro* protocol for cardiomyocyte differentiation.
- Investigate the effects of age on cardiac stem cells (cardiosphere-derived cells) in terms of isolation, expansion, phenotype, function and differentiation potential.
- Characterize cardiac morphology and function in an animal model of muscular dystrophy (causing dilated cardiomyopathy) and determine the impact of this pathology on cardiac stem cells.

Chapter 2

General methods

2.1 Animals

Experiments were performed on rats and mice in this study. Sprague Dawley (SD) rats and C57Bl/10 mice were obtained from a commercial breeder (Harlan, Oxon, UK), whereas mdx mice were bred and housed at the University of Oxford. Animals were kept under controlled conditions of temperature, light and humidity, with *ad libitum* access to water and chow. All the procedures involved in this study were reviewed and approved by the Institutional Animal Care and Use Committee (IACUC) and the Home Office, and conformed to the UK government regulations (Home Office licence: 30/2755). Adult SD rats (3-4 months old) were used in all cell culture experiments and decellularization work, described in Chapter 3. Wild-type mice (C57Bl/10) at 1.5, 6, 18 and 24 months of age and mdx at 6 and 18 months were used for experiments in Chapter 4 and Chapter 5, respectively.

2.2 Isolation and expansion of cardiac-derived stem cells

In this study, hearts from SD rats, C57Bl/10 and mdx mice were used to produce cardiac-derived stem cells (CSCs), as previously described [158, 165]. All cell culture was carried out in a humidified atmosphere of 5% CO2 and 95% air at 37^{o}C.

2.2.1 Creating explants

Animals were anesthetized with sodium pentobarbital (Euthatal, Merial, UK) administered intra-peritoneally (IP) (270 mg/kg body weight for rats and 200 mg/kg for mice, respectively). A thoractomy was performed and hearts were rapidly excised and soaked in cold phosphate buffered saline (PBS; Invitrogen, UK). The heart was washed with PBS twice to remove blood, cut into small pieces in PBS and digested in 0.05% trypsin (Invitrogen, GIBCO, 25300, UK) for 3 minutes at room temperature. Then, 2 ml of complete explant medium (CEM; Appendix: Table 1) supplemented with 20% (v/v) fetal bovine serum (FBS; Biosera, S1900, UK) was added to neutralize trypsin activity. After further mincing to 1 to 2 mm^3 in size, these smaller explant fragments were plated onto fibronectin-coated (Sigma, F1141, UK; 10 µg in 1 ml PBS) 60 x 30 mm Petri dishes (Corning, UK) with 1.5 ml CEM. The explants were then incubated

for one hour in the laminar flow cabinet, allowing them to firmly attach to the surface of pre-coated dishes. Finally, they were cultured in the incubator of a humidified atmosphere of 5% CO2 and 95% air at 37°C with medium changes every 3-4 days.

2.2.2 Harvesting explant-derived cells

After 2-3 days, explant fragments were surrounded by a layer of thin stromal-like cells over which small, round, phase-bright cells migrated. These migrating cells are termed explant-derived cells (EDCs). Once 70-80% confluent, EDCs were detached by treatment with 1 ml of 0.05% trypsin (Invitrogen, 25300, UK) for 3-5 minutes at 37°C after washing with PBS and versene (Invitrogen, Gibco, 15040, UK). EDCs could be harvested 2-3 times from the same explant at one week intervals.

2.2.3 Growing cardiospheres

EDCs were counted using a haemocytometer (Neubauer, Assistant, Germany) and seeded onto 24 multiwell plates pre-coated with poly-D-lysine (Sigma, P7280, UK; 10 µg in 0.5 ml PBS for each well) at a concentration of 3 x 10^4 cells in 300 µl of Cardiosphere Growth Medium (CGM; Appendix: Table 2.1 and 2.2). After incubation for 2 days, spherical multicellular clusters, commonly known as cardiospheres, began to form. Cardiosphere culture was carried out in a humidified atmosphere of 5% CO2 and 95% air at 37°C.

2.2.4 Expanding cardiosphere-derived cells

After approximately 4 days, loosely adherent cardiospheres were harvested by gentle pipetting. After resuspension in CEM, cardiospheres were plated into fibronectin-coated T75 flasks (Corning, UK) and expanded as monolayer cardiosphere-derived cells (CDCs). CDC culture was carried out in a humidified atmosphere of 5% CO2 and 95% air at 37°C.

2.2.5 Passaging CDCs

CDCs were passaged at 80-90% confluence by treatment with 3 ml of 0.05% trypsin (Invitrogen, 25300, UK) for 3-5 minutes at 37°C and split into two fibronectin-coated T75 flasks. The culture medium was changed every 4 days.

2.3 Cell viability and proliferation assays

2.3.1 Trypan blue viability assay

Trypan Blue (Sigma, T8154, UK) is one of several stains recommended to be used in a dye exclusion assay for determining the cell viability. Examined cells were prepared in a cell suspension by enzymatic trypsinization and stained with 0.4% Trypan Blue for about 5 minutes. Live (viable) cells with intact membrane integrity do not take up the dye and were not stained, whereas dead (non-viable) cells with defective membrane were stained blue. Cell viability was calculated with the use of the formula below:

$$\text{Cell viability (\%)} = \left(\frac{\text{Total viable cells (unstained)}}{\text{Total cells (stained \& unstained)}} \right) \times 100$$

2.3.2 AlamarBlue® cell proliferation assay

The viability and proliferation of CDCs were assessed using AlamarBlue® (AbD Serotec, BUF012A, UK), in which nonfluorescent resazurin (oxidized form, blue) was reduced to fluorescent resorufin (red) by living cells. One of AlamarBlue's advantages is that it does not interfere with the pathways of the electron transport chain, meaning that cell growth is not affected by addition of AlamarBlue® solution. CDCs were seeded into a 96 well plate in a serially decreasing number (from 5,000 to 312 cells per well) for a standard curve or at a certain density for dynamic growth evaluation and allowed to attach overnight. The cells were washed twice with PBS and incubated with 10% AlamarBlue®, diluted in phenol red-free Iscove's Modified Dulbecco's Medium (IMDM; Invitrogen, UK), at 37^{o}C. The resulting relative fluorescence intensity at 530-560 nm excitation wavelength and 590 nm emission wavelength, quantified by FLUOstar OPTIMA (BMG labtech, UK), is directly related to the number of live cells. A standard curve of fluorescence intensity with corresponding cell number was obtained, which could be used to translate the fluorescence intensity into the number of viable cells. Thereafter, the AlamarBlue® assay was carried out at different time

points to determine continuous cell growth.

2.4 Clonogenic assay

To perform a clonogenic assay, monolayered CDCs were harvested using trypsinization to produce a dissociated single cell suspension. The cell suspension was serially diluted to 50 cells in 10 ml of CEM and seeded into the wells of a 96 well plate pre-coated with fibronectin (Sigma, F1141, UK; 10 µg in 1 ml PBS) at a density of 0.5 cell per well to generate single-cell clones. The plated cells were incubated to allow for attachment at 37^{o}C for 4 hours. Each of 96 wells containing a single cell was identified under a light microscope. Thereafter, the wells previously identified were examined for growing colonies twice weekly. After two weeks, the number of wells with clones derived from a single cell was counted. Four randomly picked clones from each sample were trypsinized and further expanded in a 6-well plate to confirm the proliferation of these colony-forming cells. Clonogenicity of CDCs was determined and expressed as a percentage using the following formula:

$$\textbf{Clonal efficiency (\%)} = \frac{\textbf{Total wells with clone}}{\textbf{Total wells with single cell}} \times 100$$

2.5 Tissue sectioning

For histology and immunohistochemistry, explanted hearts were cut into half transversely, and embedded and frozen in optimal cutting temperature compound (OCT; Sakura Tissue-Tek, 4583) on dry ice, and stored at -80^{o}C. Frozen heart tissues were sliced into 10 µm sections in thickness at -20^{o}C using a cryostat (Bright 5040) and stored at -80^{o}C until use.

2.6 Histological study

2.6.1 Hematoxylin & eosin staining

Hematoxylin (Merck, HX945424, Germany) stained nuclei blue/purple whereas Eosin (Merck,

HX884852, Germany) stained cellular cytoplasm, collagenous and elastic fibers pink/red. Briefly, tissue sections were fixed in acetic alcohol for 1 min (3% acetic acid in 95% methanol), followed by washing in running tap water. Fixed slides were placed in Haematoxylin for 10 min, followed by washing in running tap water until clear. Stained sections were dipped in differentiation solution (1% HCl in 70% ethanol), blued in Scotts tap water substitute for 30 sec, and stained in Eosin for 2 min, with washing in running tap water between each step. Sections were dehydrated through serial alcohol (70%, 95% and 100%) and xylene (BDH, UN1307) and coverslips were mounted using DPX medium (BDH, HX806878, England).

2.6.2 Picro-sirius red staining

Picro-sirius red staining is one of the most widely used techniques of collagen histochemistry. Picro-sirius red stains cytoplasm yellow and collagen-based extracellular components red. To prepare sirius red solution, 0.5 g of powered direct red 80 (Sigma, UK) was dissolved in 45 ml distilled water. Absolute ethanol 50ml (99%) was added and then 1 ml of sodium hydroxide (1%). Sodium chloride (20%) was slowly added in drops until a slight precipitate persisted. The mixture was left overnight and filtered before use. Tissue sections were fixed in acid alcohol (1% HCl in 70% ethanol) for 5 min, followed by washing in acid water (1 ml acetic acid in 200 ml H_2O) for 1 min. Fixed slides were placed in picro-sirius red (10% sirius red stain in a saturated picric acid solution) for 10 min, followed by washing in acid water for 1 min twice. Stained slides were dehydrated through serial alcohol (70%, 95% and 100%) and xylene, and coverslips were mounted using DPX medium.

2.7 Immunohistochemistry

In general, frozen sections were fixed with 4% (w/v) paraformaldehyde (PFA; Sigma, P6148, UK) in PBS at room temperature for 20 min before staining. Slides were then incubated with blocking solution at room temperature for an hr. Subsequently, slides were sequentially incubated with primary antibody and secondary antibody at recommended dilutions (see Table 2.1) at room temperature for an hour in the dark. Between each staining step, slides were

washed three times (5 minutes each) with PBS. Finally, slides were covered with cover glass using mounting medium with 4', 6-diamidino-2-phenylindole (DAPI; Vectashield, Vector Laboratories, UK). The slides were placed in slide boxes, which were wrapped in foil and stored at 4°C prior to images scanning. The antibodies used for immunohistochemistry are summarized in Table 2.1.

2.8 Immunocytochemistry

Cell phenotypes were characterized by the staining of surface and intracellular markers using the immunocytochemical technique described below. The antibodies used for immunocytochemistry together with relevant information, such as dilution factors, are summarized in Table 2.2 and Table 2.3.

2.8.1 Preparation of cells to be stained

For immunophenotyping, cells were grown on fibronectin-coated cover-glasses, placed in a 24 well plate, at a density of 2 x 10^4 cells per well. The 24 well plate was then left in the incubator overnight to allow cell attachment prior to fixation.

2.8.2 Cell fixation, permeabilization and blocking

Cultured cells were washed twice with PBS after medium had been removed. The cells were fixed with 4% PFA in PBS at room temperature for 15 min, followed by washing three times with PBS, each for 5 min. If staining for surface antigens, cells were not permeabilized. To target intracellular markers, the fixed cells were permeabilized with 0.1% (v/v) Triton-X 100 (Sigma, T8787, UK) in PBS at room temperature for 10 minutes and followed by washing three times with 0.1% (v/v) Tween 20 (Sigma, P7949, UK) in PBS. Then cover-glasses were incubated with blocking solution (either 10% normal donkey serum (Sigma, D9663, UK) or 10% normal goat serum (Sigma, G9023, UK) in PBS) at room temperature for 1 h.

2.8.3 Antibody incubation, DAPI staining and mounting

Antibodies were diluted in PBS according to the dilution factors summarized in Table 2.2. After the blocking solution had been aspirated, the cover-glasses were covered with a diluted

fluorochrome-conjugated primary antibody solution (~300 µl per well) and incubated at room temperature for an hour in the dark. If using an unconjugated primary antibody, cover-glasses were incubated with diluted primary antibody at 4°C overnight in a humidified chamber. After incubation, cover-glasses were gently washed three times with PBS. During the last wash step, a diluted secondary antibody was prepared and then added to each well of a 24 well plate, which was then incubated at room temperature for an hour in the dark. After incubation, cover-glasses were washed three times in PBS. Approximately 6 µl of mounting medium containing DAPI (Vectashield, Vector Laboratories, UK) was added onto a microscope slide per coverslip. Three coverslips were placed on one microscope slide. The samples were wrapped in foil for protection from light and stored at 4°C prior to analysis.

2.9 Confocal microscopy

All immuno-labelled samples were scanned using a confocal laser scanning microscope (Zeiss LSM META 510, Germany). The laser power was maintained at a minimum and the image contrast was optimized by adjusting the detector gain and amplifier offset. The pinhole was set to ~1 to minimize background signal. Scanning was performed in 8-bit multi-track scan mode and 1024 x 1024 pixel images were acquired. Fluorochromes together with corresponding lasers and filters used are listed in Table 2.4. All images acquired were processed with the use of Zeiss LSM Image Examiner software.

2.10 Flow cytometric analysis

Flow cytometric analysis was used to quantify the expression of cell surface and intracellular antigens. A general protocol of the whole procedure is described below. The antibodies used in flow cytometry along with relevant information, such as dilution factors, are summarized in Table 2.5 and Table 2.6.

2.10.1 Preparation of cells to be analysed

In order to produce single cells for flow cytometric analysis, cells in monolayers were

harvested using 0.05% trypsin at 37°C for three minutes after washing twice with PBS. The detached cells were collected in centrifuge tubes containing CEM and spun at 1500 rpm for 3 minutes. The cell pellets were then washed in incubation buffer (Appendix: Table 3) and centrifuged at 2000 rpm for 5 min twice. Approximately one hundred thousand cells per sample were used for flow cytometric analysis.

2.10.2 Cell fixation and permeabilization

When staining for cell surface antigens, cells were not fixed and permeabilized. To stain for intracellular markers, the cells were fixed and permeabilized using BD Cytofix/CytopermTM Fixation/Permeabilization Kit (BD Bioscience, San Jose, CA) according to the manufacturer's instructions.

2.10.3 Antibody incubation

Cells were incubated in 50 µl of incubation buffer with the appropriate amount of a fluorochrome-conjugated primary antibody at 4°C for an hour in the dark (see Table 2.6). When using an unconjugated primary antibody, cells were sequentially incubated with diluted primary antibody at 4°C for an hour and secondary antibody at 4°C for an hour in the dark at the recommended concentration (see Table 2.5). After each staining, cells were washed once with the incubation buffer to remove excessive antibody. After washing and centrifugation at 2000 rpm for 5 minutes, the supernatant was discarded and cell pellets were resuspended in 500 µl of incubation buffer. Samples were then kept on ice prior to flow cytometric analysis.

2.10.4 Acquisition and analysis

For live cell labelling, the viability of examined cells was determined using Trypan Blue dye to ensure dead cells would not compromise the accuracy of results. In addition, a combination of unstained cells and an isotype-matched control or only secondary antibody-stained sample were used as negative thresholds. Cells were analyzed using a FACSCalibur flow cytometer (BD Biosciences, San Jose, CA) and each acquisition included a minimum of 10,000 events. To quantify the percentage of cells expressing specific markers, the threshold of positive

population was set above the 99th percentile of a negative control cell population. The data were analyzed using CellQuest Pro software (BD Biosciences, San Jose, CA).

2.11 Polymerase chain reaction

Polymerase chain reaction (PCR) was used to amplify specific regions of DNA (genomic and complementary) by multiple cycles of polymerization. The primers used in real-time PCR are summarized in Appendix: Table 5. DNA and RNA extraction from cultured cells and quantitative PCR are described below.

2.11.1 DNA extraction

Total genomic DNA was extracted from cultured cells to be examined using the QIAGEN® Blood and Cell Culture DNA kits (Qiagen GmbH, Hilden, Germany) according to the manufacturer's instructions. To evaluate the purity and concentration of DNA, absorbances were measured at 260 nm (A260) and 280 nm (A280) using a Nanodrop ND-1000 spectrophotometer (Nanodrop Technologies Inc., USA). A ratio of 260 nm/280 nm between 1.7 and 1.9 represented an acceptable purity of DNA.

2.11.2 RNA Extraction and cDNA synthesis

Total RNA was extracted from cultured cells with the use of the Rneasy Mini kit (Qiagen, Hilden, Germany) according to the manufacturer's instructions. The purity and concentration of RNA were determined by measuring the absorbance values at A260 and A280 using a Nanodrop ND-1000 spectrophotometer. A ratio of A260/A280 ≈ 2.0 represents an acceptable purity of RNA. The different complementary DNAs (cDNA) were generated from the RNA template (1 µg of total RNA) using the AB high transcriptase kit (Applied Biosystem, USA) according to the manufacturer's instructions.

2.11.3 Quantitative real time PCR

Real time quantitative PCR was performed using the Applied Biosystem StepOnePlus Real-Time PCR system (AB International, CA). The real-time quantitative PCR reactions were set up in 20 µl reaction volume with 10 µl AB System Sybrgreen PCR mastermix (AB

International, CA), 1 µl forward primer, 1 µl reverse primer, 1 µl cDNA and 7 µl distilled water. During the PCR, changes in temperature were used to control the steps of amplification. The polymerase was heat-activated at 95°C for 10 minutes, followed by 40 cycles of a denaturation step at 95°C for 15 seconds, an annealing step at 60°C for 30 seconds and an extension step at 72°C for 30 seconds. Dye fluorescence of amplified products was measured at the end of each extension step during PCR cycles. After amplification had been finished, a melt curve was acquired to evaluate the specificity of PCR products.

PCR efficiency for all primers was evaluated by using a standard curve of five serial dilution points. Relative mRNA expression levels were analyzed using the comparative CT method (the $2^{-\Delta\Delta CT}$ method), with normalization to an endogenous control (the housekeeping gene: glyceraldehyde-3-phosphate dehydrogenase (GAPDH)) and a calibrator (the control sample) [233-235].

2.12 Magnetic resonance imaging

In this thesis, high-resolution cine magnetic resonance imaging (MRI) was used to characterize decellularized heart matrix (Chapter 3) and evaluate mouse heart function *in vivo* (Chapter 5). In general, high-resolution cine MRI was performed using a 40 mm ^{1}H-imaging probe on a 500 MHz 11.7 T MR system consisting of a vertical magnet (Magnex Scientific, Oxon, UK), a Bruker Avance console (Bruker Medical, Ettlingen, Germany), and a shield gradient system (Magnex Scientific, Oxon, UK) (Figure 2.1), as previously described [236]. The protocols of specific procedures are explained in individual chapters.

Figure 2.1 High-resolution cine magnetic resonance imaging. *High-resolution cine magnetic resonance imaging used a 40 mm ^{1}H-imaging probe on a 500 MHz 11.7 T MR system consisting of a vertical magnet, a Bruker Avance console, and a shield gradient system.*

2.13 Statistical analysis

Data are presented as mean ± standard error of mean (SEM) if not otherwise specified. All statistical analyses were performed with the use of Excel and statistical software SPSS (Version 13.0, SPSS Inc.). Statistical significance of differences between two groups was analysed using an unpaired Student *t*-test. Multiple groups (3 or more groups) were compared using a one-way analysis of variance (ANOVA). Tukey post hoc test was applied to determine the statistical difference between groups. All experiments were performed in at least triplicates. A value of $p < 0.05$ was chosen for significant difference.

Table 2.1 List of antibodies used for immunohistochemistry

Antibody	Manufacturer	Dilution	Secondary antibody (dilution)
Cardiac troponin I	Santa Cruz sc-15368	1:100	AF488 Donkey anti rabbit (1:1000)
α-sarcomeric actin	Sigma A2172	1:500	AF488 Donkey anti mouse (1:1000)
Smooth muscle actin	Sigma A2547	1:200	AF488 Donkey anti mouse (1:1000)
Elastin	#	1:5000	DyLight 488 Donkey anti rabbit (1:100) #
Dystrophin	Abcam * ab15277	1:2500	AF594 Goat anti rabbit (1:200) *

*# Antibodies for elastin were kindly provided by Dr Jing Yu from University of Oxford; * antibodies for dystrophin were generously provided by Corinee Betts from University of Oxford.*

Table 2.2 List of antibodies used in immunocytochemistry for rat cells

Antibody	Manufacturer	Dilution	Secondary antibody (dilution)
c-kit	Santa Cruz sc-5535	1:50	AF488 Donkey anti rabbit (1:1000)
Sox 2	Santa Cruz sc-17320	1:50	AF488 Donkey anti goat (1:1000)
Oct 3/4	Santa Cruz sc-9081	1:50	AF488 Donkey anti rabbit (1:1000)
CD90	BD Pharmingen 554892	1:100	AF488 Donkey anti mouse (1:1000)
Nkx2.5	Santa Cruz sc-8697	1:50	AF488 Donkey anti goat (1:1000)
Cardiac troponin T	Abcam ab10214	1:200	AF488 Donkey anti mouse (1:1000)
Myosin heavy chain	Abcam ab15	1:200	AF488 Donkey anti mouse (1:1000)
Smooth muscle actin	Sigma A2547	1:200	AF488 Donkey anti mouse (1:1000)
α-sarcomeric actin	Sigma A2172	1:500	AF488 Donkey anti mouse (1:1000)
Von-Willebrand Factor	Santa Cruz Sc-8086	1:50	AF488 Donkey anti mouse (1:1000)

Table 2.3 List of antibodies used in immunocytochemistry for mouse cells

Antibody	Manufacturer	Dilution	Secondary antibody (dilution)
c-kit-FITC	BD Pharmingen 553354	1:50	-
Sca-1-PE	BD Pharmingen 553108	1:100	-
Sox 2	Santa Cruz sc-17320	1:50	AF488 Donkey anti goat (1:1000)
Oct 3/4	Santa Cruz sc-9081	1:50	AF488 Donkey anti rabbit (1:1000)
CD90-FITC	BD Pharmingen 553012	1:100	-
CD105	Santa Cruz sc-71042	1:200	AF633 Donkey anti mouse (1:1000)
CD45-FITC	BD Pharmingen 554877	1:50	-
CD31	AbD Serotec MCA1334G	1:50	AF488 Donkey anti mouse (1:1000)
Nkx2.5	Santa Cruz sc-8697	1:50	AF488 Donkey anti goat (1:1000)
Cardiac troponin T	Abcam ab10214	1:200	AF488 Donkey anti mouse (1:1000)
Myosin heavy chain	Abcam ab15	1:200	AF488 Donkey anti mouse (1:1000)
Smooth muscle actin	Sigma A2547	1:200	AF488 Donkey anti mouse (1:1000)

Table 2.4 Fluorochromes and corresponding lasers used for confocal microscopy

Fluorochrome	Peak excitation wavelenth	Peak emission wavelenth	Laser	Filter
DAPI	364	454	Diod (405)	BP 420-480
Alexa Fluor 488	499	519	Argon (488)	BP 420-480
FITC	495	521	Argon (488)	BP 420-480
PI	545	615	HeNe1 (543)	BP 420-480
Alexa Fluor 594	591	618	HeNe1 (543)	BP 420-480
PE	565	578	HeNe1 (543)	BP 420-480
Alexa Fluor 633	633	647	HeNe2 (633)	BP 420-480

Abbreviations: DAPI = 4´,6-diamidino-2-phenylindole; FITC = fluorescein isothiocyanate; PI = propidium iodide, and PE = R-Phycoerythrin.

Table 2.5 List of antibodies used in flow cytometry for rat cells

Antibody	Manufacturer	Dilution	Secondary antibody (dilution)
c-kit	Santa Cruz sc-5535	1:20	AF488 Donkey anti rabbit (1:1000)
CD90	BD Pharmingen 554892	1:100	AF488 Donkey anti mouse (1:1000)
Cardiac troponin T	Abcam ab10214	1:200	AF488 Donkey anti mouse (1:1000)
α-sarcomeric actin	Sigma A2172	1:500	AF488 Donkey anti mouse (1:1000)

Table 2.6 List of antibodies used in flow cytometry for mouse cells

Antibody	Manufacturer	Dilution	Secondary antibody (dilution)
c-kit-FITC	BD Pharmingen 553354	1:20	-
Sca-1-PE	BD Pharmingen 553108	1:100	-
CD90-FITC	BD Pharmingen 553012	1:100	-
FITC IgG2b, κ isotype control	BD Pharmingen 553988	1:20 or 1:100	-
PE IgG2a, κ isotype control	BD Pharmingen 553930	1:100	-
Cardiac troponin T	Abcam ab10214	1:200	AF488 Donkey anti mouse (1:1000)
Myosin heavy chain	Abcam ab15	1:200	AF488 Donkey anti mouse (1:1000)

Chapter 3

Combination of cardiac stem cells and tissue engineering for heart failure therapy

3.1 Abstract

Stem cell-based therapy has emerged as a promising approach to treat heart diseases. However, the current method of cell delivery *via* intra-myocardial injection or coronary infusion results in low retention and poor engraftment. For this reason, a variety of engineered cardiac tissues, involving the combination of biomaterials and cells, have been developed to enhance cell retention and improve cell survival in the heart. Cardiac stem cells (CSCs) can be expanded *in vitro* to improve heart function in animal studies and early phase clinical trials. The work in this chapter involved the characterization and differentiation of CSCs from rat hearts. Cardiosphere-derived cells (CDCs) were produced *via* cardiosphere formation as a mixed population, including CSCs and cardiac lineage-committed cells. CDCs were induced to differentiate into the cardiomyocyte phenotype by exposure to 5-azacytidine (5-Aza), dimethyl sulfoxide (DMSO) or ascorbic acid (AA). Furthermore, the optimised combination of 5-Aza or DMSO with AA significantly enhanced the differentiation efficiency, compared to 5-Aza or DMSO alone (1.9-fold, $p < 0.05$ or 1.8-fold, $p < 0.01$, respectively). For cardiac tissue engineering, a 3D porous alginate scaffold was developed and the growth of CDCs was optimized within the construct. CDCs within the alginate matrix survived for up to 7 weeks and proliferated over time from day 7 to 49, with a significant increase in cell number (2-fold, $p < 0.01$). To optimize cell survival within alginate scaffolds, different extracellular matrix (ECM) proteins were used to help cell attachment. Alginate scaffolds containing ECM proteins significantly increased the number of viable cells compared with control scaffolds ($p < 0.01$). An acellular whole rat heart ECM was generated using decellularization by coronary perfusion. Characterization of the decellularized heart matrix showed the absence of cellular and nuclear materials using histology and immunohistochemistry, and ECM component, elastin, remaining using immunostaining. *In vivo* MRI showed in detail that cardiac architecture, including chamber geometry and valve leaflets, was preserved. The maintenance of vasculature was revealed using Evan's blue dye. Future work would include repopulation of CDCs into the decellularized heart matrix to investigate the fate of implanted cells, determination of the optimal culture conditions for receullarization, and restoration of organ function during maturation.

3.2 Introduction

Irrespective of the aetiology, most cardiovascular diseases eventually lead to heart failure (HF), which is progressive and irreversible. Clinically, therapeutic options available for patients in terminal HF are limited. Thus there is an urgent need for the development of a novel approach to treatment of advanced and terminal HF.

Recently, cell-based cardiac repair and regeneration has emerged as a promising strategy that aims to replace cardiomyocyte loss after myocardial injury. However, the largest concern that cell transplantation therapy faces is the matter of low engrafrment of implanted cells. As an alternative to administration of cells by injection or infusion, a bioartificial patch may be fabricated by seeding cells in scaffolds which aid in supporting their survival and integration into the native myocardial tissue [238]. For this, establishing an appropriate scaffold is essential to induce the formation of functional myocardial tissue and represents the major focus in tissue engineering for cardiac repair [239]. However, myocardial patches promise to replace focal non-contractile fibrous scar tissue of damaged myocardium, but are not adequate for replacement of the whole organ in end-stage HF. In the regenerative medicine field, generating an organ is the ultimate goal, which is especially valuable for advanced and end-stage heart diseases. This is indeed challenging for the heart as it is an organ of high complexity in function and structure, composed of uniquely organized muscular bands, a delicate web of coronary vasculature and a sophisticated conduction system [53, 75, 244]. Encouragingly, Ott *et al.* developed an accellular heart scaffold and a recellularized bioartificial rat heart repopulated with neonatal rat cardiomyocytes and endothelial cells in 2008 [76].

Fetal or neonatal cardiomyocytes were one of the first cell types to be studied as a potential cell source for cardiac repair in animal experiments, which improved heart function following transplantation [157]. However, like embryonic stem cells, the use of these cells faces similar hurdles for treatment of human heart diseases, including availability, immunological rejection

and ethical issues. Furthermore, it is important to emphasize that adult cardiomyocytes lack the ability to self-renew, proliferate and differentiate, so they provide limited quantities in culture and therefore are not ideal for clinical applications [31, 245]. In addition, structurally, the heart muscle is a highly differentiated tissue comprising not only cardiac myocytes, but also endothelial cells, smooth muscle cells, fibroblasts, pacemaker cells (sinoatrial nodal cells and atrioventricular nodal cells) and purkinje fibers [67], which are required for a full recellularization of the decellularized heart.

In this study, it was hypothesized that the decellularized rat heart, generated using coronary detergent perfusion, could preserve intact 3D architecture such as vascular networks and heart valves, which are important to reconstitute a pumping heart with nourishing vessels and functional valves following cell repopulation. A number of techniques were used to confirm this, including immunohistochemisty, high-resolution magnetic resonance imaging (MRI) (not used in the previous study [76]) and Evan's blue dye perfusion. For the demonstration of differentiation potential and the purpose of reseeding engineered cardiac tissues, cardiomyocyte differentiation of CDCs was induced *in vitro* by treatment with 5-azacytidine, dimethyl sulfoxide, and ascorbic acid, as the previously used technique of differentiation by coculture would be inappropriate in tissue engineering. Furthermore, it was decided to develop a biomaterial scaffold (myocardial patch) using alginate, a biodegradable polysaccharide polymer, which is natural, hydrophilic and similar to glycol-components of the extracellular matrix [57, 246]. Additionally, it has been reported that alginate scaffolds are able to create a favourable environment for 3D culture of cardiac myocytes [57, 247, 248]. By culturing cardiosphere-derived cells (CDCs) in alginate scaffolds, knowledge of cell viability and growth dynamics of cardiac stem cells in an ECM-like environment could be obtained for the first time.

Thus, the work in this chapter focused on developing a therapy for HF using a combination of tissue engineering techniques and cardiac stem cells. To be specific, the aims were to:

- Isolate, expand and characterize cardiac-derived stem cells from adult rat hearts *in vitro*, *via* the formation of cardiospheres.
- Establish 3D myocardial patches (alginate scaffolds) and evaluate viability and proliferation of cardiac stem cells (CDCs) within the constructs.
- Prepare and characterize a bioartificial cardiac extracellular matrix from an intact rat heart using a perfusion decellularization method, followed by a pilot study of recellularization with CDCs.
- Differentiate CDCs *in vitro* into the main cardiac lineage: cardiac muscle cells (cardiomyocytes).

3.3 Methods

3.3.1 Isolation and expansion of cardiac-derived stem cells

In this study, cardiac-derived stem cells (CSCs) were cultured from the hearts of Sprague Dawley rats (SD rat; 3-4 months old) as previously described in Chapter 2. Only atrial parts of SD rat hearts were used for explantation and other experiments in this chapter. All cell culture was carried out in a humidified atmosphere of 5% CO2 and 95% air at 37°C. The whole process of isolation and expansion of cardiosphere-derived cells (CDCs) was simplified into four steps of tissue explantation, cardiosphere formation, cardiosphere-derived cell expansion and passage (subculture), as illustrated below in Figure 3.1. Isolated CDCs at passage 2 were used in cell implantation of porous alginate scaffolds. For recellularization, pre-labelled CDCs were injected or infused into the decellularized heart matrix. Furthermore, rat CDCs at passage 2 were induced to differentiate into cardiomyocytes.

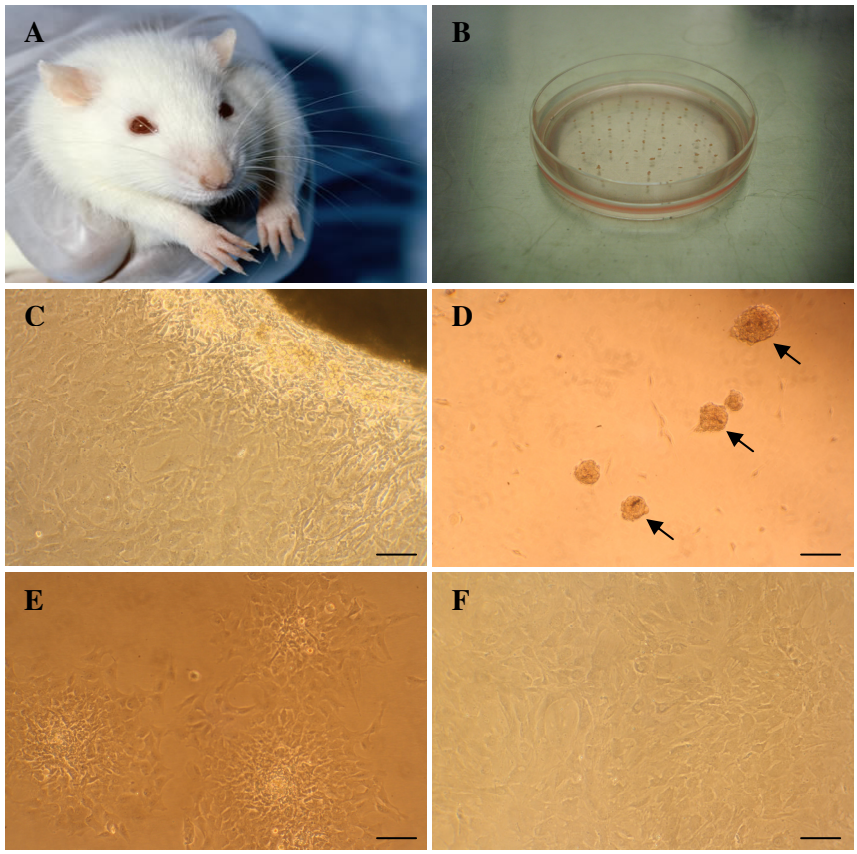

Figure 3.1 Isolation and expansion of rat cardiac-derived stem cells via the formation of cardiospheres. *(**A**) Sprague Dawley rat. (**B**) Heart fragments were explanted on a petri dish. (**C**) An explant with migrating explant-derived cells. (**D**) Cardiosphere formation (black arrow). (**E**) Cardiosphere-derived cells at passage 0. (**F**) Passage 2 CDC expansion. Scale bars = 100 μm.*

3.3.2 Preparation of three-dimensional cell-alginate constructs

Cell-alginate scaffolds (5 mm in diameter) were prepared by mixing equal volumes of 1% sodium alginate (Fluka, 7123, Norway) containing CDCs at passage 2 and 0.1 M calcium chloride (BDH, UK) as the cross-linker in a 96 well plate (Corning) (Figure 3.2). The cultures of cell-implanted scaffolds were incubated in 5% CO2 and 95% air at 37°C, with medium changes every 2 days.

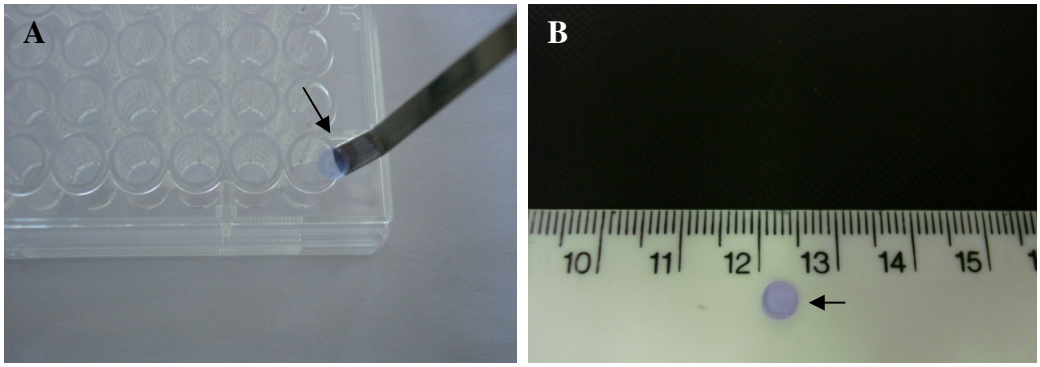

Figure 3.2 Three dimensional porous alginate scaffolds. (***A***) *Scaffolds were prepared in a 96 well plate (black arrow).* (***B***) *Showing the alginate scaffold size (5 mm in diameter).*

3.3.3 Cell viability and proliferation assay

In the viability experiment, alginate scaffolds containing CDCs were incubated with AlamarBlue® solution (AbD Serotec, BUF012A, UK) at 37°C for an optimized incubation time, depending on the number of seeded cells. In the proliferation experiment, alginate scaffolds seeded with serially decreasing numbers of CDCs (from 15,000 to 500 cells per scaffold/well) were prepared and incubated with AlamarBlue® solution for 9 hours at day 0. A standard curve of fluorescence intensity read at an emission wavelength of 590 nm with corresponding cell number was established (Figure 3.3), the cell proliferation assay was performed at different time points during a culture period. Based on the standard curve, cell growth kinetics within alginate scaffolds was presented as the number of viable cells against culture days.

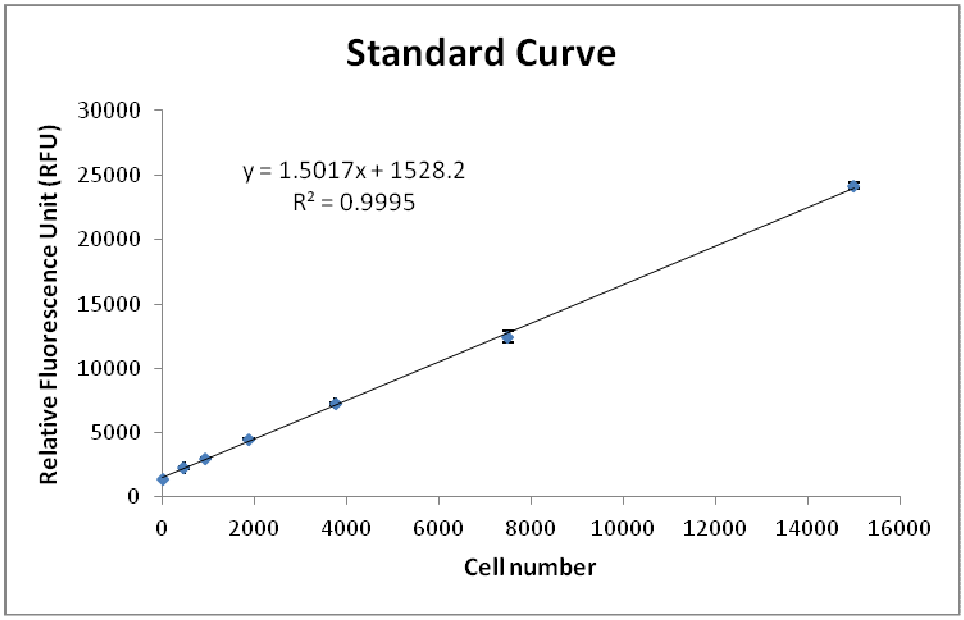

Figure 3.3 Standard curve for the cell proliferation assay using AlamarBlue®. *Relative fluorescence intensity of 0, 469, 938, 1875, 3750, 7500 and 15000 cells was read after 9 hours of incubation with AlamarBlue® solution at 37°C using FLUOstar OPTIMA. Values are presented as mean ± SEM (n = 4). Relative cell number of each sample could be calculated from relative fluorescence intensity based on the equation acquired from the standard.*

3.3.4 Effects of extracellular matrix proteins on CDC viability in porous alginate scaffold

In order to investigate the effect of pre-coating the porous alginate scaffold on cardiosphere-derived cell viability, four extracellular matrix proteins were chosen. Fibronectin (Sigma, F1141, UK), type 1 collagen (Sigma, C8919, UK), poly-D-lysine (Sigma, P7280, UK) and gelatin (Sigma, G6144, UK) were individually mixed with the sodium alginate solution to final concentrations of 0.4%, 10%, 2% and 1%, respectively, prior to mixing with CDCs and gelation with calcium chloride. CDCs were incubated overnight, followed by incubation with AlamarBlue® solution for 9 hours at 37°C before measuring the fluorescence intensity.

3.3.5 Langendorff perfusion decellularization of rat hearts

Sprague Dawley rats, aged from 3 to 4 months, were used for decellularization of hearts. Once the rat was deeply anesthetised, the heart was excised from the chest and immediately immersed in cold heparinized PBS to minimise the risk of blood clot formation. Subsequently,

the heart was suspended on a cannula by the ascending aorta, and slowly perfused with heparinized PBS to avoid the formation of air emboli (Figure 3.4). When the heart was firmly attached to the cannula, it was perfused with heparinized PBS containing 10 µM adenosine (Sigma, A40360, UK) for 30 minutes, followed by 1% (w/v) sodium dodecyl sulfate (SDS; Sigma, UK) for at least 12 hours until fully decellularized. Finally, the heart was perfused with PBS for 1 h to rinse remaining detergent out.

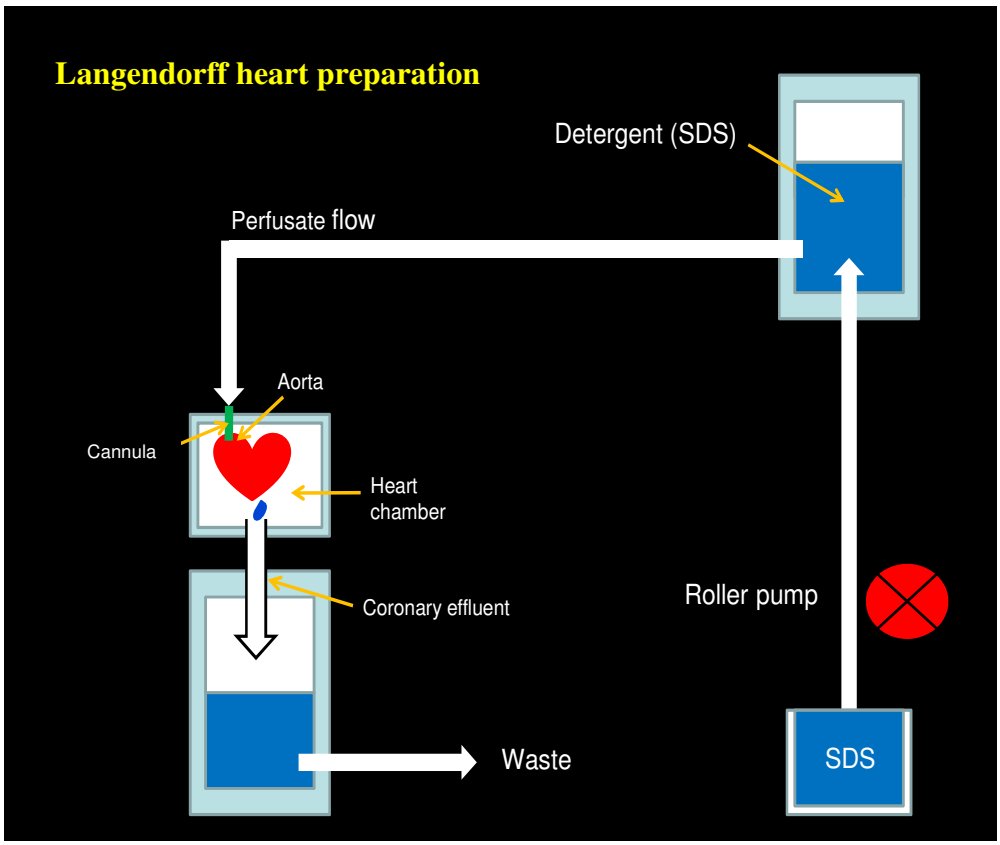

Figure 3.4 Langendorff heart preparation. *Hearts were cannulated via the ascending aorta and the perfusion fluid was delivered in a retrograde manner. Due to this flow force, the aortic valves were shut, so the perfusion fluid was directly guided into the coronary ostia, followed by the perfusion of whole heart and drainage into right atrium via the coronary sinus.*

3.3.6 Recellularization of decellularized rat hearts

To recellularize the decellularized heart matrix, cells were administered by both intramyocardial injection and intravascular infusion. CDCs were labelled with either microsized-particles of iron oxide (MPIO; encapsulated magnetic microsphere; Bangs, Fishers,

IN) for intramyocardial injection or CellTracker Vybrant® CM-DiI (Invitrogen, Molecular Probes, USA) for intracoronary infusion. In brief, CDCs at passage 2 were incubated with MPIO (30 µl in 6 ml CEM) overnight or CM-DiI (6 µl in 5 ml PBS) for 30 min at 37°C before trypsinization. For direct intramyocardial injection, approximately 6 x 10^6 CDCs suspended in 1 ml CEM were injected into the anterior wall of the left ventricle using a 27-G needle mounted on an insulin syringe. For intracoronary infusion, 10 x 10^6 CDCs were delivered in a retrograde direction down the aorta at a constant flow rate of 6 ml/min.

3.3.7 Magnetic resonance imaging

Magnetic resonance imaging (MRI) was used to characterize the morphology of extracellular matrix (ECM) of the decellularized heart construct and to investigate the internal structures following decellularization. Decellularized rat hearts were fixed in 4% (w/v) paraformaldehyde (Sigma, P6148, UK) in phosphate buffered saline (PBS; Sigma; pH 7.2) and embedded in 1% (w/v) agarose doped with gadolinium DTPA (Gd-DTPA; MagnevistTM) in a 20 mm NMR-tube. High-resolution MRI was carried out in a 20 mm quadrature-driven birdcage coil (Rapid Biomedical, Würzburg, Germany) using a fast gradient echo sequence with the following parameters: TE/TR = 1.8/30 ms, flip angle 90º, field of view: 32 x 32 x 32 mm, matrix size 512 x 512 x 512, voxel size 62.5 x 62.5 x 62.5 mm.

3.3.8 Tissue sectioning

For histology and immunohistochemistry, decellularized and recellularized heart samples were fixed in 10% formalin for 2 to 3 days. Heart tissues were embedded and frozen in optimal cutting temperature (OCT; Sakura Tissue-Tek, 4583) compound on dry ice, and stored at -80°C. The tissue block was sliced into 10 µm sections at -20°C using a cryostat (Bright 5040) and stored at -80°C until use (Figure 3.5).

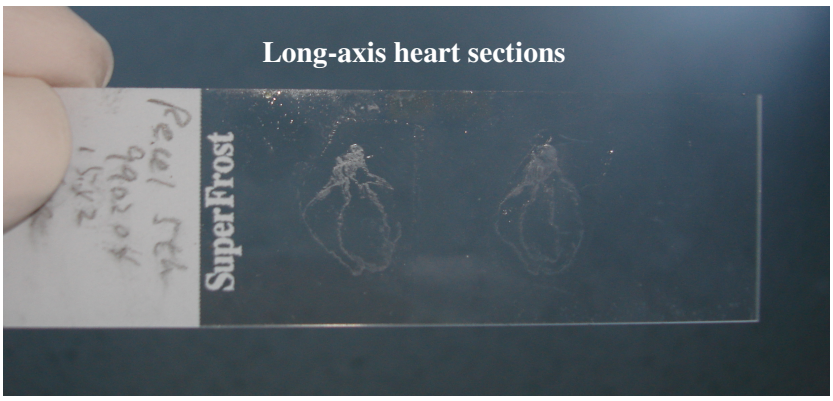

Figure 3.5 Cryosections of decellularized and recellularized hearts. *Fragile heart tissue was sliced with special caution using a cryostat and mounted on microscope slides for histology and immunohistochemistry.*

3.3.9 Hematoxylin & eosin staining

For the decellularized heart matrix, hematoxylin and eosin (H&E; HX945424 and HX884852, Merck, Germany) staining was utilized to determine if nuclear material remained. Hematoxylin stained cell nuclei blue or purple whereas eosin stained cellular cytoplasm, collagenous and elastic fibers pink or red. The staining procedures were performed according to the protocol described in Chapter 2

3.3.10 Immunohistochemistry

Immunohistochemistry was used to verify the removal of cellular and nuclear material from the decellularized heart tissue, as described in Chapter 2. Detection of nucleic acids was performed by staining the specimen with 4', 6-diamidino-2-phenylindole (DAPI; Vectashield, Vector Laboratories; blue) or propidium iodide (PI; Vectashield, Vector Laboratories; red). For the verification of the removal of intracellular material, the contractile proteins of cardiac muscle cells, including cardiac troponin I (cTnI) and alpha-sarcomeric actin (ASA), were targeted. In addition, alpha-smooth muscle actin (αSMA) of cardiac smooth muscle cells was also examined in decellularized rat hearts. As for the detection of implanted cardiosphere-derived cells in recellularized heart matrix, frozen sections were mounted following nuclear DAPI labelling, as above, without extra staining.

3.3.11 Immunocytochemistry

In this chapter, immunocytochemistry was used to characterize cultured CDCs and identify cardiomyocytes following induction of differentiation. The detailed protocol of the immunostaining is described in Chapter 2. To ensure that cardiac-specific primary antibodies, such as cardiac troponin T (cTnT), cardiac myosin heavy chain (cMHC) and alpha-sarcomeric actin (ASA), detected CDCs differentiated towards cardiomyocytes, neonatal rat cardiomyocytes were used as positive control cells, as shown in Figure 3.6 below.

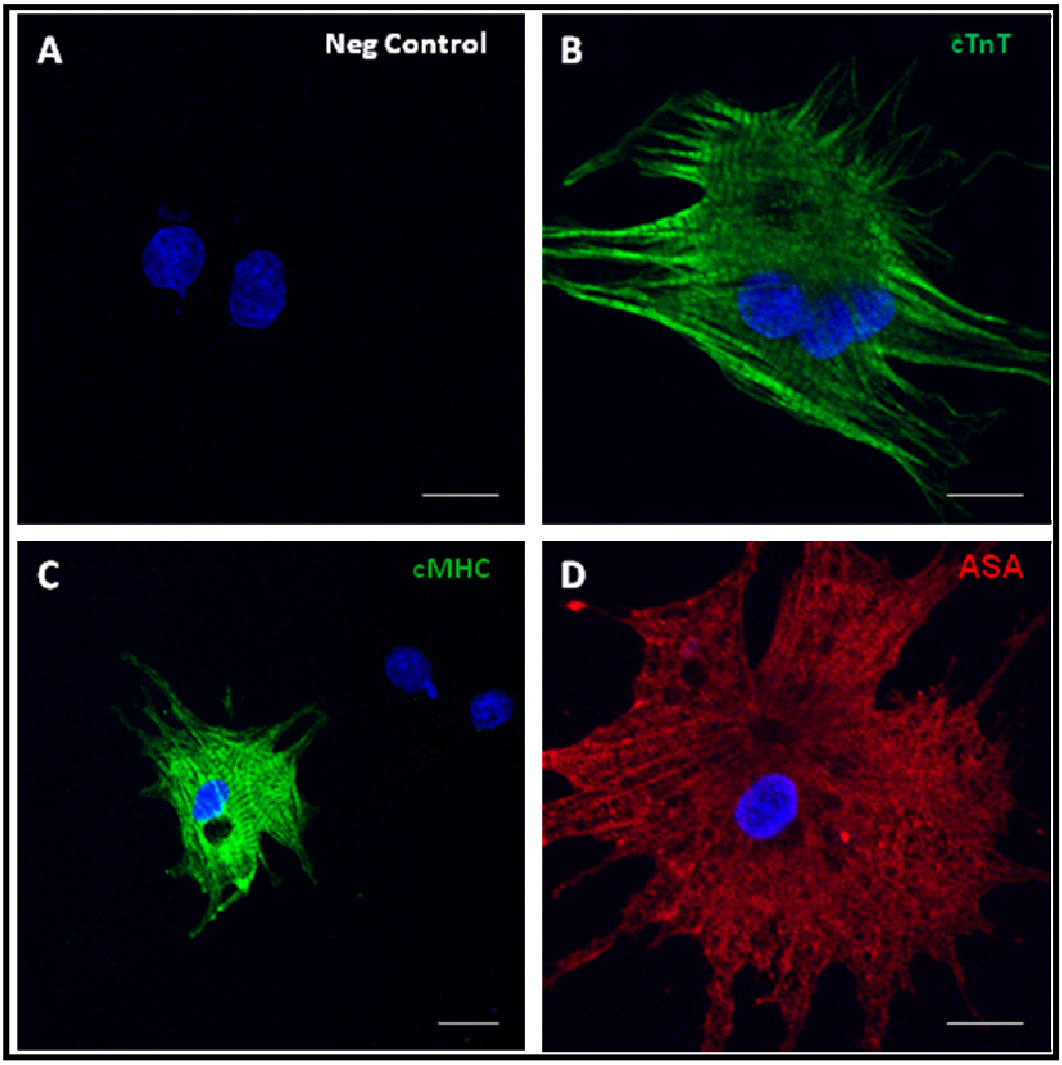

Figure 3.6 Immunofluorescent images of neonatal rat cardiomyocytes as positive control cells. *(**A**) Negative control comprised cells stained with secondary antibody without primary antibody. (**B** - **D**) Neonatal rat cardiomyocytes stained positive for cardiomyocyte markers including cardiac troponin T (B), myosin heavy chain (C), and alpha-sarcomeric actin (D). cTnT, cMHC and ASA immunostaining revealed banding patterns of sarcomeric striations. Nuclei were counterstained with DAPI (blue). Scale bars = 20 µm (C) and 10 µm (A, B and D). Abbreviations: cTnT = cardiac troponin T, cMHC = cardiac myosin heavy chain, and ASA = alpha-sarcomeric actin, DAPI = 4′, 6-diamidino-2-phenylindole.*

3.3.12 Real-time quantitative RT-PCR

Real-time quantitative reverse transcriptase polymerase chain reaction (qRT-PCR) was used to determine the expression of cardiac-specific genes in the differentiation experiments, as described in Chapter 2. The primers for genes of interest used in this chapter are listed in Appendix (Table 5). All primers gave rise to a single peak in the melting curve (dissociation curve). For example, the melting curve for cTnT (cardiac specific gene) is shown in Figure 3.7.

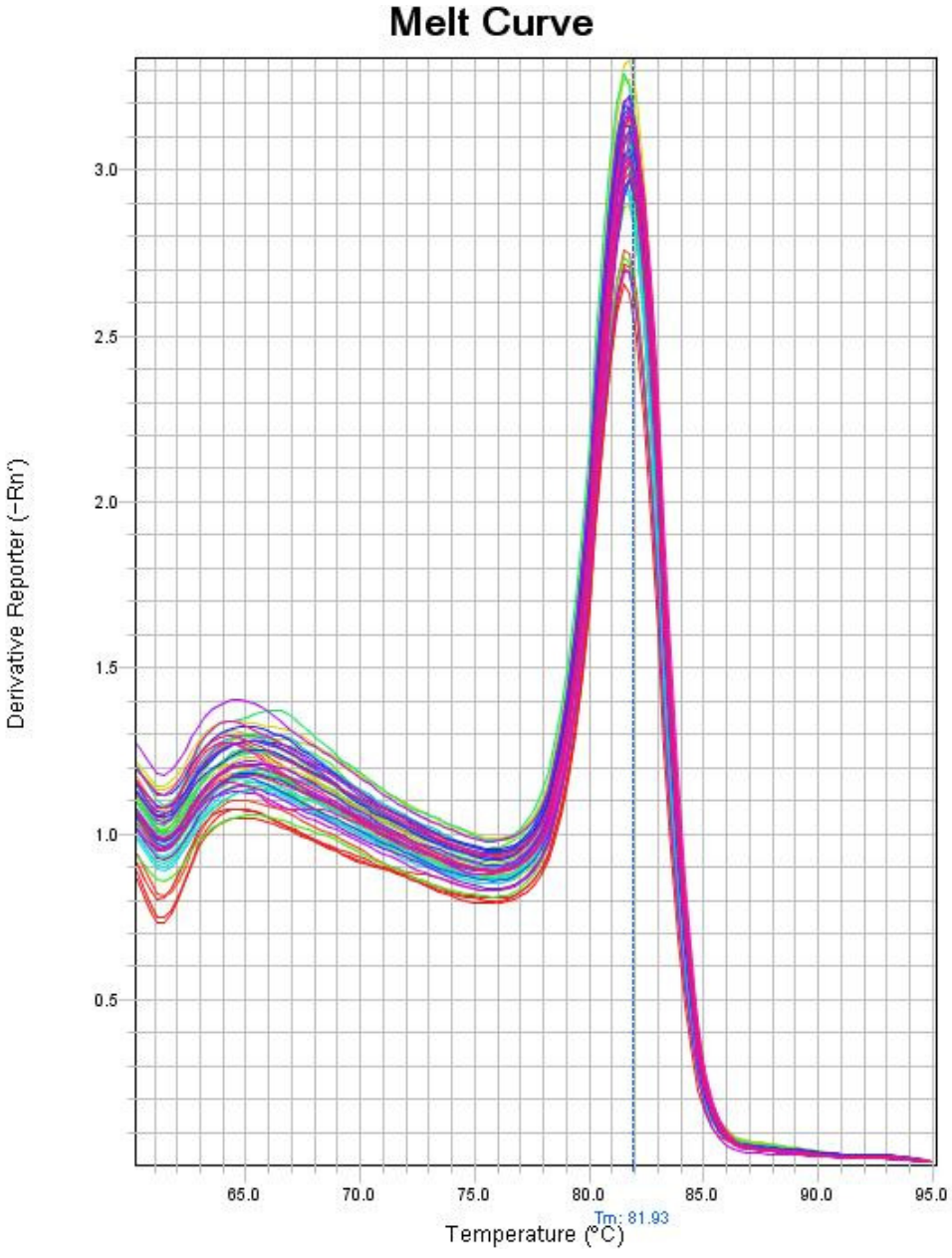

Figure 3.7 Melt curve (dissociation curve) for primers of the cardiac-specific gene cardiac troponin T.

All real-time qRT-PCR data were analysed using the arithmetic formula below based on the comparative CT method (the $\Delta\Delta C_T$ method).

Arithmetic formula ($2^{-\Delta\Delta CT}$):

$$\Delta C_T \text{ (control sample)} = C_T \text{ (gene of interest)} - C_T \text{ (housekeeping gene)}$$

$$\Delta C_T \text{ (treated sample)} = C_T \text{ (gene of interest)} - C_T \text{ (housekeeping gene)}$$

$$\Delta\Delta C_T = \Delta C_T \text{ (treated sample)} - \Delta C_T \text{ (control sample)}$$

$$\text{Relative gene expression level} = 2^{-\Delta\Delta CT}$$

The derivation of this formula has been discussed in User Bulletin #2 of Applied Biosystem (Relative Quantitation of Gene Expression; P/N 4303859).

3.4 Results

3.4.1 Isolation and expansion of cardiac-derived stem cells

3.4.1.1 Explant-derived cells

Small tissue fragments from the atrium of a Sprague Dawley rat heart were plated onto dishes coated with fibronectin (Figure 3.8 A). After 2-3 days, explant fragments were surrounded by a layer of thin stromal-like cells over which small, round, phase-bright cells migrated (Figure 3.8 B). Once confluent, the explant-derived cells were isolated from explants, one adult rat heart producing approximately 3-5 x 10^6 cells from each harvest.

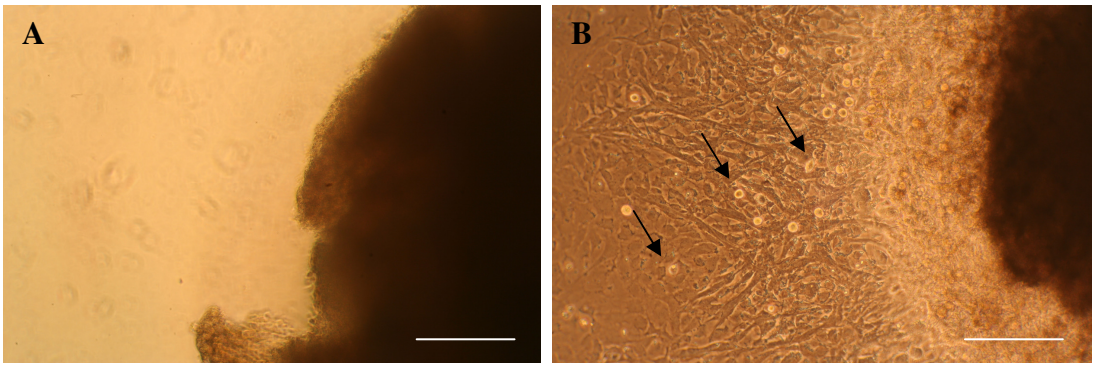

Figure 3.8 Explants and migrating explant-derived cells. *(**A**) Explant fragment plated on fibronectin-coated dish at day 0. (**B**) Small, round phase-bright cells (arrows) spread out on top of stromal-like cells from explants after 6 days. Scale bar = 250 µm.*

3.4.1.2 Cardiospheres and cardiosphere-derived cells

After incubation for 1-2 days, EDCs cultured in CGM started to self-organize into spherical multicellular clusters, termed cardiospheres, which increased in size over time (Figure 3.9 A). At day 4 of plating, approximately 300-400 cardiospheres (between 50 and 150 µm in size) were obtained in each well of the 24 multiwell plate (Figure 3.9 B). Most cardiospheres were loosely adherent to the poly-D-lysine coated surface, whereas some became detached from the culture surface. Cardiospheres could be readily isolated by mechanical trituration using a pipette.

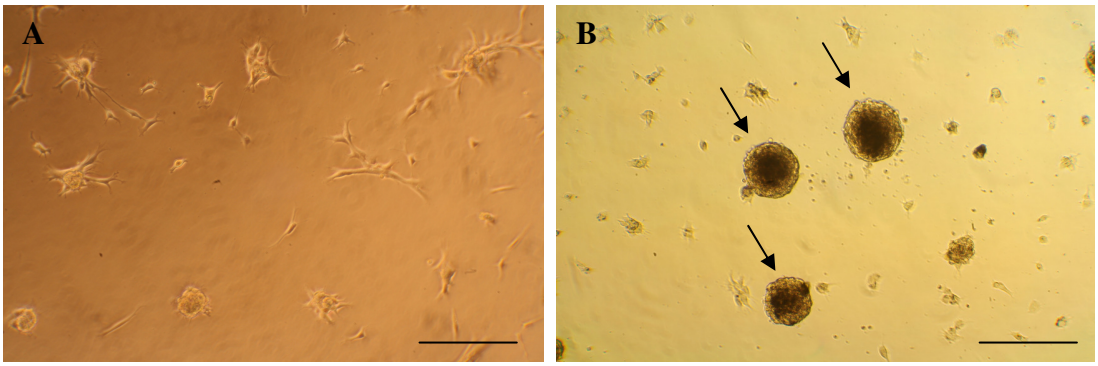

Figure 3.9 Cardiosphere formation. *(**A**) Cardiosphere-forming cells plated on poly-D-lysine for 2 days. (**B**) Fully formed cardiospheres (arrows) on day 4 after plating. Scale bar = 250 μm.*

The harvested cardiospheres were seeded into T75 flasks in CEM and grown as monolayer cardiosphere derived cells (CDCs) (Figure 3.10). When 80-90% confluent, CDCs were subcultured and split at a ratio of 1:2 for further expansion.

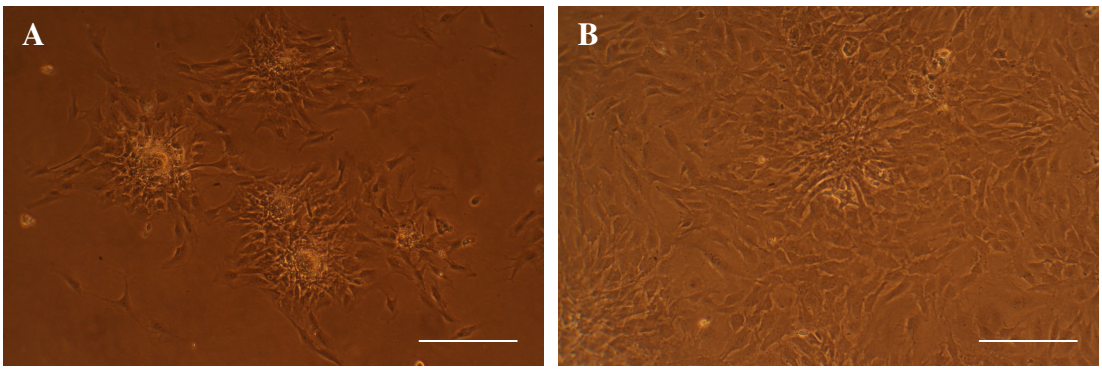

Figure 3.10 Cardiospheres and CDC expansion. *(**A**) Cardiospheres plated on fibronectin-coated culture surface for 1 day. (**B**) Expansion of CDCs on day 3 after plating. Scale bar = 250 μm. Abbreviation: CDCs = cardiosphere-derived cells.*

3.4.2 *In vitro* culture of cardiosphere-derived cells within alginate scaffolds

3.4.2.1 Three-dimensional (3D) culture of CDCs within alginate scaffolds

Ionically crosslinked alginate scaffolds were fabricated from sodium alginate and calcium chloride solutions. Varying numbers of cells (from ~500 to 45,000) were mixed with the sodium alginate solution before being added to calcium chloride solution. Gelation was achieved in less than 5 minutes. The cell viability in 1.5 mm thick alginate scaffolds was

significantly higher than that in 2.5 mm scaffolds ($p < 0.001$) (Figure 3.11). Thereafter, alginate scaffolds were prepared as 1.5 mm thick cylindrical disks.

The effect of sodium alginate and calcium ion concentrations on cell viability was examined. No combination of sodium alginate and calcium ion level revealed a significantly beneficial effect on cell survival compared to control (alginate 1% and calcium 100 mM) (Figure 3.12). The viability of CDCs in alginate scaffolds was compared with that of CDCs cultured in a monolayer. It was found that, after 24 hours incubation, the number of viable cells in the scaffold was approximately 50% that of cells in monolayer culture ($p < 0.01$) (Figure 3.13). Finally, to evaluate cell distribution within the 3D construct, CDCs labelled with Hoechst were seeded at a concentration of 4.5×10^4 cells per scaffold. CDCs were evenly distributed within the alginate scaffold (Figure 3.14).

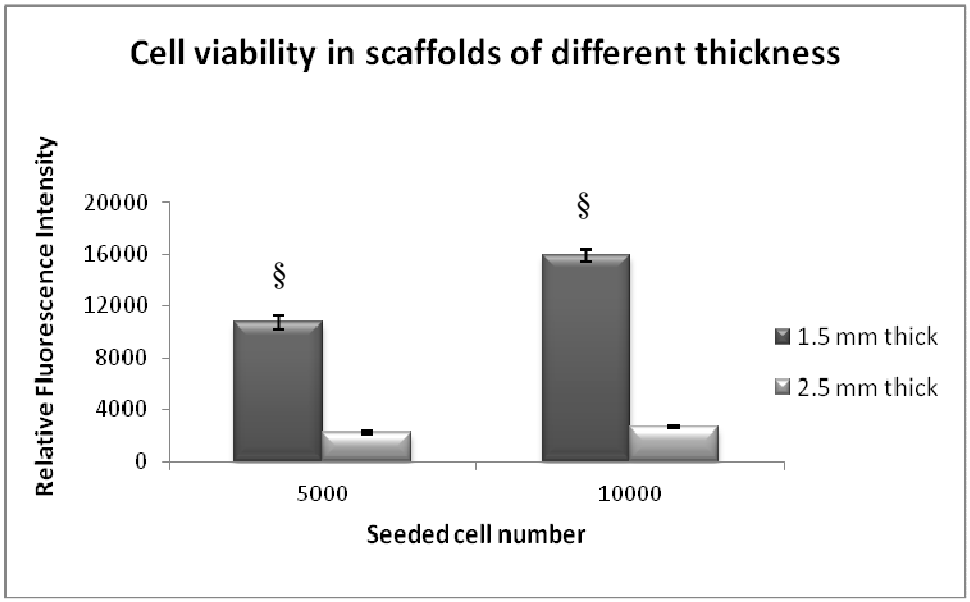

Figure 3.11 Comparison of cell viability between 1.5 mm and 2.5 mm thick alginate scaffolds. *Cell viability was higher in thinner scaffolds at cell densities of either 5000 or 10,000 cells per scaffold ($p < 0.001$). Data are presented as mean ± SEM ($n = 3$). § $p < 0.001$ vs. control (2.5 mm thickness).*

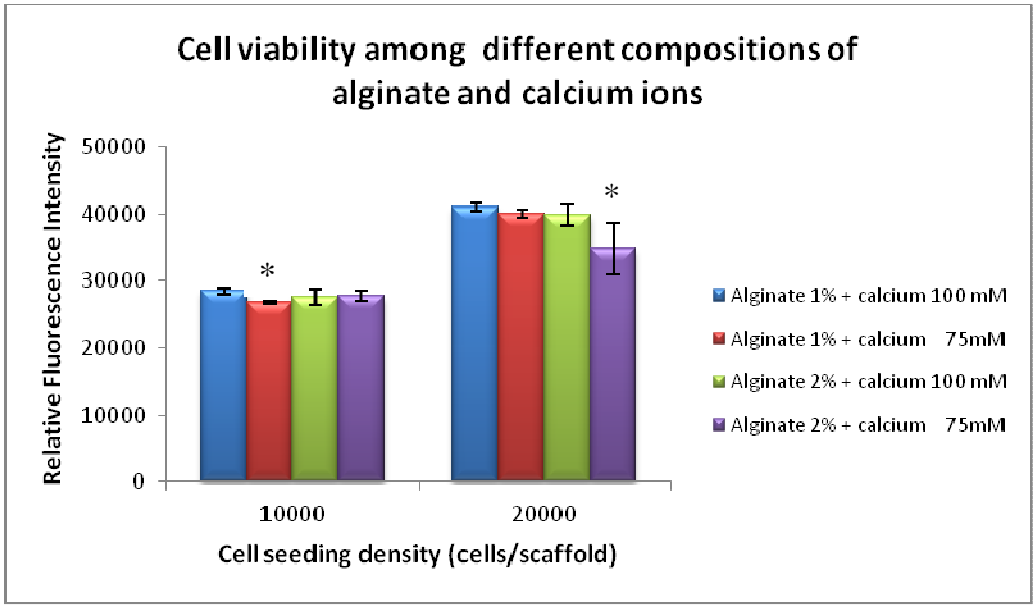

Figure 3.12 Comparison of cell viability in scaffolds from different compositions of alginate and calcium ions. *No combination significantly increased cell viability compared to control (alginate 1% + calcium 100 mM). Data are presented as mean ± SEM (n = 4). * p < 0.05 vs. control.*

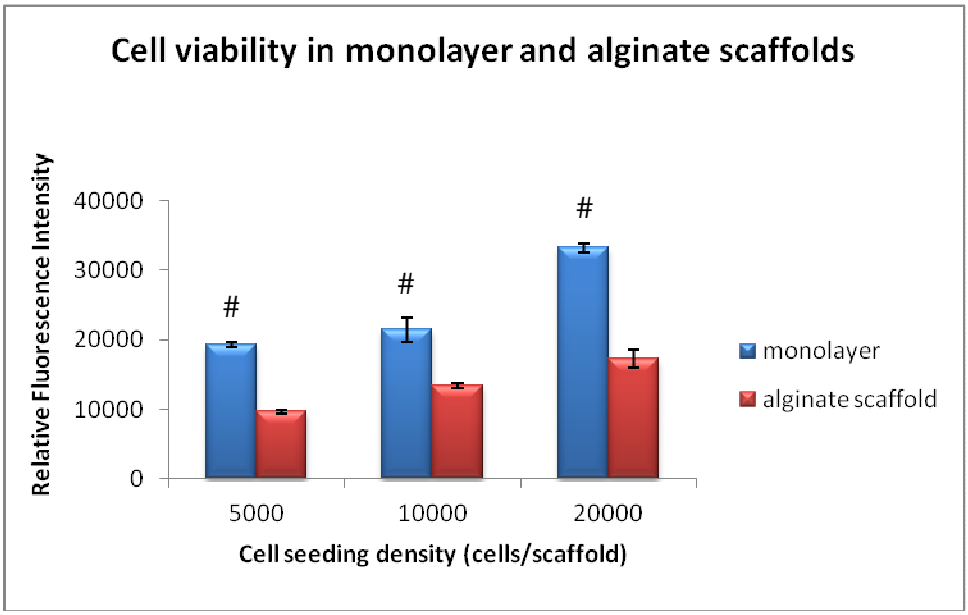

Figure 3.13 Comparison of cell viability between monolayer and alginate scaffolds at different cell seeding densities. *Cells grown in monolayer showed significantly higher viability than in the alginate scaffold (p < 0.01). Data are presented as mean ± SEM (n = 3). # p < 0.01 vs. monolayer.*

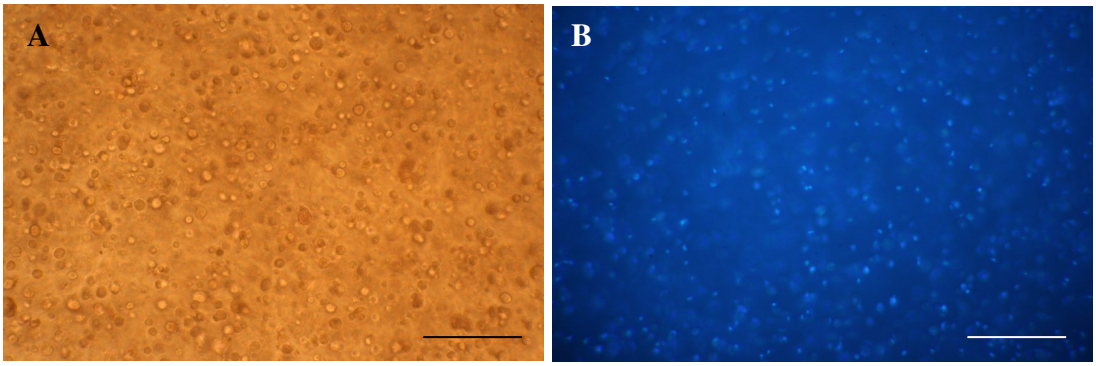

Figure 3.14 Cell distribution within alginate scaffolds at density of 4.5 x 10^4 cells per scaffold. *(**A**) Representative photomicrograph of CDCs within a 3D porous alginate scaffold by light microscope. (**B**) Fluorescence photomicrograph of CDCs stained with Hoechst. Scale bars = 250 μm. Abbreviation: CDCs = cardiosphere-derived cells.*

3.4.2.2 Cardiosphere-derived cell proliferation within alginate scaffolds

To determine the viability and proliferation of CDCs within alginate scaffolds over time, the AlamarBlue® assay was carried out at 7, 14 and 49 days. The number of viable cells significantly increased from day 7 to day 49 during the culture period ($p < 0.01$), indicating that CDCs proliferated and remained viable within alginate constructs for up to 7 weeks (Figure 3.15).

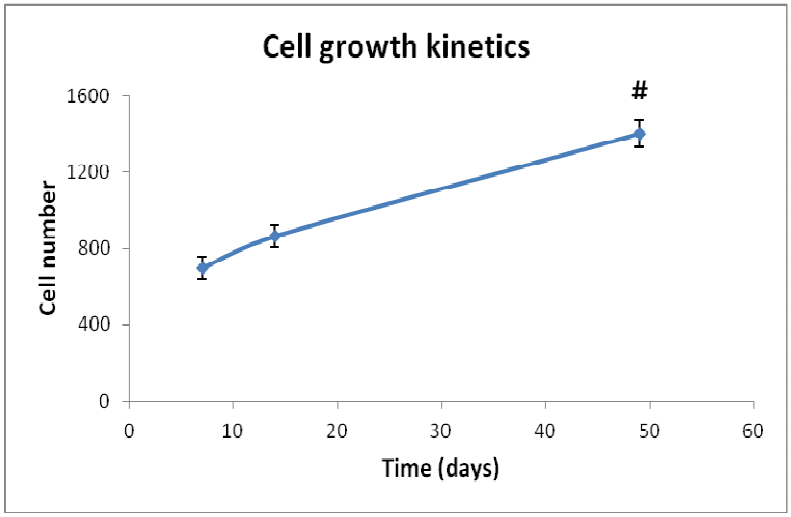

Figure 3.15 Growth curve for CDCs cultured within alginate scaffolds. *The constructs were analyzed for cell number after 7, 14 and 49 days of culture. The number of CDCs increased over time during a culture period of 7 weeks. Data are presented as mean ± SEM (n = 3). # $p < 0.01$ compared with day 7.*

3.4.2.3 Optimization of CDC survival within alginate scaffolds by adding extracellular matrix proteins

To optimize CDC survival in the alginate scaffold, extracellular matrix proteins were added to coat the surface of interconnective pores within the alginate construct. After 24 hours cultivation, cell viability was significantly increased in coated alginate scaffolds (fibronectin, type 1 collagen, gelatin and poly-D-lysine) compared with control (Figure 3.16).

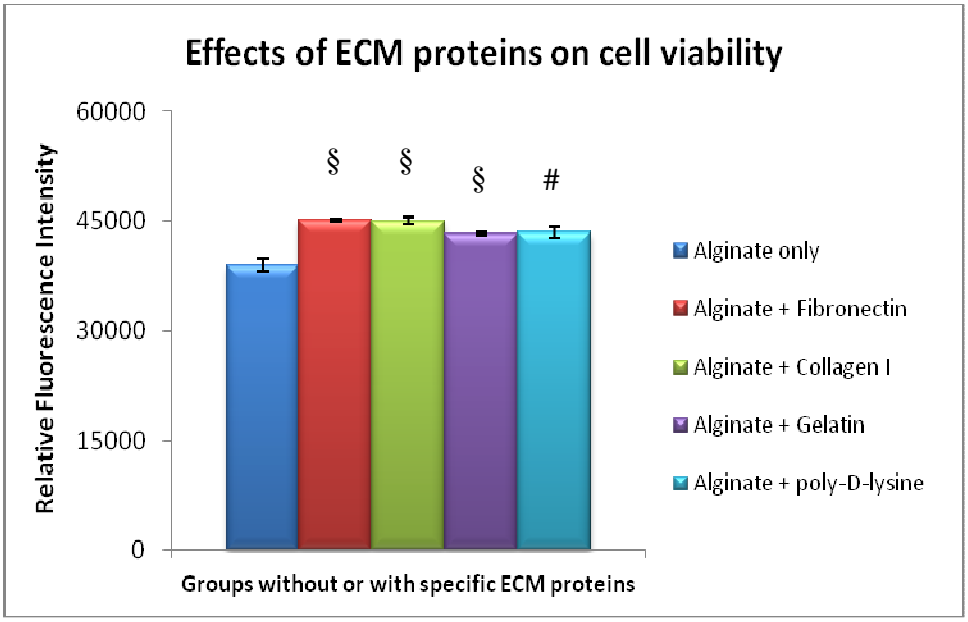

Figure 3.16 Cell viability in scaffolds after addition of extracellular matrix protein. *CDCs were cultured within various scaffolds made of alginate only, alginate containing fibronectin, alginate containing type 1 collagen, alginate containing gelatin or alginate containing PDL. Addition of ECM proteins significantly increased cell viability compared with control. Data are presented as mean ± SEM (n = 5). # p < 0.01 vs. alginate only; § < 0.001 vs. alginate only. Abbreviations: ECM = extracellular matrix.*

3.4.3 Decellularization of whole rat hearts

3.4.3.1 SDS perfusion decellularization of rat hearts using the Langendorff system

An isolated Sprague Dawley rat heart was mounted on the Langendorff apparatus *via* a cannula, and retrograde coronary perfusion of 1% SDS was carried out for 12 to 18 hours to totally decellularize the whole heart (Figure 3.17). When cellular material was removed during detergent perfusion, the heart became translucently white over time. It was observed that the heart was bleached in order from the right ventricle, then the right atrium, the left atrium and ultimately the left ventricle (Figure 3.17: **A** to **I**).

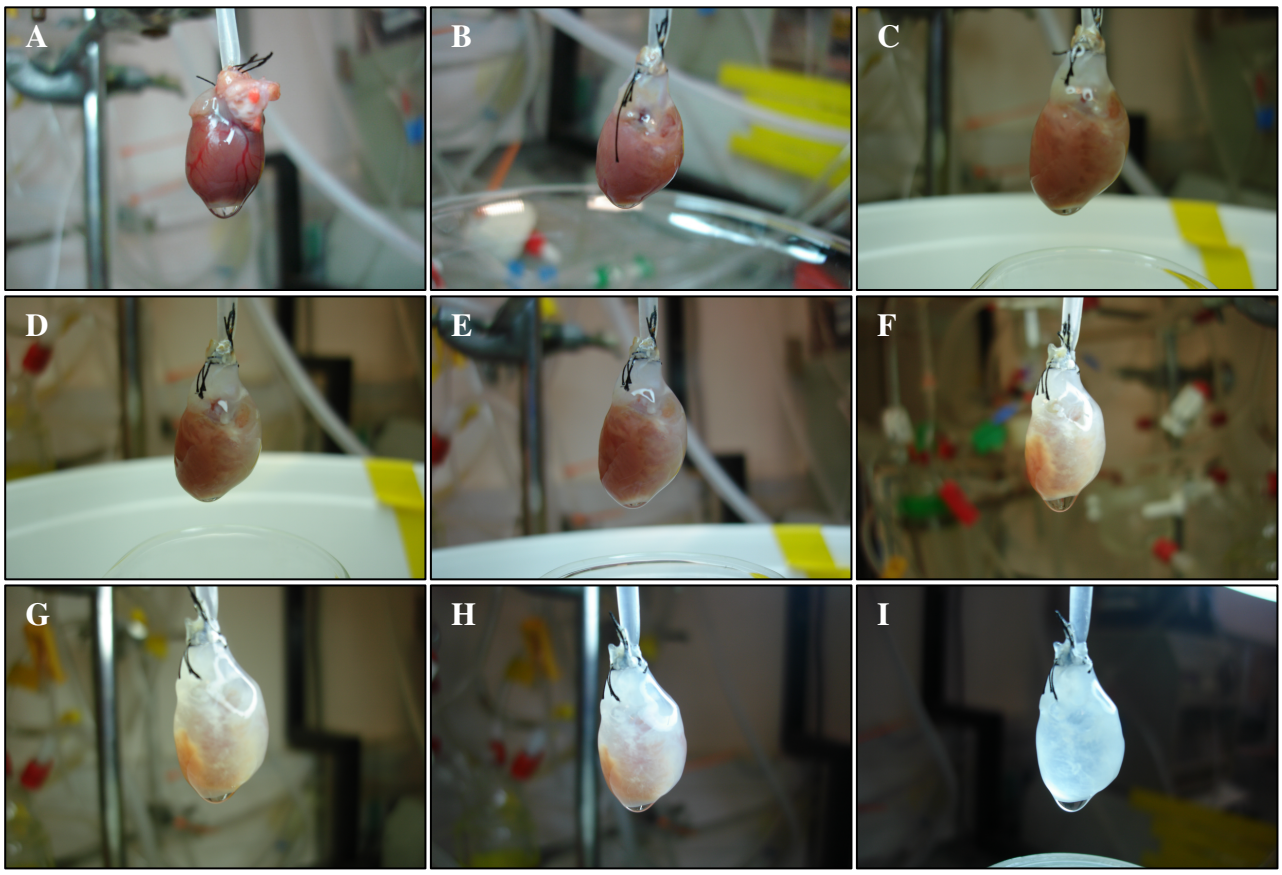

Figure 3.17 Decellularization photographs of 3 month-old Sprague Dawley rat hearts during a Langendorff perfusion. *Retrograde coronary SDS (1%) perfusion of a whole rat heart was performed over 12 hours. From beginning to end, representative images were taken with time using a digital camera (SONY, Cyber-shot, Japan; A to I). The heart turned whiter and more translucent as cells were continuously removed from the heart during the process of SDS- perfusion decellularization.*

3.4.3.2 Characteristics of the decellularized heart scaffold

Rat hearts were decellularized by retrograde coronary perfusion with 1% SDS for at least 12 hours, during which time cells were disrupted and the cellular material was washed out. Histological analysis, using H&E staining, showed no remaining nuclei after SDS-perfusion decellularization, suggesting disruption of intact cells (Figure 3.18). Immunohistochemical examination of decellularized heart samples revealed no remaining nuclei (stained by DAPI or propidium iodide) and intracellular proteins, including cardiac troponin I (cTnI), alpha-sarcomeric actin (ASA) and smooth muscle actin (SMA), compared with the control heart, further confirming that nuclear and cellular materials had been removed (Figure 3.19 and Figure 3.20).

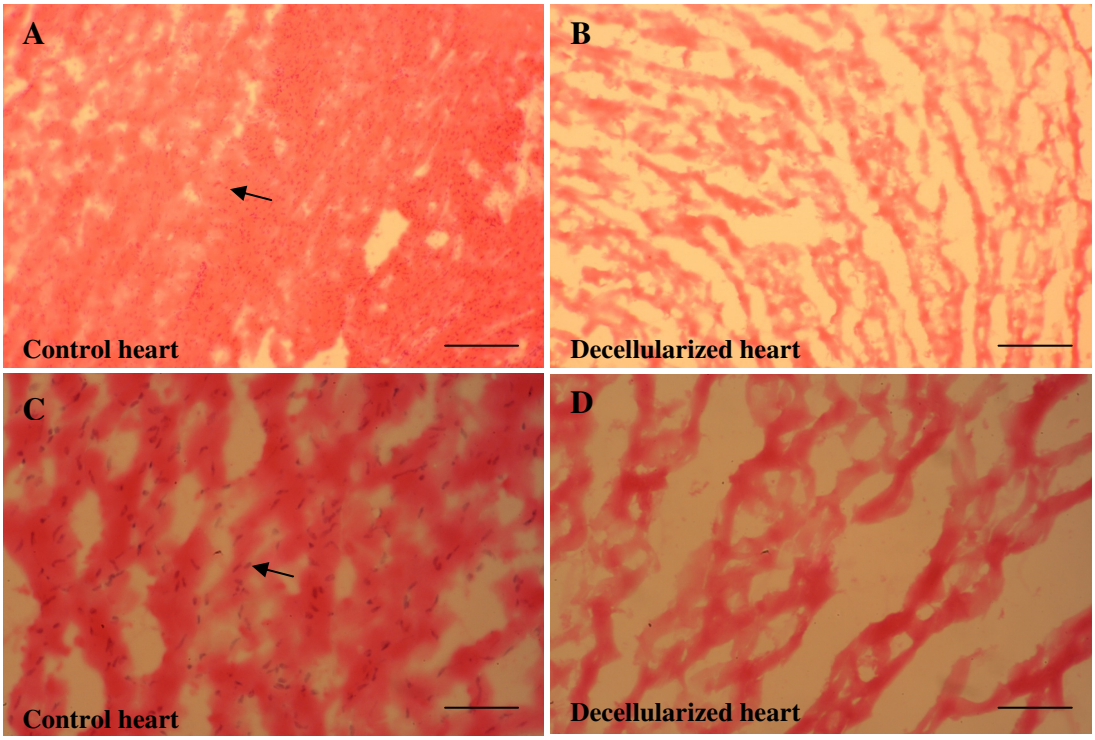

Figure 3.18 Photomicrographs of H&E staining taken using a light microscope (magnification 10x and 25x). *(**A** - **D**) Heart sections were from control rat hearts (A and C) and from decellularized rat hearts (B and D). C and D are higher magnifications. Using H&E staining, nuclei were stained purple in control heart sections (black arrows), but not found in decellularized hearts, indicating the removal of nuclei following perfusion decellularization. Extracellular matrix proteins were stained red by eosin. Scale bar = 200 μm (A and B) and 100 μm (C and D).*

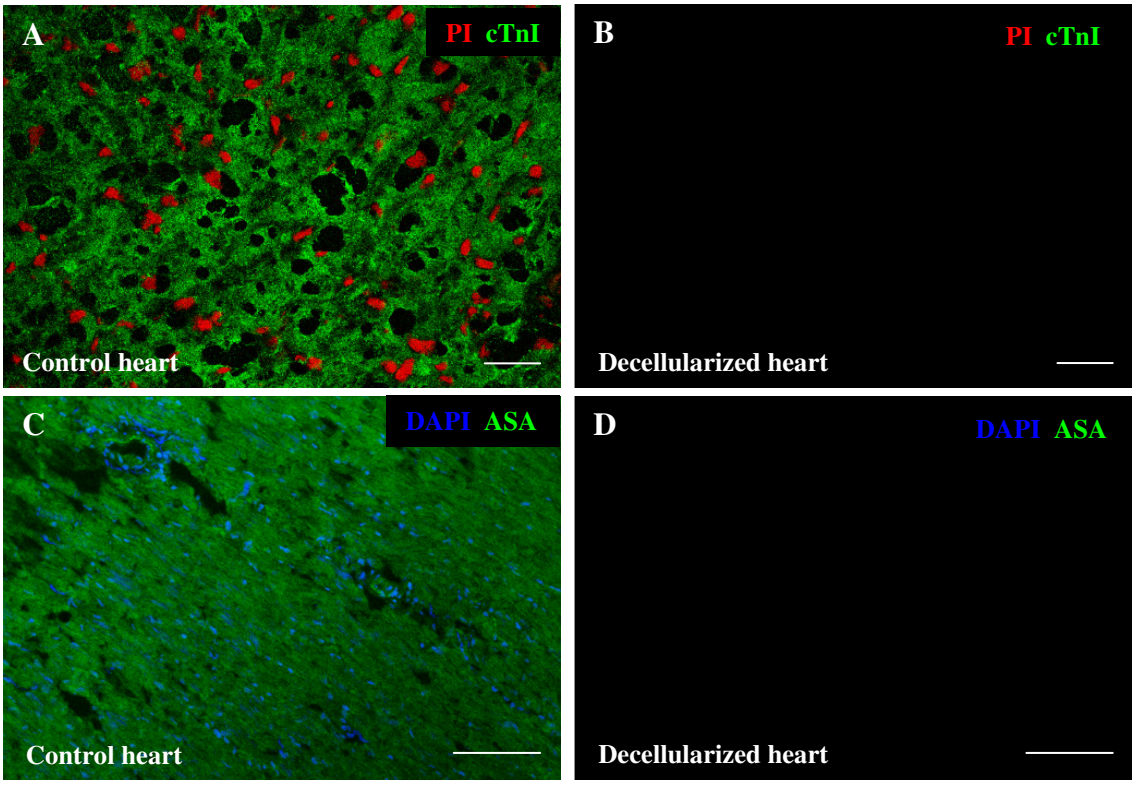

Figure 3.19 Photomicrographs of immunostaining for intracellular proteins of cardiomyocytes taken using a confocal microscope. *(**A** - **D**) Control and decellularized heart tissue sections were stained for troponin I (A and B) or alpha-sarcomeric actin (C and D). Nuclei were stained with PI (red) or DAPI (blue). PI/cardiac troponin I and DAPI/alpha-sarcomeric actin (green) staining were not detected in the decellularized heart matrix compared to control hearts. Scale bar = 100 µm (A to D). Abbreviations: PI = propidium iodide, cTnI = cardiac troponin I, DAPI = 4', 6-diamidino-2-phenylindole, and ASA = alpha-sarcomeric actin.*

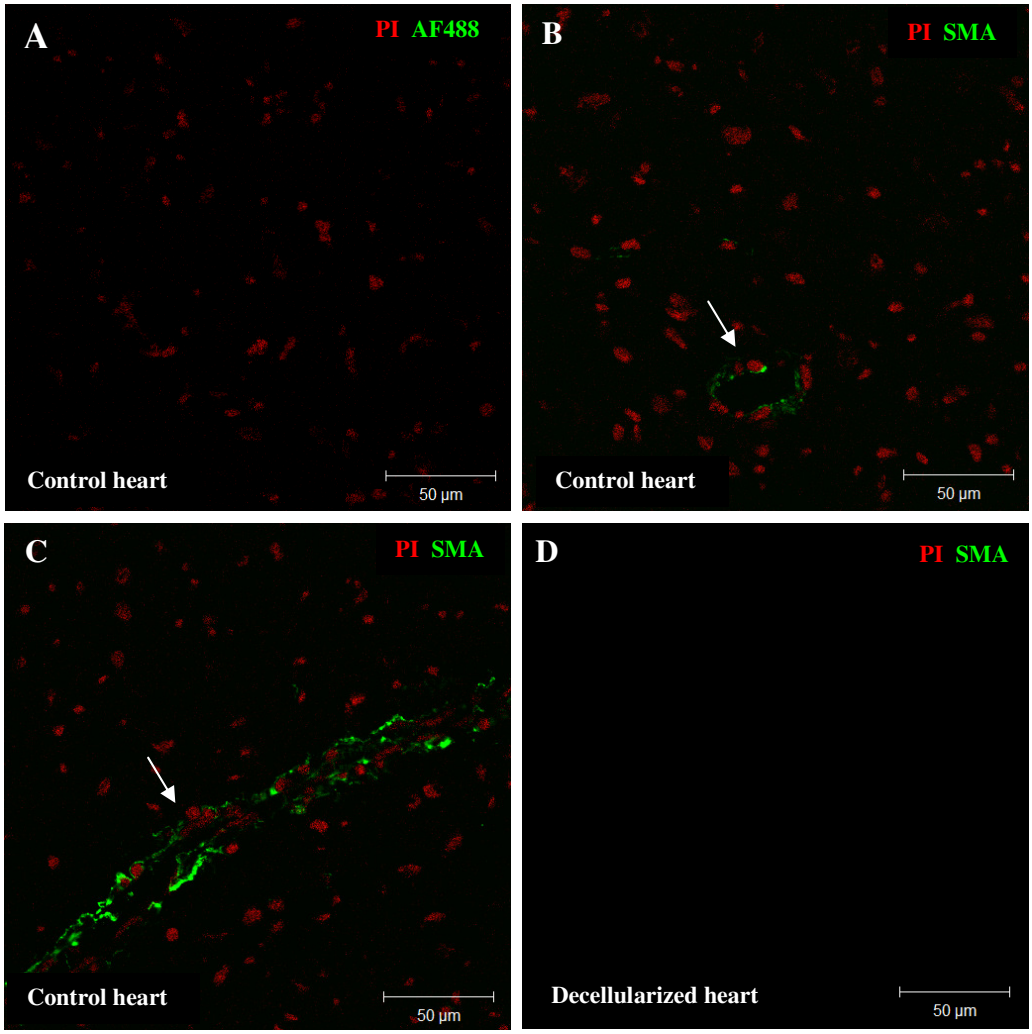

Figure 3.20 Photomicrographs of immunostaining for intracellular proteins of smooth muscle cells by confocal microscope. (***A***) *Negative control indicated control heart tissue stained with secondary antibody only (AF488, green).* (***B*** *-* ***D***) *Control and decellularized heart tissues were stained against smooth muscle actin (green). Nuclei were counterstained with propidium iodide (PI, red). A vascular lumen was shown in B (white arrow). A longitudinal vessel was shown in C (white arrow). PI and smooth muscle actin staining were not detected in decellularized heart matrix compared to control hearts in D. Scale bar = 50 µm. Abbreviations: PI = propidium iodide, AF488 = AlexFluor 488, and SMA = smooth muscle actin.*

3.4.3.3 Characterization of 3D cardiac architecture in decellularized rat heart

(I) Preservation of the extracellular matrix in decellularized heart scaffolds

Positive immunostaining of elastic fibers (red) in the decellularized heart tissue demonstrated the preservation of the extracellular matrix, elastin, after complete SDS decellularization (Figure 3.21). Moreover, high resolution magnetic resonance imaging (MRI) exhibited the arrangement and orientation of the extracellular matrix was preserved in the decellularized hearts (Figure 3.22 and Figure 3.23).

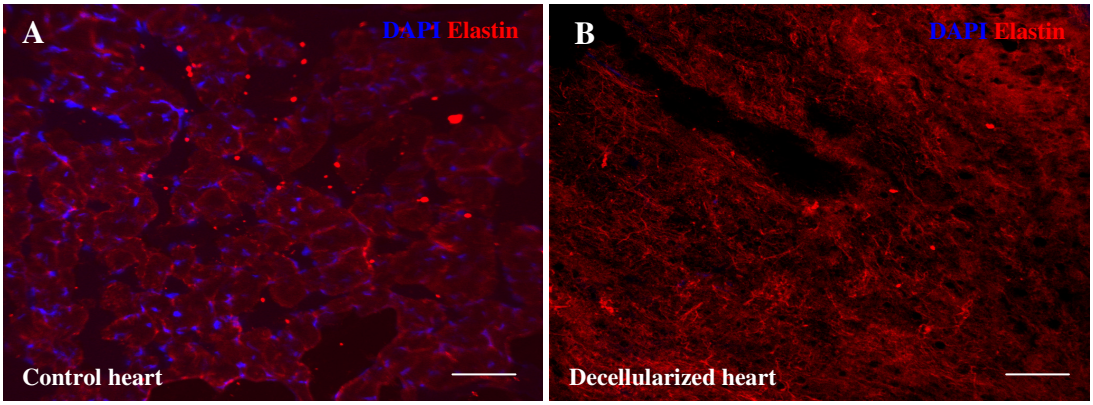

Figure 3.21 Photomicrographs of immunohistochemical staining for elastin by confocal microscope*. (**A, B**) Heart sections were stained for elastin: a control rat heart (A) and a decellularized rat heart (B). No DAPI nuclear staining (blue) was detected in the decellularized heart matrix whereas the elastin (red) of the ECM components was preserved. Scale bar = 50 μm (A) and 25 μm (B). Abbreviations: DAPI = 4′, 6-diamidino-2-phenylindole, ECM = extracellular matrix.*

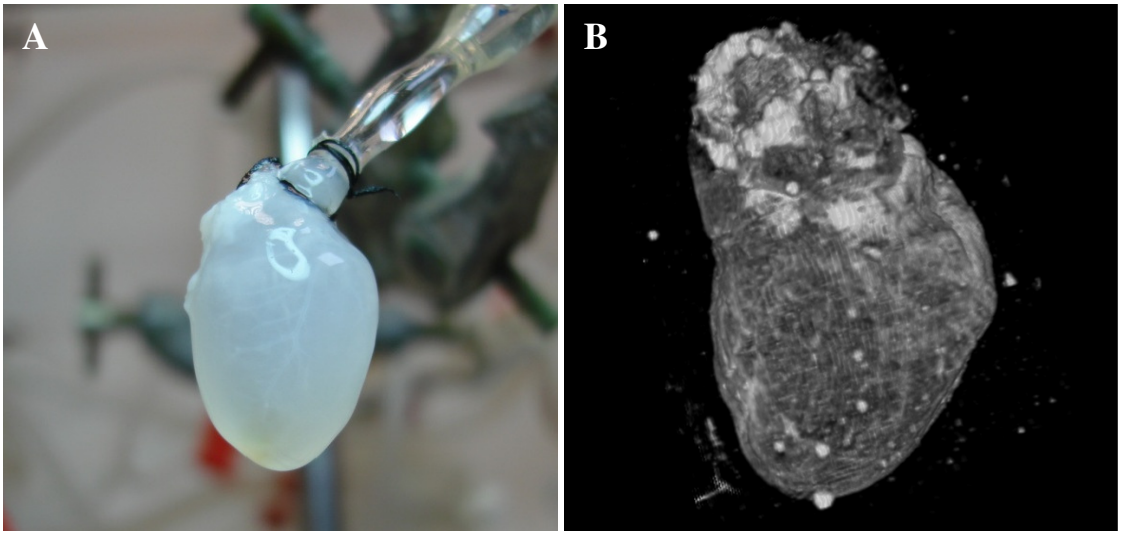

Figure 3.22 Macroscopic and MR images of the decellularized heart scaffold. *(**A**) A translucent extracellular matrix-based heart scaffold after decellularization. (**B**) Three dimensional (3D) reconstructed MR image of the decellularized heart scaffold shows the orientation of extracellular matrix components.*

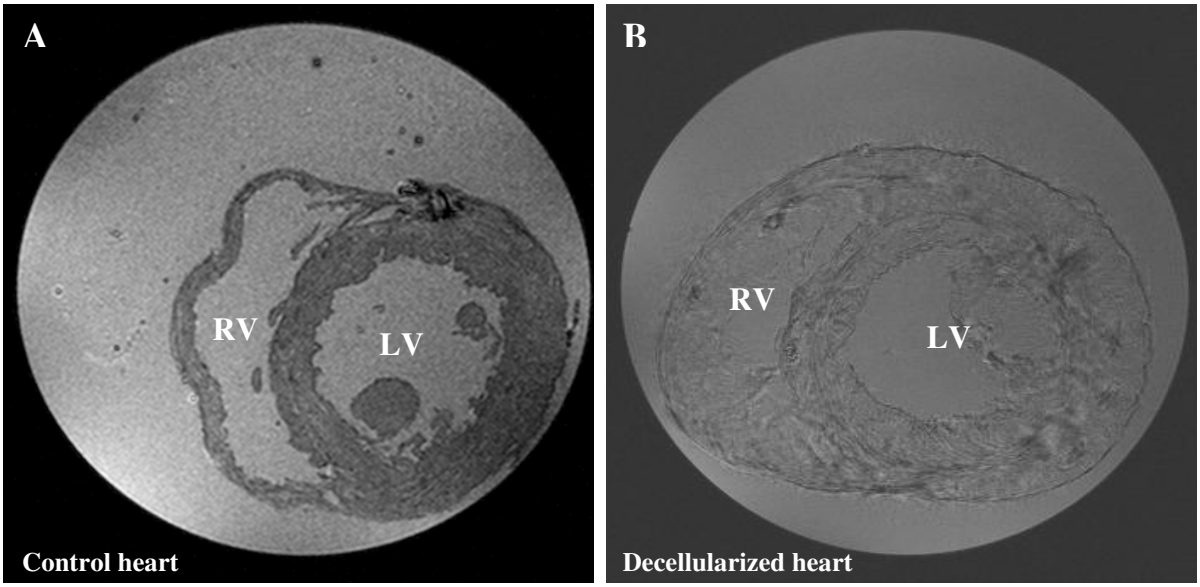

Figure 3.23 Representative images of the cross-section of normal and decellularized rat hearts using MRI. *(**A**) A cross-section view of the normal heart at papillary muscle level. (**B**) A short-axis view at the same level, showing the orientation of collagen-based extracellular matrix in the decellularized heart. Abbreviations: LV = left ventricle and RV = right ventricle.*

(II) Maintenance of intact architecture of cardiac chambers and valves

2D MR images of decellularized rat hearts revealed the intact geometry of the four chambers, papillary muscles, preserved semilunar valves (aortic and pulmonary), and conserved atrioventricular valves (tricuspid and mitral valves), which suggests the conservation of internal cardiac architecture following complete SDS-perfusion decellularization (Figure 3.24 B to I).

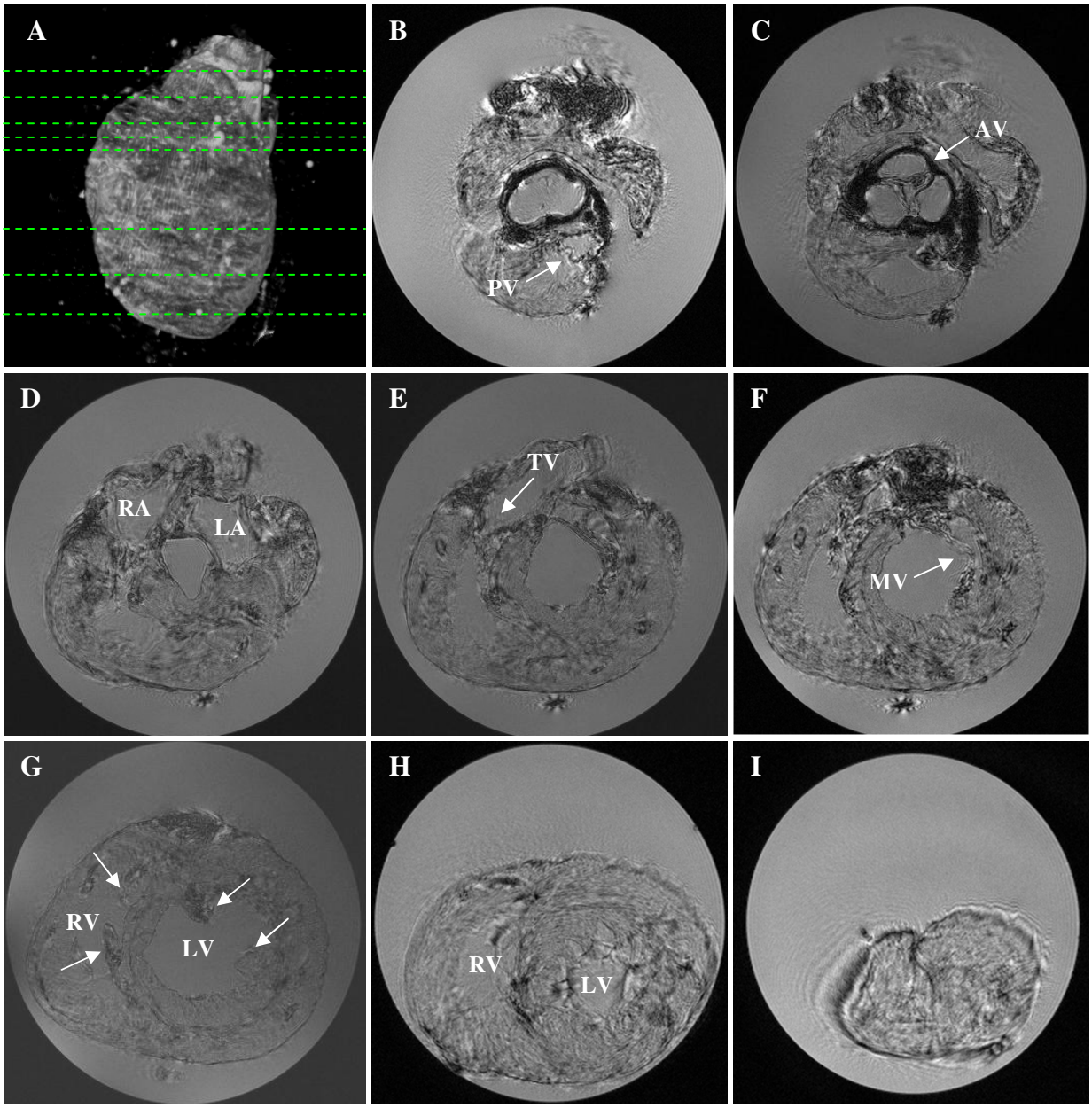

Figure 3.24 High resolution cine MR images of internal structures of a decellularized rat heart from base to apex. *(**A**) Reconstructed 3D MR long-axis image of a decellularized heart scaffold; green lines indicate the various levels of heart from base to apex with corresponding short-axis images (B to I). (**B**) Pulmonary valves. (**C**) Aortic valves. (**D**) Right and left atria. (**E**) Tricuspid valves. (**F**) Mitral valves. (**G**) Right and left ventricles at middle level (white arrows, papillary muscles). (**H**) Both ventricles at low level. (**I**) Apex. Abbreviations: PV = pulmonary valve, AV = aortic valve, TV = tricuspid valve, MV = mitral valve, RA = right atrium, LA = left atrium, RV = right ventricle, and LV = left ventricle.*

3.4.3.4 Characterization of coronary vasculature in decellularized rat hearts

(I) Macroscopic view of coronary vascular network

Under illumination, the macroscopic appearance of the decellularized rat heart demonstrated the maintenance of the coronary vascular network from the main trunk beyond the second branches following complete perfusion decellularization (Figure 3.25)

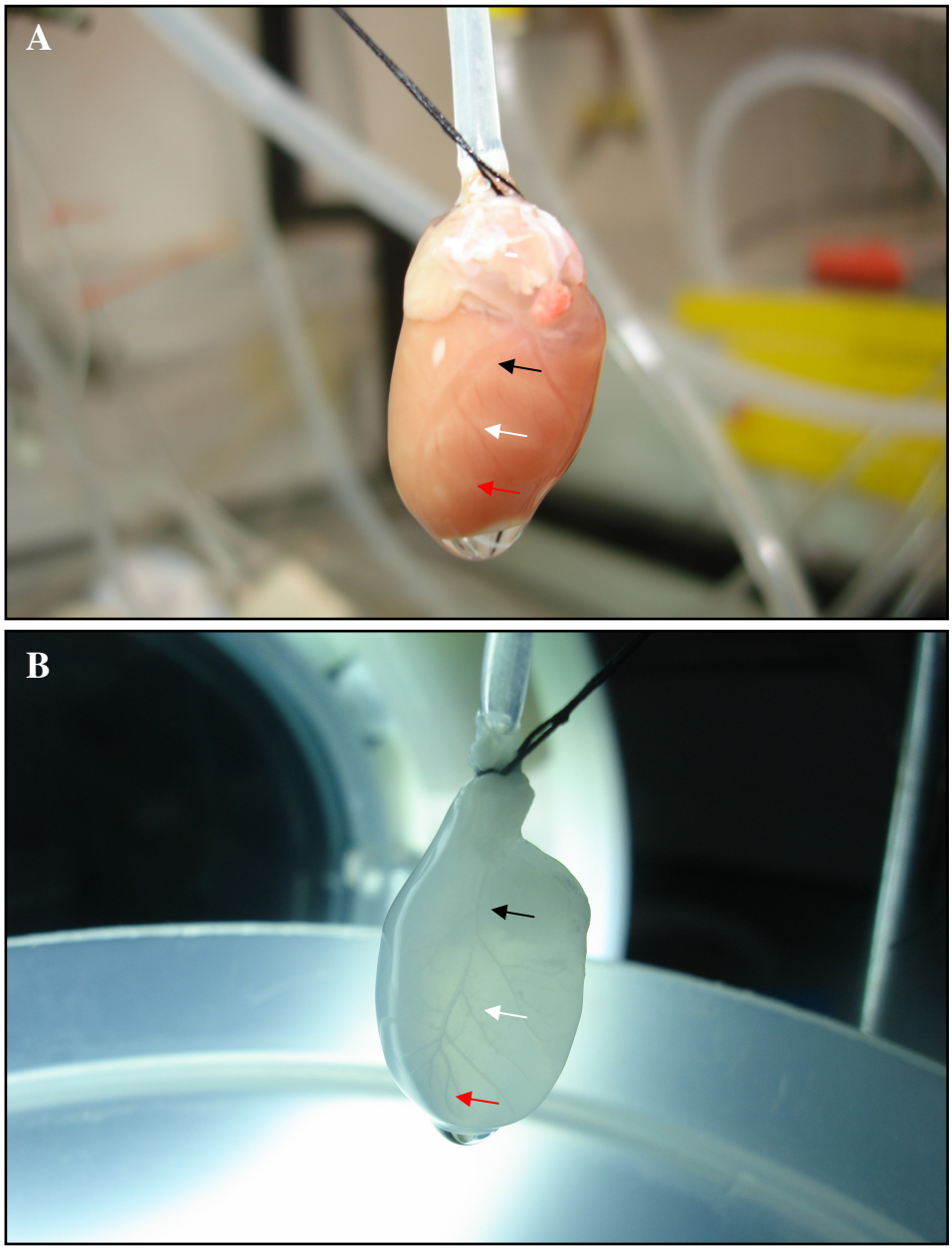

Figure 3.25 Representative images of rat hearts before and after decellularization. *(**A**) A mounted rat heart at the start of decellularization. (**B**) A completely decellularized heart. Black arrows indicate coronary main trunks, white arrows indicate the first branches and red ones indicate the second branches. It is apparent that vascular network was preserved in the decellularized heart matrix.*

(II) Confirmation of intact coronary vascular conduits using Evan's blue dye perfusion

The integrity of aortic valves and coronary vasculature was confirmed on the basis of dye movement using Evan's blue dye perfusion (Figure 3.26 and Figure 3.27).

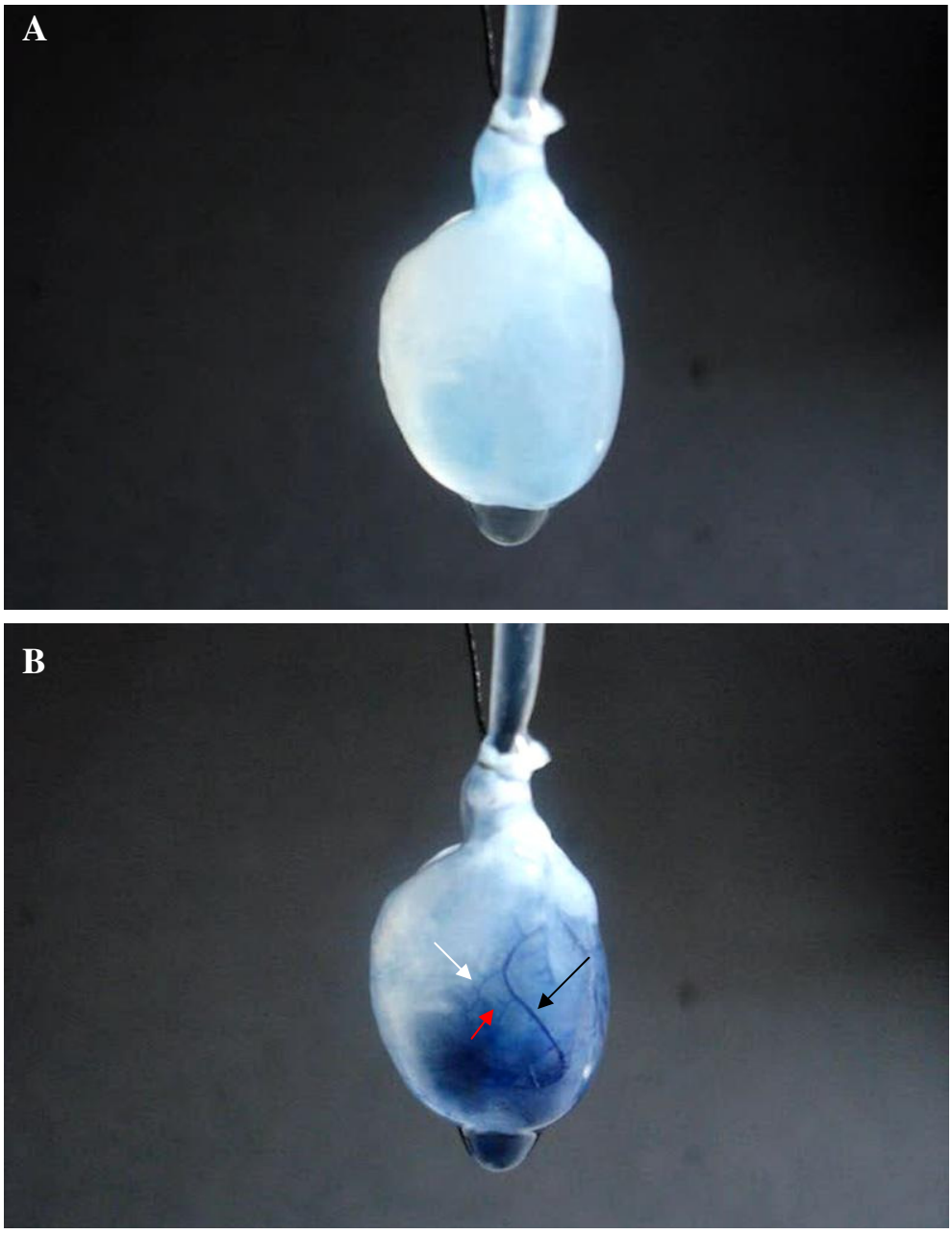

Figure 3.26 Representative images of decellularized rat hearts at the beginning and end of Evan's blue dye perfusion. *Photographs were taken using a digital camera (SONY, Cyber-shot, Japan). (**A**) At the start of dye perfusion. (**B**) At the end of dye perfusion. Macroscopic appearance of the decellularized heart revealed intact coronary artery without obvious leakage along the vessels after dye perfusion. Coronary main trunk, first branch and second branch were designated by black, white and red arrows, respectively.*

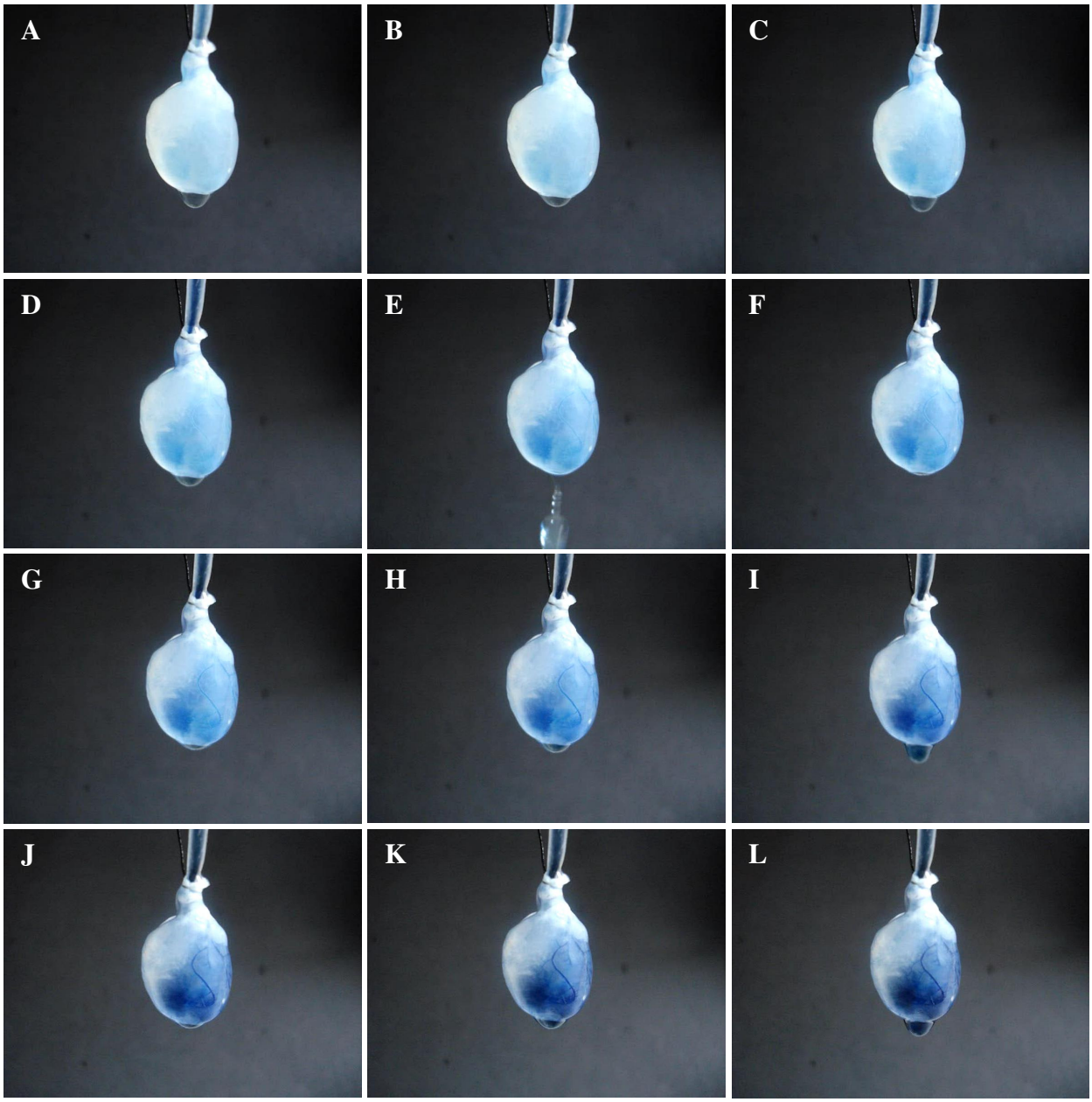

Figure 3.27 Serial images of a decellularized rat heart undergoing Evan's blue dye perfusion. *To assess the integrity of coronary vasculature, high molecular weight dye (Evan's blue dye) was used for coronary perfusion. The dye perfusion process was filmed using a digital video camera (SONY, Cyber-shot, Japan). Thereafter, moving pictures were captured individually at one second interval from start to end of perfusion (A to L). These images showed that blue dye ran through coronary vascular network (from large to small vessels) during perfusion, indicating that functional aortic valves and intact coronary vascular conduits were preserved following detergent perfusion decellularization.*

3.4.3.5 Recellularization of the dcellularized heart matrix – A pilot study

Recellularization of decellularized hearts using rat cardiac-derived stem cells

Cardiosphere-derived cells, pre-labelled with MPIO (green) or CM-DiI (red), were transplanted into a decellularized heart scaffold *via* intra-myocardial injection and coronary infusion, respectively. Following intra-myocardial administration of cells (MPIO-labelled CDCs), the cell number in the coronary effluent from the myocardium was measured using a haemocytometer shortly after injection. Approximately 60% of the administered cells were lost within 20 min. During the recellularization *via* coronary infusion, the cells in the coronary effluent were re-circulated into the heart scaffold. The number of cells (CM-DiI stained CDCs) in the coronary effluent was measured after each cycle of perfusion. The number of cells staying in the heart varied from cycle to cycle. After a total of ten cycles, around 50% of the cells (i.e., 1 x 10^5 CDCs) remained in the collagen-based heart matrix.

After CellTracker CM-DiI stained CDCs and MPIO-labelled CDCs were seeded, the recellularized heart matrix was fixed for frozen sectioning. Confocal microscopy revealed that the CDCs stayed within the preserved extracellular matrix of the decellularized heart construct. Most MPIO-labelled CDCs were found in the outer layer of left ventricular wall associated with injection sites; in contrast, CM-DiI stained CDCs distributed throughout the whole layer of the wall due to intracoronary infusion (Figure 3.28).

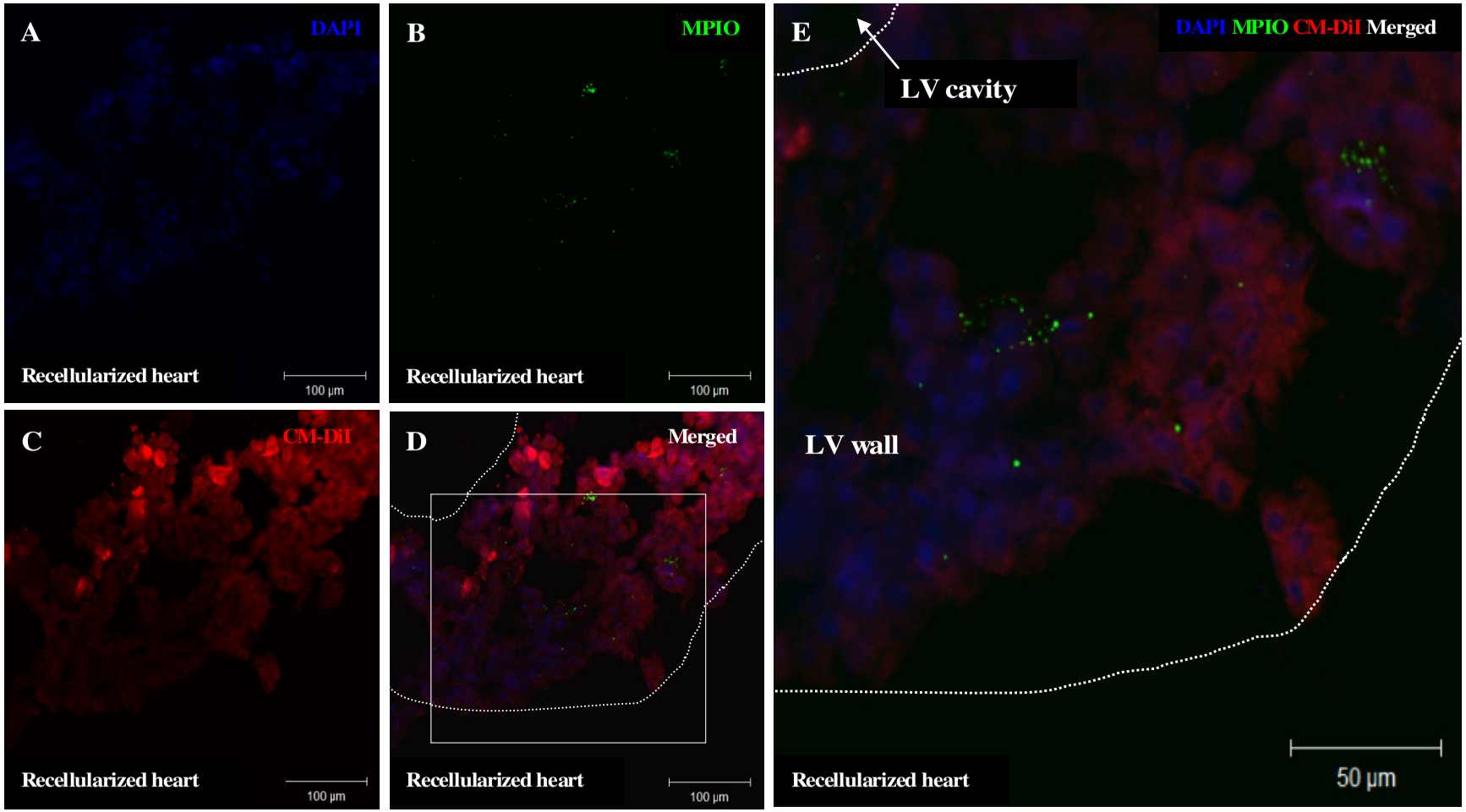

Figure 3.28 Confocal photomicrographs of the decellularized heart matrix following recellularization of labelled cardiosphere-derived cells. *CDCs, pre-labelled with MPIO (green) or CM-DiI (red), were transplanted into a decellularized heart scaffold via intra-myocardial injection and coronary infusion, respectively. Nuclei were counterstained with DAPI (blue). The square image in* ***D*** *was enlarged as* ***E****. White dotted lines indicate inner and outer margin of LV wall. Scale bar = 100 µm (****A to D****) and 50 µm (****E****). Abbreviations: DAPI = 4′, 6-diamidino-2-phenylindole, MPIO = microsized-particles of iron oxide, and LV = left ventricle*

3.4.4 Cardiomyocyte differentiation of cardiosphere-derived cells

3.4.4.1 Characterization of rat cardiosphere-derived cells

Flow cytometric analysis identified c-kit and CD90 expressing cells (3 ± 0.2 % and 65 ± 6 %, respectively) in expanded CDCs, as shown in Figure 3.29. Immunocytochemistry revealed that rat CDCs (passage 2) were composed of mixed subpopulations including cardiac-derived stem cells (c-kit, Oct3/4 and Sox2), mesenchymal stem cells (CD90), cardiac lineage-committed cells (Nkx2.5 and cTnT), smooth muscle cells (αSMA) and endothelial-related cells (vWF) (Figure 3.30).

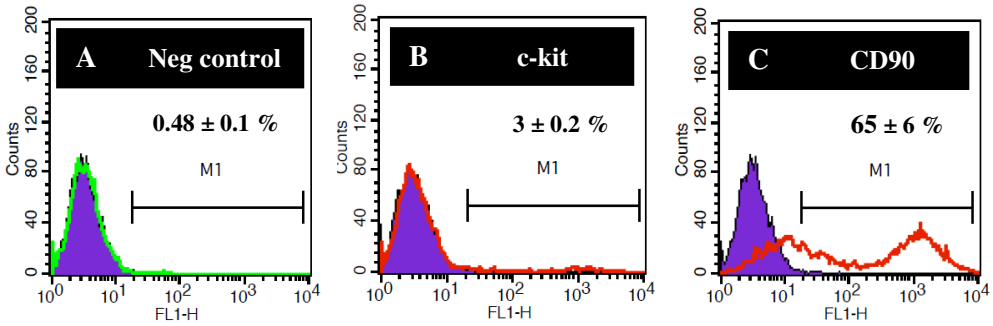

Figure 3.29 Flow cytometric analysis of CDCs isolated from 3 month-old rats. *(**A**) Negative control of cells stained only with secondary antibody (green line). (**B**, **C**) Passage 2 CDCs were analysed after staining for cardiac stem cell markers, c-kit (B) or mesenchymal cell marker CD90 (C) using flow cytometry. Cells present in region M1 were defined as the positive population. Purple region: unstained cell control. Red line: corresponding stained samples. Data are presented as mean ± SEM (n = 3). Abbreviation: CDC = cardiosphere-derived cell.*

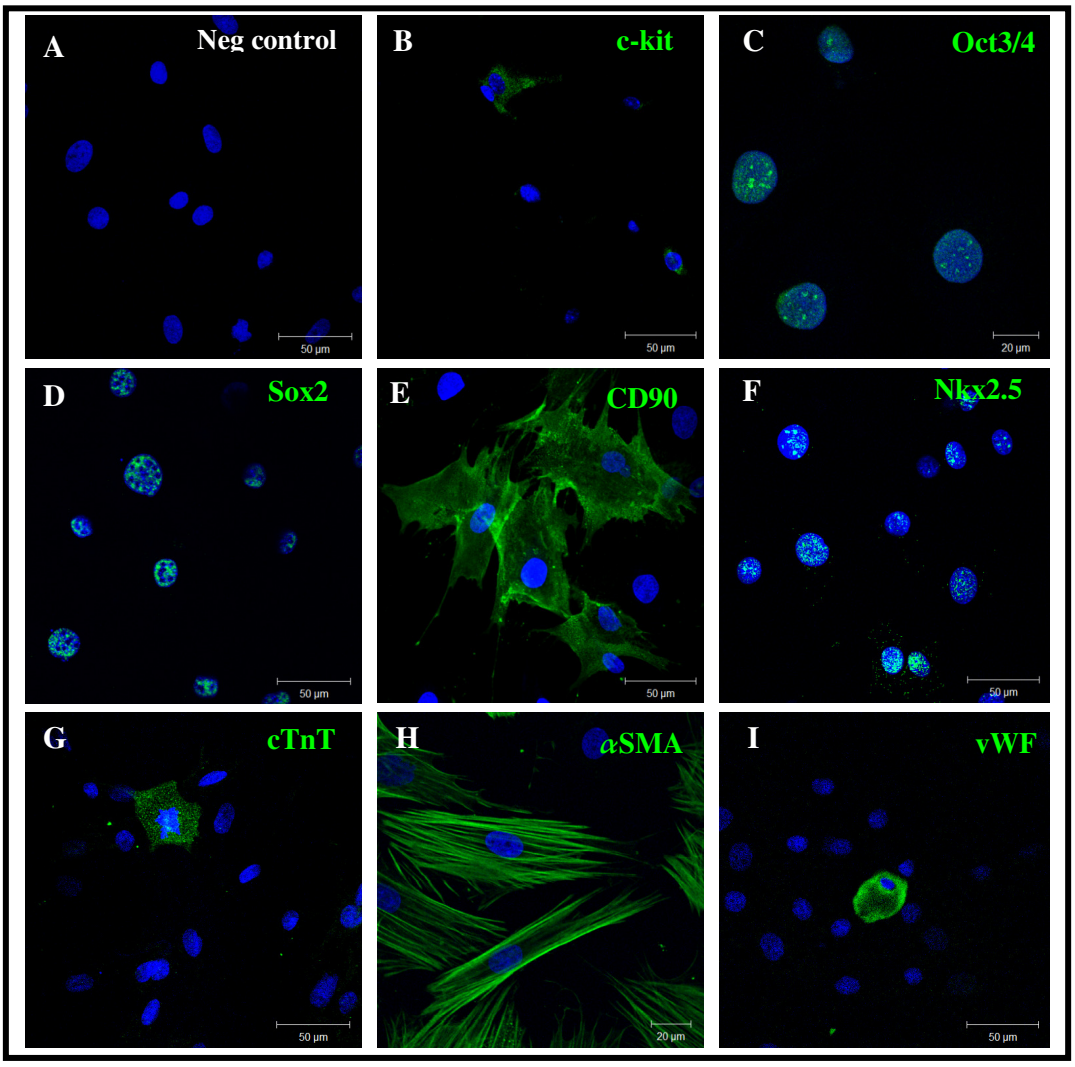

Figure 3.30 Immunophenotype characterization of rat CDCs at passage 2. *(**A**) Negative control indicated cells stained with secondary antibody only (AF488, green). (**B** - **I**) Confocal images revealed that CDCs represented a mixed cell population consisting of cardiac stem and progenitor cells expressing c-kit (B, green), Oct3/4 (C, green) and Sox2 (D, green), mesenchymal stem cells expressing CD90 (E, green), cardiac lineage-commited cells expressing Nkx2.5 (F, green), cardiac differentiated cells expressing cTnT (G, green), cardiac smooth muscle cells expressing αSMA (H, green), and endothelial cells expressing vWF (I, green). Nuclei were counterstained with DPAI (blue). Scale bars = 20 µm (C and H) and 50 µm (others). Abbreviations: CDCs = cardiosphere-derived cells, AF488 = AlexFluor 488, cTnT = cardiac troponin T, αSMA = alpha-smooth muscle actin, and vWF = von Willibrand Factor.*

3.4.4.2 Effects of low serum and 5-Aza on differentiation of cardiosphere-derived cells

Reduction of CDC proliferation and induction of differentiation in culture by low serum or 5-Aza

During the culture period with 5-Aza (10 μM), cell death occurred. Floating cells with small vacuoles (dead cells) were observed in suspension. At the end of differentiation, micrographs of CDCs were taken (Figure 3.31) and cells were counted using a haemocytometer. Serum 2% and 5-Aza 10 μM significantly reduced cell proliferation compared with 20% serum (Figure 3.32). Quantitative RT-PCR showed that cardiac-specific gene expression of cTnT was significantly up-regulated in differentiated CDCs induced by 2% serum, 20% serum+5-Aza and 2% serum+5-Aza, compared with control (Figure 3.33).

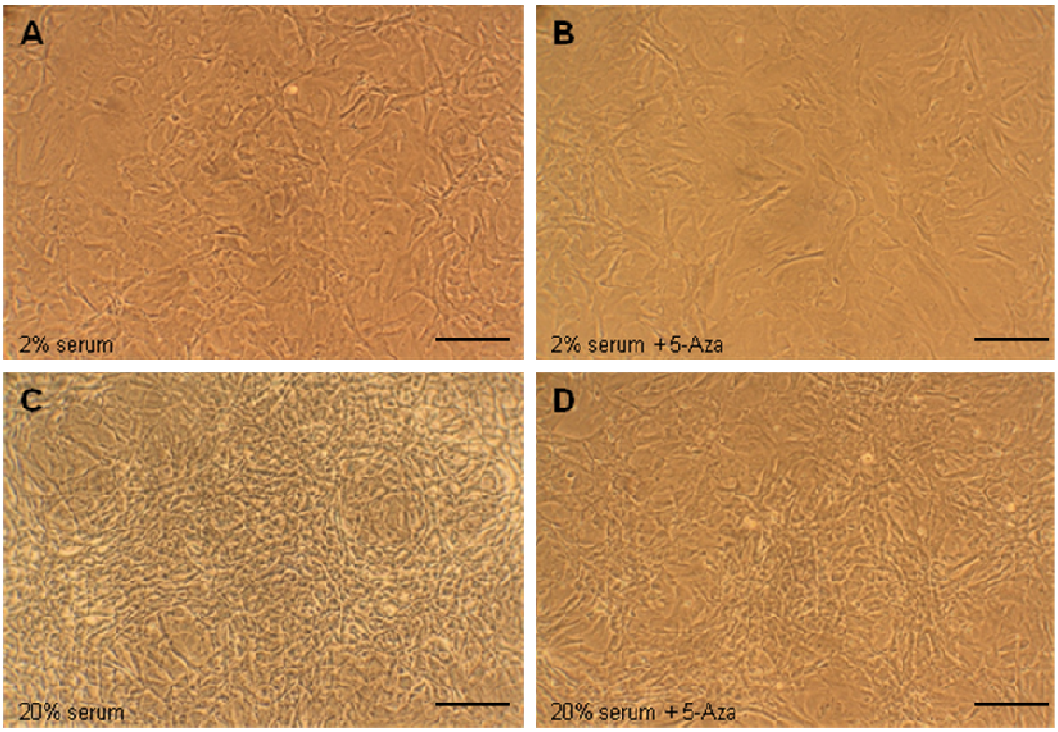

Figure 3.31 Morphological characteristics of CDCs grown in various culture media (magnification x10). *CDCs were grown in 6 well plates under various treatments for one week to induce cardiac differentiation. CDCs were found to proliferate at different speeds among the four groups during the culture period. Representative images were captured at the end of one week culture. Scale bar = 200 μm. Abbreviations: CDCs = cardiosphere-derived cells and 5-Aza = 5-azacytidine.*

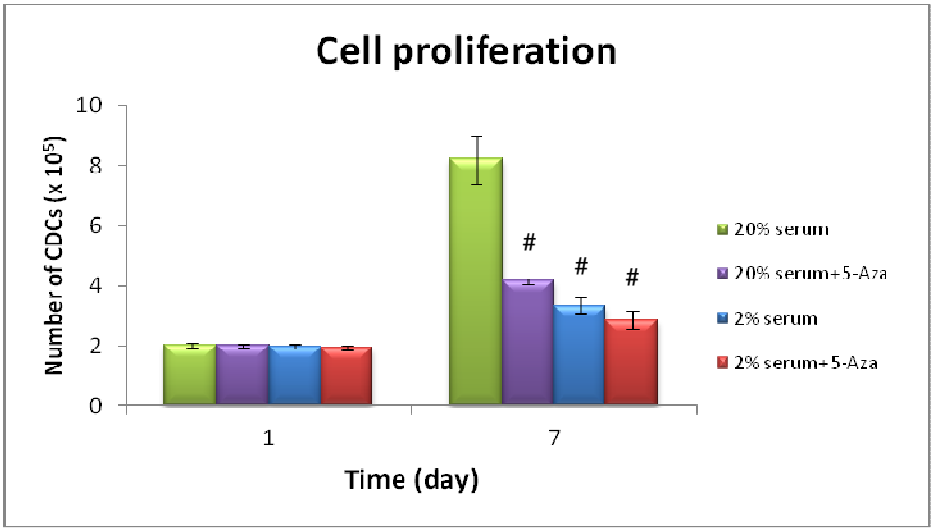

Figure 3.32 Proliferation of CDCs grown in different media. *Passage 2 CDCs (2 x 10^5) were cultured in 6 well plates with different media, containing various concentrations of serum and 5-Aza, for one week. CDCs were counted manually using a hemocytometer at day 1 and day 7 post plating. Serum 2% and 5-Aza gave a significantly lower number of CDCs after one week of culture. Data are presented as mean ± SEM (n = 3). # p < 0.01 vs. control (20% serum). Abbreviations: CDCs = cardiosphere-derived cells and 5-Aza = 5-azacytidine.*

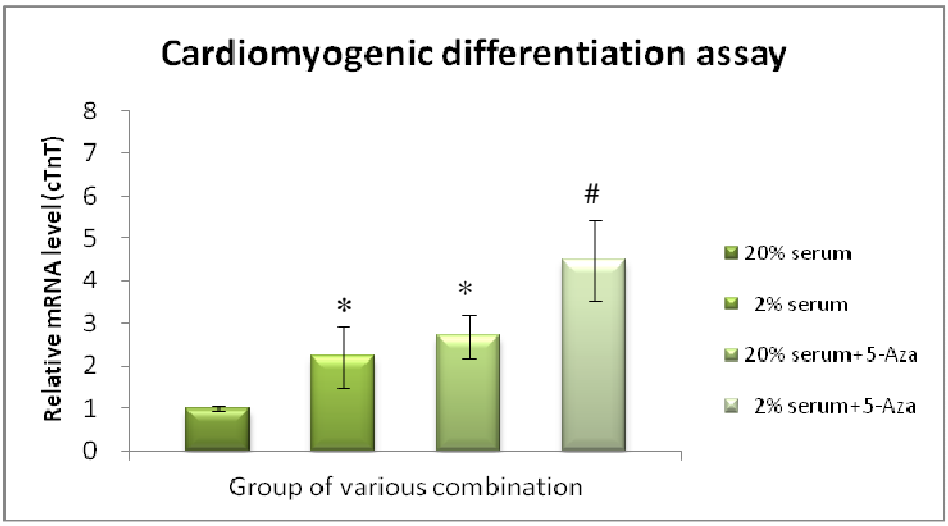

Figure 3.33 Quantitative RT-PCR showing the relative mRNA expression of cTnT in CDCs cultured in different media. *Passage 2 CDCs were grown in media containing 2% or 20% of serum, with or without 5-Aza (10 μM), for one week. All values were normalized to the housekeeping gene (GAPDH). The fold change of mRNA expression is reported relative to control containing 20% serum (n = 3). * p < 0.05 vs. 20% serum; # p < 0.01 vs. 20% serum. Abbreviations: cTnT = cardiac troponin T, CDCs = cardiosphere-derived cells and 5-Aza = 5-azacytidine.*

3.4.4.3 Determination of the optimal concentration of 5-azacytidine and DMSO for cardiac differentiation

5-Aza or DMSO were added to the basal differentiation medium (BDM; Appendix: Table 4), containing 2% FBS, at various concentrations to investigate the optimal differentiating concentration.

Cardiomyocyte differentiation by treatment with 5-Aza or DMSO at various concentrations

P2 CDCs were cultured in 6 well plates pre-coated with 0.1% gelatin. In the 5Aza group, for the first three consecutive days, BDM with 5-Aza was added to each well at indicated concentrations (0, 1, 5 or 10 μM, respectively). Thereafter, BDM was changed every 2-3 days for the rest of two weeks. As shown in Figure 3.34, 5-Aza inhibited CDC proliferation in a dose-dependent manner. Quantitative RT-PCR revealed that the treatment with 1 μM 5-Aza significantly increased the expression of cardiomyocyte-specific genes among four groups (Figure 3.35).

In the DMSO group, BDM with DMSO was added to each well every two days (day 1, 3 and 5) at indicated concentrations (0, 1, 10 or 100 mM, respectively; Figure 3.36). For the rest of two weeks, BDM was refreshed every 2-3 days. As shown in Figure 3.37, DMSO (1 mM) treatment was found to be the strongest inducer of cardiomyogenic differentiation.

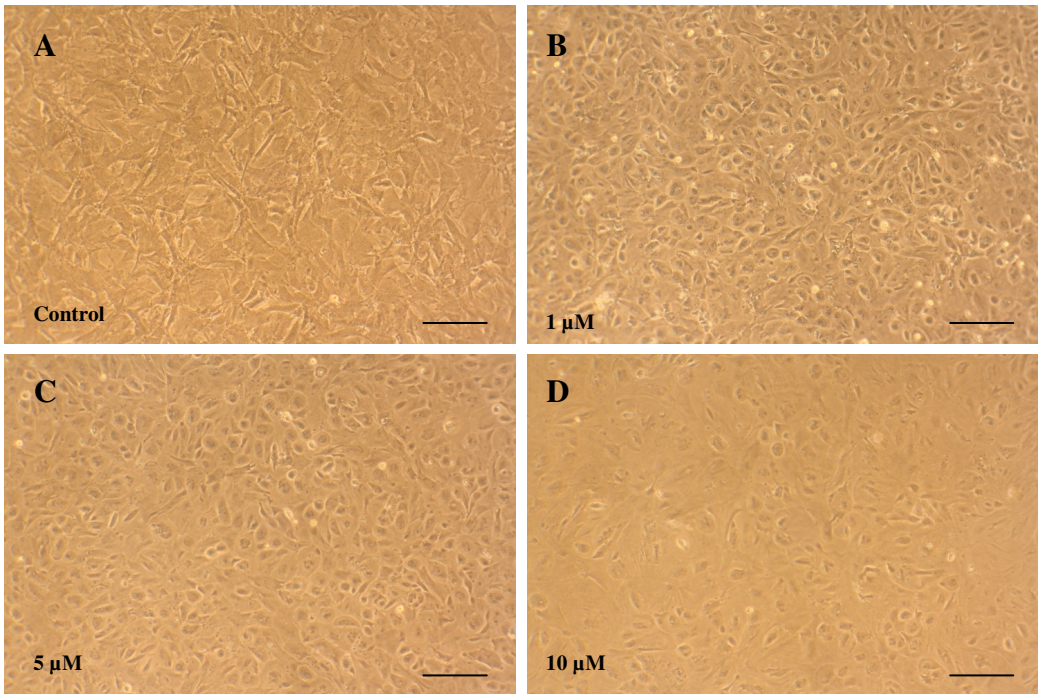

Figure 3.34 Morphological characteristics of CDCs grown in media containing various concentrations of 5-Aza (magnification x10). *Passage 2 CDCs were treated for the first three consecutive days with 0, 1, 5 or 10 µM of 5-Aza, respectively, and then BDM for two weeks. (**A** - **D**) Representative images were captured at the end of differentiation induction (A, B, C and D, respectively). Scale bar = 200 µm. Abbreviations: CDC = cardiosphere-derived cell, 5-Aza = 5-azacytidine, and BDM = basal differentiation medium.*

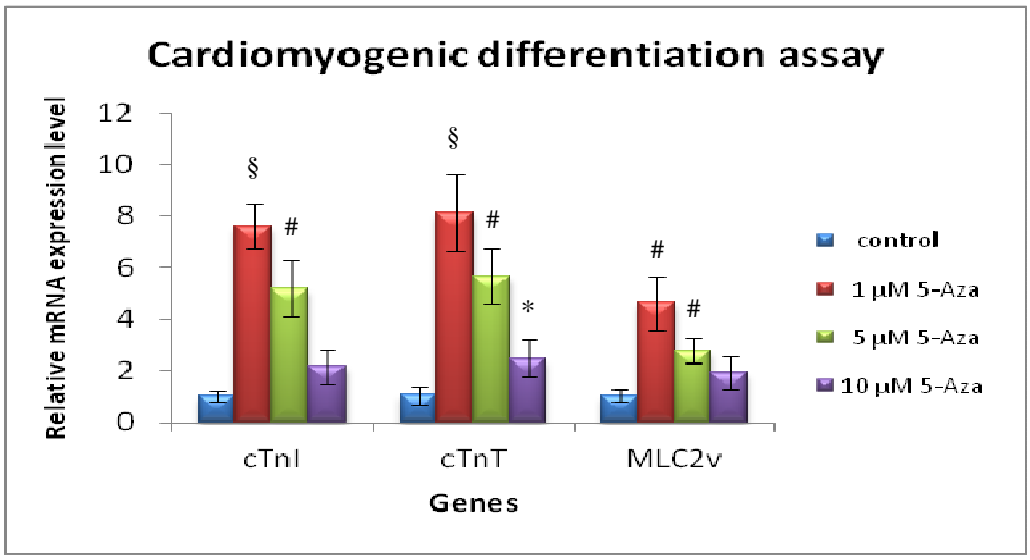

Figure 3.35 The relative mRNA expression level of cardiac-specific genes in differentiated CDCs using qRT-PCR. *Passage 2 CDCs were treated with 0, 1, 5 or 10 µM of 5-Aza, respectively. Cardiac-specific gene expression of cTnI, cTnT and MLC2v were measured using qRT-PCR. All values were normalized to GAPDH and mRNA level was reported relative to control treated with BDM (n = 3). * $p < 0.05$ vs. control; # $p < 0.01$ vs. control; § $p < 0.001$ vs. control. Abbreviations: CDC = cardiosphere-derived cell, cTnI = cardiac troponin I, cTnT = cardiac troponin T, MLC2v = myosin light chain-2v, 5-Aza = 5-azacytidine, and BDM = basal differentiation medium.*

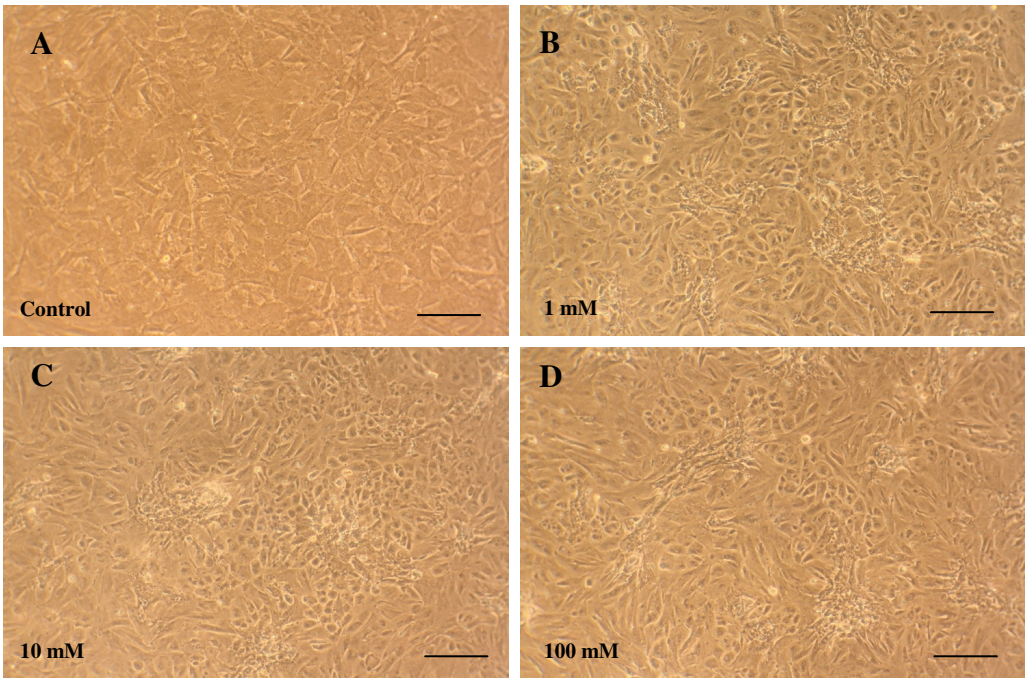

Figure 3.36 Morphological characteristics of CDCs grown in media containing various concentrations of DMSO (magnification x10). *Passage 2 CDCs were treated with 0, 1, 10 or 100 mM DMSO, every two days and then with BDM for two weeks. (**A** - **D**) Representative images were taken at the end of one week induction of differentiation (A, B, C and D, respectively). Scale bar = 200 µm. Abbreviations: CDC = cardiosphere-derived cell, DMSO = dimethyl sulfoxide, and BDM = basal differentiation medium.*

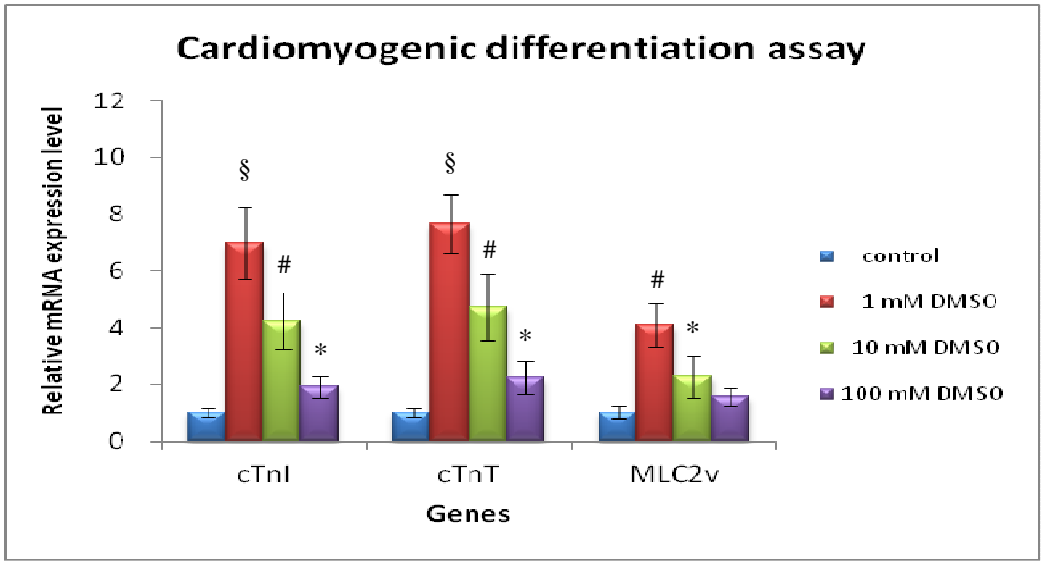

Figure 3.37 The relative mRNA expression level of cardiac-specific genes in differentiated CDCs using qRT-PCR. *Passage 2 CDCs were treated with with 0, 1, 10 or 100 mM DMSO, respectively. The expression of cardiac-specific genes cTnI, cTnT and MLC2v was examined by qRT-PCR. All values were normalized to GAPDH and mRNA expression was reported relative to control treated with BDM (n = 3). * $p < 0.05$ vs. control; # $p < 0.01$ vs. control; § $p < 0.001$ vs. control. Abbreviations: CDC = cardiosphere-derived cell, cTnI = cardiac troponin I, cTnT = cardiac troponin T, MLC2v = myosin light chain-2v, DMSO = dimethyl sulfoxid , and BDM = basal differentiation medium.*

3.4.4.4 Effects of combined ascorbic acid and 5-Aza or DMSO on cardiomyogenic differentiation

(I) Induction of cardiomyocyte differentiation by ascorbic acid at various concentrations

BDM with ascorbic acid was added to each well every two days (day 1, 3 and 5) at indicated concentrations (0, 10^{-6}, 10^{-5}, 10^{-4}, or 10^{-3} µM, respectively). For the remainder of two weeks, BDM was changed every 2-3 days. Interestingly, ascorbic acid promoted cell proliferation in a dose-dependent manner (Figure 3.38). Moreover, it was found that cells treated with 10^{-4} µM of ascorbic acid significantly expressed cardiac-specific genes (cTnI, cTnT and MLC2v) among five groups using qRT-PCR (Figure 3.39).

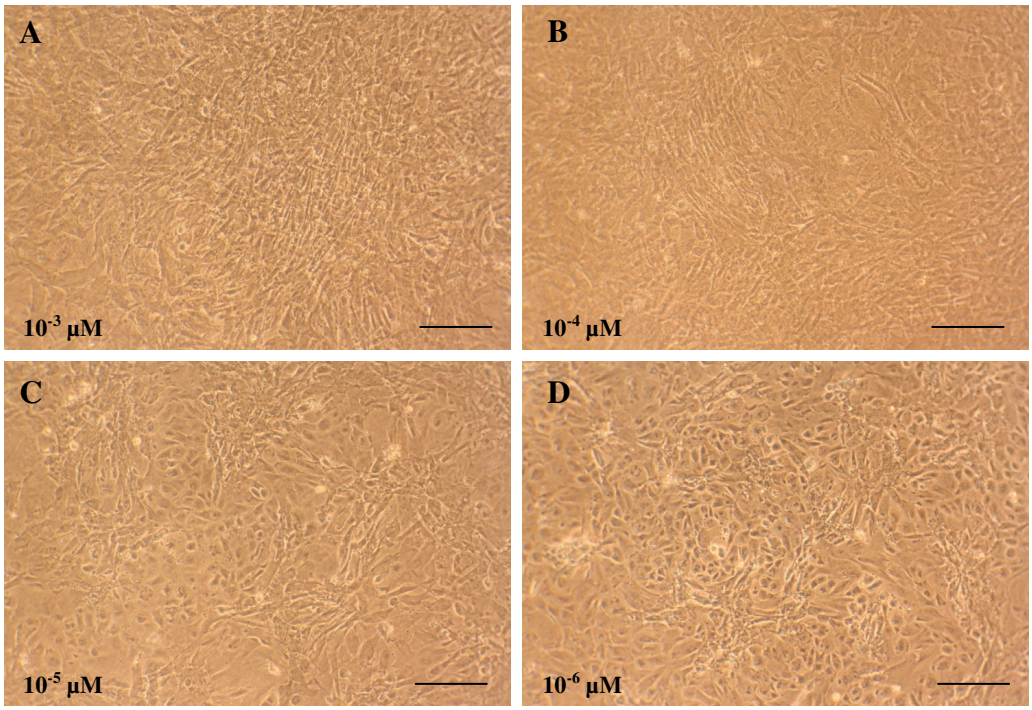

Figure 3.38 Morphological characteristics of CDCs grown in media containing different concentrations of ascorbic acid (magnification x10). *Passage 2 CDCs were treated with 0, 10^{-6}, 10^{-5}, 10^{-4} or 10^{-3} µM of ascorbic acid, respectively, every two days and then BDM for the remainder of two weeks. (**A - D**) Representative images were taken at the end of differentiation induction (A: 10^{-3}, B: 10^{-4}, C: 10^{-5}, and D: 10^{-6} µM of ascorbic acid). Scale bar = 200 µm. Abbreviations: CDC = cardiosphere-derived cell and BDM = basal differentiation medium.*

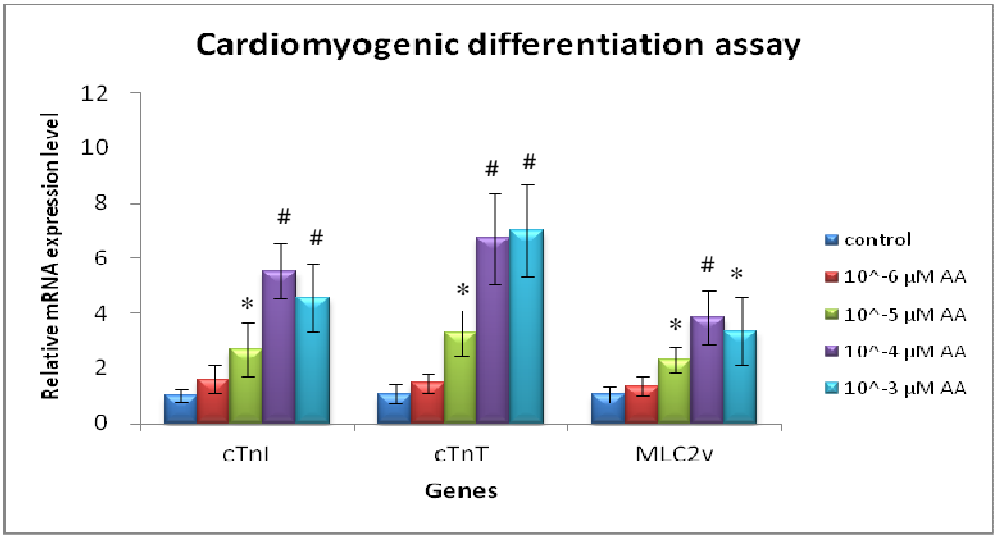

Figure 3.39 The relative mRNA expression level of cardiac-specific genes in differentiated CDCs using qRT-PCR. *Passage 2 CDCs were treated with 0, 10^{-6}, 10^{-5}, 10^{-4} or 10^{-3} μM of ascorbic acid, respectively. The expression levels of cardiac-specific genes cTnI, cTnT and MLC2v were quantified using qRT-PCR. All values were normalized to the housekeeping gene (GAPDH). mRNA expression was reported relative to control treated with BDM (n = 3). * $p < 0.05$ vs. control; # $p < 0.01$ vs. control. Abbreviations: CDC = cardiosphere-derived cell, cTnI = cardiac troponin I, cTnT = cardiac troponin T, MLC2v = myosin light chain-2v, AA = ascorbic acid, and BDM = basal differentiation medium.*

(II) Enhanced cardiomyogenic differentiation of CDCs by addition of ascorbic acid (10^{-4} μM)

Based on the results of Section **3.4.4.3**, DMSO (1 mM) or 5-Aza (1 μM) were combined with ascorbic acid. For DMSO and 5-Aza only groups, 5-Aza (day 1, 2, and 3) or DMSO (day 1, 3, 5) was added to each well with BDM as indicated and BDM was then changed every other day after the last treatment of each agent for the remainder of two weeks. For DMSO+AA and 5-Aza+AA groups, DMSO or 5-Aza was given as above and AA (10^{-4} μM) was added to each well with BDM every other day after the last administration of each agent until two weeks. Over the induction period, cells gradually grew into dense clusters (Figure 3.40). At the end of two week culture, cells were harvested for qRT-PCR, which showed that addition of AA significantly up-regulated gene expression of cardiac troponin T compared to DMSO only or 5-Aza only, suggesting the synergistic effect of AA on cardiac differentiation (Figure 3.41).

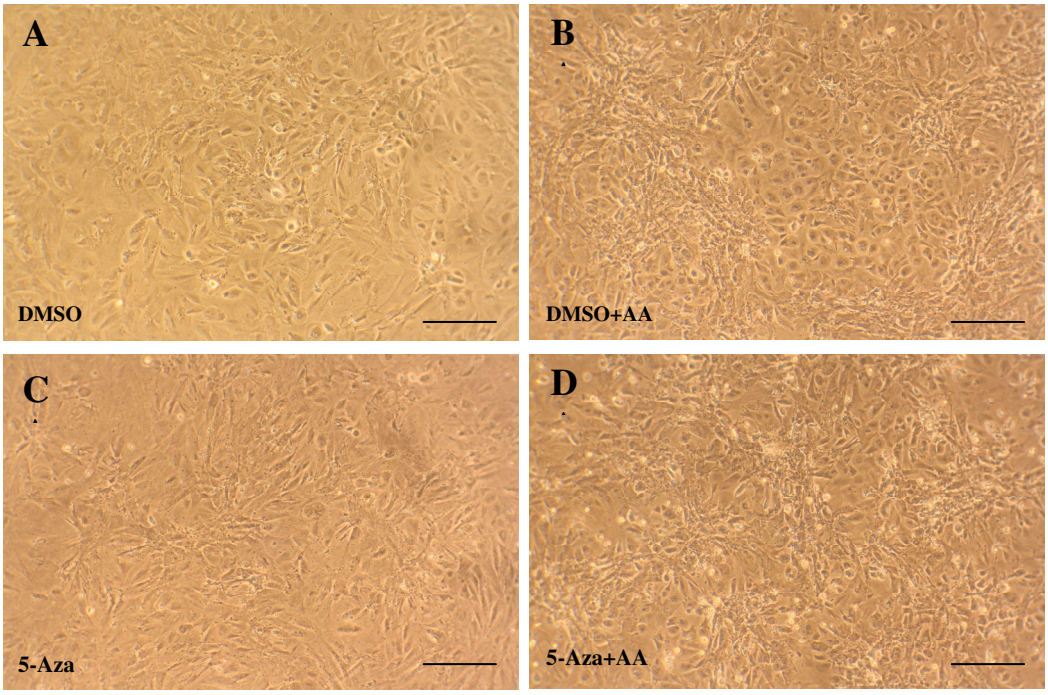

Figure 3.40 Morphological characteristics of CDCs grown in medium containing various differentiating inducers (magnification x10). *(**A - D**) Representative images were taken at the end of differentiation process. Passage 2 CDCs were treated with DMSO only (A), DMSO and then AA (B), 5-Aza only (C), or 5-Aza and then AA (D), respectively. Scale bar = 200 μm.*

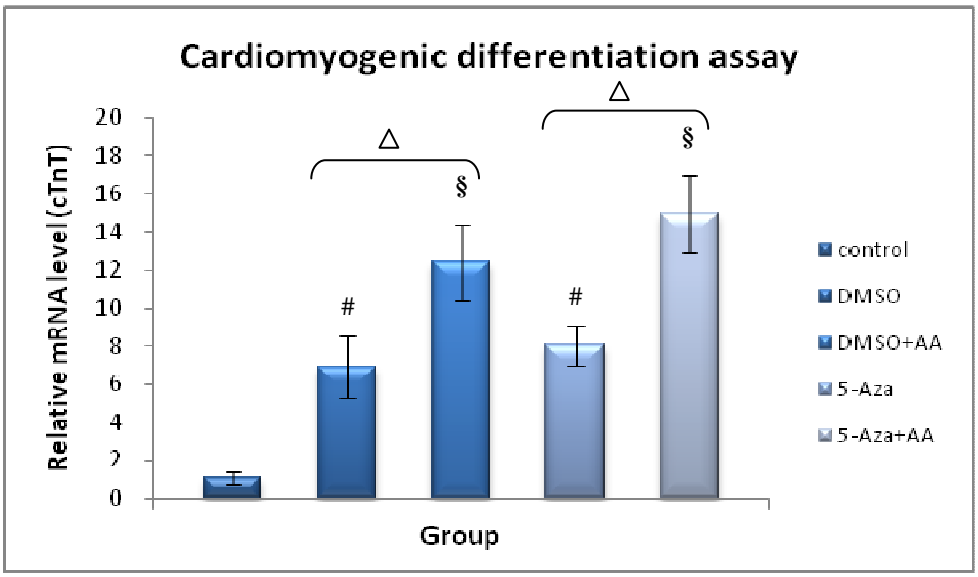

Figure 3.41 Quantitative RT-PCR showing the relative mRNA expression level of cTnT in CDCs treated with various inducers. *Passage 2 CDCs were induced for cardiac differentiation using various agents. All values were normalized to GAPDH and mRNA level was expressed relative to control treated with BDM (n = 3). # $p < 0.01$ vs. control; § $p < 0.001$ vs. control; △ $p < 0.01$ vs. DMSO or 5-Aza. Abbreviations: CDC = cardiosphere-derived cell, cTnT = cardiac troponin T, DMSO = dimethyl sulfoxide, 5-Aza = 5-azacytidine, AA = ascorbic acid, and BDM = basal differentiation medium.*

3.4.4.5 Confirmation of cardiomyogenic differentiation by flow cytometry and immunocytochemistry

To confirm the findings of cardiomyocyte differentiation from qRT-PCR, cardiac-related protein expression was detected using flow cytometry and immunocytochemistry.

(I) Cardiac-specific protein expression by flow cytometry

The expression of intracellular cardiac-specific proteins (cTnT and ASA) was determined and quantified in the differentiated CDC population using flow cytometry (Figure 3.42).

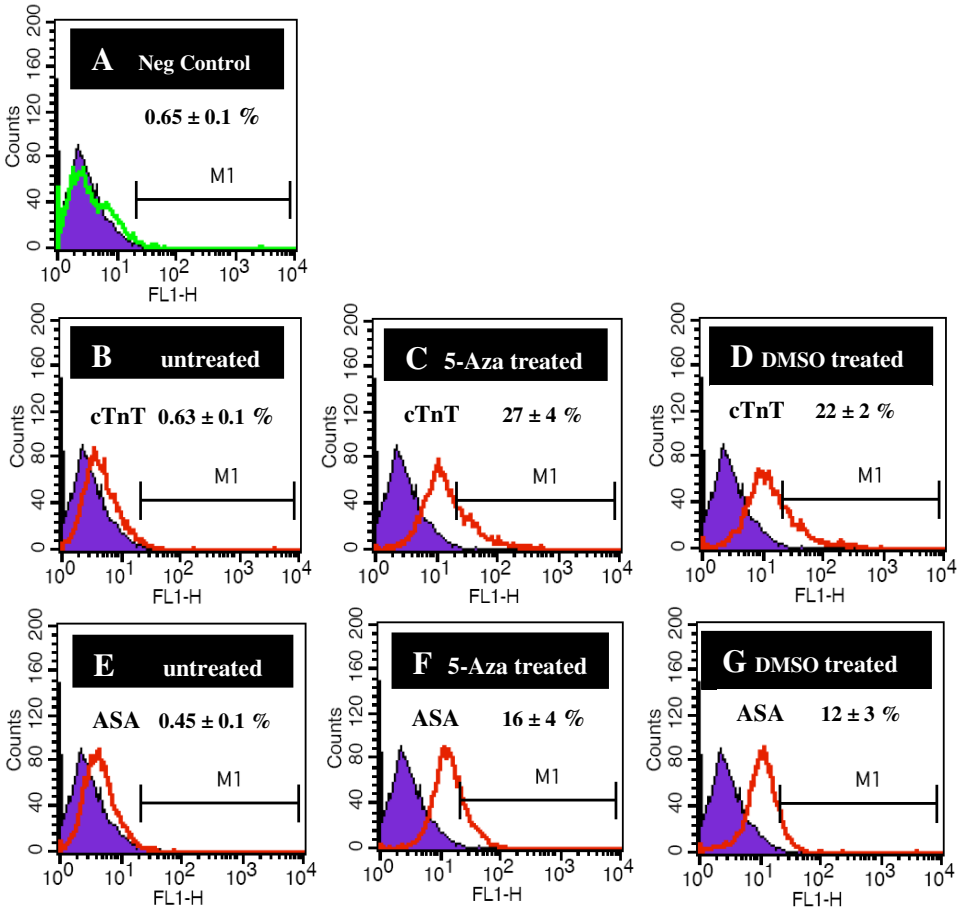

Figure 3.42 Flow cytometric analysis of cardiomyogenic differentiation of rat CDCs. *Passage 2 CDCs were treated with either 5-Aza plus AA or DMSO plus AA to induce differentiation into cardiomyocytes. (**A**) Cells which were stained only with secondary antibody served as a negative control (green line). (**B**-**G**) Flow cytometric analysis identified the presence of cardiac-specific markers in the induced CDC populations and determined the expression percentages of these markers including cTnT (middle panel) and ASA (lower panel). Cells present in region M1 were defined as the positive population. Purple region: unstained cell control. Red line: corresponding stained samples. Data are presented as mean ± SEM (n = 3). Abbreviations: CDC = cardiosphere-derived cell, 5-Aza = 5-azacytidine, DMSO = dimethyl sulfoxide, AA = ascorbic acid, cTnT = cardiac troponin T, and ASA = alpha-sarcomeric actin.*

(II) Cardiac-related protein expression in immunocytochemistry

Immunofluorescence staining was used to detect the expression of the specific cardiac structural protein (cMHC) in the differentiated CDC population after treatment with 5-Aza or DMSO plus ascorbic acid (Figure 3.43).

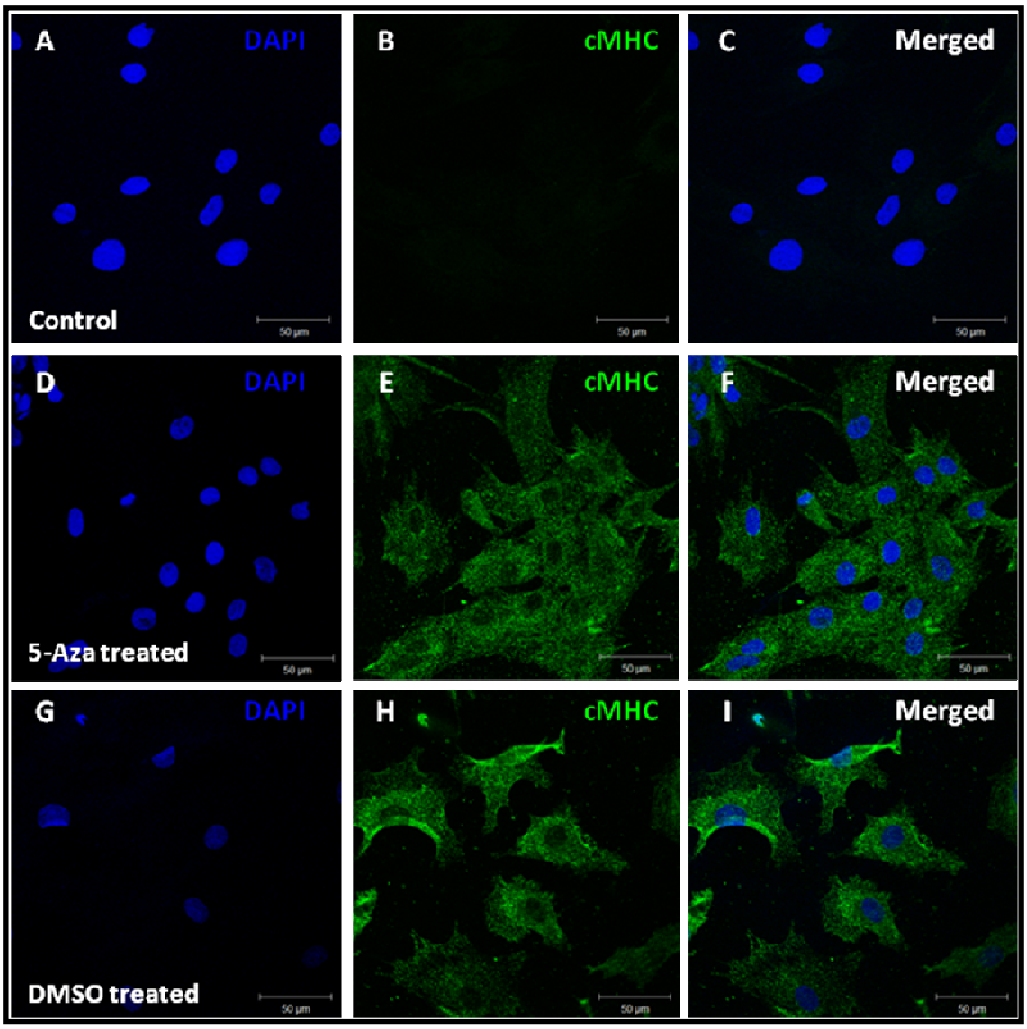

Figure 3.43 Immunocytochemical detection of cMHC in CDCs after cardiomyogenic differentiation. *For differentiation into cardiomyocytes, CDCs at passage 2 were treated with either 5-Aza or DMSO, followed by addition of ascorbic acid. After two weeks of treatment, cells were stained for cardiac myosin heavy chain (cMHC) for immunocytochemistry. Upper panel indicates control cells without differentiating agent treatment. Middle panel indicates 5-Aza-treated CDCs expressing cMHC (green, AF 488). Lower panel indicates DMSO-treated CDCs expressing cMHC (green). Nuclei were counterstained with DPAI (blue). Scale bars = 50 µm. Abbreviations: CDC = cardiosphere-derived cell, 5-Aza = 5-azacytidine, DMSO = dimethyl sulfoxide, AF 488 = AlexaFluor 488, cMHC = cardiac myosin heavy chain, and DAPI = 4′, 6-diamidino-2-phenylindole.*

3.6 Discussion

For myocardial injury and chronic HF, the clinical application of stem cell therapy strategies using cell transplantation is limited by low retention and poor survival of donor cells. Thus, the work in this chapter focused on the potential of stem cell culture in combination with cardiac tissue engineering for use in the treatment of HF at various stages.

Isolation, expansion and characterization of rat CDCs

A variety of adult stem cell types have been investigated for the purpose of cardiac repair in animal and clinical studies. Among them, cardiac stem cells have recently emerged as a promising cell source due to their advantages including autologous origin, cardiac committment and multipotent capacity. Although it remains uncertain which resident cardiac stem cell is the ideal candidate in the clinical setting, cardiosphere-derived cells (CDCs) have been successfully isolated and expanded to yield therapeutically-relevant numbers from tiny human endomyocardial biopsies [37].

In the present study, CDCs were isolated from adult rat hearts and expanded *via* the formation of cardiospheres. These cells were characterized using immunocytochemistry and flow cytometry targeting specific proteins associated with the identification and differentiation of cardiac stem cells. In agreement with the previous report by Smith *et al.* [165], the immunocytochemical analysis showed that *in vitro* cultured CDCs were a mixed population containing cardiac stem and progenitor cells (expressing c-kit, Oct3/4, and Sox2), mesenchymal stem cells (CD90), cardiac-committed cells (Nkx2.5) and differentiating cardiomyocytes (cTnT). Flow cytometric analysis further confirmed and quantified the percentages of cells expressing c-kit or CD90 in the CDC population.

The adult heart muscle is a mosaic tissue consisting of many types of differentiated cells, including not only cardiomyocytes (30%), but also fibroblasts (60%), vascular smooth muscle, endothelial cells, specialized cells (i.e., pacemaker cells) and purkinje fibers [67]. To generate a functional bioartificial heart, therefore, in addition to repopulation of cardiomyocytes, it is also

necessary to provide the heart with other cell types resident in the normal myocardium for optimal cardiac function [249]. Thus, cultured cardiosphere-derived CSCs represent a plausible autologous cell source for the population of biomaterial-based scaffolds and bioengineered decellularized heart matrix due to their composition of multiple lineages.

Cardiac tissue engineering

Myocardial patch - alginate scaffolds

Due to its biocompatibility and unique gelation property, alginate may be used in cardiac tissue engineering [48]. Leor and colleagues prepared 3D porous alginate scaffolds seeded with fetal rat cardiac cells using a freeze-drying technique. After the scaffolds were implanted onto the injured myocardium as a pericardial patch in a rat model of MI, the biografts enhanced neovascularization, attenuated left ventricular dilation and improved heart function [57].

This is the first study where cardiac stem cells (CDCs) have been grown in alginate hydrogel scaffolds precoated with ECM proteins. In contrast to freeze-drying, a rapid-curing gelation method was adopted here to fabricate alginate scaffolds [250]. CDCs were evenly distributed in the porous alginate constructs because the cells were pre-suspended in sodium alginate before gelation instead of onto dry alginate scaffolds.

Under the same concentration of sodium alginate (2% or 1%), calcium ion levels did not affect CDCs viability. Similarly, a study by Simpson *el al.* reported that βTC3 cell growth within alginate gels with high mannuronate content were not affected by different calcium concentrations [251]. Although CDCs were metabolically active in alginate constructs after 24 hours, the number of active CDCs was approximately 50% of that formed when cells were grown in a monolayer, suggesting that cell survival was significantly lower within the thicker construct. This cell death could be explained by poor cell attachment and oxygen/nutrient diffusion restrictions in 3D alginate scaffolds. ECM proteins (e.g., collagen and fibronectin) are components that play important functions in the interactions between cells and ECM, such as cell attachment, proliferation and migration, through integrins (cell surface receptors) [67]. To

help CDCs remain and grow within alginate constructs following seeding, ECM proteins were first added to facilitate cell adhesion by coating the surface of the interconnective pores, resulting in increased cell viability.

CDCs grew and survived for up to 49 days within the scaffold with a two-fold increase in cell number from day 7. This indicated that culture of CDCs in alginate constructs is possible, but limited by sluggish diffusion of nutrients through the matrix. In terms of mechanical integrity, alginate scaffolds remained intact when handled at day 49. *In vitro* culture of CDCs within alginate scaffolds enables us to be familiar with growing cells in 3D environment in a synthetic or bioengineered extracellular matrix.

Heart decellularization and recellularization

Creating a whole heart is complicated by its intricate structure due to the anisotropic orientation of muscular bands and collagen fibers (Figure 3.44). Another challenge is to establish and arrange epicardial coronary arteries and their gradual branching vessels, intercalating through cardiac muscle itself, which are critical to nourish a variety of cells for normal heart function [244].

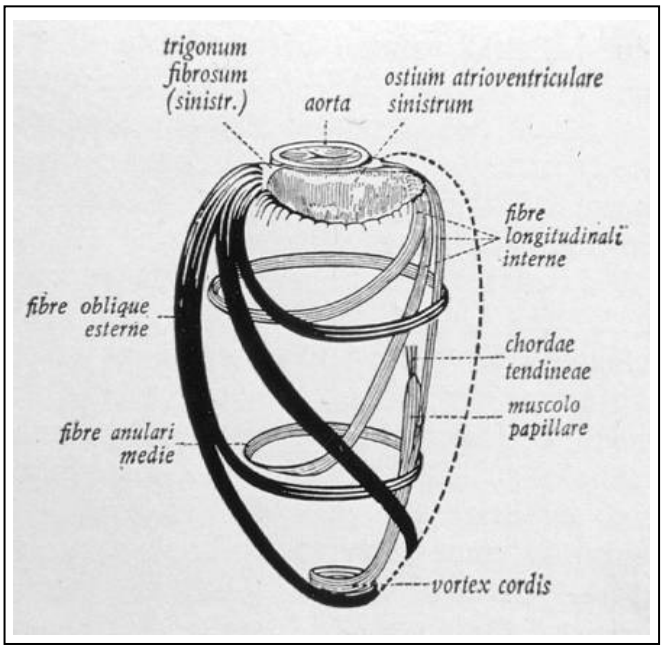

Figure 3.44 Cardiac muscle orientation. *(http:/biomed.brown.edu/courses/BII08/2006-108websites)*

Acellular ECM of cardiovascular tissues, such as pericardium, vascular wall, and valve leaflets, has been engineered with the use of immersion decellularization technique [58, 59]. The current study described an efficient and reproducible method of perfusion decellularization for the intact adult rat heart. In this work, some modifications to the decellularization process were adopted, including two washes with cold heparinised PBS, longer perfusion with heparinized PBS containing adenosine before the start of decellularization and PBS perfusion for 1 h at the end to facilitate the efficiency of detergent perfusion during the process and full removal of detergent in the end. After coronary perfusion with detergent for 12 hours, decellularization of rat hearts was confirmed by histological and immunohistochemical analyses. Furthermore, the structural and functional characterization of decellularized heart constructs was performed using immunohistochemistry, high-resolution magnetic resonance imaging (MRI) and Evan's blue dye. It is well known that MRI provides excellent evaluation of anatomical details. High resolution 2D and 3D MRI exhibited the weave and orientation of the remaining extracellular matrix following decellularization, which corresponded to native muscular fiber bands. Compared with immunohistochemistry, without the need of tissue sectioning, cine-MRI can directly give detailed 2D and 3D information of cardiac structures (e.g., intact valve leaflets), which can serve as predictors of a structurally preserved bioartificial heart. Moreover, MRI is able to be used for functional assessment of a recellularized heart during maturation. The presence of an organ-specific ECM may provide not only cues for engrafted cells to drive their migration, alignment, and integration but also signals to guide their differentiation and proliferation [244, 252]. Apart from cardiac architecture and myocardial interlacing pattern, coronary vascular trees were macroscopically identified up to second branching vessels and functionally confirmed based on the movement of Evan's blue dye. The remaining vascular network functions as a conduit for distribution of infused cells throughout the whole heart and for transfer of culture media to support cell viability and proliferation [244, 252].

As shown by Ott *et al.* [76], the acellular heart matrix generated is a suitable scaffold for cardiac organ engineering in terms of the prerequisites of decellularization and ECM preservation. The decellularized heart construct was reseeded with CDCs *via* both intramyocardial injection and

intracoronary infusion in a pilot study. Confocal microscopy confirmed the presence of MPIO-labeled and DiI-stained CDCs in the recellularized heart tissue, indicating that cells were retained in the heart extracellular matrix.

Wainwright *et al.* have described the methodology of perfusion decellularization for a large porcine heart and demonstrated the preserved passive mechanical behaviour and capability of supporting heart cells on decellularized porcine hearts [252]. Additionally, a number of groups have investigated the possibility of perfusion decellularization for various organs, including lungs [253, 254], liver [255, 256] and kidneys [257, 258], in animal models. In a clinical case, Macchiarini and colleagues implanted a bioengineered airway, made using a decellularization-recellularization technique, to a patient with end-stage airway disease and found that there were no anti-donor antibodies detected up to two months after operation [259].

Subsequently, the decellularized rat heart matrix will be repopulated with either CDCs only or a mixture of CDCs and differentiated CDCs (cardiomyocytes) prior to cultivation for a period of time, depending on the progress of maturation. The use of undifferentiated and differentiated CSCs (i.e., cardiac myocytes, endothelial and smooth muscle cells etc) to reseed a decellularized heart matrix is a novel and exciting direction of research in the regenerative medicine field. It is planned to optimize the recellularization in a sterile culture system, which mimics *in vivo* physiological conditions, including suitable temperature, oxygen/carbon dioxide levels and substrates and provides pulsatile flow and synchronized pacing. The designed culture system equipped with pulsatile flow will create an environment with preload and afterload, which allows the recellularized heart construct to mature.

Although this technique provides a prospective promise for whole organ engineering, there is still a long way to go before the clinical application becomes practical in the real world. Cell expansion *in vitro* will need to be optimised to generate tha large number of cells required to repopulate the decellurised scaffold. Functional assessment of the engineered bioartificial heart should be made, including hemodynamic measurement (LVP and afterload) using a pressure transducer and electrophysiological studies (ECG tracings with and without electric or drug

stimulation). Using MRI, systolic and diastolic function of the LV can be evaluated *in vitro* at various time points. Magnetic resonance spectroscopy (MRS) will be used to investigate energy metabolism within the recellularized heart. Also, calcium imaging can be considered to determine the status of intracellular Ca^{2+}, related to electrical impulse conductivity and cardiac muscle contraction.

Differentiation of CDCs into the cardiomyocyte lineage

There are a variety of strategies that could possibly be utilized to direct and control the cardiomyogenic differentiation of stem cells *in vitro,* such as coculture, inducing factors and physical stimuli [248]. With coculture, several studies have reported transdifferentiation of adult stem cells into cardiomyocytes [145, 260, 261]. Furthermore, cardiac stem cells, including cardiac SP cells and Isl-1^+ progenitors, can differentiate into cardiomyocytes by coculture with adult or neonatal cardiomyocytes [188, 196]. In addition, rat CDCs were found to differentiate toward spontaneously beating cardiac myocytes when co-cultured with neonatal rat cardiomyocytes in our lab (unpublished data). In the clinical scenario, however, it would not be practical to induce differentiation of stem cells into cardiac myocytes through coculture with an allogenic or xenogenic cell source as co-culture of two distinct cell populations may bring a hidden danger of pathogen transmission (e.g., viruses). Another major limitation of this technique is the difficulty in the separation of co-cultured cell populations [248].

A number of cytokines, growth factors and synthetic chemicals have the potential for induction of cardiomyogenic differentiation in embryonic and adult stem cells. Among the synthetic chemicals, 5-azacytidine, DMSO, ascorbic acid and retinoic acid are well known to induce *in vitro* cardiomyogenic differentiation [248, 262]. 5-azacytidine (5-Aza), a synthetic nucleoside, is commonly used as an inhibitor of DNA methylation in the treatment of cancers [248, 262]. It is an effective inducer of cardiomyocyte differentiation in various stem cell types, such as embryonic [263], mesenchymal [264-266] and cardiac [179, 184, 267] stem cells. Nevertheless, the exact mechanism of 5-Aza on the induction of cardiomyocyte differentiation remains somewhat unclear, but is postulated to be linked to the mediation of gene activation *via* the

demethylating process [179, 268]. Dimethyl sulfoxide (DMSO) has been commonly used for cryoprotection but also encourages cardiomyogenic activity in embryonic stem cells [269] as well as embryonal carcinoma cells [270]. It has been reported that DMSO triggers the expression of Nkx2.5 and Gata4, and increases intracellular Ca^{2+} levels [262]. The molecular mechanism by which DMSO induces cardiomyogenic differentiation is not well elucidated. There are reports showing that DMSO treatment activated both the canonical Wnt pathway and the PI3K pathway [271]. Ascorbic acid, also called vitamin C, is well known for its antioxidative properties. Richard and his colleagues screened 880 FDA-approved compounds and found that ascorbic acid enhances the differentiation of cardiac myocytes from embryonic stem cells [272]. However, the molecular mechanism of ascorbic acid promoting cardiomyogenic differentiation is still unascertained. Moreover, this seems to be independent of its antioxidative activity as other antioxidants, including N-acetylcysteine, Tiron and vitamin E, do not induce the differentiation of embryonic stem cells into cardiomyocytes [262, 272].

Although a large number of studies have investigated differentiation of various stem cell types into cardiomyocytes, there is little research focusing on the *in vitro* directed cardiomyogenic differentiation of cardiac stem cells. Furthermore, previous studies mainly inspected the differentiation of c-kit$^+$ or Sca-1$^+$ stem cells. It should be emphasized that this was the first time to induce the cardiomyocyte differentiation of CDCs *in vitro* using low serum and chemical reagents (5-Aza, DMSO, and ascorbic acid). Here, I examined the cardiogenesis-inducing effect of these chemicals on CDCs and determined the optimal concentrations by treating cells with different levels of these inducers. I also explored the effect of serum concentration on the cardiomyogenic differentiation of CDCs. Similar to the findings demonstrated by Tang *et al.* [183], our results showed that CDCs have a tendency to differentiate towards cardiomyocyte lineage (spontaneous differentiation) in low serum. Interestingly, there were several reports describing that serum-free culture condition has a permissive effect on differentiation in various cell types, such as skeletal myoblasts and undifferentiated neuroblastoma cells [273-275]. In addition, it was revealed by Sachinidis *et al.* that serum plays an inhibitory role in cardiomyocyte differentiation of mouse embryonic stem cells [276]. This phenomenon seems to

suggest that stem cells prefer differentiation to proliferation when cultured in low serum concentrations. However, it should be noted that as the composition of serum is complex and poorly defined, cardiogenic stimulatory and inhibitory factors may both exist in serum and be involved in multiple signalling pathways mediating cardiogenesis [248, 275]. Accordingly, whether stimulation or inhibition of cardiomyogenic differentiation predominates in culture depends on when serum is added and its concentration during the induction period [275].

With respect to the impact of 5-Aza on cardiomyogenic differentiation, the expression of a cardiac-related gene (cTnT) was significantly up-regulated under the treatment with 5-Aza (10 μM) compared to the control (0 μM), but 5-Aza led to a substantial inhibition of cell proliferation. 5-azacytidine has been shown to kill cells [184], and inhibit cell proliferation in a dose-dependent manner [268]. In the comparison of efficiency of various concentrations, it was shown that treatment of CDCs with 1 μM 5-Aza gave rise to the greatest up-regulation of cardiomyocyte-related marker levels (cTnI, cTnT, and MLC2v) among four groups of 0, 1, 5, and 10 μM of 5-Aza in the BDM. Similarly, Choi *et al.* cultured P19 embryonic stem cells in medium containing 0, 0.5, 1, 2, 5, and 10 μM of 5-Aza and found that treatment with 1 μM significantly increased the expression of cardiac specific markers, such as Gata4 and β-MHC relative to the undifferentiated control [268]. Furthermore, Yoon and colleagues showed that 0.1 μM of 5-Aza significantly enhanced the expression level of cardiac-specific transcription factors (Nkx2.5 and Gata4) and genes (ANP, α/β-MHC, and MLC2v), and simultaneously increased the number of beating cells among different 5-Aza treatment groups of 0, 0.1, 1 and 10 μM [277]. This means that the concentration of 5-Aza is critical in the differentiation efficiency of stem cells into cardiomyocytes due to the compromise from its concomitant toxic effect [277]. Moreover, it is important to note that the optimal dose of 5-Aza for cardiomyocyte differentiation depends on the type of stem cells and the culture conditions.

Again, four concentrations of DMSO in BDM (i.e., 0, 1, 10, and 100 mM) were chosen to induce cardiomyocyte differentiation. A significant increase in the expression level of cardiomyocyte-related markers (cTnI, cTnT, and MLC2v) was detected by qRT-PCR when

CDCs were treated with 1 mM of DMSO, compared to that of the untreated control. Furthermore, CDCs were exposed to BDM containing ascorbic acid at various concentrations to examine its role, as well as the optimal dosage in cardiomyocyte differentiation. This is in agreement with the work by Takahashi *et al.,* who found ascorbic acid significantly increased the efficiency of cardiomyogenic differentiation of CGR8 embryonic stem cells, but determined the optimal concentrations of ascorbic acid for cardiac differentiation at between 10^{-4} and 10^{-3} μM [272]. In the current study, CDCs were significantly differentiated into cardiac phenotype at the concentration of 10^{-4} μM.

It has been suggested that heart development and cardiac cell lineage differentiation are associated with complex molecular mechanisms and multiple signalling pathways during embryogenesis [262, 278, 279]. Wang *et al.* investigated the effect of combined treatment of 5-Aza and ascorbic acid on cardiomyocyte differentiation of human embryonic stem cells and found that dual treatment produced significantly more cardiomyocytes compared to single treatment [280]. In the present study, it was also demonstrated that the combination of either 5-Aza and ascorbic acid or DMSO and ascorbic acid is superior to the treatment with 5-Aza or DMSO alone in the induction of cardiac myocyte differentiation, suggesting that the addition of ascorbic acid further enhanced the extent of differentiation. On the other hand, there was no significant difference of the differentiation efficiency in the differentiated CDC population with the combined treatment. Furthermore, Smits *et al.* isolated human cardiomyocyte progenitor cells (hCMPCs) using mouse anti-Sca-1 antibody, and differentiated these Sca-1-like stem cells into functionally mature cardiomyocytes with great efficiency (80-90%) using a combination treatment of 5-Aza, followed by transforming growth factor beta-1 (TGF-β1) and ascorbic acid (3 weeks of induction period in total). Interestingly, they found that while treatment with 5-Aza and AA induced the expression of cardiac and contractile genes, addition of TGF-β1 further led to a highly significant improvement in efficiency of differentiation and extent of maturation [184].

Taken together, after treatment with 5-Aza, DMSO or ascorbic acid, qRT-PCR showed the up-

regulated expression of cardiomyocyte-specific genes including cTnI, cTnT and MLC2v. Flow cytometry and immunocytochemistry identified the expression of cardiac-related structural proteins (cTnT, ASA and MHC) in the differentiated CDC population. All of these results indicated that CDCs were directed to differentiate into the cardiomyocyte phenotype when treated with inducers *in vitro*. However, there were no beating cardiomyocytes found during the two weeks induction. This might suggest that the induced cardiomyocytes may be not mature enough or they need extrinsic triggering stimuli to initiate contraction *in vitro*. Thus, a longer period of differentiation culture could be used or the differentiating myocytes provided with additional factors or stimulation such as TGF-β1, electrical pulses or pharmacological stimulants (e.g., norepinephrine).

Study limitations

I am aware of several limitations in this study. Firstly, CDCs could be differentiated towards cardiomyocyte-like cells based on the expression of cardiac-specific genes and proteins; however no beating cells were observed due to immature phenotype or no extrinsic stimulation. Secondly, to recellularize a bioartificial decellularized heart matrix, in addition to cardiac myocytes, a variety of other cardiac cells are also needed such as endothelial cells, smooth muscle cells, pacemaker cells and purkinje fibers. Optimistically, CSCs have been shown to be able to give rise to vascular cells and sinus node-like cells following induction [160, 377].

Additionally, despite repopulation with proliferating stem cells and various specialized cells, substantial *ex vivo* expansion is still required to produce sufficient cell numbers to reseed an accellular whole heart. Hence, there is a need of an optimal method to efficiently grow cells without causing chromosomal instability and phenotypic shift. Finally, tissue and/or organ engineering approach for cardiac repair involves invasive surgery of implantation, matrix integration into native myocardium, and tensile strength and functional maturation of engineered scaffolds, which have not yet been investigated.

3.6 Conclusion

In the present study, cardiosphere-derived cells were isolated and expanded *via* the formation of cardiospheres from adult rat hearts, which comprised cardiac stem/progenitor cells, mesenchymal cells, endothelial progenitors and cardiac lineage-committed cells based on phenotype characterization. Furthermore, cardiosphere-derived stem cells could be differentiated towards the cardiomyocyte lineage when exposed to 5-Aza, DMSO or ascorbic acid alone and it was found that combined treatment of 5-Aza or DMSO with ascorbic acid significantly enhanced the differentiation efficiency compared to 5-Aza or DMSO alone. Many studies have suggested that there are multiple signalling pathways implicated in the cardiomyogenic process of stem cells in the natural environment. As a result, if a variety of approaches (i.e., inducing factors and stimuli) were utilized in combination, cardiomyocyte differentiation may be further enhanced and fully completed in terms of efficiency and maturity as needed.

With regard to stem cell-based tissue/organ engineering, it was shown that the whole rat heart can be decellularized using coronary perfusion of detergents. The key advantages of this approach include the preservation of the complex 3D architecture and perfusable vascular networks, which would enable the generation of a clinically applicable bioartificial heart after recellularization and organ maturation without concern of immune rejection. Collectively, although there is still much research to be done, the strategy of generating a bioartificial organ has paved the way for transplantation of a tissue-engineered heart in the future.

Chapter 4

Characterization of cardiac-derived stem cells and effects of age on isolation and function

4.1 Abstract

Age is a major risk factor for a variety of cardiovascular diseases. Increased age may result in a progressive decline in number and/or function of available CSCs. Also, stem cell behaviour is determined by cardiac niches where CSCs reside. Therefore, the objectives of this study were to investigate the impacts of aging and sampling location on CSC isolation and function *in vitro*. CSCs were isolated as explant-derived cells (EDCs) and expanded to cardiosphere-derived cells (CDCs) *via* cardiosphere formation from the hearts of C57Bl/10 mice. Adult mouse CDCs comprised stem cells expressing c-kit, Sca-1, Oct3/4, and Sox2 and mesenchymal cells expressing CD90 and CD105. CDCs isolated from atria contained more c-kit or Sca-1 positive cells than those from ventricles (c-kit: 13 % vs. 3.4%, $p < 0.01$; Sca-1: 82% vs. 53%, $p < 0.01$, respectively). In addition, atrium-derived CDCs possessed greater clonogenic and proliferative potential than ventricle-derived cells. To investigate the effects of age, CSCs were cultured from mice aged 1.5, 6, 18 and 24 months old. Younger mice produced significantly more EDCs, cardiospheres, and CDCs per mg tissue, compared with 24 month-old mice. CDCs derived from 1.5 month-old mice exhibited substantially higher expression of cardiac stem cell markers including c-kit and Sca-1 than those from 24 month-old mice (c-kit: $p < 0.01$; Sca-1: $p < 0.001$, respectively). EDCs and CDCs from aged mice showed decreased distance of migration, compared with those from young animals. Higher proliferative ability and clonogenic efficiency were also found in CDCs from younger mice. Following induction of cardiomyogenic differentiation, it was found that CDCs from young mice displayed a higher expression of the cardiomyocyte-specific markers, cTnT and cMHC. Shortened telomere length and down-regulated telomerase activity were observed in CDCs from older animals. In conclusion, the atrium may represent a desirable region for biopsy collection. CSCs can be isolated and expanded from young and old mice; however, from aged animals, a reduced number of cardiac-derived stem cells were generated with the CSCs showing impaired proliferation, migration, clonogenicity and differentiation.

4.2 Introduction

Within the adult heart, cardiac stem cells (CSCs) are stored in cardiac niches that offer a specialized microenvironment to replenish lost myocardial cells and maintain a balance of survival, proliferation and self-renewal of CSCs [159]. CSC clusters are spread throughout the myocardium in adult hearts; however, the distribution of cardiac niches seems to be conditioned by the different level of wall stress [281]. At the cellular level, physical load, mechanical deformation and high wall tension play roles in the regulation of cell behaviour and fate. In other words, external forces modulate cell migration, proliferation, differentiation and death [282-286].

Although CSCs can be isolated from different regions of a heart for *ex vivo* expansion, they exist in small numbers *in vivo* (one CSC per 30,000-40,000 myocardial cells) [169, 286]. The relationship between the sampling location in the heart and the *in vitro* expansion and properties of CSCs has not yet been completely determined. Here, CDCs were generated from two areas with distinct pressure and volume loads (i.e., atrium and mid-portion ventricle) to explore the impact of the wall stress on the isolation and characteristics of CSCs, which might provide better understanding of the optimal sampling region for endogenous stem cells in terms of therapeutic potential.

It has been proposed that there is a general decline in the number and/or function of stem cells with increased age in various stem cell types [221]. Hill *et al.* demonstrated an inverse correlation between the number of circulating endothelial progenitor cells and age [287]. A study by Scheubel *et al.* also reported that aging inhibits endothelial progenitor cell mobilization in patients undergoing CABG [288]. Moreover, other researchers have shown that aging is involved in mediating intrinsic characteristics of stem cells, such as cell growth, proliferation, differentiation, and senescence [37, 217-219, 289].

Clearly, epidemiological studies show that heart diseases are prevalent among the elderly population [290]. To take advantage of the therapeutic capability of autologous CSCs, the impacts of age on CSC isolation, expansion and regenerative potential need to be fully

investigated. In the present study, CDCs were isolated and expanded *in vitro* from hearts of young (1.5 month-old), middle-aged (6 month-old), old (18 month-old) and very old (24 month-old) mice to determine age-related alterations in stem cell characteristics and test the hypothesis that older animals have lower numbers of CDCs due to exhaustion and that these cells might have impaired biological properties.

Taken collectively, both high wall stress and aging may deplete the stem/progenitor cell reservoir and impair their inherent biological characteristics [221]. The hope is that this study will provide further insight into the effects of the cardiac region and chronological aging on CSCs in terms of cell culture yield and relevant therapeutic potential, which are directly associated with clinical applicability.

The work in this chapter focused on the characterization of mouse cardiosphere-derived stem cells and the understanding of effects of age on isolation and function of CSCs. Specifically, the aims were to:

- Isolate, expand and characterize cardiac-derived stem cells *in vitro via* the formation of cardiospheres from wild-type adult mouse hearts.
- Generate CDCs from different regions of the heart and determine the correlation between the location of biopsy and CSC biological characteristics.
- Investigate the impacts of age on the therapeutic potential of CDCs in terms of isolation and biological properties.

4.3 Methods

This chapter comprised of two studies: (I) *in vitro* isolation, expansion, characterization and differentiation of cardiac stem cells from different regions of the mouse heart, and (II) effects of age on isolation, characterization and function of cardiac stem cells from mouse hearts.

(I) *In vitro* isolation, expansion, characterization and differentiation of cardiac stem cells from different regions of mouse hearts

4.3.1 Isolation and expansion of cardiac stem cells from atria and ventricles

In this study, C57Bl/10 mice (6 weeks old) were used to generate cardiac stem cells (CSCs). All cell culture was carried out in a humidified atmosphere of 5% CO_2 and 95% air at 37^{o}C. Cardiosphere-derived stem cells were produced *via* the formation of cardiospheres from heart explants, as described in Chapter 2. To make explant cultures, heart tissues were divided into atrial and ventricular (mid-portion) parts, which were then plated in separate dishes to grow explant-derived cells (EDCs). Subsequently, EDCs were harvested and seeded on poly-D-lysine coated multiwell plates to generate cardiospheres when reaching 70-80% confluency. Cardiospheres were cultured on fibronectin-coated flasks to grow into monolayer cardiosphere-derived cells (CDCs). Once confluent, CDCs were trypsinized and further expanded up to passage 2 for experiments. All the procedures were processed according to the protocols described in Chapter 2 with modifications of the culture period, as mouse cell growth was slower than that of rat cells. A simplified flow scheme was presented below to depict the steps (Figure 4.2).

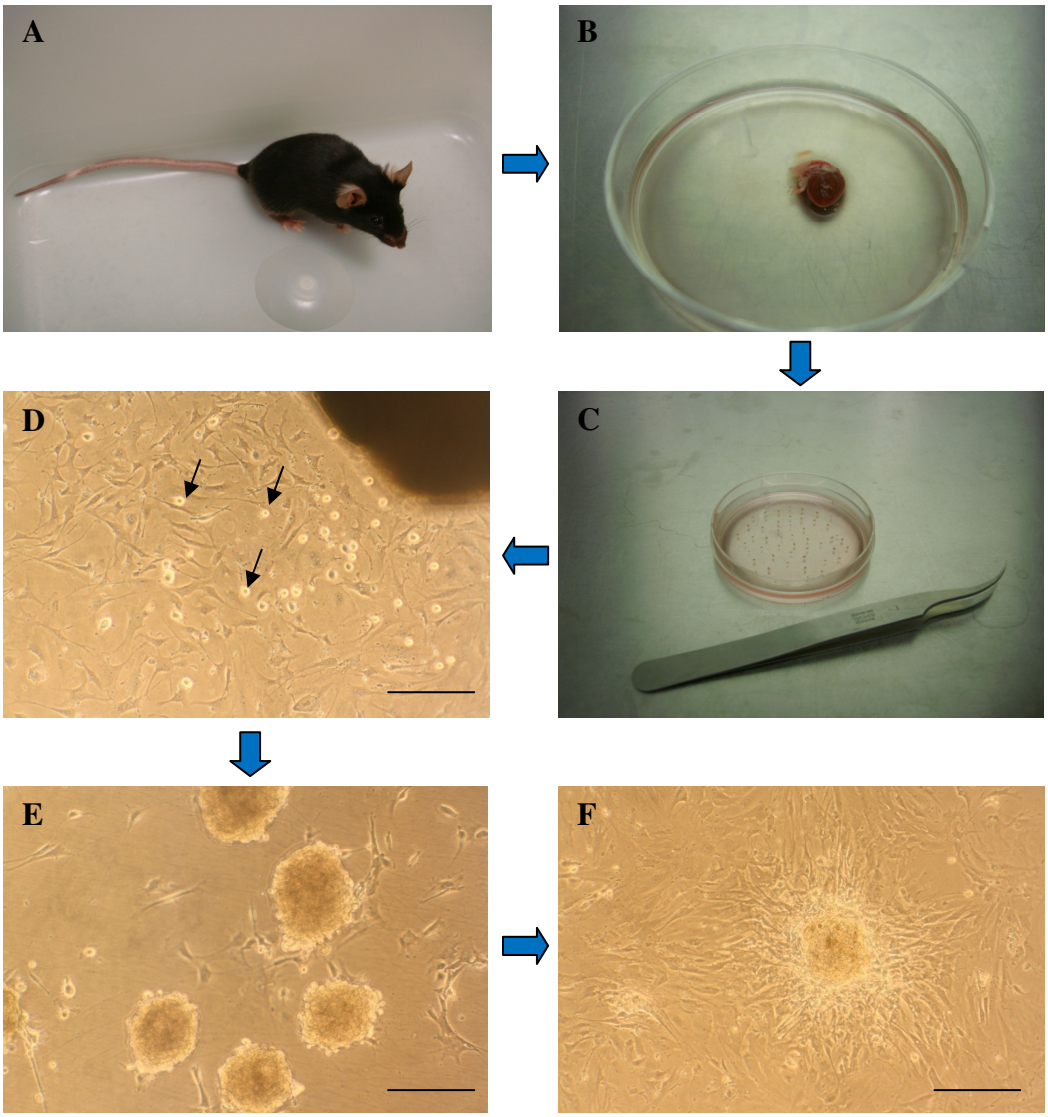

Figure 4.2 Heart sample processing for cardiosphere growth and cardiosphere-derived cell expansion. *(**A**) A mouse ready for heart removal. (**B**) Excised heart washed in PBS in a petri dish. (**C**) Explant fragments plated on a fibronectin-coated dish. (**D**) Explant-derived cells consisted of stromal-lke cells and phase bright cells (black arrow). (**E**) Fully formed cardiospheres in a poly-D-lysine coated well. (**F**) Cardiospheres grew into a monolayer of cardiosphere-derived cells on a fibronectin-coated culture flask. Scale bars = 200 μm.*

4.3.2 Cell proliferation assay

Cardiosphere-derived cells were seeded into 96 well plates at a density of 500 cells per well and proliferation measured using AlamarBlue® according to the protocol described in Chapter 2. The proliferation of CDCs derived from different age groups (n = 4 from each group) was determined at day 1, day 2, day 3, day 5 and day 7. The statistical differences between the four age groups were analyzed using one-way ANOVA with Tukey post hoc test.

4.3.3 Clonogenic assay

For clonogenic analysis, CDCs isolated from different age groups, 1.5, 6, 18 and 24 months, were cultured (n = 4 for each group). CDCs at passage 2 were trypsinized and seeded at a single cell per well of 96 well plates. A total of 4 plates were analyzed for each sample. The wells containing a single cell were identified and followed up for two weeks. The clonogenic efficiency of CDCs was measured by counting the number of wells generating single clones in each 96 well plate as described in Chapter 2. The statistical differences of the clonogenicity of CDCs derived from different age groups were analyzed using one-way ANOVA with Tukey post hoc test.

4.3.4 Phenotypic characterization of cardiac stem cells

Phenotypes of cardiac stem cells were characterized using immunocytochemistry and flow cytometric analysis, based on the expression of cell surface and intracellular markers, including cardiac stem cell markers (c-kit and Sca-1), pluripotent stem cell markers (Oct3/4 and Sox2), mesenchymal stem cell markers (CD90 and CD105), hematopoietic stem cell marker (CD45), endothelial cell marker (CD31), early cardiac transcription factor (Nkx 2.5) and cardiac lineage-committed markers (cardiac troponin T (cTnT), cardiac myosin heavy chain (cMHC) and smooth muscle actin (SMA)).

4.3.5 Cardiomyogenic differentiation of cardiosphere-derived cells

To assess the potential of cardiomyogenic differentiation of CDCs *in vitro*, cells at passage 2 were induced to differentiate into the cardiac myocyte lineage. CDCs were treated with either 5-azacytidine (5-Aza; Sigma, A2385, UK) or dimethyl sulfoxide (DMSO; Sigma, D2650, UK) using the protocol established in Chapter 3. Finally, cells were collected at the end of two weeks for detection of cardiac-specific markers (cTnT and cMHC) using immunocytochemistry or flow cytometry.

(II) Effects of age on isolation, characterization and function of cardiac-derived stem cells from mouse hearts *in vitro*

4.3.6 Isolation and expansion of cardiac-derived stem cells from young and old mice

In this study, CSCs were isolated and expanded via the formation of cardiospheres from the hearts of C57Bl/10 mice at 1.5, 6, 18 and 24 months (n = 4 for each group). The procedure to obtain cardiac stem cells (CSCs) was outlined in Chapter 2. Since the cell number of EDCs obtained from the ventricle was low, according to the results of study (I), only atrial tissues were utilized to generate CSCs in study (II). In addition, due to the variation of the time required for cell growth from mice of different ages, EDC and CDC harvesting was based on confluence instead of a set time period. Therefore, EDCs were harvested when a confluent layer of stromal-like cells and overlying phase bright cells were found using an inverted light microscope. To study the effects of age on CSC isolation and expansion, the yield of EDCs from four age groups was examined in terms of the number of EDCs produced per milligram of tissue. Cardiosphere number and size were compared among these four groups. Likewise, the number of CDCs produced was determined using an advanced Neubauer hemocytometer when reaching confluency.

4.3.7 Migration assay of explant-derived cells

Heart explant fragments were plated on 60 mm petri dishes pre-coated with fibronectin (10 µg/ml in PBS). To observe and compare EDC migration, images of explants with EDCs were taken at 1, 3, 5, 7, 9 and 12 days post plating using a light microscope (Nikon TMS, Japan) fitted with a digital camera (Canon EOS 1000D, Canon Inc., Japan). A total of 12 plated tissue explants were randomly chosen for analysis from each age group. The maximal distance of EDCs migrating away from explants was measured in mm at day 5 after plating using ImageJ (Figure 4.3). The difference of migration of EDCs derived from mice of different ages was analyzed using one-way ANOVA with Tukey post hoc test.

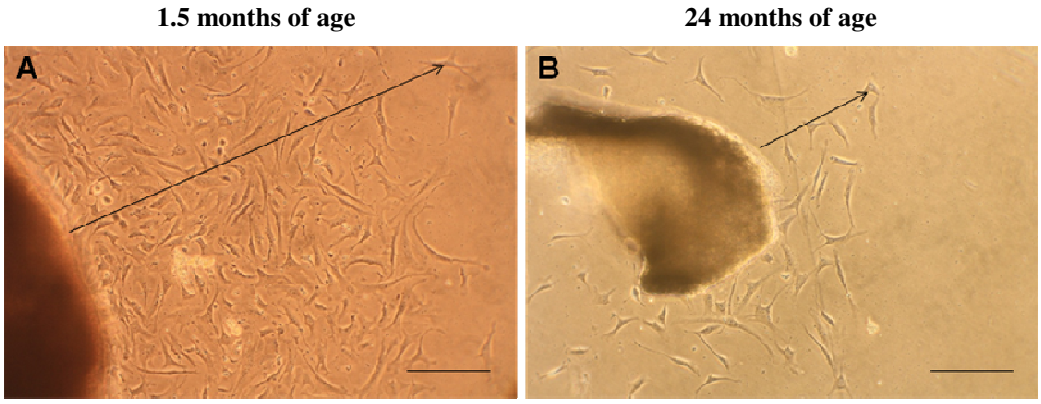

Figure 4.3 Representative images of migrating explant-derived cells (magnification x10). *(**A, B**) Explants with EDCs from wild-type mice aged 1.5 months (A) and 24 months (B). The maximal distance of cell migration was determined after 5 days in culture using ImageJ. Scale bars = 200 μm.*

4.3.8 Migration assay of cardiosphere-derived cells

Cardiospheres were plated into fibronectin-coated culture flasks and expanded as monolayer CDCs. Images of cardiospheres with expanding CDCs were captured at 18 and 30 hours post plating, as above. A total of 12 cardiospheres were analyzed from each of 4 different age groups. The maximal distance of CDCs migrating out of cardiospheres was measured at 18 and 30 hours after plating using ImageJ software (Figure 4.4). The statistical significance of CDC migration among four age groups was analyzed using one-way ANOVA with Tukey post hoc test.

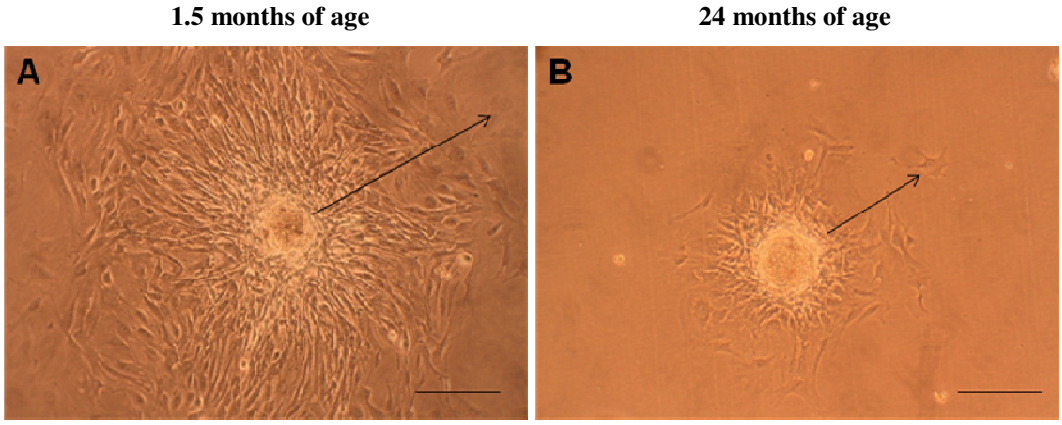

Figure 4.4 Representative images of cardiopshere-derived cells migrating from cardiospheres (magnification x10). *(**A, B**) A cardiosphere from 1.5 month-old mouse and expanding CDCs (A) and a cardiosphere from 24 month-old mouse (B) at 30 hours post plating. The maximal distance of cell migration was measured using ImageJ. Scale bars = 200 μm.*

4.3.9 Immunocytochemistry

For phenotype characterization by immunocytochemistry, mouse cardiospheres and CDCs were cultured on glass coverslips, as outlined in Chapter 2. The following antibodies were used: c-kit-FITC (BD Pharmingen, UK), Sca-1-PE (BD Pharmingen, UK), CD90-FITC (BD Pharmingen, UK), CD105 (Santa Cruz Biotech, UK), CD31 (AbD Serotec, UK), CD45-FITC (BD Pharmingen, UK), Sox2 (Santa Cruz Biotech, UK), Oct3/4 (Santa Cruz Biotech, UK), Nkx2.5 (Santa Cruz Biotech, UK), α-SMA (Sigma, UK), cTnT (Abcam, UK) and cMHC (Abcam, UK). Corresponding secondary antibodies and relevant dilution factors are summarized in Table 2.3 (Chapter 2). To ensure that cardiac-specific primary antibodies (cTnT and cMHC) detected cardiomyocytes, HL-1 cells, derived from transgenic mouse cardiomyocytes (375, 376), were used as positive control cells. Confocal fluorescence imaging was performed on Zeiss LSM META 510 and processed with Zeiss LSM Image Examiner software. As shown in Figure 4.5, HL-1 cardiomyocytes were unequivocally positive for cTnT and cMHC staining, demonstrating that these cardiac-specific antibodies can be used to identify the cardiomyocyte-directed cells following the induction of cardiomyogenic differentiation.

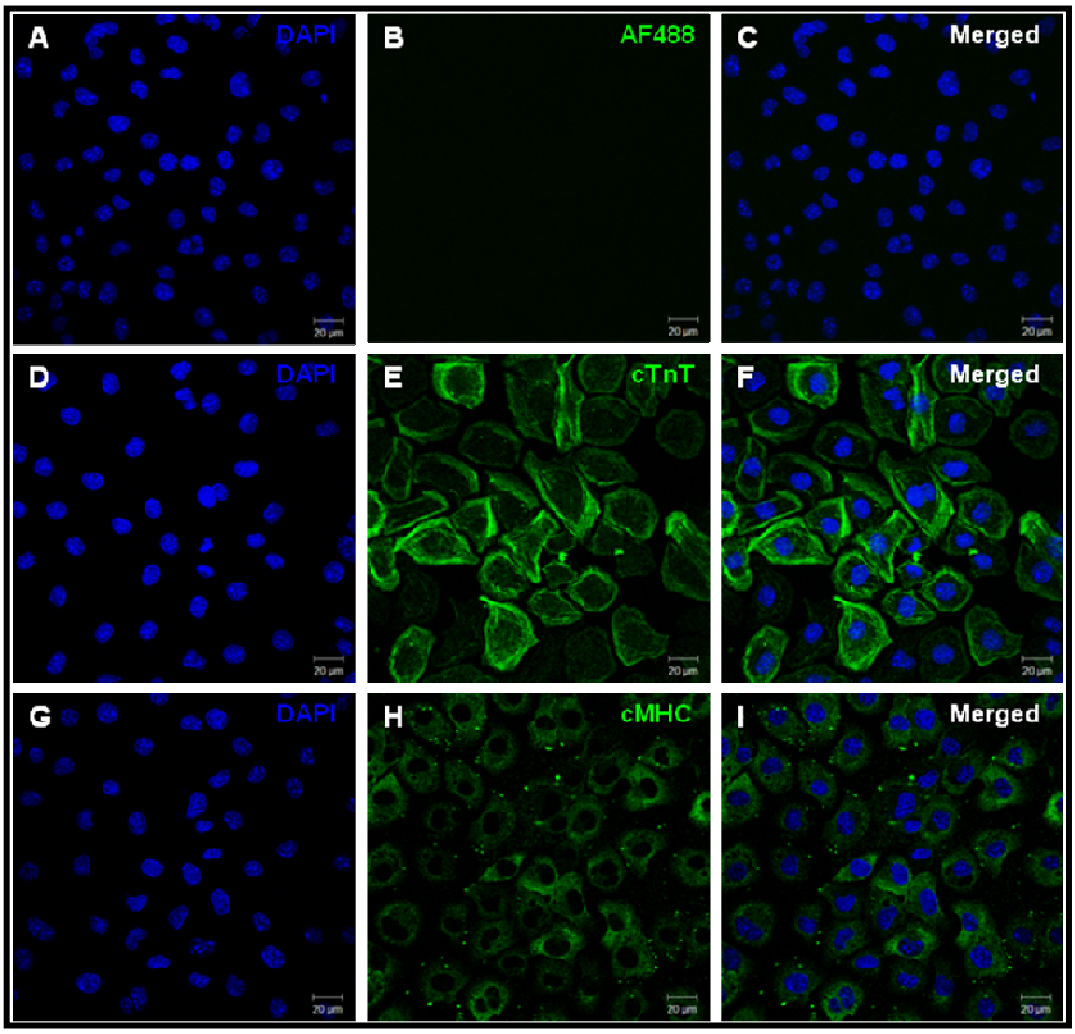

Figure 4.5 Representative confocal images of HL-1 cardiomyocytes used as positive control cells. *HL-1 cardiomyocytes were grown on fibronectin-coated wells overnight and stained for cardiac-specific markers, including cardiac troponin T (cTnT) and cardiac myosin heavy chain (cMHC). Upper panel represented negative control of HL-1 cells stained with secondary antibody only (AlexaFluor 488, green). Middle panel shows cells stained with anti-cTnT antibody. Lower panel shows cells stained with anti-MHC antibody. HL-1 cells were both cTnT and cMHC positive. Nuclei were counterstained with DAPI (blue). Scale bars = 20 µm. Abbreviations: cTnT = cardiac troponin T, cMHC = cardiac myosin heavy chain, and DAPI = 4′, 6-diamidino-2-phenylindole.*

4.3.10 Flow cytometric analysis

Cells were prepared and stained according to the protocol described in Chapter 2. For characterization of mouse CDCs, the following conjugated antibodies and corresponding isotype-matched control antibodies were used: c-kit-FITC (BD Pharmingen, UK), CD90-FITC

(BD Pharmingen, UK), Sca-1-PE (BD Pharmingen, UK), FITC IgG2bκ isotype control (BD Pharmingen, UK) and PE IgG2aκ isotype control (BD Pharmingen, UK) (see Table 2.6 in Chapter 2). Isotype-matched control antibodies were used to set up negative thresholds. In addition, flow cytometry was utilized to quantify the degree of CDCs differentiation into cardiomyocytes. For quantification of cells expressing cardiac-specific markers at the end of the induction of differentiation, the following primary antibodies and appropriate secondary antibodies were used: cTnT (Abcam, UK), MHC (Abcam, UK) and AF488 Donkey Anti-mouse (Invitrogen, UK) (see Table 2.6 in Chapter 2). In this part, an identical experiment was run as a negative control with secondary antibody only. For live cell labelling, the viability of cells was determined before flow cytometric analysis using Trypan Blue dye. The cell viability always exceeded 95% (97 ± 1%). Cells were analyzed using a FACSCalibur flow cytometer (BD Bioscience, San Jose, CA) and each acquisition included a minimum of 10,000 events. The data were analyzed using CellQuest Pro software (BD Bioscience, San Jose, CA).

4.3.11 Telomere length and telomerase activity assays

To compare telomere length of cardiosphere-derived stem cells from young and old mice, relative telomere lengths were determined using quantitative real-time PCR, as described previously [373]. Total DNA was extracted from cultured cells in a monolayer as described in Chapter 2. Telomeric DNA was amplified using specific primer pairs (Appendix Table 5). The amplification of telomeric DNA was normalized to a single copy gene (SCG) – 36B4 (Appendix Table 5). For the comparison of telomerase activity, total cellular RNA was isolated and the telomerase expression of CDCs was determined based on the mRNA level of telomerase reverse transcriptase (TERT) enzyme and normalized to a housekeeping gene – GADPH.

4.4 Results

(I) Isolation, expansion and characterization of cardiac-derived stem cells from mouse heart explants

4.4.1 Isolation and expansion of cardiac-derived stem cells

It should be emphasized that mouse CDC culture was established for the first time to characterize CSCs in the lab.

4.4.1.1 Explant-derived cells

Hearts from 6 week-old C57Bl/10 mice were separated into atria and ventricles for individual explant cultures. After plating, explant fragments adhered onto the fibronectin-coated surface. A monolayer of stromal-like cells started to appear due to cells migrating out of explants 3 days post plating. After approximately 5 days, small, round phase bright cells could be seen over the monolayer. These explant-derived cells (EDCs) continued to proliferate and expand prior to harvest for creating cardiospheres. As shown in Figure 4.6, explants from atria generated more EDCs than those from ventricles. Importantly, some explant fragments from ventricles were found not to give rise to EDCs at all throughout the culture process. Explants from atria produced approximately 3.3-fold more EDCs per milligram of tissue than those from ventricles ($1.6 \pm 0.1 \times 10^4$ vs. $0.5 \pm 0.1 \times 10^4$ EDCs per mg tissue; $p < 0.001$; Figure 4.7).

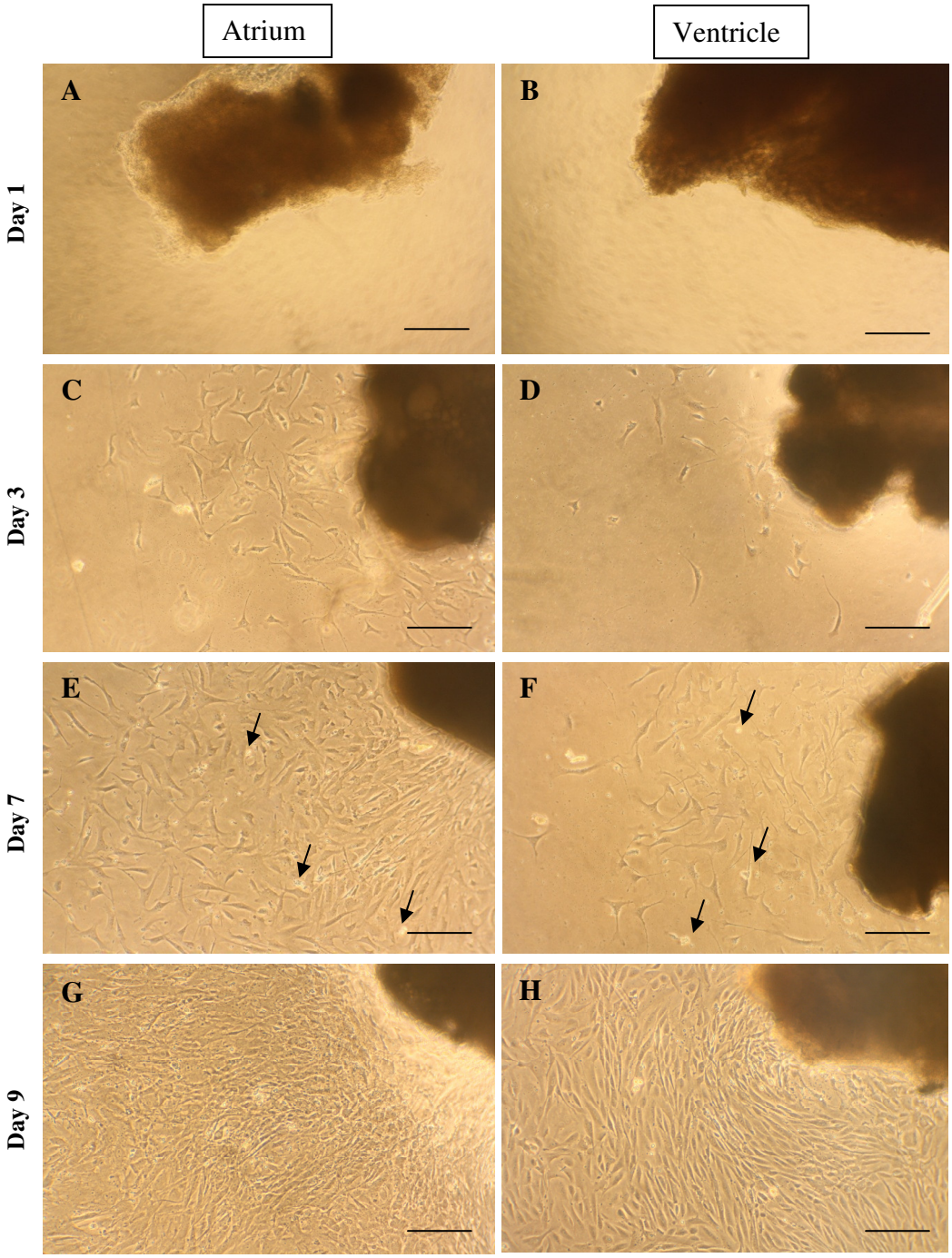

Figure 4.6 Representative micrographs of explants and explant-derived cells from atria and ventricles (magnification x10). *Images of explants were taken at different time points. (**A**, **B**) At day 1, explants adhered onto fibronectin-coated culture surface post plating. (**C**, **D**) At day 3, cells started to arise from explant edges. (**E**, **F**) At day 7, a monolayer of fibroblast-like cells formed with phase bright cells over it (arrow). (**G**, **H**) At day 9, cells became more confluent. Scale bars = 200 µm.*

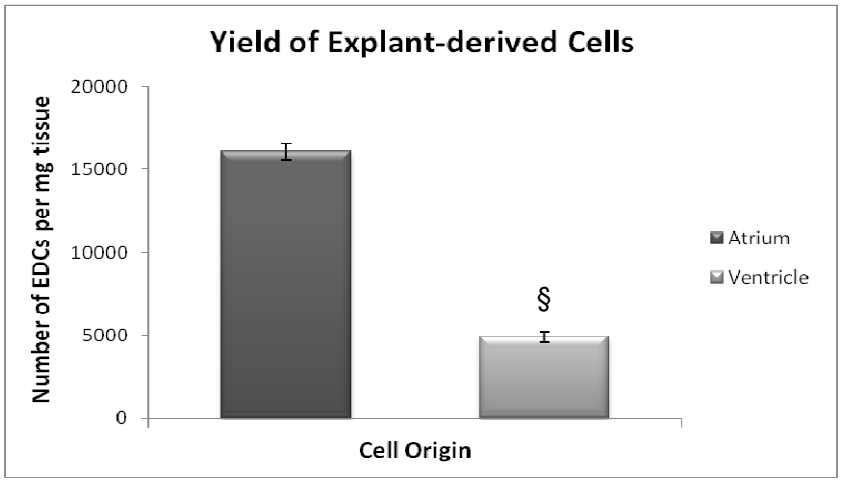

Figure 4.7 Yield of explant-derived cells isolated from atria and ventricles. *EDCs were enzymatically digested and counted using a haemocytometer at day 7 post plating. Atrial explants gave a significantly higher number of EDCs than ventricular explants (1.6 ± 0.1 x 10^4 vs. 0.5 ± 0.1 x 10^4 EDCs/mg tissue; $p < 0.001$). Data are presented as mean ± SEM (n = 4). § $p < 0.001$ vs. atrium.*

4.4.1.2 Cardiospheres

After plating on poly-D-lysine, floating EDCs adhered onto the culture surface and started to proliferate. Subsequently, adherent cells gradually self-assembled into clusters, termed cardiospheres. From day 3 post plating, cardiospheres increased in size with time, and fully formed approximately 5 days after plating (Figure 4.8). The size of cardiospheres, measured using ImageJ, did not differ significantly between atrial and ventricular origins (0.025 ± 0.003 vs. 0.027 ± 0.001 mm^2; p = NS; Figure 4.9). There was a significant difference in number per well between atrium and ventricle-derived cardiospheres (94 ± 5 vs. 77 ± 6; $p < 0.05$; Figure 4.10). Since the atrial explants generated more EDCs, the total number of cardiospheres from atria was higher than that from ventricles in terms of yield per milligram of tissue.

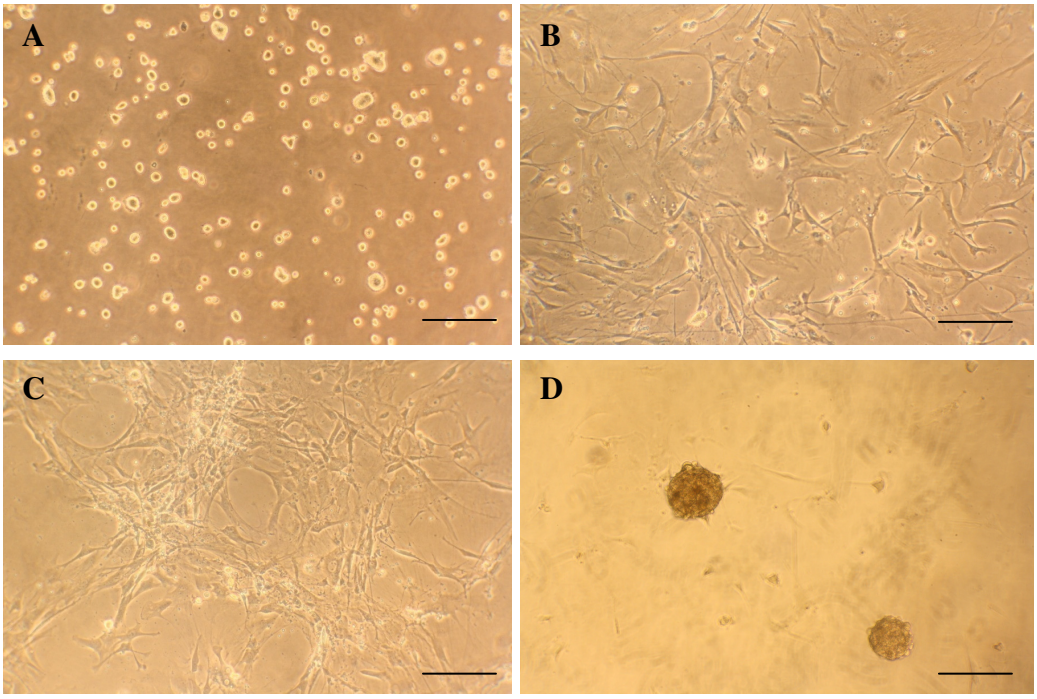

Figure 4.8 The process of cardiosphere formation in CGM. *(**A**) Explant-derived cells (cardiosphere-forming cells) were plated onto 24 multiwell plates pre-coated with poly-D-lysine. (**B**) Adhered cells on day 2 post plating. (**C**) Cells proliferated and aggregated into clusters on day 3 post plating. (**D**) Fully formed cardiospheres 5 days post plating. Scale bars = 200 μm. Abbreviation: CGM = cardiosphere growth medium.*

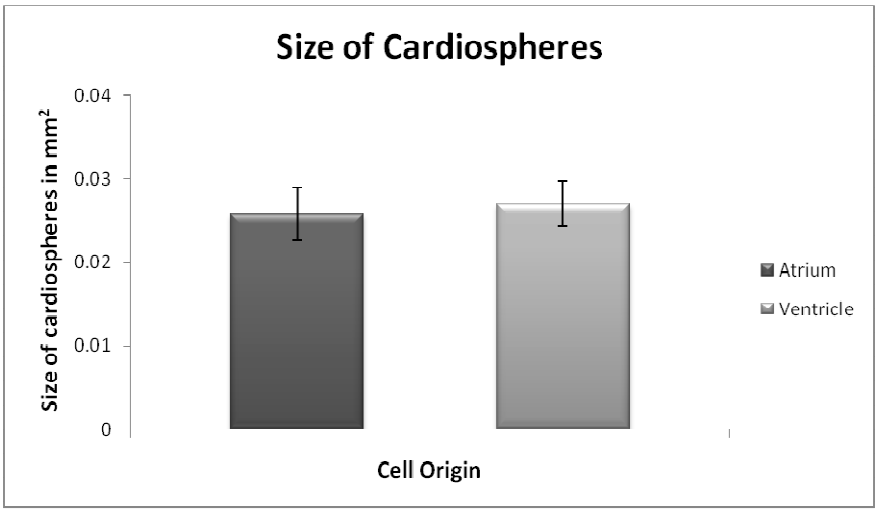

Figure 4.9 Size of cardiospheres derived from atria and ventricles. *Representative images of cardiospheres were taken under a light microscope from both atria and ventricles. Cardiosphere sizes were measured using ImageJ. There was no significant difference in size of cardiopsheres from atrial and ventricular tissue (0.025 ± 0.003 vs. 0.027 ± 0.001 mm²; p = NS). Data are presented as mean ± SEM (n = 20).*

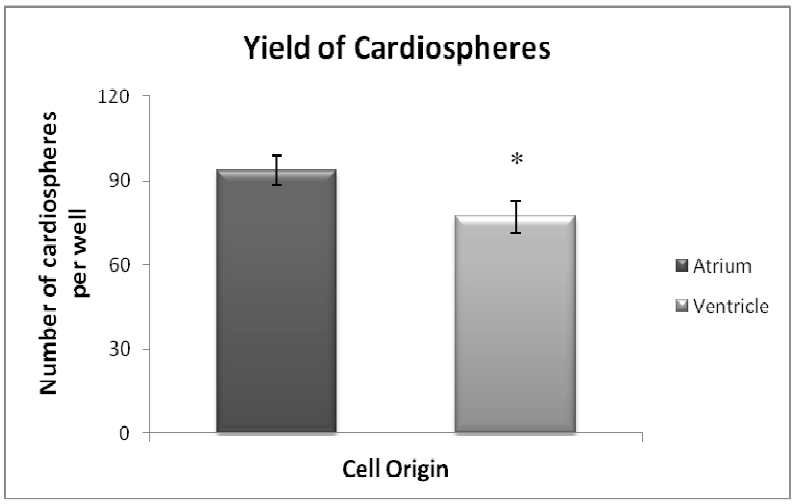

Figure 4.10 Yield of cardiospheres derived from atria and ventricles. *Cardiospheres were grown in 24 well plates coated with poly-D-lysine. The number of cardiospheres from both atrial and ventricular tissue per well was determined (94 ± 5 vs. 77 ± 6 cardiospheres per well; $p < 0.05$). Data are presented as mean ± SEM ($n = 4$). * $p < 0.05$ vs. atrium.*

4.4.1.3 Cardiosphere-derived cells

Cardiospheres plated on the fibronectin-coated surface started to give rise to cardiosphere-derived cells (CDCs), which spread out radially. When reaching confluency, CDCs were passaged for further expansion up to passage 2. CDCs from atria and ventricles exhibited similar cell morphology through passages P0 to P2, regardless of the cell origin (Figure 4.11). Atrial tissues were found to generate approximately 3.7-fold more CDCs per milligram of tissue than ventricular tissues ($2.4 \pm 0.2 \times 10^4$ vs. $0.6 \pm 0.2 \times 10^4$ CDCs/mg tissue; $p < 0.001$; Figure 4.12).

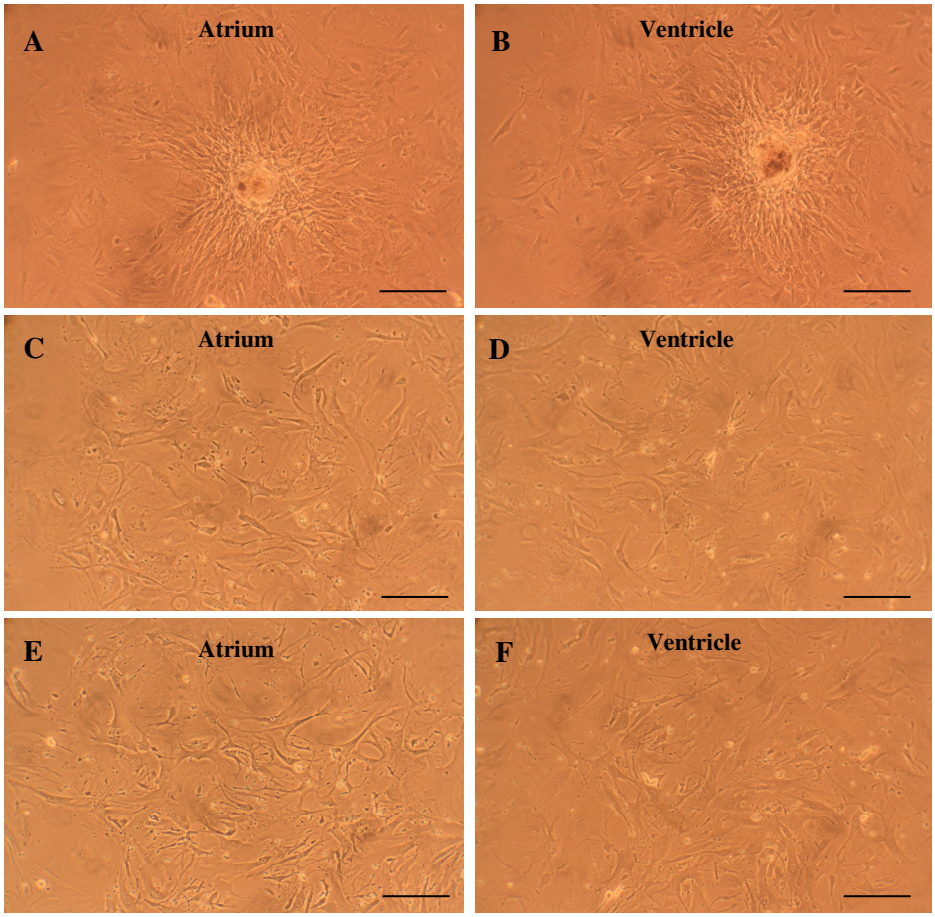

Figure 4.11 Representative micrographs showing morphology of cardiosphere-derived cells from atria and ventricles (magnification x10). *(**A**, **B**) Cardiospheres cultured from the atrium and ventricle gave rise to cardiosphere-derived cells (CDCs) at passage 0 on the fibronectin-coated culture surface. (**C** - **F**) When confluent, cells were further passaged for expansion from passage 1 (C, D) to passage 2 (E, F). CDCs generated from both origins showed similar morphological pattern under a light microscope. Scale bars = 200 μm*

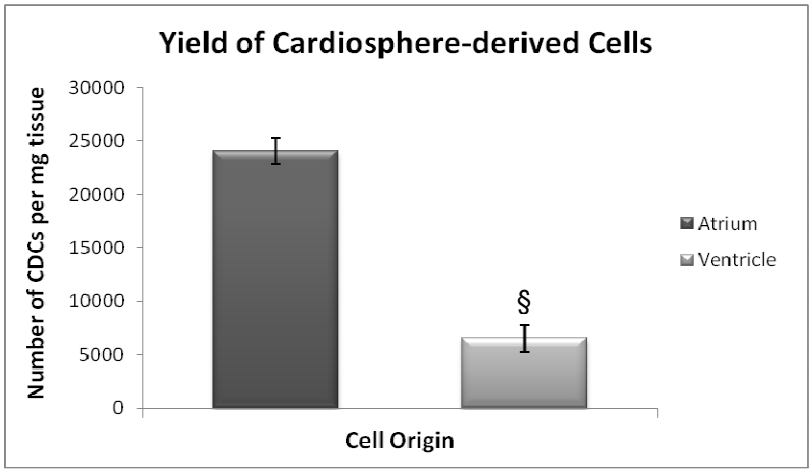

Figure 4.12 Yield of cardiosphere-derived cells from atrial and ventricular tissues. *To compare cell yield from atrial and ventricular tissue, passage 2 CDCs were trypsinized and counted using a hemocytometer when confluent. Atrial explants produced a significantly higher number of CDCs than ventricular explants ($2.4 \pm 0.2 \times 10^4$ vs. $0.6 \pm 0.2 \times 10^4$ CDCs/mg tissue; $p < 0.001$). Data are presented as mean ± SEM ($n = 4$). § $p < 0.001$ vs. atrium.*

4.4.2 Proliferation of cardiosphere-derived cells

The proliferative potential of cardiac stem cells derived from atria and ventricles was measured using AlamarBlue®. It was found that the number of atrium-derived CDCs was 1.2-fold higher than that of ventricle-derived CDCs ($p < 0.05$) after 1 day of culture (Figure 4.15). Higher cell numbers of atrium-derived CDCs were maintained during the culture period, with the cell number being 1.7-fold higher than ventricle-derived cells at day 7 ($p < 0.001$; Figure 4.13).

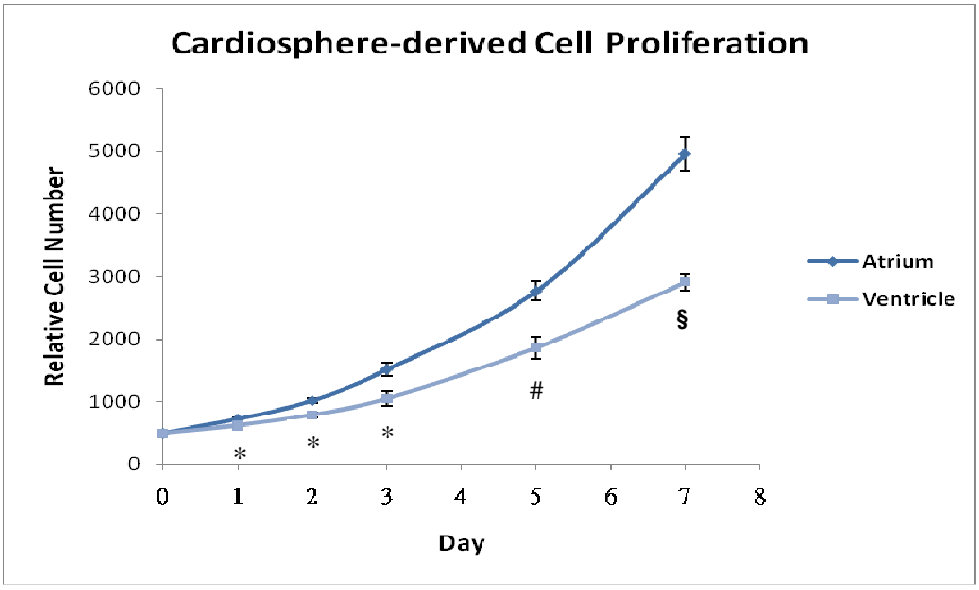

Figure 4.13 Proliferation of cardiosphere-derived cells grown from atria and ventricles. *Passage 2 CDCs were seeded onto 96 well plates pre-coated with fibronectin at a density of 500 cells per well. Relative fluorescence intensity was read using FLUOstar OPTIMA at day 0, day 1, day 2, day 3, day 5, and day 7. There was a significant difference in the cell number between CDCs from atrial and ventricular tissue through the culture period. Data are presented as mean ± SEM (n = 4). * $p < 0.05$ vs. atrium; # $p < 0.01$ vs. atrium; § $p < 0.001$ vs. atrium.*

4.4.3 Clonogenicity of cardiosphere-derived stem cells

Since clonal expansion is one of the important characteristics of stem cells, clonogenicity of passage 2 CDCs was examined and compared between atrium and ventricle-derived CDCs. As shown in Figure 4.14, CDCs from both atria and ventricles were clonogenic, but the former revealed a higher clonal efficiency than the latter (45 ± 5% vs. 31 ± 5%; $p < 0.01$), suggesting that atrium-derived CDCs contained a larger amount of stem cells.

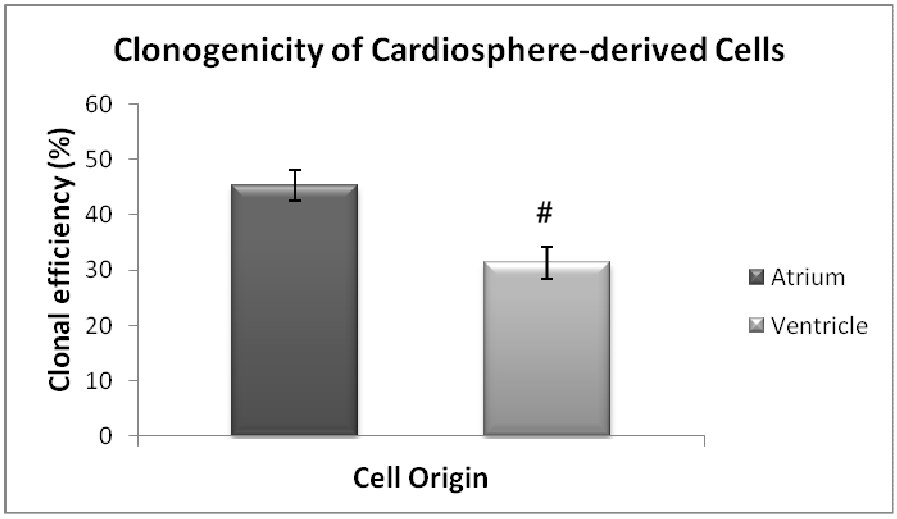

Figure 4.14 Comparison of cardiosphere-derived cell clonogenicity between atrial and ventricular CDCs. *Passage 2 CDCs were seeded on fibronectin-coated 96 well plates at a density of a single cell per well. The total number of wells containing colonies was counted after two weeks of culture. The CDCs from atria exhibited a significantly higher clonal efficiency than those from ventricles (45 ± 5% vs. 31 ± 5%; $p < 0.01$). Data are presented as mean ± SEM ($n = 4$). # $p < 0.01$ vs. atrium.*

4.4.4 Characterization of cardiac stem cells

Cardiac stem cell phenotype was characterized using immunocytochemistry and flow cytometry to identify and quantify the expression of cell surface and intracellular markers.

4.4.4.1 Immunophenoype characterization of cardiospheres and CDCs

Phenotypic analysis of newly developed cardiospheres, formed from EDCs, revealed expression of c-kit and Sca-1 (cardiac stem cell markers), Oct3/4 and Sox2 (pluripotent stem cell markers), CD90 and CD105 (mesenchymal stem cell markers), CD31 (endothelial stem cell marker), and Nkx2.5 (early cardiac transcription factor), but was negative for CD45 (hematopoietic stem cell marker) (Figure 4.15), suggesting cardiospheres comprised cardiac stem/progenitor cells and mesenchymal stem cells. Immunostaining showed that migrating CDCs from plated cardiospheres were composed of c-kit$^+$, Sca-1$^+$ and CD90$^+$ cells (Figure 4.16). Furthermore, immunophenotypic analysis demonstrated that passage 2 CDCs stained positive for c-kit, Sca-1, Oct3/4, Sox2, Nkx2.5, cTnT and α-SMA (cardiac lineage-related proteins), and CD90 (Figure

4.17). Taken together, the results indicated that CDCs represent a heterogeneous heart-derived cell population comprised of cardiac stem cells, mesenchymal stem cells, endothelial cells and cardiac lineage-committed cells.

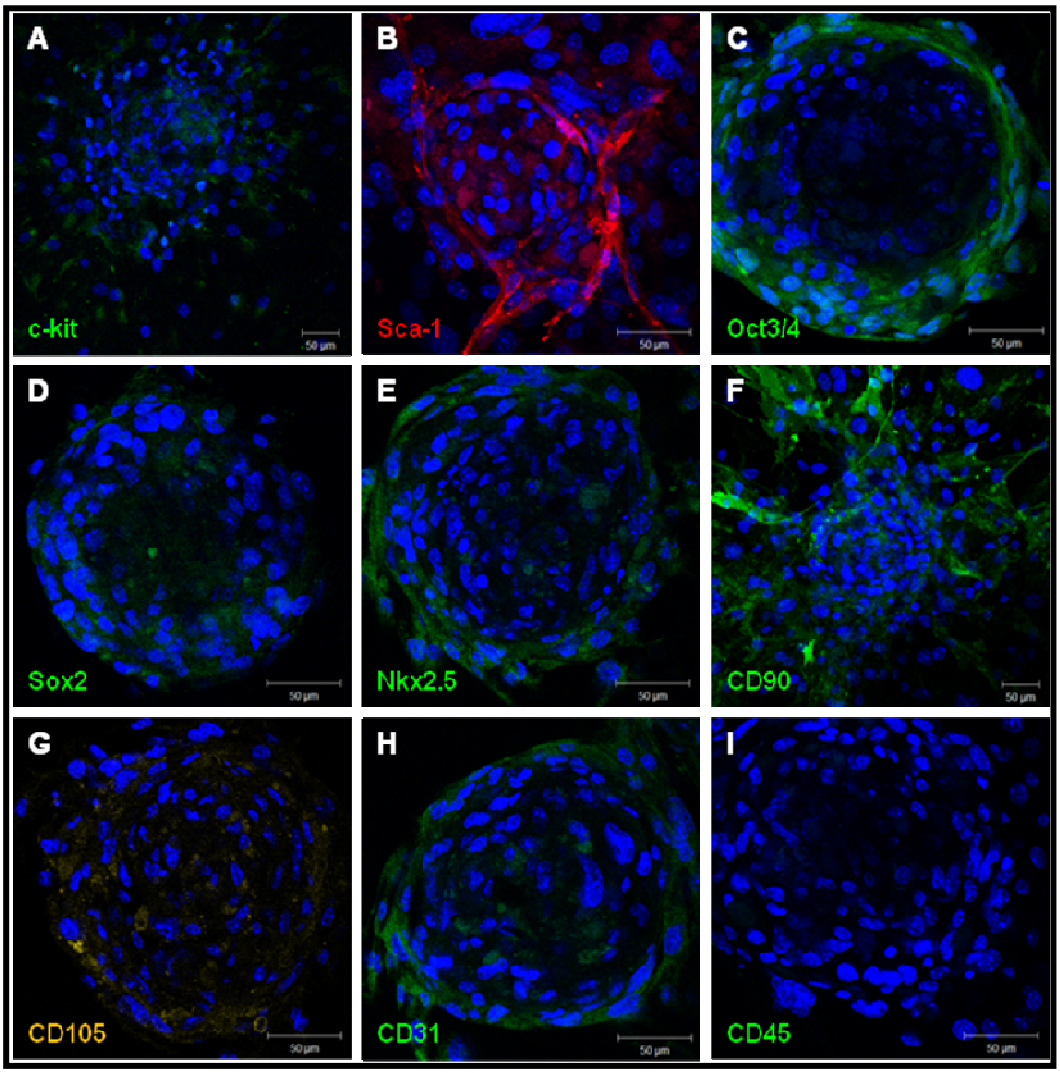

Figure 4.15 Immunophenotyping of mouse cardiospheres. *Cardiospheres generated from explant-derived cells, isolated from mice, were grown for immunostaining. Representative confocal images of immunostained cardiospheres showed the expression of specific cell surface markers. (**A**, **B**) Cardiac stem cell-related proteins - c-kit (green) and Sca-1 (red). (**C**, **D**) Pluripotent-related proteins - Oct3/4 (green) and Sox2 (green). (**E**) Early cardiac transcription factor - Nkx2.5 (green). (**F**, **G**) Mesenchymal-related proteins - CD90 (green) and CD105 (yellow). (**H**) Endothelial-related protein - CD31 (green). (**I**) However, cardiospheres expressed little or no hematopoietic-related protein - CD45. Nuclei were counterstained with DAPI (blue). Scale bars = 50 μm. Abbreviations: CDC = cardiosphere-derived cell and DAPI = 4′, 6-diamidino-2-phenylindole.*

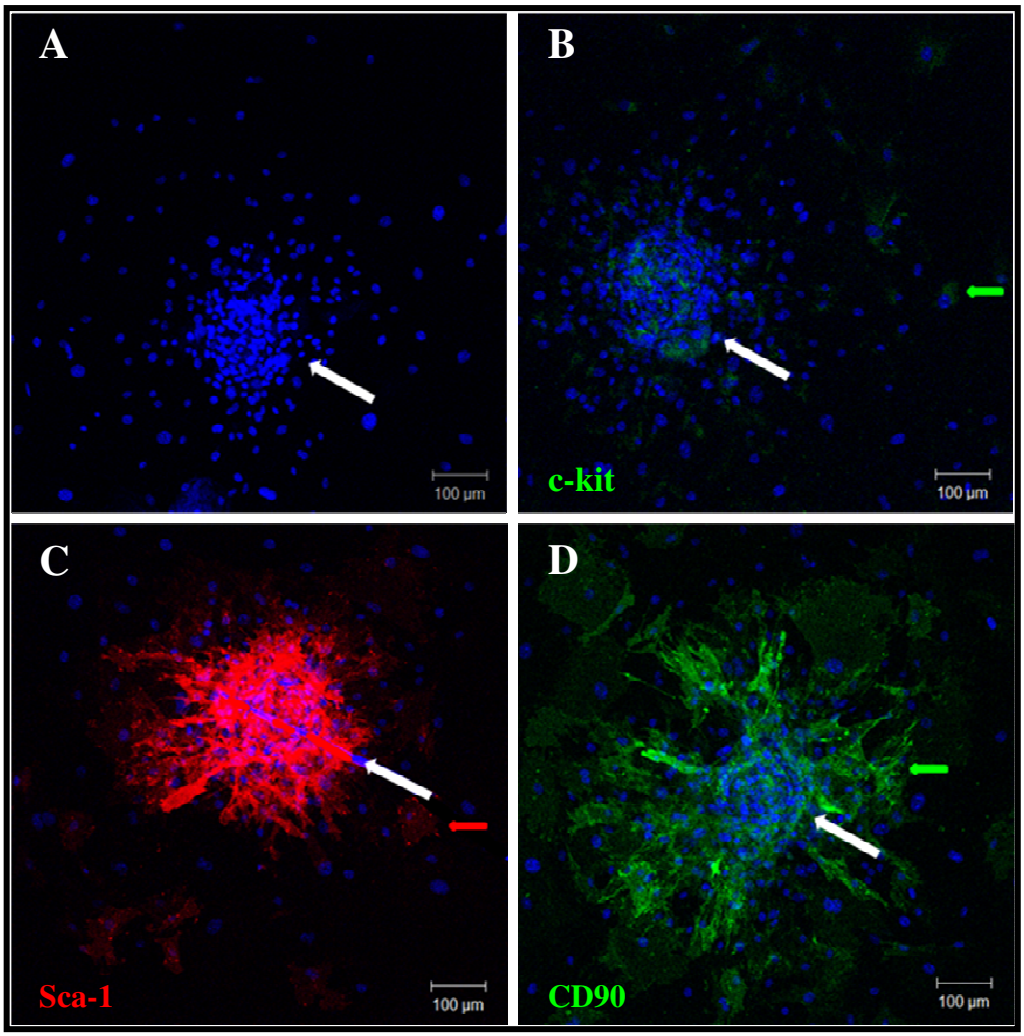

Figure 4.16 Immunophenotyping of cardiospheres with migrating cardiosphere-derived cells. *Cardiospheres, plated on the fibronectin-coated culture surface, gave rise to cardiosphere-derived cells, which were stained for immunophenotype characterization. (**A**) Negative control indicated cells stained with isotype-matched antibody. (**B** - **D**) Representative confocal images showed that cardiospheres and migrating cardiosphere-derived cells expressed cardiac stem cell markers - c-kit (B, green) and Sca-1 (C, red) and mesenchymal cell marker - CD90 (D, green). Nuclei were counterstained with DAPI (blue). White arrows indicate cardiospheres. Color arrows indicate migrating CDCs expressing c-kit, Sca-1 or CD90. Scale bars = 100 µm. Abbreviations: CDC = cardiosphere-derived cell and DAPI = 4', 6-diamidino-2-phenylindole.*

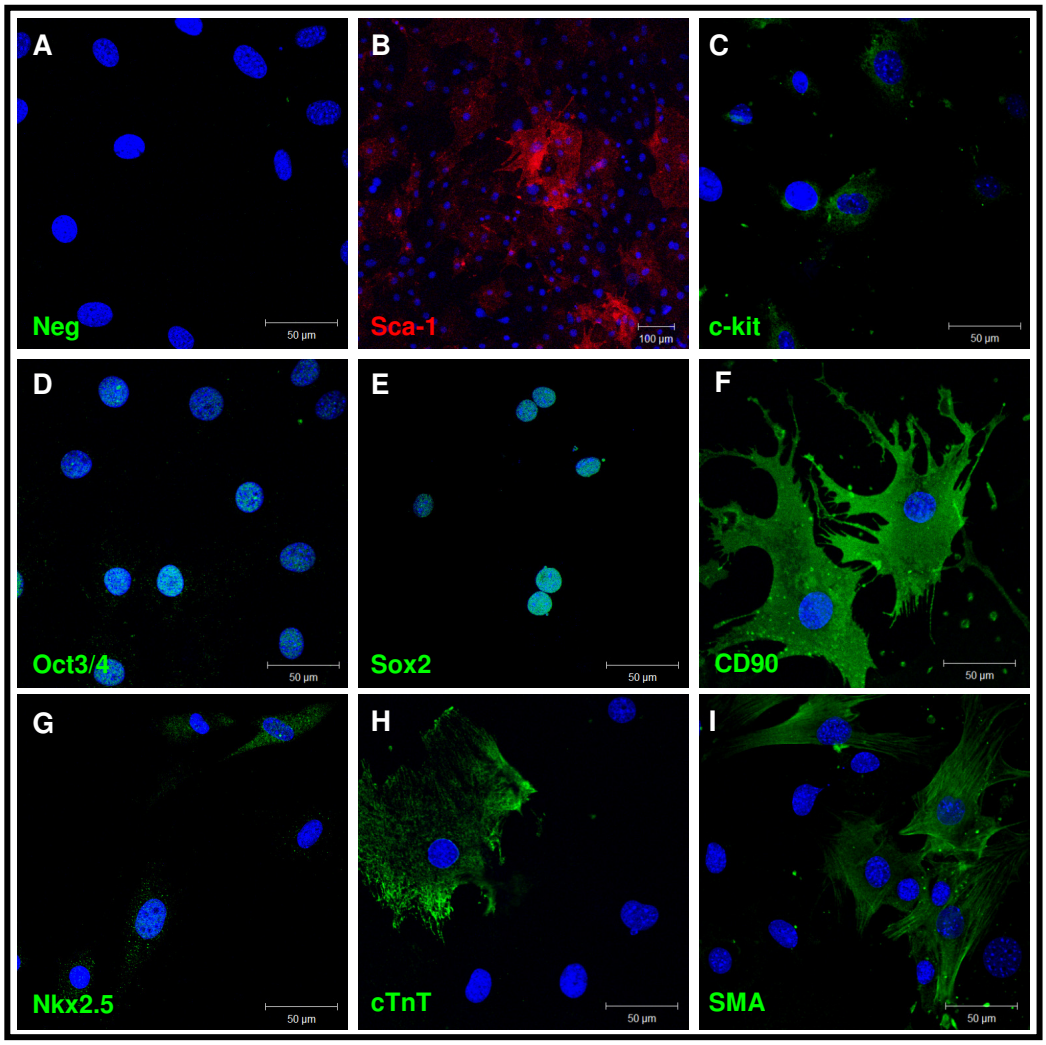

Figure 4.17 Immunophenotyping of cardiosphere-derived cells. *Cardiosphere-derived cells at passage 2 were grown and stained for immunophenotype characterization. (**A**) Negative control indicated cells stained with secondary antibody only (AlexFluor 488, green). Representative confocal images showed that cardiosphere-derived cells represented a mixed cell population. (**B** - **E**) Cardiac stem and progenitor cells expressing Sca-1 (B, red), c-kit (C, green), Oct3/4 (D, green) and Sox2 (E, green). (**F**) Mesenchymal stem cells expressing CD90 (green). (**G**) Cardiac lineage-committed cells expressing Nkx2.5 (green). (**H**) Cardiac differentiated cells expressing cTnT (green). (**I**) Cardiac smooth muscle cells expressing α-SMA (green). Nuclei were counterstained with DAPI (blue). Scale bars = 50 µm (A), 100 µm (B) and 50 µm (C to I). Abbreviation: DAPI = 4', 6-diamidino-2-phenylindole.*

4.4.4.2 Phenotype characterization of CDCs using flow cytometric analysis

Based on flow cytometry, passage 2 CDCs derived from atria were found to contain higher amount of c-kit$^+$ (13 ± 2%) and Sca-1$^+$ (82 ± 4%) cells than those from ventricles (3.4 ± 0.5% and 53 ± 4%; $p < 0.01$ and $p < 0.01$, respectively; Figure 4.18 and 4.19). However, the percentage of CD90$^+$ cells was higher in CDCs from ventricles compared to those from atrium (58 ± 2% and 48 ± 3%; $p < 0.05$; Figure 4.18 and 4.19). The results confirmed that CDCs are a mixed stem cell population and revealed that atrial tissues generated more cardiac stem cells than did ventricular tissues. In addition, quantitative flow cytometry demonstrated that most CDCs exhibited a mesenchymal phenotype, regardless of cell origins.

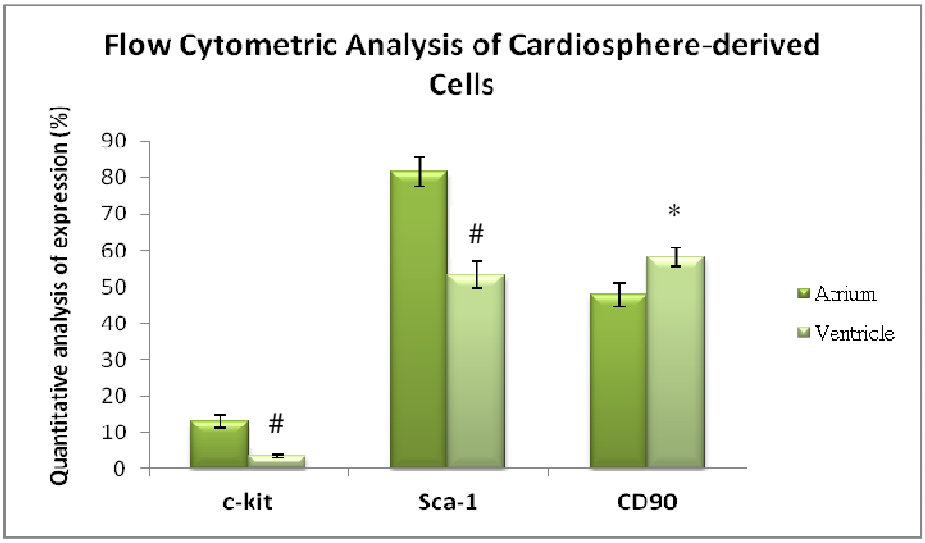

Figure 4.18 Flow cytometric analysis of cardiosphere-derived cells for phenotype characterization. *The expression of c-kit, Sca-1 and CD90 on CDCs, including those derived from atria and ventricles, was analyzed using flow cytometry and shown as a percentage of positive cells. CDCs (atria vs. ventricles) were positive for c-kit (13 ± 2% vs. 3.4 ± 0.5%; $p < 0.01$), Sca-1 (82 ± 4% vs. 53 ± 4%; $p < 0.01$), and CD90 (48 ± 3% and 58 ± 2%; $p < 0.05$). Data are presented as mean ± SEM ($n = 4$). * $p < 0.05$ vs. atrium; # $p < 0.01$ vs. atrium.*

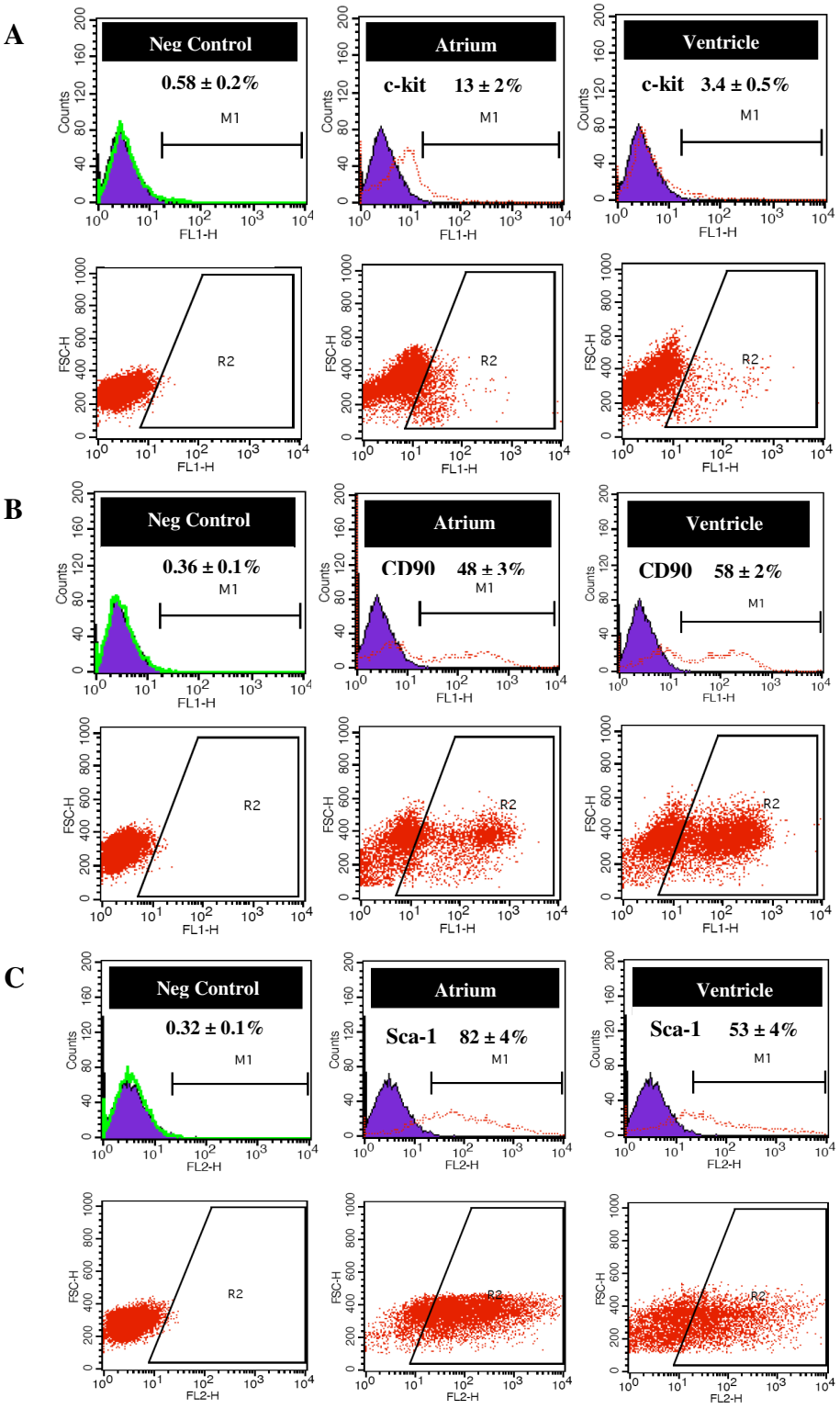

Figure 4.19 Flow cytometric analysis of passage 2 cardiosphere-derived cells from both atria and ventricles. *Atrium- and ventricle-derived CDCs at passage 2 were labelled for characterization using flow cytometry. (**A** - **C**) Histograms (upper panel) and scatter plots (lower panel). CDCs expressed cardiac stem cell markers - c-kit (A) and Sca-1 (C) and mesenchymal cell marker - CD90 (B). Negative control denoted cells stained with isotype-matched antibodies (green line; A for c-kit, D for CD90, and G for Sca-1). Cells present in region M1 and R2 were defined as the positive population. Purple region: unstained cell control. Red dotted line: corresponding stained samples. Data are presented as mean ± SEM (n = 3). Abbreviation: CDC = cardiosphere-derived cell.*

4.4.5 *In vitro* cardiomyogenic differentiation potential of mouse CDCs

Both 5-Aza and DMSO were effective in inducing differentiation of CDCs towards the cardiomyocyte phenotype. Based on flow cytometric results, differentiated CDCs significantly increased the expression of cardiac-related proteins, including cTnT and cMHC, compared with CDCs cultured in CEM (Figure 4.20). Immunofluorescence further confirmed the presence of cardiomyocyte-like cells in differentiated cell populations using the specific cardiomyocyte marker - cardiac troponin T (Figure 4.21). No spontaneous beating was observed during the induction process. However, the results clearly demonstrated that CDCs contained cardiac stem and progenitor cells, which were able to differentiate along the cardiac myocyte lineage *in vitro* and acquire cardiomyocyte-like phenotype following 5-Aza or DMSO.

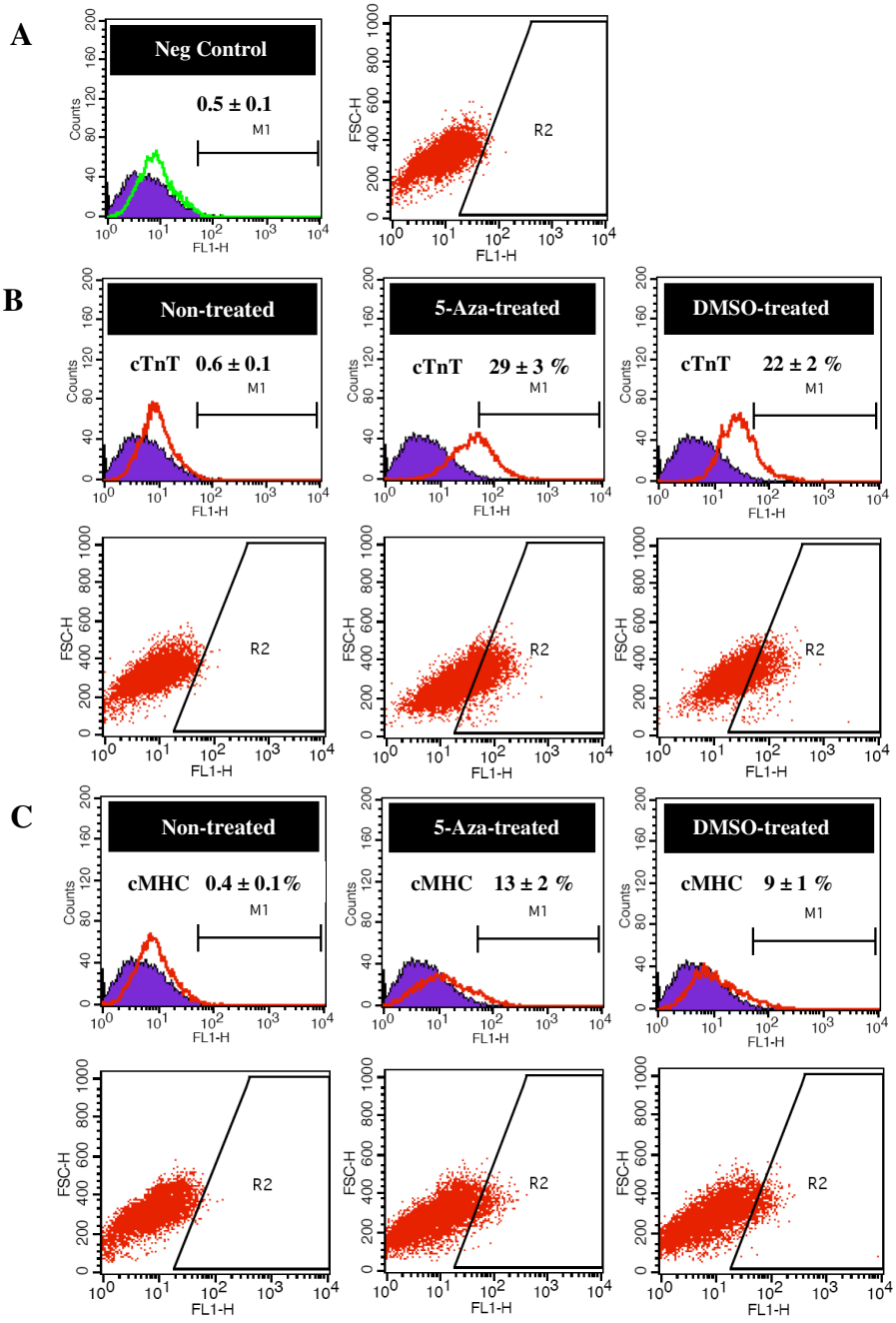

Figure 4.20 Flow cytometric analysis of cardiomyogenic differentiation of mouse cardiosphere-derived cells. *Passage 2 cardiosphere-derived cells were induced to differentiate into cardiomyocytes when treated with either 5-Aza or DMSO. Following two weeks of induction, flow cytometric analysis identified the presence of cardiomyocyte-like cells with cardiac-specific markers. (**A**) Negative control on histogram and scatter plot was cells stained only with secondary antibody (green line). (**B**, **C**) Histograms and scatter plots for cTnT (B) and cMHC (C). The results suggested that CDCs were potentially cardiomyogenic. Cells present in region M1 were defined as the positive population. Purple region: unstained cell control. Red line: corresponding stained samples. Data are presented as mean ± SEM (n = 3). Abbreviations: CDC = cardiosphere-derived cell, 5-Aza = 5-azacytidine, DMSO = dimethyl sulfoxide, cTnT = cardiac troponin T, and cMHC = cardiac myosin heavy chain.*

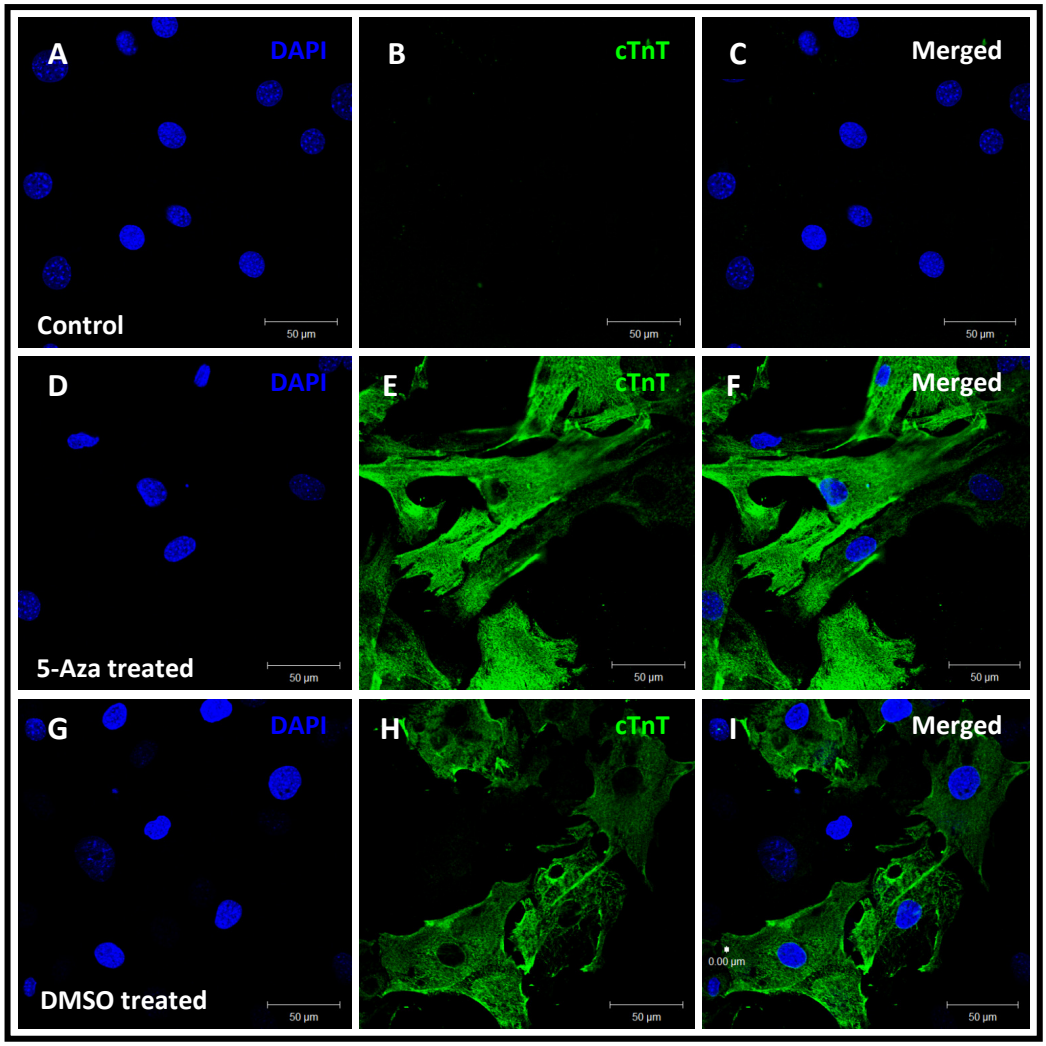

Figure 4.21 Immunocytochemical analysis of cardiac-related protein cTnT after cardiomyogenic differentiation of cardiosphere-derived cells. *CDCs at passage 2 were treated with either 5-Aza or DMSO. After two weeks, cells were stained for cardiac troponin T (cTnT). Upper panel indicates control cells without differentiating agent treatment. Middle panel indicates 5-Aza-treated CDCs expressing cTnT (green, AF 488). Lower panel indicates DMSO-treated CDCs expressing cTnT (green, AF 488). Nuclei were counterstained with DAPI (blue). Scale bars = 50 µm (A - I). Abbreviations: CDC = cardiosphere-derived cell, cTnT = cardiac troponin T, 5-Aza = 5-azacytidine, DMSO = dimethyl sulfoxide, and AF 488 = AlexaFluor 488, and DAPI = 4', 6-diamidino-2-phenylindole.*

(II) Effects of age on cardiac stem cells in isolation, proliferation, clonogenicity and differentiation

4.4.6 Effects of age on isolation and expansion of cardiac-derived stem cells

4.4.6.1 Explant-derived cells

Atrial tissues from hearts of C57Bl/10 mice at 1.5, 6, 18, and 24 months of age were plated as explants on petri dishes pre-coated with fibronectin. The morphological pattern of explant-derived cells (EDCs) was similar among the four age groups. It was observed, however, that the rate of expansion of EDCs differed. Representative microphotographs of expanding EDCs at day 5, 7 and 9 are presented below (Figure 4.22). The majority of explants was found to give rise to EDCs between 3 and 5 days of culture in complete explant medium (CEM) post plating. EDCs were harvested when a confluent layer of stromal-like cells with overlying phase bright cells was observed, rather than at a set time period, due to the wide variability in the time for culture. Quantitative analysis showed that there was a significant decrease in the number of EDCs (EDCs/mg tissue) from 6 to 24 month-old mice by 26%, 45%, and 58%, respectively, compared to 1.5 month-old mice (Figure 4.23).

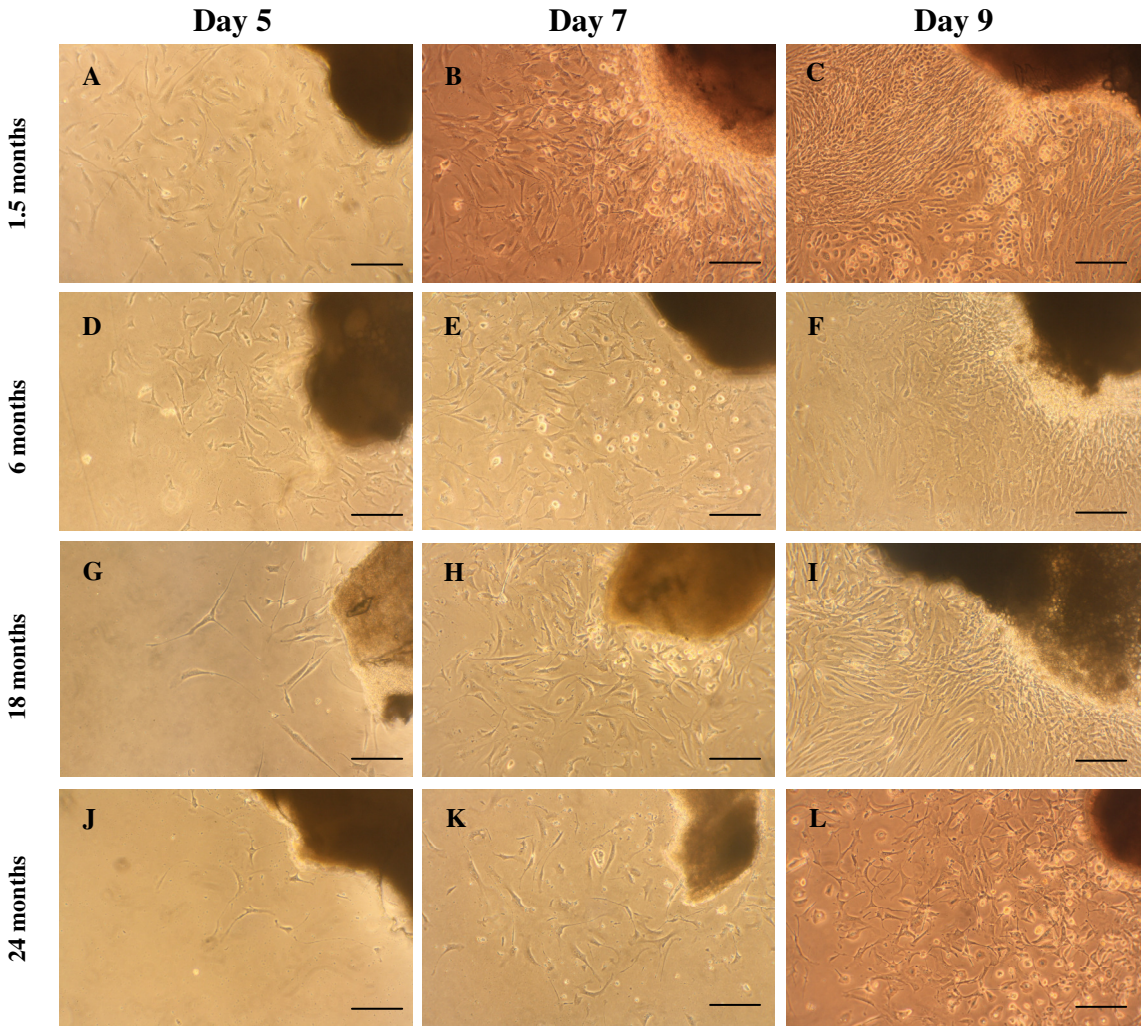

Figure 4.22 Representative micrographs of cultured explants with migrating explant-derived cells from different age groups at different time points (magnification x10). *Explants from atrium, excised from hearts of CL57Bl/10 mice at 1.5, 6, 18, and 24 months of age, were plated on fibronectin-coated petri dishes. Images of explants were captured to assess expansion and migration of EDCs at different time points, including day 5, day 7 and day 9 post plating (left, middle and right columns, respectively). Explants from older mice took a longer time to give rise to EDCs and reach confluence compared with those from younger mice. Scale bars = 200 μm.*

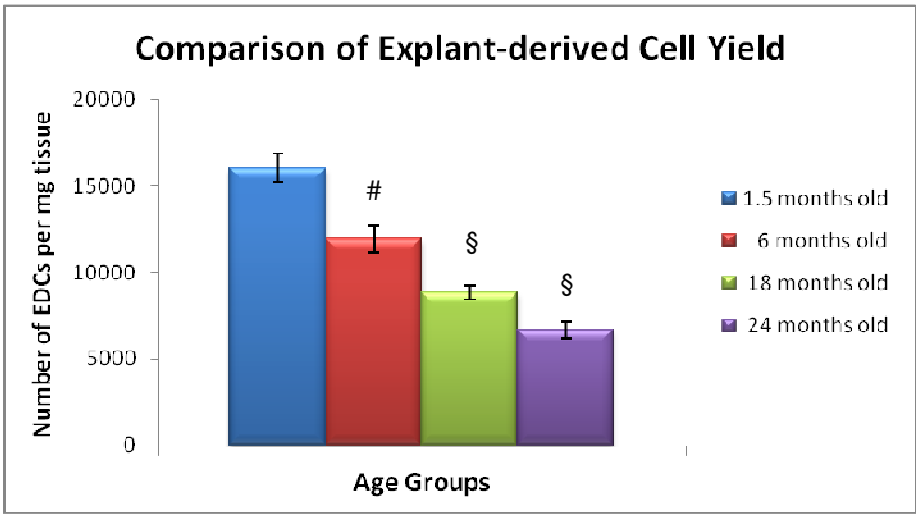

Figure 4.23 Effects of mouse age on explant-derived cell yield. *Atrial explant fragments from hearts of C57Bl/10 mice at 1.5, 6, 18, and 24 months of age were cultured on fibronectin-coated petri dishes. When confluent following plating, EDCs were enzymatically digested and counted using a haemocytometer. There was a close correlation between mouse age and EDC yield. With increasing age, the number of EDCs generated per milligram of tissue significantly declined from 1.5 to 24 month-old mice (1.6 ± 0.1 x 10^4 to 0.7 ± 0.1 x 10^4 EDCs/mg tissue). Data are presented as mean ± SEM (n = 4). # p < 0.01 vs. 1.5 months old; § p < 0.001 vs. 1.5 months old.*

4.4.6.2 Cardiospheres

Explant-derived cells (cardiosphere-forming cells) were plated onto 24 well plates at a density of 3 x 10^4 cells per well, to form cardiospheres. No difference in morphology and size of cardiospheres from four age groups was found (Figure 4.24 and Figure 4.25). However, EDCs from older mice required a longer time to form cardiospheres than those from younger mice (24 vs. 1.5 month-old, 8 ± 1 vs. 5 ± 1 days; $p < 0.01$). When compared to 1.5 month-old mice, 24 month-old mice gave a significantly lower number of cardiospheres (24 vs. 1.5 month-old, 43 ± 5 vs. 90 ± 7 cardiospheres per well; $p < 0.01$; Figure 4.26).

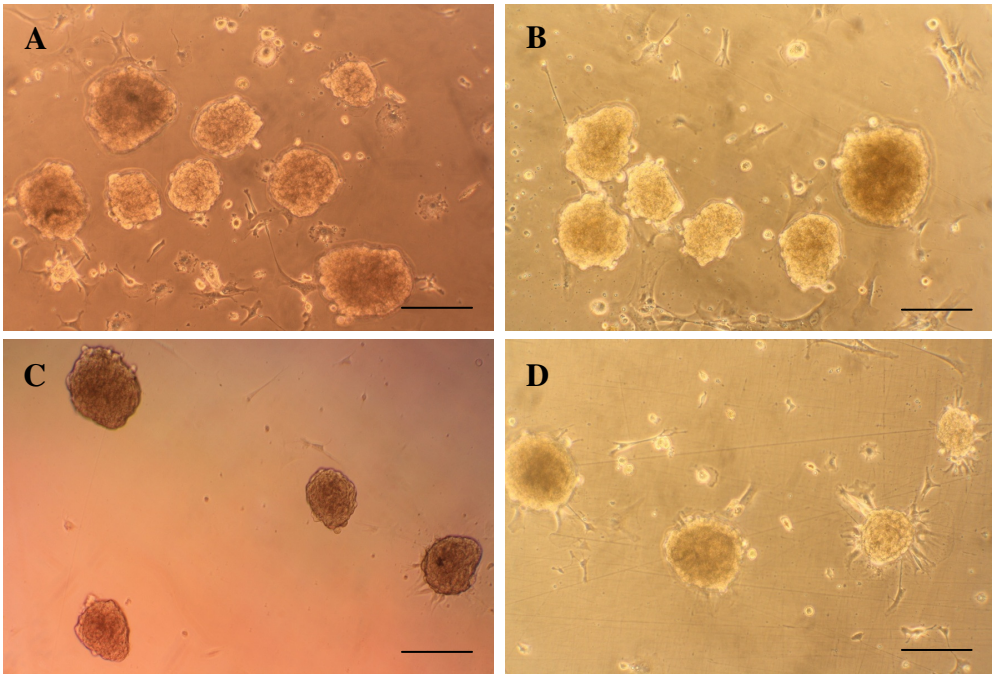

Figure 4.24 Representative micrographs of cardiospheres grown from mice of different ages (magnification x10). *When confluent, explant-derived cells were harvested and seeded on poly-D-lysine coated multiwell plates. Over time, cardiospheres increased in size and some detached and floated in suspension. (**A – D**) Cardiospheres formed from 1.5 month-old mice (A), 6 month-old mice (B), 18 month-old mice (C), 24 month-old mice (D). There was no difference in morphology of cardiospheres from the four age groups. Scale bars = 200 µm.*

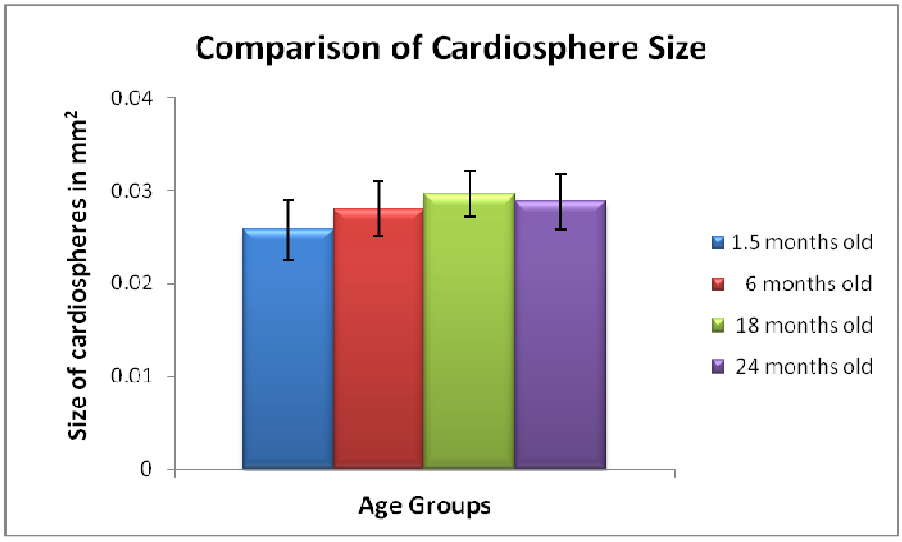

Figure 4.25 Effects of mouse age on cardiosphere size. *Representative images of cardiospheres were taken from mice at 1.5, 6, 18, and 24 months of age under an inverted light microscope. Cardiosphere sizes were measured using ImageJ. There was no significant difference in size between four age groups (p = NS vs. 1.5 months old). Data are presented as mean ± SEM (n = 20).*

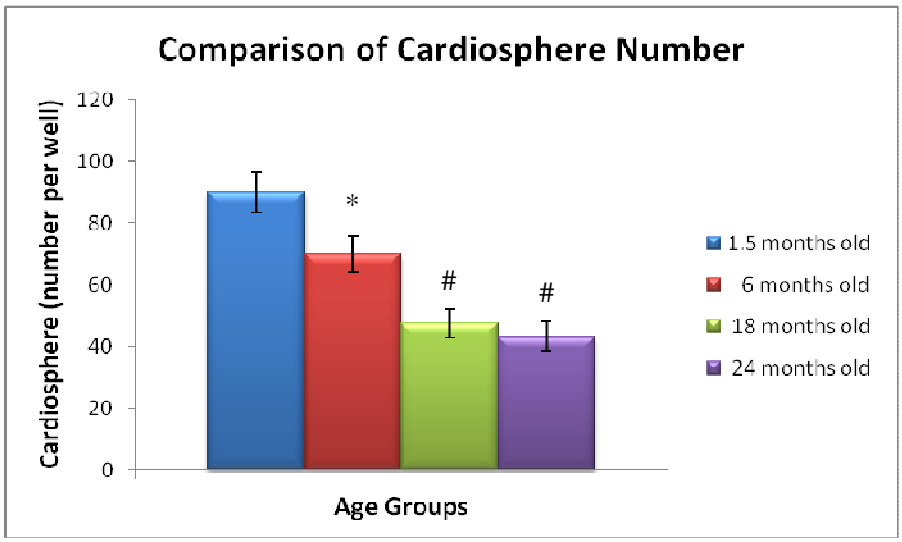

Figure 4.26 Effects of mouse age on cardiosphere number per well. *Cardiospheres were grown in 24 well plates coated with poly-D-lysine. The number of cardiospheres per well was determined from the four age groups. There was a gradual reduction in the number of cardiospheres derived from 1.5, 6, 18, to 24 months of age (90 ± 7 vs. 70 ± 6 vs. 47 ± 5 vs. 43 ± 5 cardiospheres per well). Data are presented as mean ± SEM (n = 4). * p < 0.05 vs. 1.5 months old; # p < 0.01 vs. 1.5 months old.*

4.4.6.3 Cardiosphere-derived cells

Harvested cardiospheres were plated onto fibronectin-coated flasks to produce cardiosphere-derived cells. Once confluent, CDCs were subcultured up to passage 2. Representative images of CDCs at passage 2 from 1.5, 6, 18, and 24 month-old mice are illustrated below in Figure 4.27, showing no difference in morphology. In terms of cell yield, however, there was a significant reduction in the number of CDCs generated per milligram tissue (CDCs/mg tissue) from 6, 18, and 24 month-old mice by 25%, 44% and 55%, respectively, compared to 1.5 month-old (Figure 4.38).

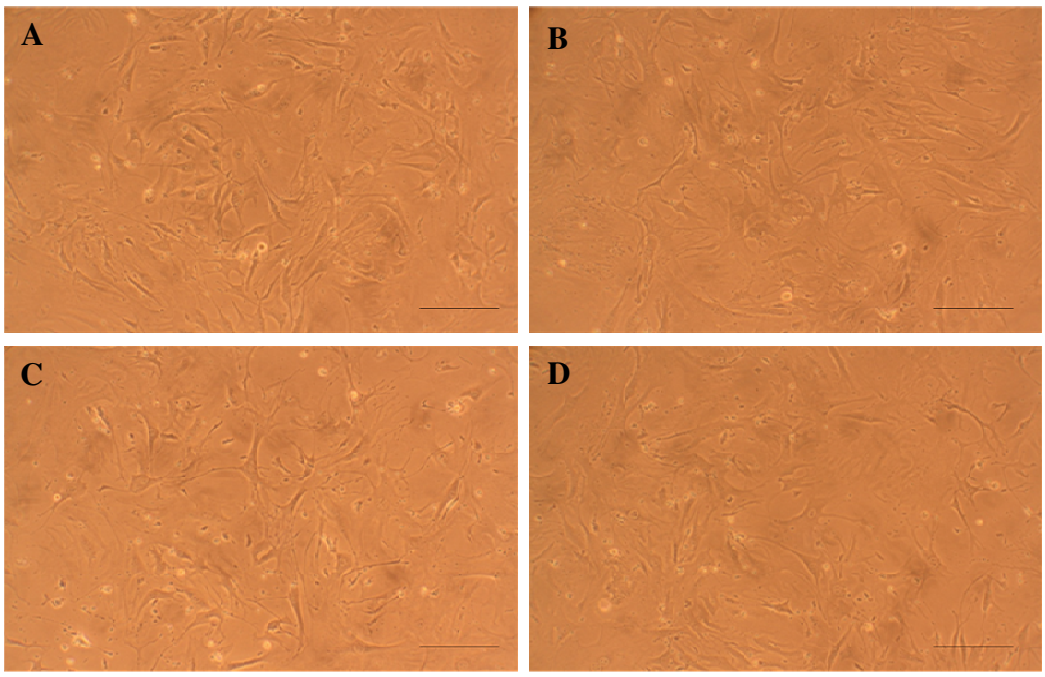

Figure 4.27 Representative micrographs showing morphology of cardiosphere-derived cells grown from mice of different ages (magnification x10). *(**A** - **D**) Passage 2 CDCs were produced from 1.5 month-old (A), 6 month-old (B), 18 month-old (C), and 24 month-old (D) mice. All showed a similar morphology. Scale bars = 200 μm.*

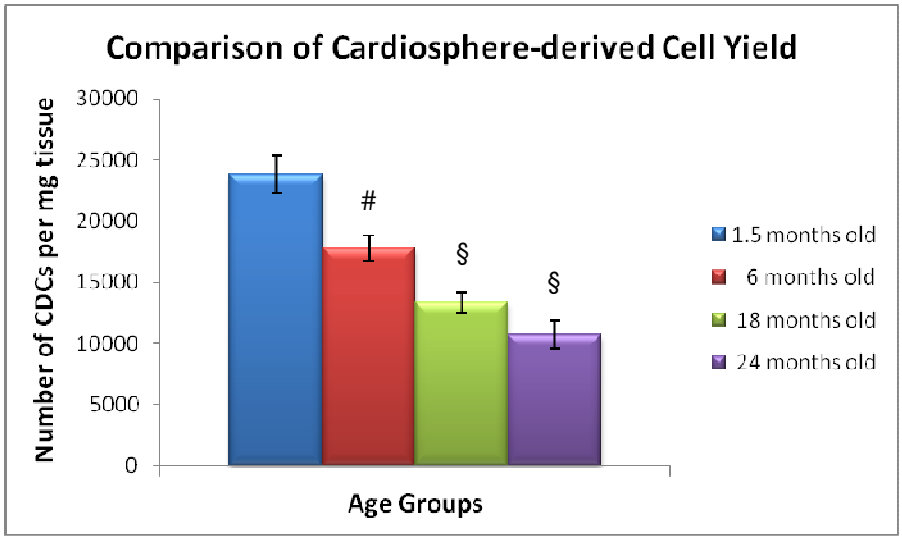

Figure 4.28 Effects of mouse age on cardiosphere-derived cell yield. *Passage 2 CDCs were harvested when reaching confluency. With increasing age, the numbers of CDCs generated per milligram of tissue from 1.5 to 24 month-old mice significantly declined ($2.4 \pm 0.2 \times 10^4$ to $1.1 \pm 0.2 \times 10^4$ CDCs/mg tissue). Data are presented as mean ± SEM (n = 4). # $p < 0.01$ vs. 1.5 months old; § $p < 0.001$ vs. 1.5 months old.*

4.4.7 Effects of age on phenotypic characteristics of cardiosphere-derived cells

From the first study, it was known that cardiosphere-derived cells were a heterogeneous population consisting of cells which expressed cardiac stem cell markers (c-kit and Sca-1) and mesenchymal cell marker (CD90). In order to investigate the effects of age on stem cell subpopulations in the CDC population, flow cytometry was performed to determine the percentage of cells expressing these markers in cells isolated from young to old mice. CDCs derived from 1.5 month-old mice exhibited significantly higher expression of cardiac stem cell markers than those from 24 month-old mice (c-kit: 13 ± 2% vs. 3 ± 1% and Sca-1: 82 ± 4% vs. 46 ± 4%; $p < 0.01$ and $p < 0.001$, respectively; Figure 4.29). However, the expression of the mesenchymal cell marker CD90 was higher in older mice than those from younger mice (24 vs. 1.5 month-old, 69 ± 4% vs. 48 ± 3%; $p < 0.01$; Figure 4.29).

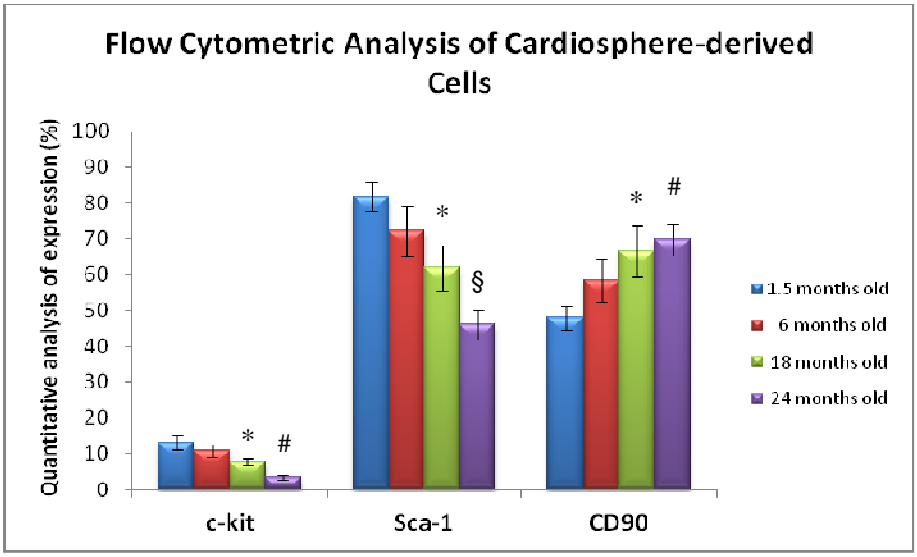

Figure 4.29 Flow cytometric analysis of cardiosphere-derived cells from mice at four ages. *The expression of c-kit, Sca-1 and CD90 on CDCs, was analyzed using flow cytometry and shown as a percentage of positive cells. CDCs derived from 24 month-old mice had significantly lower percentage of cardiac stem cells, expressing c-kit or Sca-1, than those from 1.5 month-old mice (c-kit: 3 ± 1% vs 13 ± 2%; Sca-1: 46 ± 4% vs 82 ± 4%; $p < 0.01$ and $p < 0.001$, respectively). CD90 expression significantly increased in CDCs from 24 month-old mice compared to those from 1.5 month-old mice (69 ± 4% vs. 48 ± 3%; $p < 0.01$). Data are presented as mean ± SEM ($n = 4$). * $p < 0.05$ vs. 1.5 months old; # $p < 0.01$ vs. 1.5 months old; § $p < 0.001$ vs. 1.5 months old.*

4.4.8 Effects of age on cellular senescence of CDCs

Cellular senescence was evaluated using telomere length and telomerase activity (determined by the expression of TERT enzyme). Total RNA and DNA were extracted from CDCs cultured from 1.5, 6 and 24 month-old mouse hearts. Real-time PCR showed that telomeres were shortened by 25% and 50%, respectively, in CDCs from 6 and 24 month-old mice, compared to those in CDCs from 1.5 month-old mice (Figure 4.30). Furthermore, TERT mRNA was significantly down-regulated from 1.5 month-old mice to 24 month-old mice (100% vs. 70% vs. 30%; Figure 4.31).

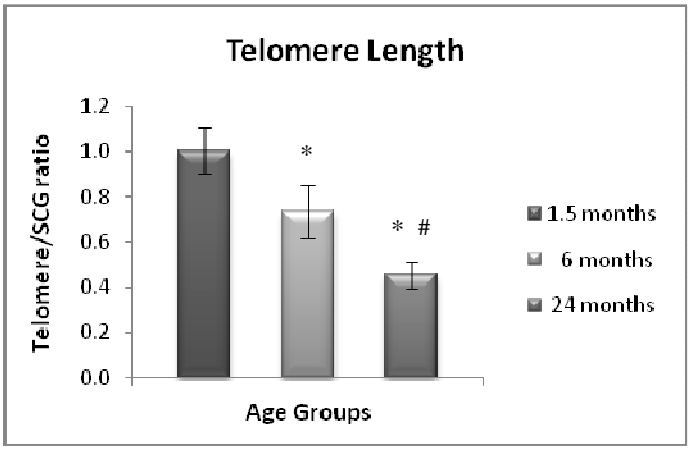

Figure 4.30 Telomere length of CDCs from young and old mice. *Telomere length was measured in passage 2 CDCs cultured from 1.5, 6, and 24 month-old mice using real-time qRT-PCR (n = 3). * p < 0.05 vs. 1.5 months old; # p < 0.05 vs. 6 months old. Abbreviations: SCG = single copy gene.*

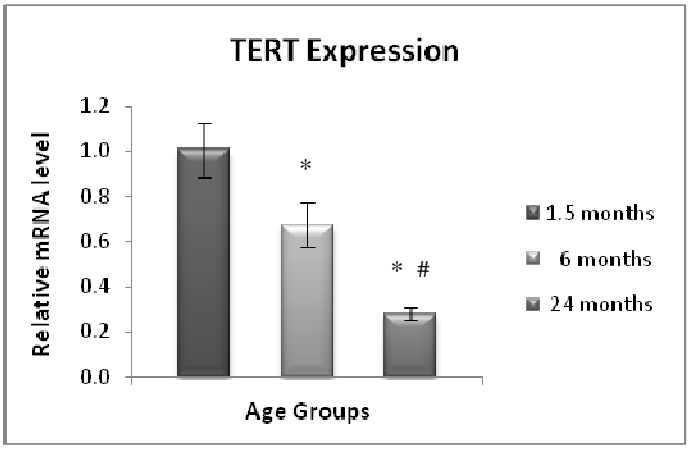

Figure 4.31 TERT mRNA expression in CDCs from young and old mice. *TERT mRNA expression was measured in passage 2 CDCs from 1.5, 6, and 24 month-old mice using real-time qRT-PCR. All values were normalized to GAPDH and reported relative to 1.5 months old (n = 3). * p < 0.05 vs. 1.5 months old; # p < 0.05 vs. 6 months old.*

4.4.9 Effects of age on biological properties of cardiac-derived stem cells

In addition to quantitative changes in cell number, it is important to examine the effect of age on functional performance of cardiac-derived stem cells in terms of migration, clonogenicity, proliferation and cardiomyogenic differentiation as this is directly related to therapeutic potential in stem cell-based therapy.

4.4.9.1 Effects of age on migration of explant-derived cells

EDCs from older mice showed significantly decreased migratory distances at a given time compared with those from 1.5 month-old mice (0.7 ± 0.07 mm for 6 months, 0.5 ± 0.04 mm for 18 months, and 0.4 ± 0.03 mm for 24 months, respectively, vs. 1.0 ± 0.08 mm for 1.5 months; Figure 4.32).

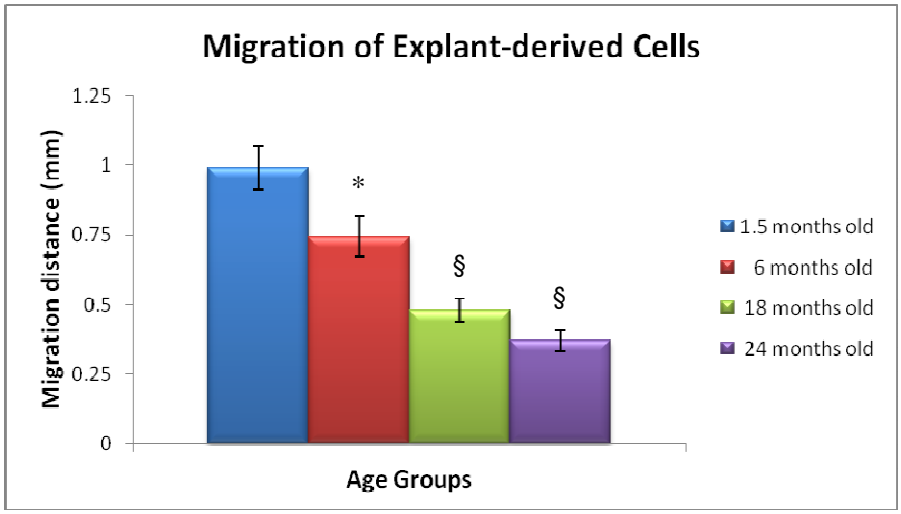

Figure 4.32 Effects of mouse age on explant-derived cell migration. *Heart explants, from 1.5, 6, 18, and 24 month-old C57Black10 mice, were plated on fibronectin-coated petri dishes. Images of explants with migrating EDCs were taken in culture 5 days post plating. The maximal distance of EDC migration was determined from randomly selected explant tissues, using ImageJ. Data are presented as mean ± SEM (n = 12). * p < 0.05 vs. 1.5 months old; § p < 0.001 vs. 1.5 months old.*

4.4.9.2 Effects of age on migration of cardiosphere-derived cells

After cardiospheres adhered to the culture surface, CDCs started to migrate out radially. Again, it was found that the cells from older mice moved slowly relative to those from younger ones at a given time (18 or 30 hours post plating; Figure 4.33). In agreement with the results from EDCs,

the migration distances of CDCs from older mice were significantly shorter at 30 hours following plating with increasing age (6 months: 0.4 ± 0.02 mm, 18 months: 0.3 ± 0.02 mm, and 24 months: 0.2 ± 0.01 mm, respectively), compared with those from 1.5 month-old ones (0.6 ± 0.03 mm) (Figure 4.34).

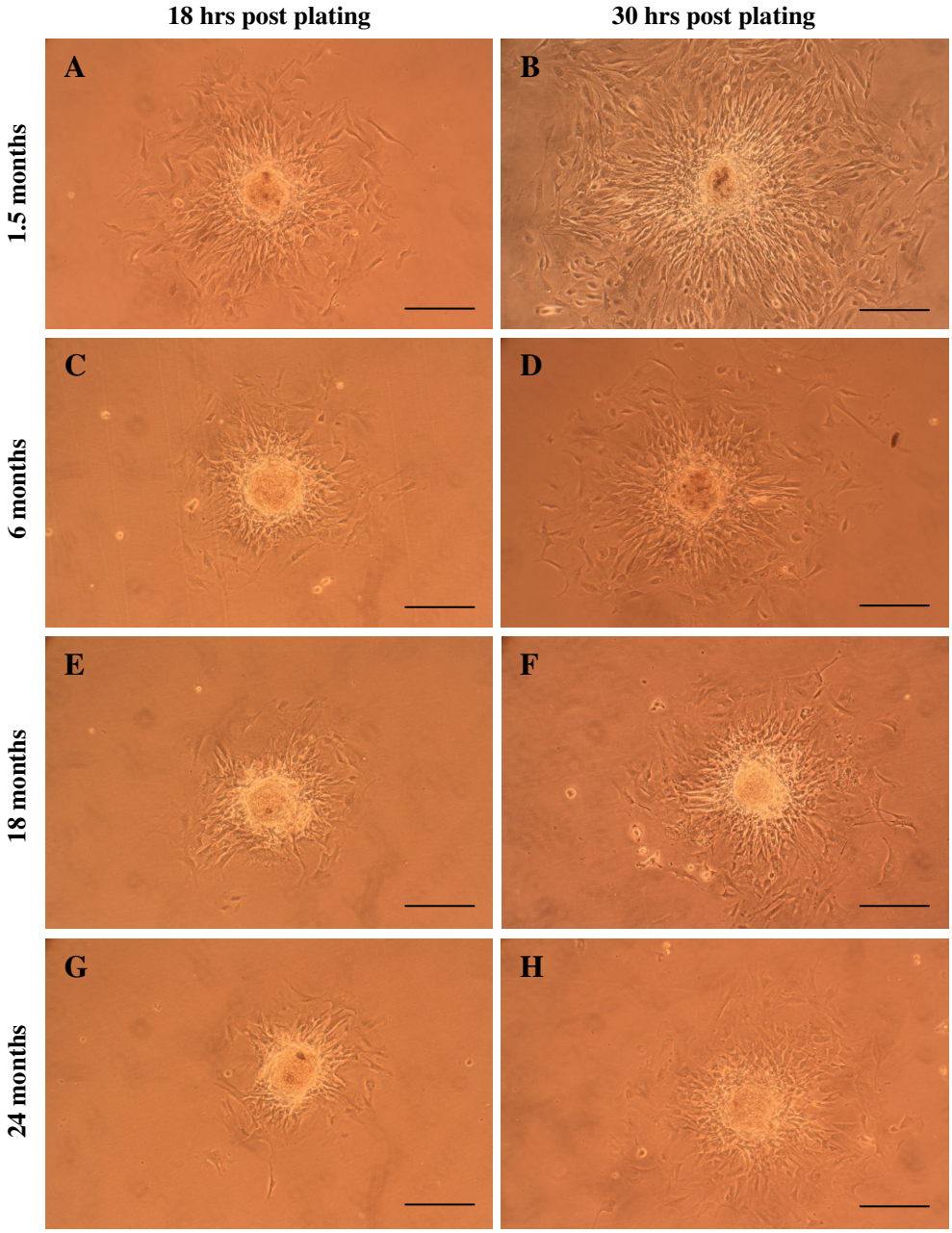

Figure 4.33 Representative micrographs of cardiosphere-derived cells migrating out of cardiospheres (magnification x10). *Cardiospheres were grown on a fibronectin-coated culture surface. The migration of CDCs was recorded at 18 hours (left column) and 30 hours (right column) after plating using a digital camera attached to a light microscope. CDCs from 1.5 month-old mice were found to spread quickly away from cardiospheres. In contrast, CDCs from 24 month-old ones spread slowly. Scale bars = 200 μm.*

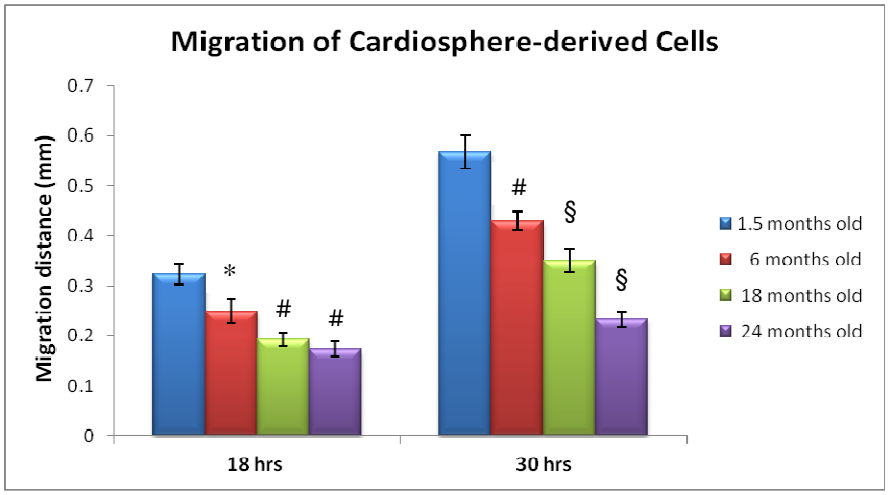

Figure 4.34 Effects of mouse age on cardiosphere-derived cell migration. *Images of cardiospheres with expanding CDCs were taken in culture at 18 and 30 hours post seeding. The maximal distance of CDCs migration was determined from randomly selected cardiospheres, using ImageJ. It was found that CDCs from older mice migrated significantly shorter distances than those from younger mice at a given time. Data are presented as mean ± SEM (n = 10). * p < 0.05 vs. 1.5 months old; # p < 0.01 vs. 1.5 months old; § p < 0.001 months old.*

4.4.9.3 Effects of age on clonogenicity of cardiosphere-derived cells

Passage 2 CDCs from 6, 18, and 24 month-old mice revealed impaired clonogenic efficiency of 42 ± 4%, 33 ± 3%, and 26 ± 5%, respectively, compared with that from 1.5 month-old ones at 45 ± 5% (Figure 4.35), suggesting that age might play a vital role in regulating clonal expansion capacity of cardiac-derived stem cells.

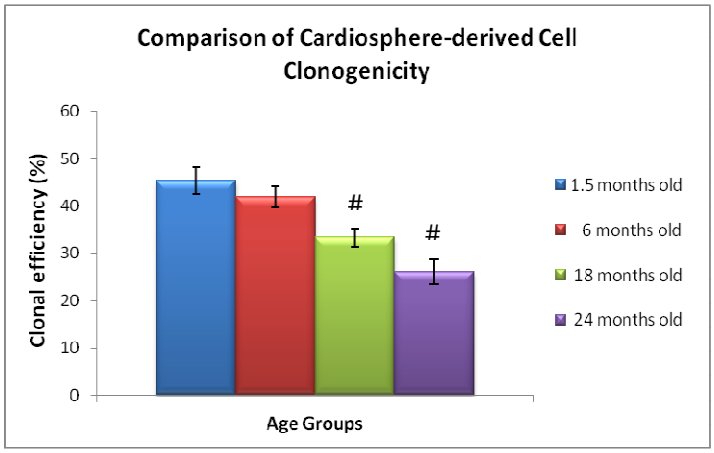

Figure 4.35 Effects of mouse age on cardiosphere-derived cell clonogenicity. *CDCs at passage 2 were prepared by serial dilution and seeded onto 96 well plates. Wells with a single cell were identified post plating and checked for colonies after two weeks of culture. Clonal efficiency consistently declined with increasing age (1.5: 45 ± 5%, 6: 42 ± 4%, 18: 33 ± 3%, and 24: 26 ± 5%, respectively). Data are presented as mean ± SEM (n = 4). # p < 0.01 vs. 1.5 months old.*

4.4.9.4 Effects of age on proliferation of cardiosphere-derived cells

The impact of age on proliferation capacity of cardiosphere-derived cells was investigated using AlamarBlue®. As shown in Figure 4.38, it was found that CDCs from older mice proliferated more slowly than those from younger mice. At day 7, the number of CDCs from 1.5 month-old mice was approximately 1.5, 1.8 and 2.3-fold higher than those from 6, 18, and 24 month-old mice, respectively (Figure 4.36), indicating the deleterious effect of aging on CDC proliferative potential.

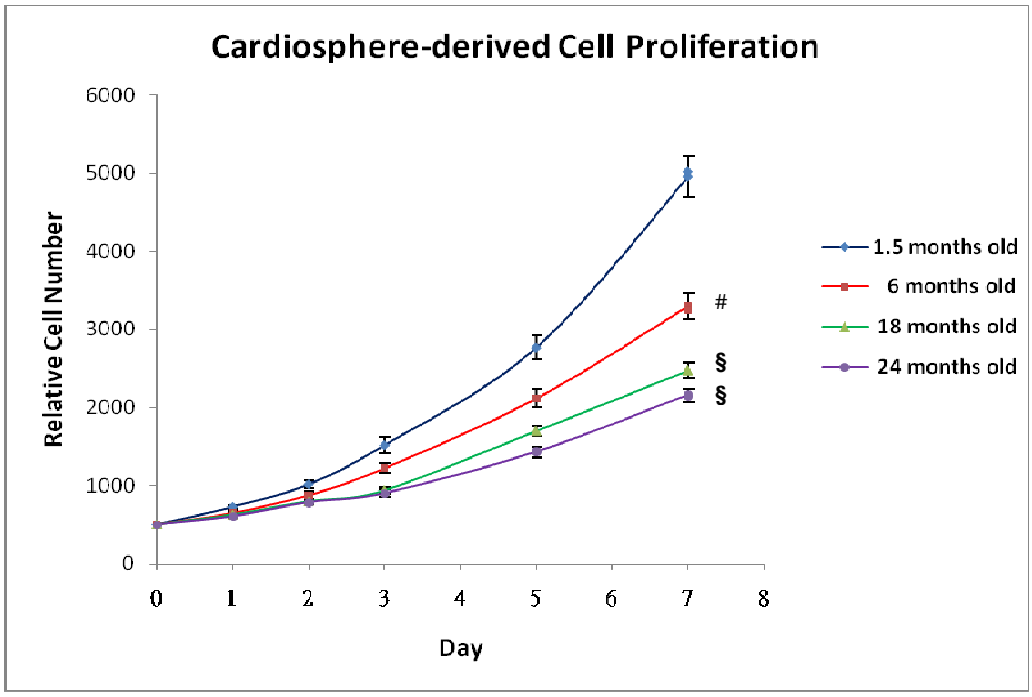

Figure 4.36 Effects of mouse age on cardiosphere-derived cell proliferation. *Passage 2 CDCs were seeded on fibronectin-coated 96 well plates at a density of 500 cells per well. Relative fluorescence intensity was measured at day 0, day 1, day 2, day 3, day 5, and day 7 and converted into relative cell number based on the standard curve. CDCs from older mice showed significantly reduced proliferation capacity relative to those from 1.5 month-old mice at day 7. Data are presented as mean ± SEM (n = 4). # p < 0.01 vs. 1.5 months old; § p < 0.001 months old.*

.

4.4.9.5 Effects of age on cardiomyogenic differentiation of cardiosphere-derived cells

For the study of age effects on the potential of CDCs to differentiate into cardiomyocytes, differentiation was induced in passage 2 CDCs from mice at 1.5, 6 and 24 months of age using 5-Aza. Flow cytometric analysis for cTnT and cMHC showed that CDCs from both young and

old mice were able to differentiate along cardiomyocyte lineage. However, CDCs from younger mice had more cells expressing cTnT and cMHC than those from older mice ($p < 0.05$; Figure 4.37), suggesting that cardiomyogenic differentiation capacity in cardiac-derived stem cells was reduced with increased age.

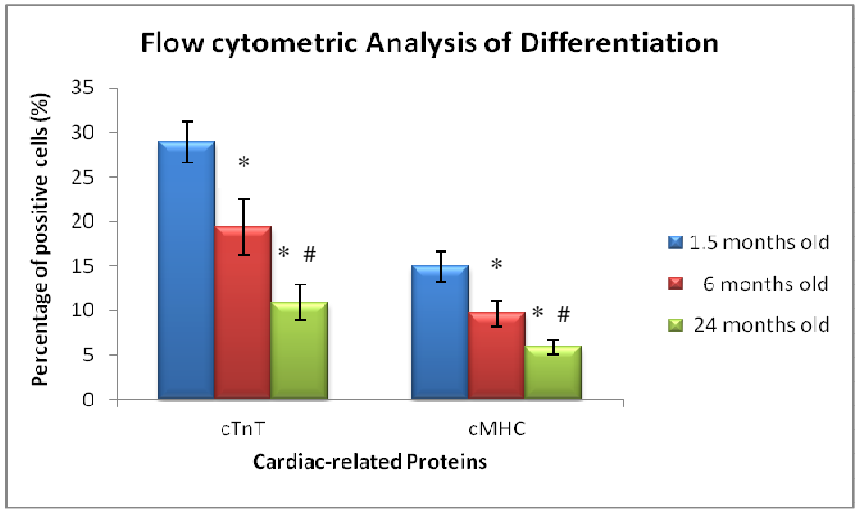

Figure 4.37 Effects of mouse age on cardiomyogenic differentiation. *Passage 2 CDCs were induced to differentiate using 5-Aza. After two weeks of culture, cells were washed and labelled with cardiac troponin T (cTnT) and myosin heavy chain (cMHC) antibodies for flow cytometric analysis. CDCs from older mice presented significantly lower efficiency of cardiomyocyte differentiation than those from 1.5 month-old ones. Data are presented as mean ± SEM (n = 3). * $p < 0.05$ vs. 1.5 months old; # $p < 0.05$ vs. 6 months old. Abbreviations: CDCs = cardiosphere-derived cells, 5-Aza = 5-azacytidine, cTnT = cardiac troponin T, and cMHC = cardiac myosin heavy chain.*

4.5 Discussion

In this chapter, the hypothesis was investigated that with advancing age, murine cardiac stem cells (CSCs) become depleted and show progressive impairment in biological characteristics. Hence, the aims of the work were to isolate and characterize mouse CDCs (cardiosphere-derived cells), investigate the association between the location of cardiac biopsy samples and stem cell properties, and determine the age-related changes of stem cell growth and function.

Characterization of mouse cardiospheres and cardiosphere-derived cells

In this study, cardiac-derived stem cells were isolated from atrial tissues of C57Bl/10 mice at 6 weeks of age, using explantation, and expanded in monolayer culture from cardiospheres, using protocols adapted from those established in our lab for the culture of rat CDCS. The purpose of forming cardiospheres, as a pivotal step, is to provide a consistent starting material for cell expansion and to minimize fibroblast contamination [165]. Cardiospheres had a complex mixed cell phenotype, consistent with previous studies [158, 165], and CDCs comprised both of c-kit and Sca-1 expressing subpopulation cells (13 ± 2 % and 82 ± 4 %, respectively), similar to previously published data [165, 291]. Interestingly, it has been reported by other studies that Sca-1 positive stem/progenitor cells are the predominant stem cell population in the mouse heart [179, 180, 286]. Sca-1^+ cells were found to be 100- to 700-fold more frequent than c-kit^+ cells in the mouse heart [160, 286].

On the other hand, due to no purification using antigenic selection or cell-sorting, CDCs include other subpopulations of mesenchymal cells and cardiac lineage-committed cells apart from cardiac stem cells [165]. Here, passage 2 CDCs contained a significant subpopulation of mesenchymal cells that expressed CD90 based on immunocytochemistry and flow cytometry (CD90: 48 ± 3%), as shown by other investigators [165, 182, 291]. The proportion of c-kit-positive cells co-expressed with CD90 ranged from 45% to 64% in a human CDC population [292]. Another report showed that co-expression of Sca-1 with CD90 was approximately 65% in CSCs from L2G85 transgenic mice (FVB strain background) [291]. This indicates that cardiac

stem cells exhibit a mesenchymal phenotype, essentially reflecting their origin in mesoderm [182, 292, 293]. It has been proposed that the mesenchymal cell population might help cardiac stem cell subpopulations to proliferate and function through physical support and paracrine effects [165, 193]. Importantly, in an experiment with transplantation of various human CDCs into a mouse model of MI, unselected human CDCs were functionally superior to c-kit- or CD90-purified CDCs, as measured by improvement in ejection fraction [294]. Further research work is warranted to elucidate the underlying mechanism.

Cells expressing either c-kit or Sca-1, used as cardiac stem cell markers, have been shown to be capable of differentiating into cardiomyocytes [160, 179, 180, 183]. In agreement with previous work, here, mouse CDCs were induced to differentiate using 5-Aza or DMSO towards cardiomyocyte-phenotype cells, as documented by positive staining for cardiac troponin T and cardiac myosin heavy chain. Smith *et al.* demonstrated that human and porcine CDCs acquired a cardiomyocyte phenotype through differentiation rather than cell fusion when co-cultured with cardiac myocytes *in vitro* [165]. Tateishi *et al.* showed that human CDCs cultured in differentiation medium can differentiate into cardiomyocytes, as shown by positive cardiac troponin T and connexin 43 staining [182]. Intriguingly, Anversa and colleagues showed that the regenerative capability of c-kit$^+$ cells is greater than Sca-1-like CSCs in the dog heart, by demonstrating that clones from c-kit-positive CSCs are 5.9-fold larger than Sca-1-like-positive clones and that c-kit$^+$ clonogenic cells form more differentiated cardiac cells than Sca-1-like-positive cells [295]. Clearly, understanding the association between stem cell antigens and biological properties of cardiac stem cells can provide valuable information for cell-based cardiac therapy in the future [295].

Shenje and colleagues suggested that explant-derived cells were unable to differentiate into functional cardiomyocytes [296]. In a separate study, Andersen *et al.* argued that murine explant-derived cells and cardiospheres were not a source of cardiac stem cells but that CDCs were composed of fibroblasts and CD45$^+$ hematopoietic cells without cardiomyogenic potential [297]. However, it was found here that cardiospheres were immunophenotypically negative for

the marker of hematopoietic cell lineage CD45. The CDCs expressed pluripotent stem cell markers (Oct3/4 and Sox2) and the early cardiac transcription factor (Nkx2.5). Furthermore, they differentiated into a cardiomyocyte phenotype when induced *in vitro*. Additionally, Davis *et al.* explored the origin of CDCs using lineage tracing and demonstrated that these cells are clonogenic, multipotent and self-renewing *in vitro* [192]. Moreover, the same authors demonstrated that human CDCs differentiated to endothelial, smooth muscle cells and functionally integrated cardiomyocytes *in vivo* after transplanted into infarcted SCID mice [298]. It is possible that technical variances of manipulation due to modifications in the culture process led to resultant differences in cell phenotype [298, 299].

Effects of cardiac niche location on characteristics of cardiosphere-derived stem cells

Adult tissue-specific stem cells reside in particular microenvironments known as niches that are located deep in the tissue for protection from extrinsic damaging stimuli [300]. The protective niches are composed not only of stem cells, but also neighbouring differentiated progenies and surrounding supporting cells, which secrete and organize a structural and functional milieu of extracellular matrix and other factors that allow stem cells to manifest their unique intrinsic traits, such as the ability to self-renew and differentiate [301]. In mammals, stem cell niches have been documented in a variety of tissues and organs. For example, the epithelial stem cell niches were found in the bulge area of hair follicles [302], and the intestinal stem cell niche was identified near the crypt base [303].

Resident cardiac stem cells have been detected in adult hearts and their niches found throughout the myocardium [160, 169, 281]. However, it is not fully clear whether the location of the niche is associated with pool size, properties and fate of cardiac stem cells in adult hearts. In the present study, it was found that atrial tissues yielded significantly higher numbers of EDCs (3.3-fold vs. ventricular tissues; $p < 0.001$) and CDCs (3.7-fold vs. ventricular tissues; $p < 0.001$). The results are in line with a previous study by Davis *et al.,* reporting that culture yield of rat EDCs from the atria markedly exceeded other regions [304]. In the current study, it was shown

that CDCs isolated from atria comprised a higher percentage of cardiac stem cells than those from ventricles (c-kit: 13% vs. 3.4%; $p < 0.01$ and Sca-1: 82% vs. 53%; $p < 0.01$, respectively). Intriguingly, Urbanek *et al.* demonstrated that atrial niches were ~ 2-fold larger than ventricular niches and the number of niches in atrial and apical myocardium per mm^3 was ~ 8-fold higher than that at the base to midregion of the ventricle [159]. In addition, Itzhaki-Alfia *et al.* reported that the biopsy location determined the amount of acquired human cardiac progenitor cells and that the right atrium generated higher percentages of c-kit^+ cells compared to left atrium, right and left ventricles [267]. More recently, Mishra and colleagues found that the number of c-kit-positive cells was significantly higher in human CDCs grown from atria than ventricles [292]. Marban *et al.* cultured human CDCs from septum apex on the right ventricular side *via* percutaneous endomyocardial biopsy and obtained therapeutically-relevant quantities; this appears consistent with the above-mentioned studies [165]. Altogether, these findings indicate that atria and apex are the preferential storage sites of endogenous CSCs, compared to the base-midregion of the ventricles [159].

Leri *et al.* proposed that the density of CSC clusters was inversely related to the hemodynamic load and wall stress sustained by the specific anatomical regions of the heart [281]. The very high level of wall stress at the basal to middle region of the left ventricle may contribute to the more frequent turnover rate to replace apoptotic and injured cells through differentiation of stem cells into lineage-committed cells, which gradually depletes CSC reservoirs. In contrast, CSCs resident in the atrial microenvironment experience less wall stress and may be better preserved for the maintenance of the stem cell pool through symmetric division and self-renewal [286].

Apart from the comparison of CSC quantity, *in vitro* functional assays were performed in order to assess the potential to clonally expand and proliferate. CDCs isolated from atria exhibited higher clonal efficiency than those from ventricles (45% vs. 31%; $p < 0.01$), persistently proliferated faster than ventricle-derived CDCs and produced 1.7-fold more cells ($p < 0.001$) after one week. Mishra *et al.* also observed that human CDCs from the atrium exhibited greater differentiation capacity [292]. Although the exact mechanism underlying the findings remains to

be elucidated, there is evidence showing that local mechanical forces are involved in the modulation of cell proliferation, migration, differentiation and apoptosis by changing intracellular responses through the biomechanical interactions with stem cell niches [283, 285, 286]. On the other hand, it should be pointed out that CDC populations containing more c-kit- or Sca-1-positive cells logically display greater functional ability (e.g., proliferation), as shown by atrium-derived CDCs. This is an inherent property that should be taken into consideration. More functional assays, independent of cell number, such as telomere length, telomerase activity and senescence expression might offer further insights. In this case, nevertheless, the results suggest that the atrium is an optimal source for generating CDCs due to an abundance of c-kit$^+$ or Sca-1$^+$ stem cells with higher proliferative and clonogenic potential. It should be noted that clinically, percutaneous endomyocardial biopsy (EMB) is the most widely used technique to obtain heart samples as it is a minimally invasive catheter-based procedure, whereas using atrial biopsies to culture cells for the purpose of regenerative therapy has the need of surgical procedures which are relatively more risky and may be a potential limitation to vulnerable patients.

Effects of age on isolation and function of cardiosphere-derived stem cells

CSCs were isolated and cultured from hearts of C57Bl/10 mice aged 1.5, 6, 18 and 24 months. This was the first time to look at the effects of such a range of chronological age on CDCs; the data is intriguing and informative as the age groups are equivalent to teenage, adult, old and very old subjects in humans. The results of the study clearly displayed a correlation between age-dependent reduction in the quantity of CSCs and impairment of properties, including migration, clonogenicity, proliferation and differentiation. First, it was found that the numbers of EDCs, cardiospheres and CDCs were significantly reduced from the older animals relative to the 1.5 month-old mice. In addition, the amount of cardiac stem cells which expressed c-kit or Sca-1 was persistently down-regulated in CDC populations with increasing age. This is consistent with a human CDC study, which confirmed that c-kit expression declined with advancing age ranging from neonates to teenagers [292]. Likewise, some studies have shown a link between age and decreased self-renewing ability in various stem cell populations, such as endothelial progenitor

cells [305], c-kit positive cells in the testis and epididymis of rats [306] and neural stem cells [307].

In contrast, the expression of CD90 (Thy-1) was up-regulated in CDCs isolated from older mice compared to younger mice. The rise in the proportion of $CD90^+$ mesenchymal cells could be considered as a consequence of a decline in the proliferation rate of cardiac stem cells in aged CDC populations. Additionally, it should be noted that markers currently used to identify MSCs, such as CD90 and CD105, are also expressed in other cell types such as fibroblasts [135, 308, 309]. Thus, more likely, it was the case that the increased expression of CD90 originated from culturing both MSCs and cardiac fibroblasts within the aged CDC population. Recently, it has been demonstrated that CD146 was expressed only in MSCs so that this antigen can be used to distinguish MSCs from cardiac fibroblasts [309, 310]. Alternatively, these two cell types could be discriminated based on the expression of discoidin domain receptor-2 (DDR-2: collagen type I), a specific marker for fibroblasts [311].

Further, this data revealed that EDCs and CDCs from the aged animals had decreased migratory capacity. Flores *et al.* reported that telomere shortening inhibited mobilization of epidermal stem cells from their niches and impaired hair growth, leading to suppressed proliferation of stem cells *in vitro* [312]. There was a substantial reduction in the proliferation rate of mouse CDCs in the aged groups. Similarly, Mishra *et al.* found that human CDC proliferation was greatest in neonates and decreased with age [292]. Reduced proliferative capacity was related to the shortening of telomeres in stem cells [219, 295, 313]. Aged animal-derived CDCs contained a lower percentage of clonogenic cells compared to those from younger groups. Interestingly, Samper *et al.* described hematopoietic stem cells from genetically telomerase-deficient mice that had a limited colony-forming capacity, suggesting age-related down-regulation of telomerase activity might be involved in impairment of clonogenicity [314]. With respect to the cardiomyogenic differentiation of CDCs, the aging process had a negative effect on the capacity for differentiation. There was a considerable reduction in the number of differentiated cells with a cardiomyocyte phenotype, as identified by positive staining of cTnT and cMHC, from the

older animal group. Aging reduced differentiation of bone marrow-derived MSCs into adipocytes and chondrocytes [315, 316]. The degeneration in differentiation potential of stem cells could result from abnormal self-renewal due to telomere shortening and telomerase deficiency in aged stem cells shown here and by others [219, 317]. Importantly, based on the work concerning the impact of aging on pure c-kit-positive CSCs, Torella *et al.* found that the percentage of c-kit^{+} cells showing evidence of senescence expression (i.e., p16^{INK4a}), shortened telomere length and apoptosis was elevated in older wild-type mice; however, interestingly, IGF-1 protected CSCs against adverse aging effect [318].

Telomeres are chromatin structures of repetitive DNA sequence at the end of chromosomes, which maintain chromosomal stability and cell viability [319]. During cell division, incomplete telomeric DNA replication results in telomere shortening in the absence of telomerase activity, which is one of the major causes of telomere dysfunction in human cells [295]. Telomerase, active in stem cells, delays telomere erosion and prevents chromosomal instability by elongating telomeres to protect against the loss of DNA during replication [169, 320, 321]. In the present investigation, there was an inverse relationship between telomere length and age in CDC population. Similarly, the expression of telomerase enzyme was down-regulated in CDCs with aging. In line with this data, Kajstura *et al.* indicated that chronological age is associated with declined telomerase activity and shorter telomere length in human CSCs [322]. With time, when telomere shortening exceeds a critical length limit, cells enter senescence and initiate apoptotic processes which relate to irreversible growth arrest in G1 with resulting loss of crucial functions including cell migration, colony-forming potential, proliferation and differentiation [222, 322]. It is thought that the telomere-telomerase system contributes to age-related changes of stem cell phenotype [318, 323]. Taken together, the length of telomeres may be viewed as a biological marker of aging which is closely linked to the reduced regenerative potential of cardiac stem cells, as suggested by Anversa *et al.* [295].

Finally, it is important to note that the underlying mechanisms by which biological properties of stem cells are mediated over time have not been fully elucidated. Growth factor-receptor

systems, including IGF-1-IGF-1R and RAS, seem to participate in the regulation of CSC growth and apoptosis [222, 318]. Expression of $p14^{ARF}$, $p16^{INK4a}$, $p19^{ARF}$, $p27^{kip1}$, and p53, induced by a variety of stimuli, such as reactive oxygen species (ROS), oxidative DNA damage and activation of certain oncogenes, may be involved in growth arrest and senescence [213, 295, 318]. More importantly, these factors interact with the telomere-telomerase system *via* complex signalling pathways to control stem cell behaviour and fate in response to chronological age and pathophysiology [222, 318, 324]. More research is required to clarify the role of various systems and their relationships in the biology of stem cells, as this is likely to contribute significantly to the development of novel therapeutic strategies in the clinic.

Study limitations

There were a few limitations in this present study. First, no positive staining controls were performed in the immunostaining for characterizating the phenotype of CDCs (e.g., c-kit, Sca-1, CD90, etc.) in flow cytometry and immunocytochemistry as the antibodies utilized here were selected from published papers [179, 182, 183, 192]. Ideally, a positive control should be used to confirm the specificity of an antibody in labelling in cells containing the protein, but not other cells [378]. Furthermore, the use of negative staining control distinguishes specific staining from artifactual staining by detecting nonspecific binding [378]. Here, as negative controls for immunocytochemistry (e.g., Nkx2.5, Oct3/4, Sox2, etc.), cell samples stained with only secondary antibody served as negative thresholds, which may not be adequate to exclude the false positivity. Future experiments would include samples stained with isotype-matched antibody as negative controls in order to optimize the specificity of results.

In addition, the capabilities of cell migration and proliferation were used to compare CDC functions between different age groups. However, these biological properties of stem cells were limited in assessing the true efficacy of CDCs for cardiac therapy. Functional assays such as engraftment, secretion of paracrine factors and *in vivo* regenerative ability following transplantation might better reflect CSC function in terms of therapeutic potential.

4.6 Conclusions

In summary, CDCs grown from mouse hearts consisted of a mixture of resident cardiac stem cells and accompanying mesenchymal cells. Mouse CDCs expressed cardiac stem cell markers (c-kit and Sca-1) and pluripotent cell markers (Oct3/4 and Sox2), and exhibited cardiomyogenic differentiation potential *in vitro*. Atrial tissues harboured more c-kit$^+$ or Sca-1$^+$ CSCs, which demonstrated greater migration and proliferation capacity than CSCs from ventricular tissues, suggesting that the atrium seems to be an optimal source for generating CSCs for clinical applications. CSCs could be isolated and expanded from young and old hearts; however, cell yield and their regenerative potential gradually decreased with age. Shortened telomere length and down-regulated telomerase activity were observed in older animals. Both cell-extrinsic environment and cell-intrinsic aging were involved in the regulation of CSC characteristics. In conclusion, these findings have implications for prospective applications of CSCs as therapeutic cell sources, in particular for cardiac therapy in elderly patients with cardiovascular disease.

Chapter 5

Characterization of heart function and cardiac stem cells in dystrophic mice

5.1 Abstract

Duchenne muscular dystrophy (DMD), an X-linked recessive disease, is characterized by a systemic lack of dystrophin protein in the sarcolemma, and affects skeletal and cardiac muscles. Current therapies have increased life span in DMD patients, but this has led to the majority of surviving patients developing dilated cardiomyopathy (DCM). Recently, stem cell-based therapy has emerged as a promising approach to treat cardiovascular diseases, however, little is known about the characteristics of endogenous cardiac stem cells (CSCs) in patients with DMD or whether CSCs could be used to prevent DCM in patients. This study aimed to measure heart function using high field magnetic resonance imaging (MRI) and to characterize CSCs in the wild-type and mdx mouse, an animal model of human muscular dystrophy, at two different ages, 6 and 18 months. Six month-old mdx mice showed right ventricular (RV) dilatation and reduced RV ejection fraction (EF) in comparison to young wild-type mice. Old mdx mice displayed significant RV and LV dilatation and decreased EF in both ventricles compared with age-matched wild-type mice. Older mdx mice also had significantly greater dystrophic cardiac fibrosis than younger mdx and age-matched control animals. Endogenous CSCs could be isolated from atrial biopsy samples *via* the formation of cardiospheres at both ages. The numbers of explant-derived cells (EDCs), cardiospheres and cardiosphere-derived cells (CDCs) from mdx mouse hearts were comparable to those from age-matched wild-type mice. There were no significant differences in expression of cardiac stem cell markers (c-kit and Sca-1) between age-matched mdx and wild-type mice. Furthermore, atrial CDCs from mdx dystrophic hearts were not distinguishable from atrial CDCs from wild-type hearts in *in vitro* culture, as measured by migration, clonal efficiency and proliferative capacity. In conclusion, the mdx mouse, a disease model of human DMD, is associated with impaired cardiac function due to DCM, but atrial CDCs, consisting of cardiac progenitor cells, could be generated and grown from young and old mdx mice without detectable differences from those cultured from wild-type mice.

5.2 Introduction

In addition to the adverse impact of age (discussed in Chapter 4), endogenous stem cells are affected by cardiovascular diseases, independent of the underlying cause, which lead to impairment in endogenous repair of the injured heart and decline in the efficacy of patient-specific cells for the purpose of autologous therapy [222]. In particular, most experimental studies have focused on the effects of ischemic heart disease, both acute and chronic, on stem cells. It has been reported that the number of c-kit expressing cells had a ~3-fold increase in mouse adult hearts following acute myocardial infarction (AMI) [379], whereas the c-kit$^+$ CSC pool size was exhausted with impaired clonogenic and differentiation capacity in chronic ischemic heart failure (HF) [169, 370].

Importantly, although the aetiology of ischemic origin accounts for the majority of LV systolic dysfunction, non-ischemic heart diseases can result in progressive HF in the clinic. On the basis of previous studies, approximately 10-30 % of HF patients have no history of AMI or coronary artery disease [9, 380]; these subjects suffer from HF due to non-ischemic cardiomyopathy [157]. Pathophysiologically, non-ischemic dilated cardiomyopathy (DCM) could be caused by either valvular heart diseases, genetic abnormalities (hereditary DCM) or previous myocarditis [157, 381]. Duchenne muscular dystrophy (DMD), a genetic disease, is caused by mutations (e.g., deletion or point mutation) in the dystrophin gene on the X chromosome, which lead to the absence of dystrophin expression in cardiac muscles, characterized by dystrophic necrosis and fibrosis [227, 325]. According to the Pediatric cardiomyopathy Registry, DMD patients are diagnosed with DCM at the average of 14.4 years [223, 228]. Moreover, Finsterer *et al.* reported that noticeable cardiomyopathy becomes clinically evident after the age of 10 years and increases in incidence with age; until it is occurring in nearly all patients above the age of 18 years [224].

It seems plausible that a combination of stem cell and dystrophin restoration may offer a possible approach to restore cardiac function in DMD patients, as the pathology of DMD is

associated with the loss of both dystrophin and myocardial cells. In chronic ischemic HF, after occlusion of a major vessel, CSCs experience apoptosis and necrosis similar to surrounding myocardial cells due to interrupted oxygen supply and blocked vascular perfusion [382]. Furthermore, telomeric DNA damage occurs due to reactive oxygen species (ROS) [384], which further reduces turnover of CSCs [222]. Meanwhile, constant demand on CSCs to replace mature cells lost during injury gradually depletes CSC reservoir [159]. However, there is extremely limited research regarding CSC characteristics and therapeutic potential in the non-ischemic DMD heart (so far, there seems to be only one paper describing CSCs in GRMD dog model of DMD [336]), which is a prerequisite to the development of cell-based regenerative strategies for DMD patients in the future.

A number of animal models, which are genetic equivalents to the human DMD, including mice [329-331], cats [332, 333] and dogs [334-336], have been used to understand the molecular mechanisms and pathophysiology of dystrophin-associated muscular dystrophy [227]. As a model of dystrophic cardiomyopathy, the mdx mouse has been extensively studied [227, 329-331, 337-341]. The mdx mouse, a naturally-occurring mutant, has a complete loss of dystrophin protein due to a point mutation in the DMD gene, and shares many of the features of DMD patients, including muscular fibrosis, skeletal muscle dystrophy, and cardiomyopathy [227, 339]. Although the mdx mouse is a mild phenotype of muscular dystrophy, it has been the most commonly used animal model for the characterization of dystrophin-deficient cardiomyopathy and the exploration of potential novel therapies [331, 342].

In this present study, dystrophic hearts of 6 and 18 month-old mdx mice were characterized for cardiac morphology and function using high-resolution cine-MRI and histology. Furthermore, to test the hypothesis that compared with wild-type mouse hearts, mdx mouse hearts grow fewer CSCs *in vitro* and these cells have impaired intrinsic characteristics, CDCs were isolated and expanded from young and old mdx mouse hearts to investigate the biological differences from age-matched control mice, and to correlate observed differences with changes in cardiac function. To the best of my knowledge, this was the first time to determine cell culture yield and

characteristics of CDCs *in vitro* from dystrophic heart using an mdx model of DMD. By studying both young and old mdx mice, it was possible to learn the progression of pathology in the dystrophic heart with time and to use old mdx mice as a better equivalent of DMD patients.

The work in this chapter concentrated on the characterization of cardiac morphology/function in 6 and 18 month-old dystrophic mice and cardiosphere-derived stem cells cultured from young and old mdx mice. Specifically, the aims were to:

- Assess cardiac morphology and function in dystrophic mdx mice at 6 and 18 months of age using high-resolution cine MRI.
- Characterize necrosis and fibrosis using histology in mdx mice of 6 and 18 months compared with age-matched wild-type mice.
- Isolate, culture and characterize cardiac-derived stem cells *in vitro* from adult mdx and wild-type mice for comparison of number and properties.

5.3 Methods

5.3.1 Animals

Mice at 6 and 18 months of age (including C57Bl/10 control (wild-type) and mdx for each group) were used in this study. After MRI had been performed, mice were sacrificed and their hearts removed for cardiac stem cells culture and histological and immunohistochemical analyses.

5.3.2 Magnetic resonance imaging

Cardiac cine MRI of mouse hearts was conducted as previously described [372]. Mice were first anaesthetized with 4% vaporized isoflurane (Abbott, IsoFlo®, UK) in pure oxygen. After body weights were measured, they were transferred into a purpose built cradle in supine position (Figure 5.1), and maintained at 2% isoflurane at 1.5 L/min oxygen flow throughout the MRI scanning period using a vertical bore 11.7 T (500 MHz) system with a Bruker console and 40 mm birdcage coil. To monitor heart rate and respiration, electrocardiogram (ECG) leads were inserted into the forepaws and a respiration sensor loop was applied to the anterior chest (Figure 5.1). Once the animal was positioned in the magnet, ECG and respiration trigger thresholds were adjusted to ensure that acquisitions were initiated at the same point during the cardiac cycle.

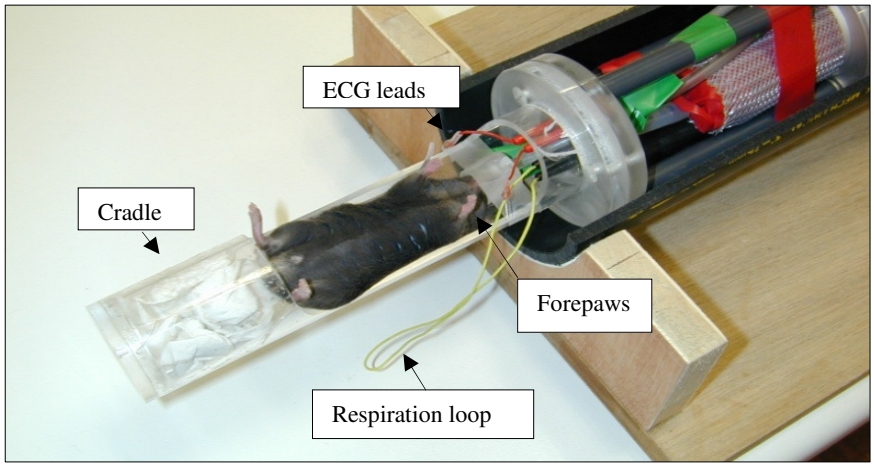

Figure 5.1 Mouse positioned in the purpose built cradle. *ECG leads were inserted into the forepaws to monitor heart rate/rhythm and a loop of wire was taped onto the chest to check respiration.*

Scout images were acquired to set up a true short-axis view. Firstly, a stack of 4 axial images

were acquired and used to adjust the position of the heart in the magnet (Figure 5.2 A to D). Two perpendicular long-axis images were acquired (Figure 5.2 E and F), from which a true short-axis image was established (Figure 5.2 G). The coil was tuned and matched, and shim coils were utilized to homogenize the magnetic field across the whole heart. Contiguous 1.0 mm short-axis slices were acquired to cover the whole heart (through base to apex, including left and right ventricles) (Figure 5.3) using an ECG-triggered and respiration-gated fast low-angle shot (FLASH) sequence (field of view 51.2 mm^2, matrix size 256 x 256, echo time/repetition time (TE/TR) 1.43/4.6 ms, 17.5^o pulse, 25-35 frames per cardiac cycle).

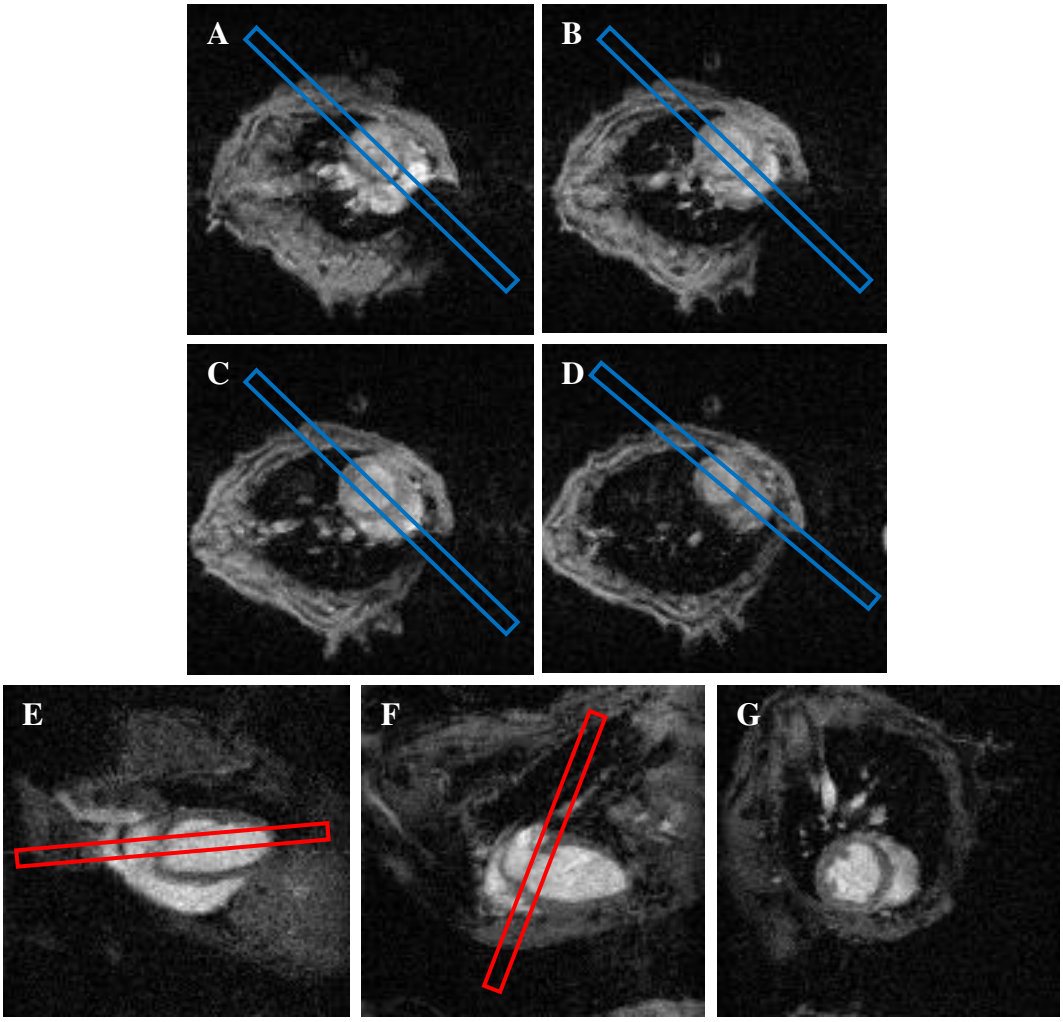

Figure 5.2 Establishing a true short-axis image. *(**A** - **D**) A stack of four axial images were acquired (from base to apex of a heart) on which a 4 chamber long axis acquisition was planned (blue rectangles across both ventricles). (**E**) A 2 chamber long-axis image was planned on the 4 chamber image (red rectangle parallel to long-axis). (**F**) Second long-axis image perpendicular to the first one was acquired. True short axis images were planned using both the 4 and 2 chamber long axis images (red rectangle across both ventricles). (**G**) A true short-axis image.*

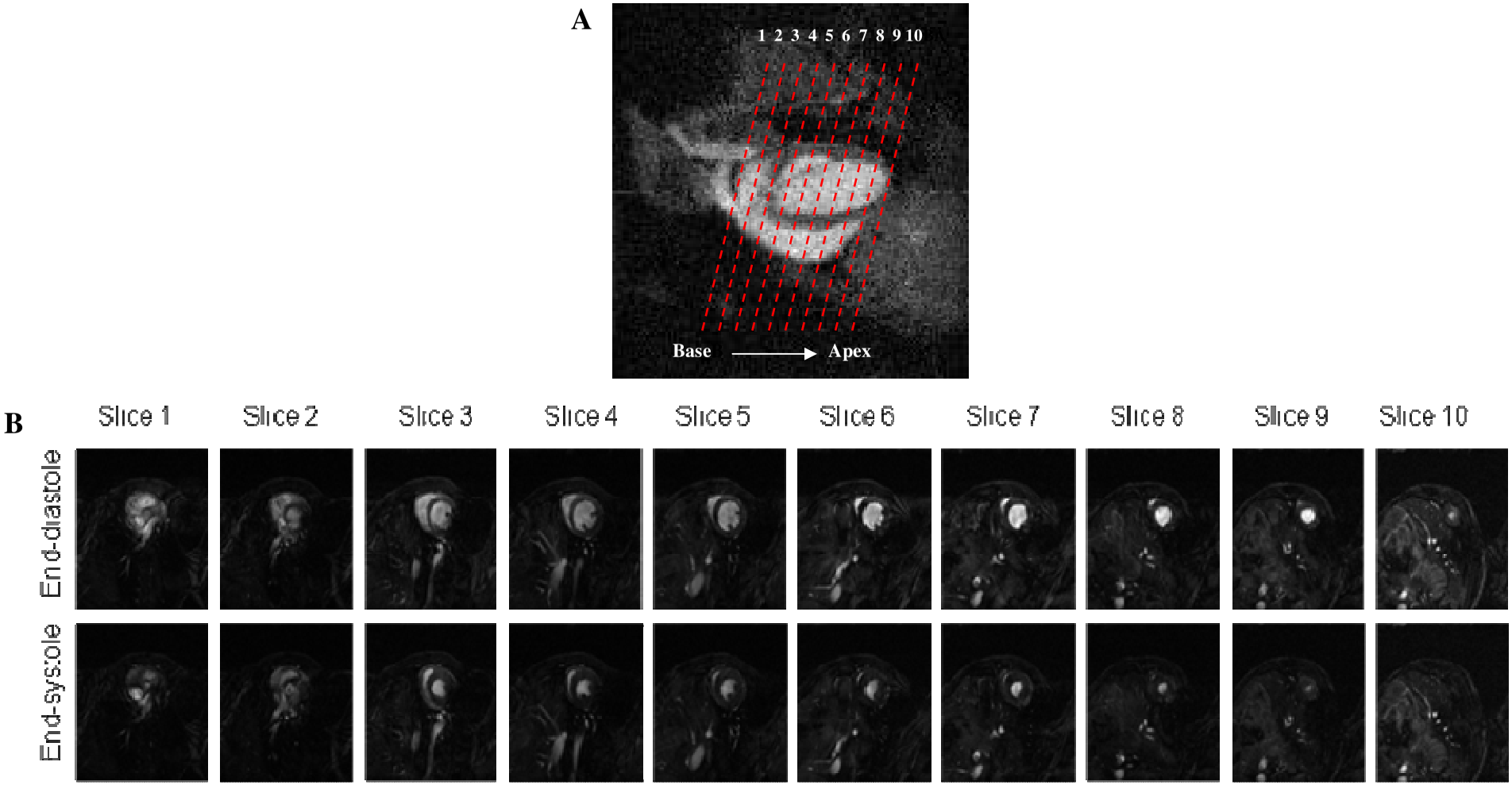

Figure 5.3 MR images of serial contiguous slices of a whole heart. *(**A**) Red dotted lines indicate various levels of imaged slices ventricles from base to apex using MRI. (**B**) High-resolution cine MRI images were acquired from the basal slice 1 to apical slice 10 in 1 mm slice thickness to cover the whole left and right ventricles. For each slice, end-diastolic (top row) and end-systolic (bottom row) short-axis images were selected to measure parameters of cardiac function.*

5.3.3 Image analysis

Once the MRI data were collected, image analysis was done using ImageJ. For each slice, end diastolic (ED) and end systolic (ES) frames were selected in accordance with maximal and minimal ventricular areas (Figure 5.3). There were two sets of analyses done individually on two different occasions, which had about 5% variability between them, and the data were finally presented as the average of two values. Image analysis was not blinded in performing the measurements of wild-type and mdx mice. The epicardial and endocardial borders of every slice were outlined using the free hand drawing function (Figure 5.4 and Figure 5.5). Left and right ventricular volumes were derived by summing all segmental volumes. From the ED and ES volumes, characteristics of heart function including stroke volume (SV = EDV–ESV), ejection fraction (EF = SV/EDV), cardiac output (CO = SV x heart rate) and cardiac index (CI = CO/body mass) were calculated. Left ventricular (LV) mass was calculated by multiplying the LV wall volume by the specific gravity of the myocardium (1.05 g/cm^3). Due to the slice positioning strategy employed as described above, cine-MRI offers excellent reproducibility in the measurements of these parameters [383].

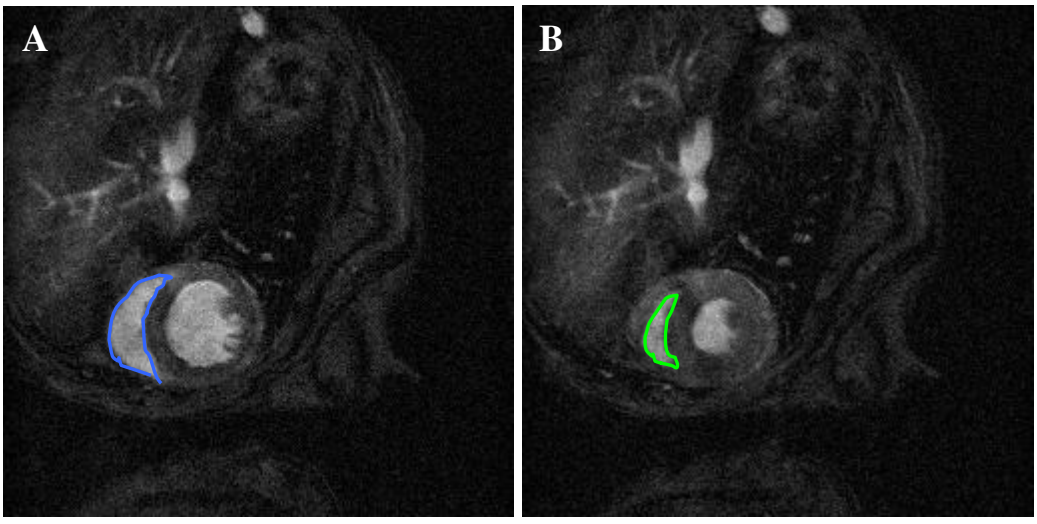

Figure 5.4 Segmentation of the right ventricle. *(**A, B**) End-diastolic (A) and end-systolic (B) frames on each slice were selected according to maximal and minimal ventricular areas. The endocardial borders on ED and ES frames (blue in A and green in B) were delineated using the free hand drawing function. RV ED and ES volumes were calculated. Abbreviations: ED = end-diastolic, ES = end-systolic, and RV = right ventricle.*

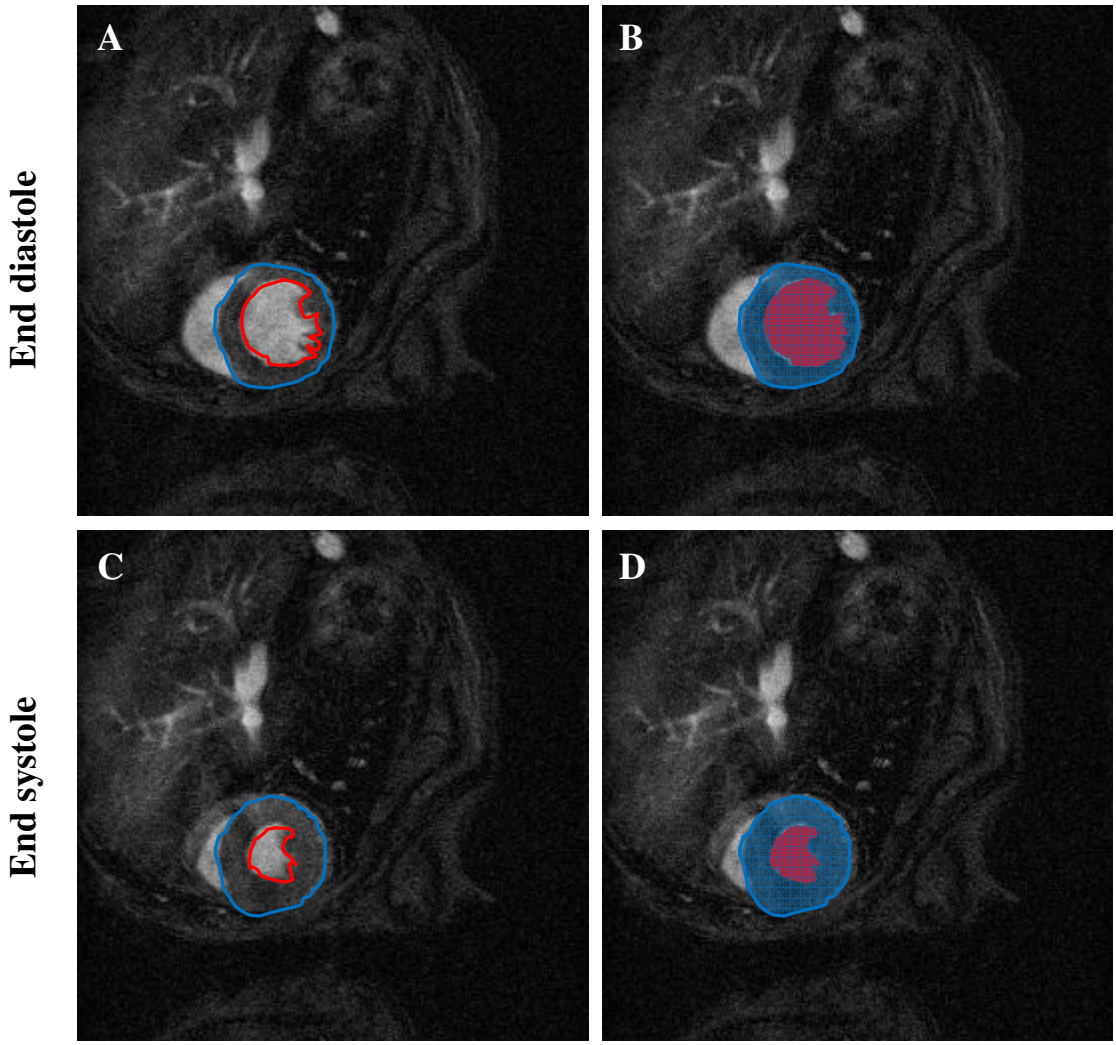

Figure 5.5 Segmentation of the left ventricle. *(**A**, **B**) End-diastolic and (**C**, **D**) end-systolic frames on each slice were selected according to maximal and minimal ventricular areas. The epicardial perimeter (open blue in A and C) and endocardial perimeter (open red in A and C) were delineated using the free hand drawing function. The LV cavity area (filled pink in B and D) and LV wall area (filled blue in B and D) were calculated to obtain EDV/ESV and LV wall volume.*

5.3.4 Tissue sectioning

For histology (hematoxylin & eosin and picro-sirius red staining) and immunohistochemistry (dystrophin staining), isolated hearts of control (wild-type) and mdx mice were immediately washed in cold PBS to get rid of blood. Heart samples were cut into half transversely, and embedded and frozen in optimal cutting temperature (OCT, Sakura Tissue-Tek) compound on dry ice, and stored at -80^{o}C. Heart tissues were horizontally sliced into 10 µm sections at -20^{o}C using a cryostat (Bright 5040) and stored at -80^{o}C until use.

5.3.5 Immunohistochemistry

Cryosections of heart tissue from control (wild-type) and mdx mice were fixed in 4% PFA for immunohistochemistry, which was used to detect dystrophin proteins in heart muscle cells. The protocol for the process is outlined in Chapter 2.

5.3.6 Assessment of cardiac fibrosis

According to the protocol described in Chapter 2, 10 µm sections were stained with picro-sirius red solution, a collagen selective stain, to quantify collagen content, which represents fibrotic areas in heart tissue. The analysis of cardiac fibrosis was performed on five regions from each heart, including right ventricle, inter-ventricular septum, and left ventricle (anterior wall, lateral wall, and posterior wall). Images were captured at 10 and 25 x magnification on a Nikon light microscope attached to a digital Canon camera (EOS 1000D, Canon Inc., Japan). The percentage of cardiac fibrotic area for wild-type and mdx mice was measured from digital grey-scale images using ImageJ (Figure 5.6).

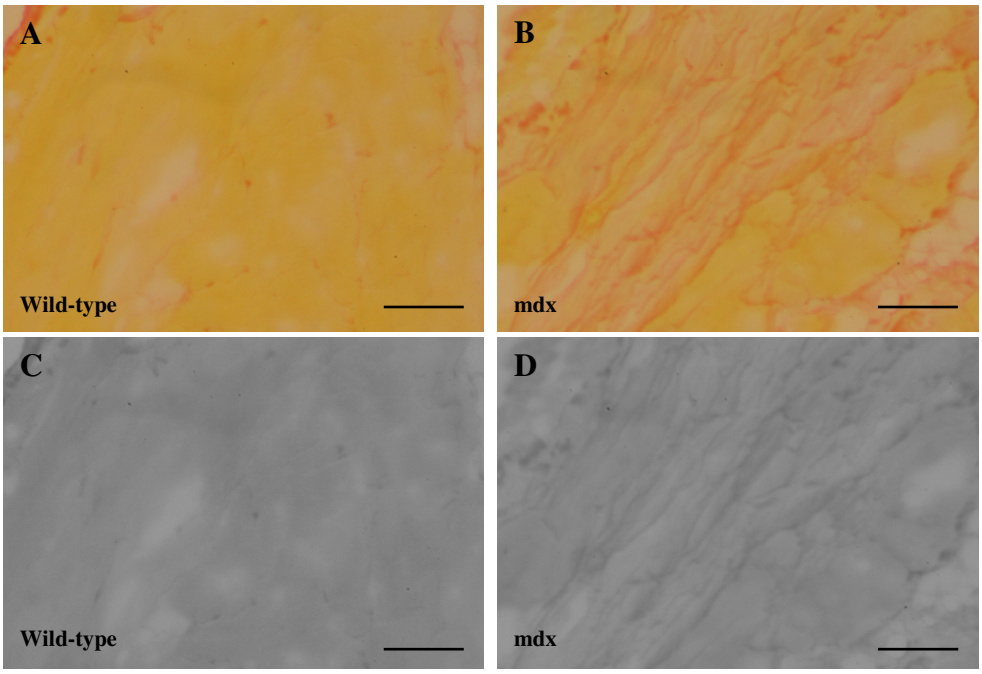

Figure 5.6 Representative original and grey-scale digital images of control (wild-type) and mdx cardiac fibrosis. (***A*** - ***D***) *Photomicrographs of picro-sirius red stained heart sections were taken (top panel) and converted to digital gray-scale images for quantification of fibrosis (bottom panel) using ImageJ analysis software. Wild-type cardiac tissue (A and C). mdx cardiac firbosis (B and D). Scale bar = 100 µm.*

5.3.7 Explantation and cardiac-derived stem cell culture

Heart fragments were explanted from control (wild-type) and mdx mice aged 6 and 18 months old. Explant-derived cells were harvested and counted. Isolated EDCs were plated to form cardiospheres, which were counted and measured for number and size. Further, cardiospheres were cultured into a monolayer cardiosphere-derived cells, which were subcultured up to passage 2 CDCs, as previously described in Chapters 2 and 4.

5.3.8 Migration assay of explant-derived cells and cardiosphere-derived cells

For the explant-derived cell migration assay, heart tissue explants, from control (wild-type) and mdx mice at both 6 and 18 months of age, were plated on 60 mm petri dishes pre-coated with fibronectin (10 µg/ml in PBS). For cardiosphere-derived cell migration analysis, isolated cardiospheres were plated into the fibronectin-coated culture flasks and expanded as a monolayer of CDCs. The procedures for these experiments were performed, based on the protocols described in Chapter 4.

5.3.9 Study design

Experiments in this study involved *in vivo* MRI for cardiac function and morphology, histology and immunohischemistry of heart tissue, and isolation and characterization of cardiac-derived stem cells in wild-type and mdx mice at 6 and 18 months of age. The design of this study is summarized in a simplified flow chart below (Figure 5.7).

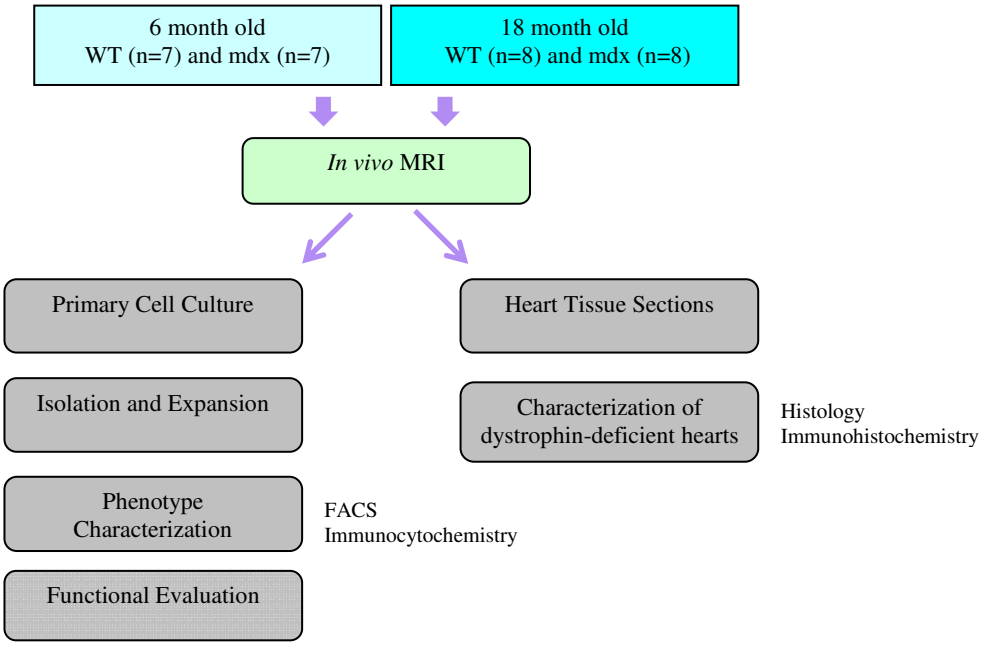

Figure 5.7 Flow diagram showing an overview of the study design.

5.4 Results

Before and after MRI scanning, mice were generally examined and seemed to be well and alert. It is important to note that, from their gross appearance, there were no overt symptoms of heart failure, such as peripheral edema, in control (wild-type) or mdx mice at both ages of 6 and 18 months. There was no significant difference in body weight between wild-type and mdx mice at either 6 or 18 months old (Table 5.1). Heart rates, adjusted under anaesthesia during imaging, were similar at around 430 bpm, which may potentially mask pathophysiological differences.

5.4.1 Cardiac morphology of left and right ventricles using high-resolution cine MRI

5.4.1.1 Cardiac morphology of both ventricles in control (wild-type) and mdx mice

As shown in Figure 5.8, the right ventricle was dilated, but the left ventricle was not, in 6 month-old mdx mice. With disease progression over time, both right and left ventricles developed chamber dilatation in 18 month-old mdx mice, compared to age-matched wild-type mice (Figure 5.8). It is important to note that there was no localized thinning of ventricular wall at the end of systole in mdx mice, which is consistent with the pattern of generalized pathological lesions. In addition, no focal hypokinesis or akinesis was observed during cardiac cycles at either age in mdx mice.

Table 5.1 In vivo MRI measurement of cardiac function in 6 and 18 month-old control and mdx mice

		6 months (n = 7)	18 months (n = 8)
Body weight (g)	con	34 ± 1	27±2
	mdx	33 ± 1	28±1
Heart rate (bpm)	con	452 ± 9	445 ± 20
	mdx	405 ± 27	412 ± 24
Right ventricle			
End diastolic volume (ul)	con	60 ± 2	61 ± 8
	mdx	67 ± 7	**84 ± 8***
End systolic volume (ul)	con	18 ± 2	27 ± 5
	mdx	**27 ± 3***	**44 ± 6***
Stroke volume (ul)	con	42 ± 1	34 ± 2
	mdx	40 ± 5	39 ± 4
Ejection fraction (%)	con	70 ± 2	58 ± 3
	mdx	**60 ± 2***	**47 ± 2***
Cardiac output (ml/min)	con	19 ± 1	15 ± 1
	mdx	16 ± 2	15 ± 1
Left ventricle			
End diastolic volume (ul)	con	67 ± 5	52 ± 3
	mdx	63 ± 4	66 ± 6
End systolic volume (ul)	con	22 ± 3	18 ± 2
	mdx	24 ± 3	**30 ± 3***
Stroke volume (ul)	con	45 ± 2	34 ± 2
	mdx	39 ± 4	36 ± 4
Ejection fraction (%)	con	68 ± 3	66 ± 2
	mdx	62 ± 4	**55 ± 2#**
Cardiac output (ml/min)	con	20 ± 1	15 ± 1
	mdx	**16 ± 1***	14 ± 1
LV mass (mg)	con	110 ± 9	91 ± 6
	mdx	106 ± 6	**114 ± 8***
Mass/body weight ratio	con	3.2 ± 0.2	3.4 ± 0.3
	mdx	3.2 ± 0.2	4.1 ± 0.2

*Data are presented as mean ± SEM. * $p < 0.05$ vs. control (wild-type); # $p < 0.01$ vs. control. Stroke volume = end-diastolic volume - end-systolic volume; Ejection fraction = stroke volume/end-diastolic volume; Cardiac output = stroke volume x heart rate.*

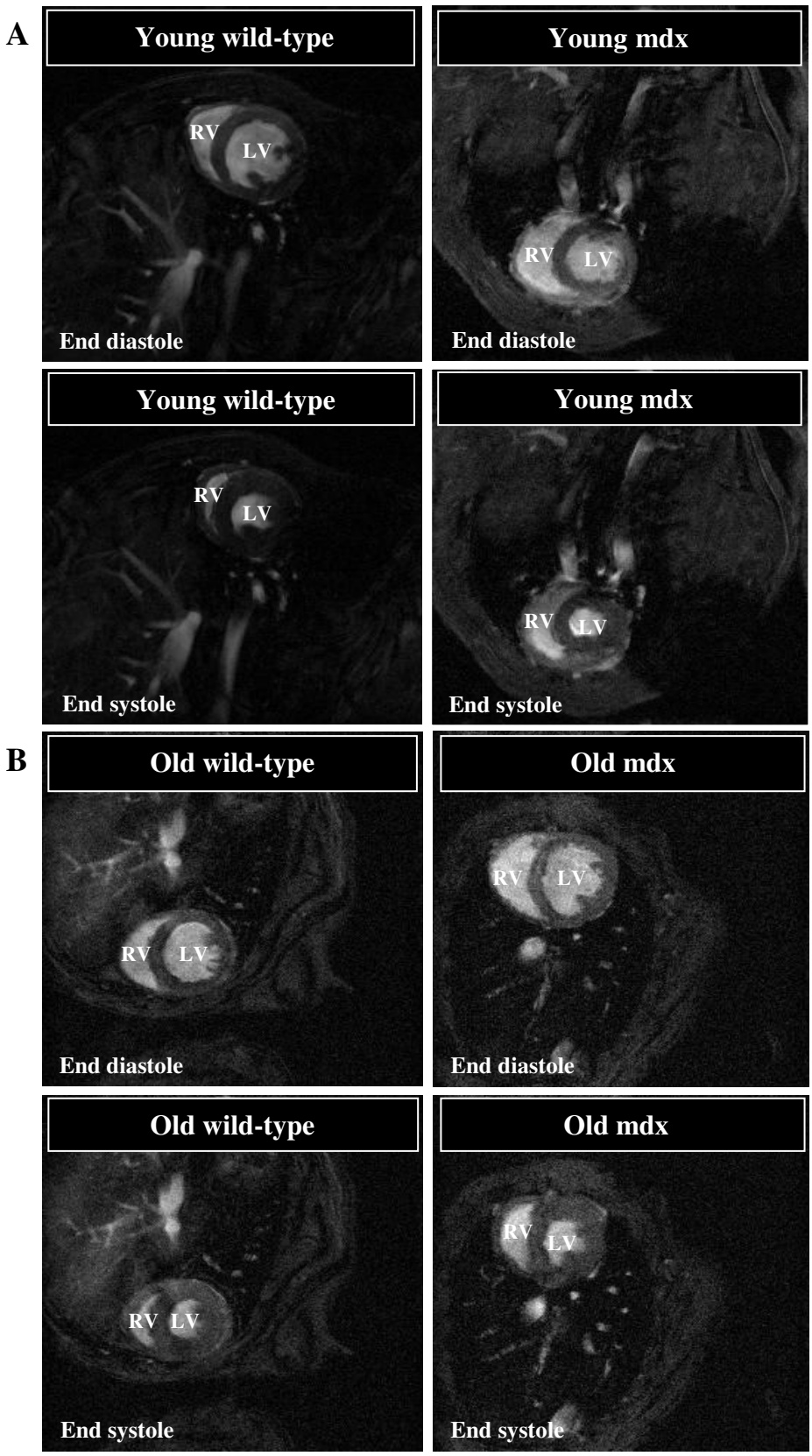

Figure 5.8 Cardiac morphology of both ventriclesin wild-type and mdx mice at both young and old ages. *(**A**, **B**) Representative in vivo short-axis MR images at end diastole and end systole were analysed from 6 (A) and 18 (B) month-old wild-type and mdx mice. Six month-old mdx mouse heart showed right ventricular dilatation during the cardiac cycles compared to that of age-matched control mouse heart. Mdx mouse heart at 18 months old was found to have dilated right and left ventricles, compared with those of age-matched control mouse heart. Abbreviations: RV = right ventricle and LV = left ventricle.*

5.4.2 Cardiac function of left and right ventricles using i*n vivo* MRI

Using *in vivo* high resolution cine MRI, left and right ventricular function was determined including end diastolic volume (EDV), end systolic volume (ESV), stroke volume (SV), ejection fraction (EF) and cardiac output (CO).

5.4.2.1 Cardiac function in 6 month-old wild-type and mdx mice

For young mice (6 month-old), no alterations to left ventricular EDV, ESV, SV, and EF were found in mdx mice, except cardiac output ($p < 0.05$), in comparison to control mice (Figure 5.9 and Table 5.1). This may be explained by the fact that although the differences in heart rate and stroke volume were not significant, cardiac output in the mdx mouse heart became significantly reduced after the combination of these two factors. In contrast, right ventricular ESV was significantly increased and EF was significantly decreased in mdx mice compared with age-matched control mice ($p < 0.05$ and $p < 0.01$, respectively; Figure 5.10 and Table 5.1).

5.4.2.2 Cardiac function in 18 month-old control and mdx mice

For aged mice (18 month-old), left ventricular ESV was significantly increased and EF was significantly reduced in mdx hearts compared to control mice ($p < 0.05$ and $p < 0.01$, respectively; Figure 5.11 and Table 5.2). Furthermore, there was a significant difference in left ventricular mass (greater in mdx mouse hearts, $p < 0.05$; Table 5.1). Similarly, right ventricular EDV and ESV were significantly higher ($p < 0.05$ and $p < 0.05$, respectively) and EF was significantly lower in mdx mouse hearts ($p < 0.05$; Figure 5.12 and Table 5.1).

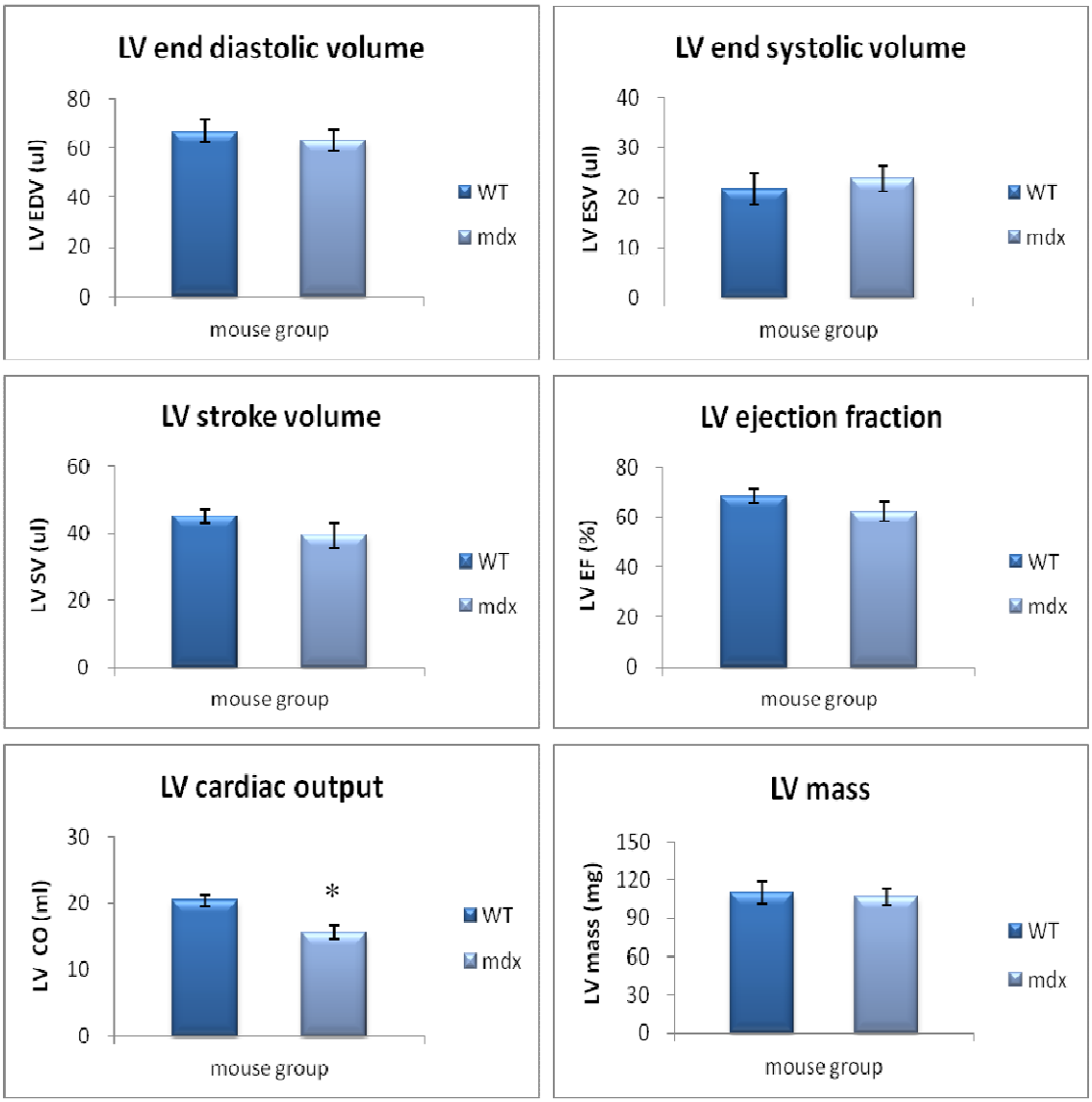

Figure 5.9 Quantitative analysis of left ventricular function at the age of 6 months. *Both wild-type and mdx mice were imaged using in vivo MRI. No significant differences of EDV, ESV, SV, EF, and mass were identified in 6 month-old mdx mice. Data are presented as mean ± SEM (n = 7). * $p < 0.05$ vs. wild-type; # $p < 0.01$ vs. wild-type. Abbreviations: LV = left ventricle, WT = wild-type, EDV = end diastolic volume, ESV = end systolic volume, SV = stroke volume, EF = ejection fraction, and CO = cardiac output.*

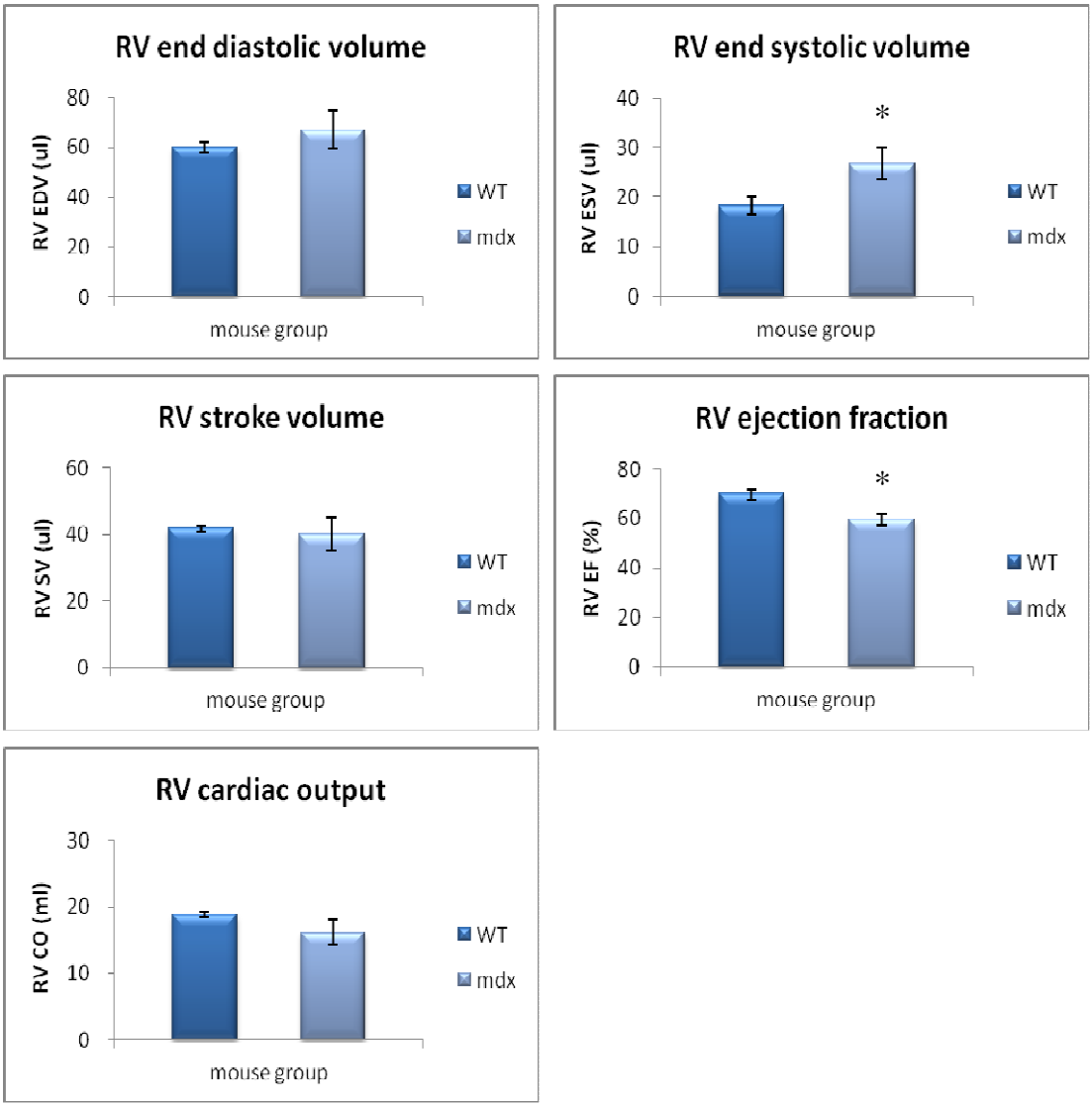

Figure 5.10 Quantitative analysis of right ventricular function in mice at 6 months of age. *In vivo MRI was used to determine right ventricular function of wild-type and mdx mice. There were statistical differences in ESV and EF between 6 month-old wild-type and mdx mice ($p < 0.05$ and $p < 0.01$, respectively). Data are presented as mean ± SEM ($n = 7$). * $p < 0.05$ vs. wild-type; # $p < 0.01$ vs. wild-type. Abbreviations: RV = right ventricle, WT = wild-type, EDV = end diastolic volume, ESV = end systolic volume, SV = stroke volume, EF = ejection fraction, and CO = cardiac output.*

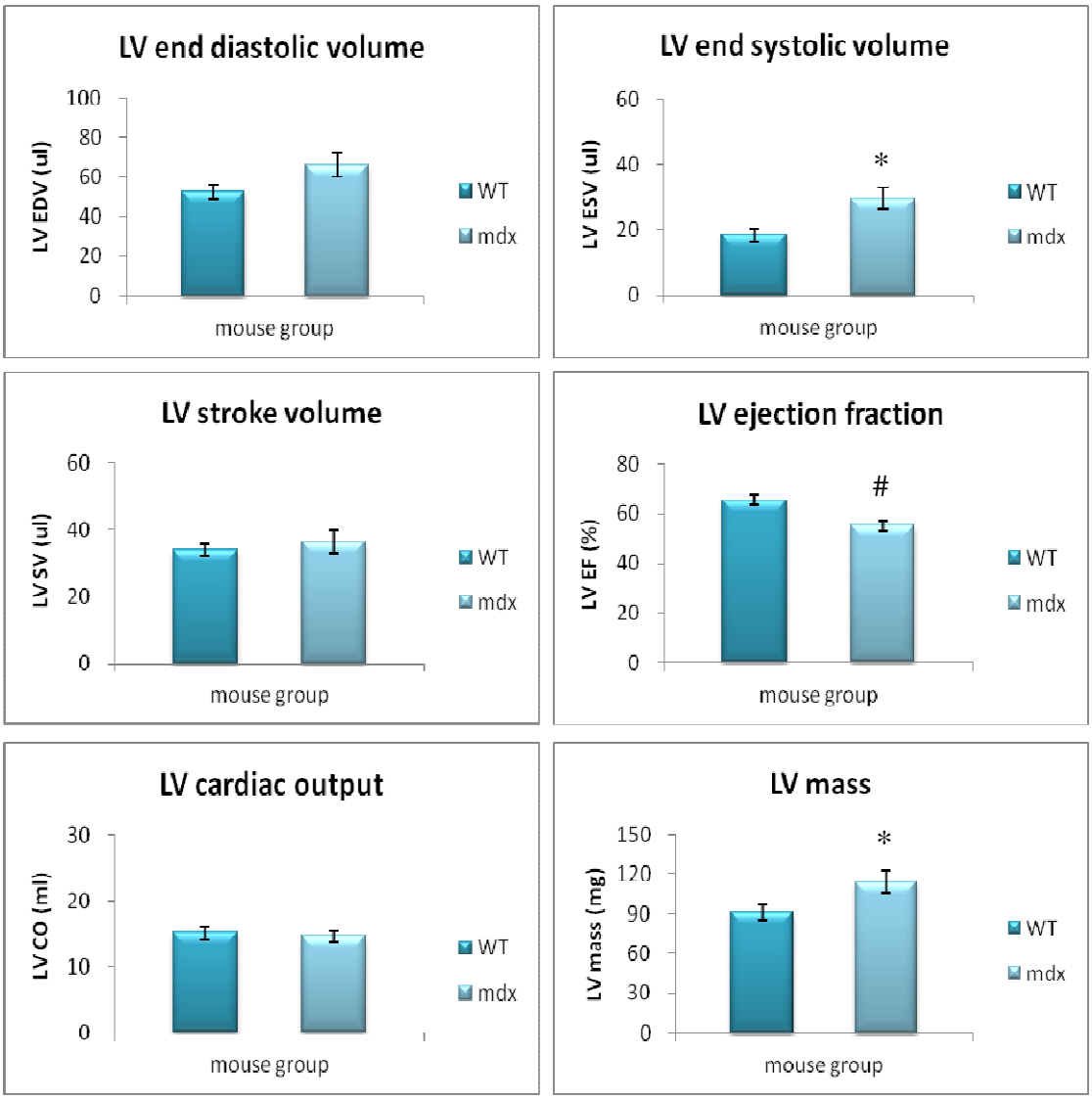

Figure 5.11 Quantitative analysis of left ventricular function at 18 months of age. *Both wild-type and mdx mice were scanned for measurement of cardiac function using in vivo MRI. There was a significantly larger ESV and lower EF in 18 month-old mdx mice compared with age-matched wild-type control mice ($p < 0.05$ and $p < 0.01$, respectively). Data are presented as mean ± SEM ($n = 8$). * $p < 0.05$ vs. wild-type; # $p < 0.01$ vs. wild-type.*

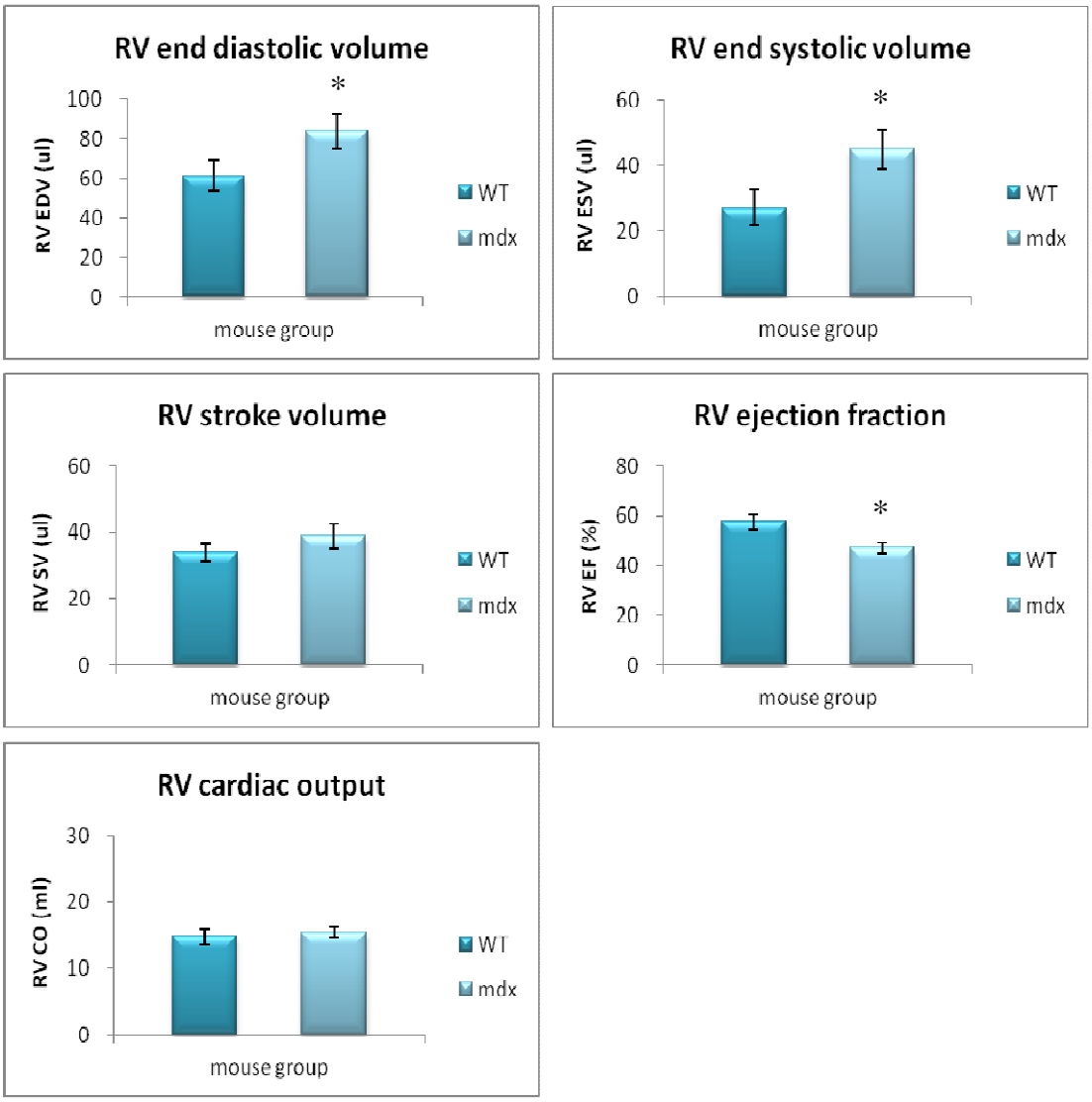

Figure 5.12 Quantitative analysis of right ventricular function at 18 months age. *In vivo MRI was used to evaluate right ventricular function of 18 month-old wild-type and mdx mice. Significantly increased EDV and ESV were found and significantly decreased EF in 18 month-old mdx mice compared to age-matched wild-type mice. Data are presented as mean ± SEM (n = 8). * $p < 0.05$ vs. wild-type; # $p < 0.01$ vs. wild-type. Abbreviations: RV = right ventricle, WT = wild-type, EDV = end diastolic volume, ESV = end systolic volume, SV = stroke volume, EF = ejection fraction and CO = cardiac output.*

5.4.3 Characterization of dystrophin-deficient heart of mdx mice using immunohistochemistry

Mdx mouse hearts are characterized by the absence of dystrophin in muscle tissues. To confirm this, immunohistochemical analysis was performed. Cardiac muscle sections revealed normal staining of dystrophin protein near the sarcolemma in wild-type mouse hearts, but no dystrophin staining was detected in heart sections derived from mdx mice (Figure 5.13).

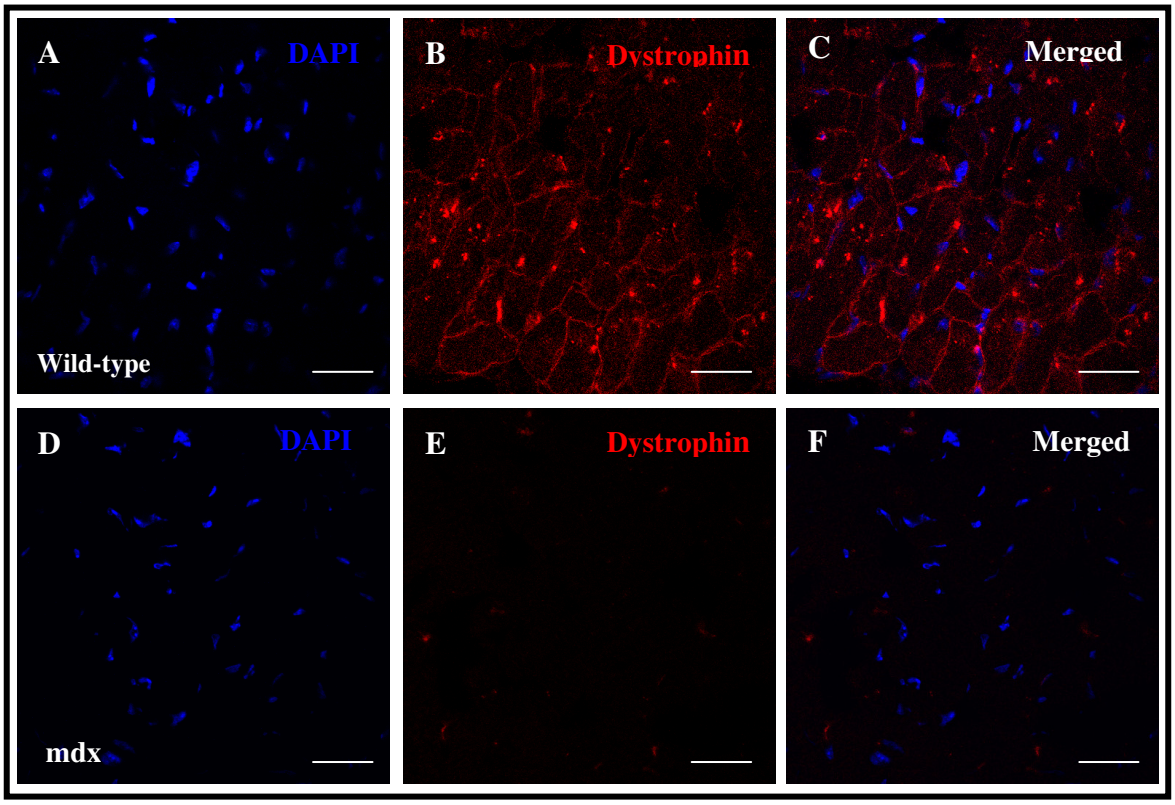

Figure 5.13 Immunostaining of heart muscle tissue cross-sections for detection and localization of dystrophin expression from control (wild-type) and mdx mice. *Heart sections from control and mdx mice were stained with anti-dystrophin antibody. Confocal images of wild-type mouse heart exhibited dystrophin expression (red; upper panel), whereas mdx mouse heart lacked dystrophin expression (lower panel). Nuclei were counterstained with DAPI (blue). Scale bars = 20 μm. Abbreviation: DAPI = 4', 6-diamidino-2-phenylindole.*

5.4.4 Assessment of cardiac necrosis and fibrosis using histology

5.4.4.1 Identification of myocardial necrosis and fibrosis

Morphological analysis of myocardial necrosis and fibrosis was performed in 6 and 18-month-old mdx and wild-type hearts. As shown in Figure 5.14 and 5.15, haematoxylin & eosin staining showed necrotic lesions (infiltration of inflammatory cells), and picro-sirius red staining revealed fibrotic areas (red, collagen content) in mdx hearts but not in control hearts at 6 months of age. Furthermore, 18-month-old mdx mouse hearts had more necrosis and fibrosis compared with age-matched control hearts (Figure 5.14 and Figure 5.15).

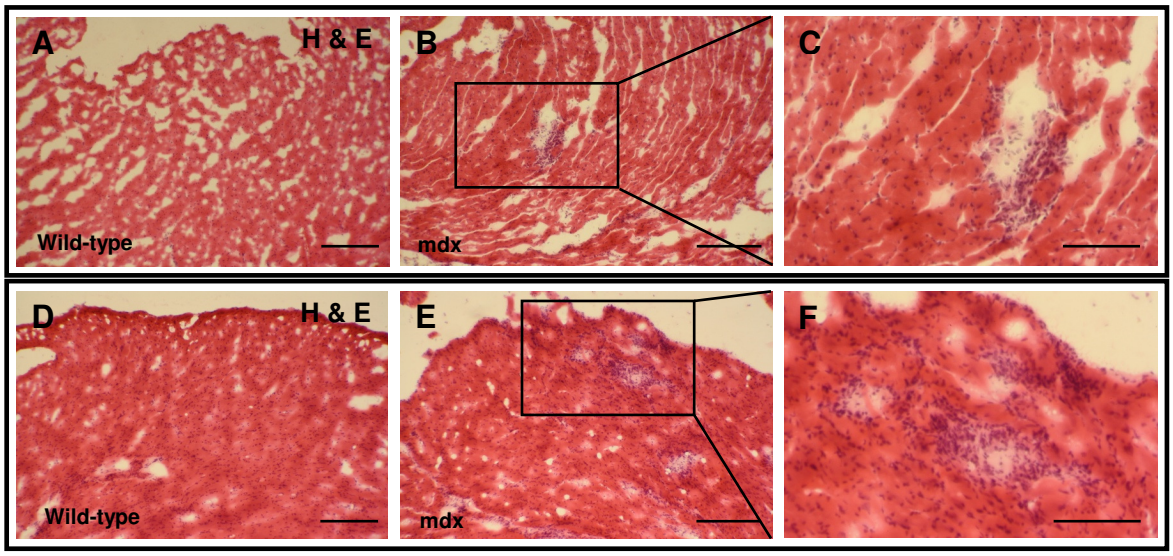

Figure 5.14 Representative photomicrographs of H&E staining on control (wild-type) and mdx mouse heart tissues at 6 and 18 months of age (magnification x10 and x25). *(**A** - **C**) Six month-old wild-type and mdx mouse hearts at top panel. The box image in B was enlarged as C. (**D** - **F**) Eighteen month-old wild-type and mdx mouse hearts at bottom panel. The box image in E was enlarged as F. H&E-stained sections of 6 and 18 month-old mdx mouse hearts showed necrotic lesions (infiltration of inflammatory cells), whereas those of age-matched control mouse hearts did not. Furthermore, aged mdx mouse heart had more necrosis than that of young mdx mouse heart. Scale bars = 200 μm (A, B, D and E); 100 μm (C and F).*

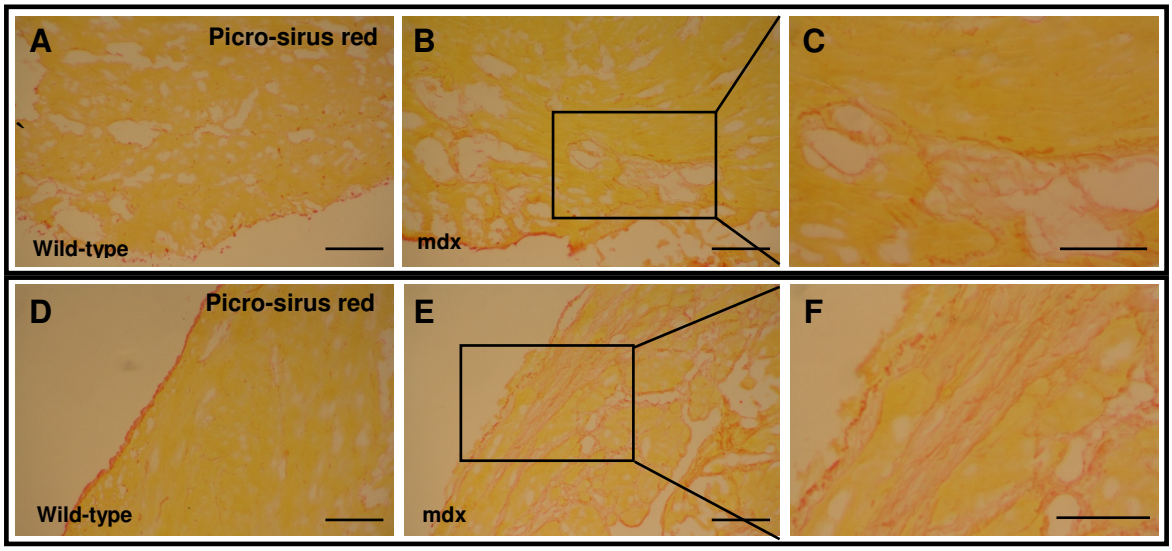

Figure 5.15 Representative photomicrographs of picro-sirius red staining on control (wild-type) and mdx mouse heart at 6 and 18 month of age (magnification x10 and x25). *(**A** - **C**) Six month-old wild-type and mdx mouse hearts at top panel. The box image in B was enlarged as C. (**D** - **F**) Wild-type and mdx mouse hearts at 18 months of age at bottom panel. The box image in E was enlarged as F. Picro-sirius red-stained sections of 6 and 18 month-old mdx mouse hearts showed fibrotic lesions in myocardium (collagen component: red), and those of age-matched control mouse hearts did not. Moreover, older mdx mouse hearts had more necrosis than that of younger mdx mouse heart. Scale bars = 200 μm (A, B, D and E); 100 μm (C and F).*

5.4.4.2 Quantification of cardiac fibrosis

Both age groups of mdx mice had more myocardial fibrosis than did age-matched wild-type mice, independent of the ventricular wall region (6 months $p < 0.05$ and 18 months $p < 0.01$, respectively; Figure 5.16). In mdx mice, the analysis also showed that the extent of RV fibrosis was greater than that in LV (i.e., average of AW, LW and PW fibrosis) at age of 6 or 18 months ($p < 0.05$ for both ages). There were significant differences of cardiac fibrosis between young and old mice for both mouse types, however the percentage difference in mdx groups was higher than that in wild-type groups (2.3- vs. 1.3-fold; Figure 5.17).

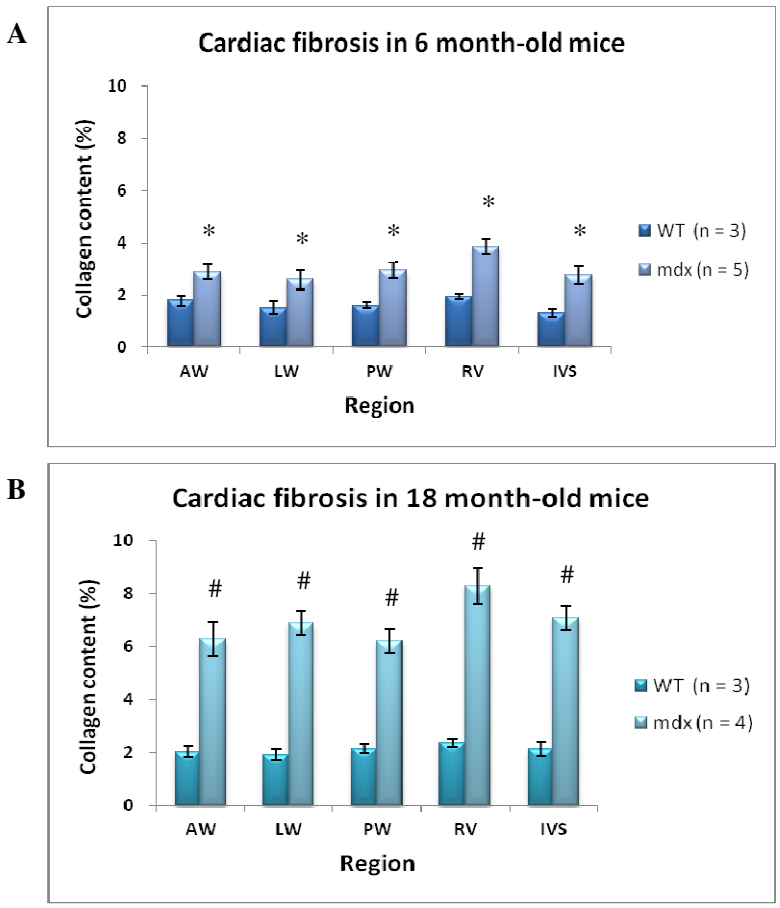

Figure 5.16 Cardiac fibrosis in five distinct regions of hearts from wild-type and mdx mice at 6 and 18 months of age. *(**A**, **B**) Regardless of the area, there was significantly more cardiac fibrosis in mdx mice compared to wild-type in both 6 month-old mice (A) and 18 month-old mice (B). Data are presented as mean ± SEM. * $p < 0.05$ vs. wild-type; # $p < 0.01$ vs. wild-type. Abbreviations: AW = anterior wall, LW = lateral wall, PW = posterior wall, RV = right ventricle, IVS = inter-ventricular septum.*

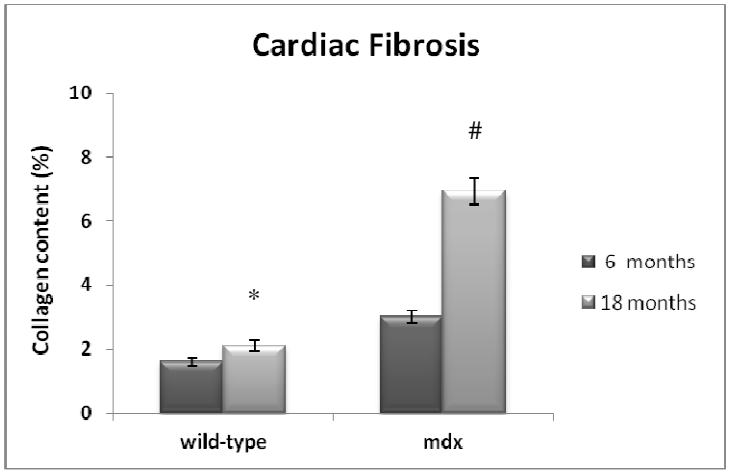

Figure 5.17 Cardiac fibrosis of whole hearts in 6 and 18-month-old wild-type and mdx mice. *Cardiac fibrosis significantly increased from 6 to 18 months of age in mdx mice. Similarly, there was also significant difference of fibrosis with increasing age in wild-type mice. Data are presented as mean ± SEM. * $p < 0.05$ vs. 6 month-old wild-type mice, # $p < 0.001$ vs. 6 month-old mdx mice.*

5.4.5 Isolation and expansion of cardiac-derived stem cells from wild-type and mdx mice

Following MRI measurements, wild-type and mdx mice were sacrificed for removal of hearts for explant culture. It should be emphasized that mouse CDC culture was established for the first time to characterize mdx mouse-derived CSCs and compare with wild type-derived CSCs in the lab.

5.4.5.1 Explant-derived cells

As observed in young and old wild-type mice (see Chapter 4), EDCs grew and migrated faster from young mdx mice (6 month-old) than old mice ones (18 month-old). However, the growing speed and cell density of EDCs from mdx mice seemed comparable to those of age-matched wild-type mice (Figure 5.18). When reaching confluence, EDCs were harvested and cell numbers counted to compare mdx with wild-type mice. For 6 month old mice, explants from mdx and wild-type mice generated 1.1 ± 0.09 x 10^4 and 1.1 ± 0.07 x 10^4 EDCs per mg of heart tissue, respectively (p = NS; Figure 5.20). Likewise, 18 month-old mdx and wild-type produced the comparable numbers of EDCs (0.8 ± 0.07 x 10^4 vs. 0.9 ± 0.07 x 10^4 EDCs/mg heart tissue; p = NS; Figure 5.19).

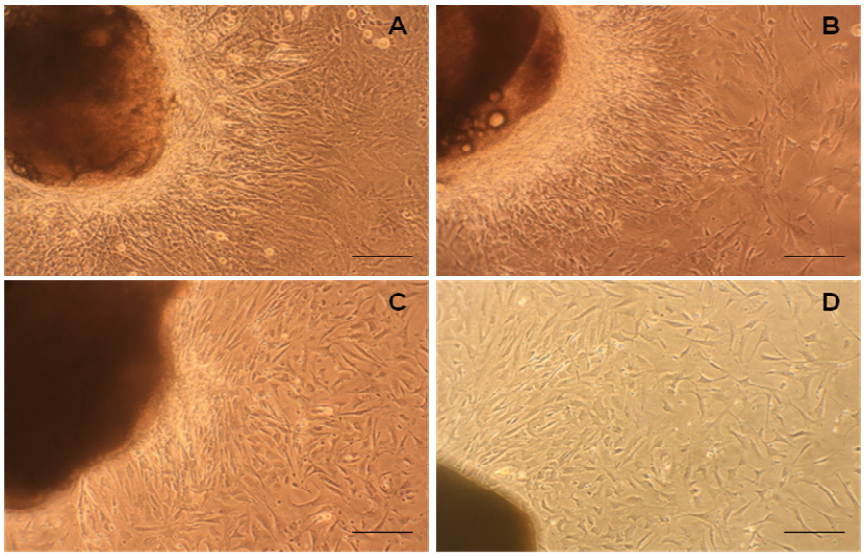

Figure 5.18 Representative photomicrographs of explants with explant-derived cells (magnification x10). *(**A** - **D**) Explants from atrial heart tissues were plated on fibronectin-coated petri dishes and images were taken at day 9 post plating, including 6 month-old wild-type (A), 6 month-old mdx (B), 18 month-old wild-type (C), and 18 month-old mdx (D). In age-matched wild-type and mdx mice, there was generally a similar cell density of EDCs. Scale bars = 200 μm. Abbreviation: EDC = explant-derived cell.*

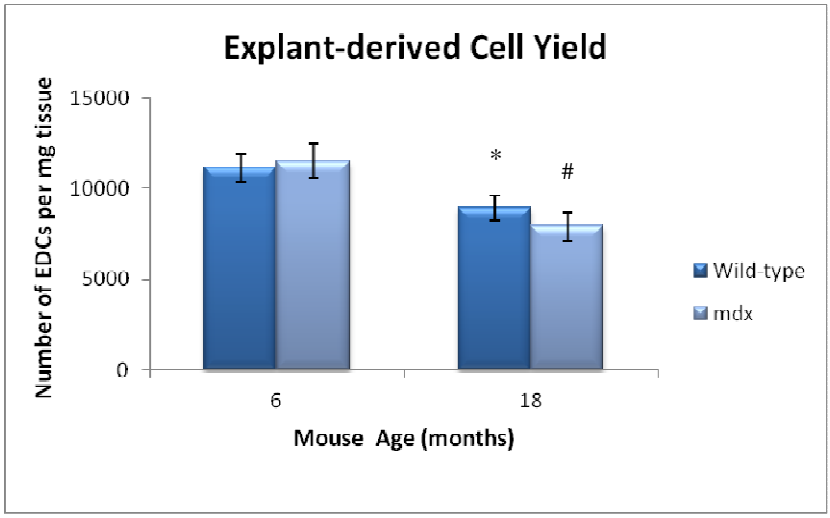

Figure 5.19 Yield of explant-derived cells isolated from wild-type and mdx mice at 6 and 18 months. *When confluent, EDCs were harvested and counted for comparison of cell yield. At the age of 6 months, there was no statistical difference between wild-type and mdx mice. Nor was a significant difference found at the age of 18 months. Data are presented as mean ± SEM. * $p < 0.05$ vs. 6 month-old wild-type; # $p < 0.05$ vs. 6 month-old mdx. Abbreviation: EDC = explant-derived cell.*

5.4.5.2 Cardiospheres

Cardiospheres showed no difference in morphology and size, whether from mdx or wild-type mice (Figure 5.20). In 6 month-old mice, the mdx group yielded 66 ± 4 cardiospheres/well, compared to 69 ± 6 cardiospheres/well in the wild-type group (p = NS). Similarly, there was no significant difference in number of cardiospheres between older mdx and wild-type mice (46 ± 5 vs. 44 ± 3 cardiospheres per well; p = NS; Figure 5.21). As for the comparison of cardiosphere size, irrespective of age, no difference was found between mdx and wild-type mice (Figure 5.22).

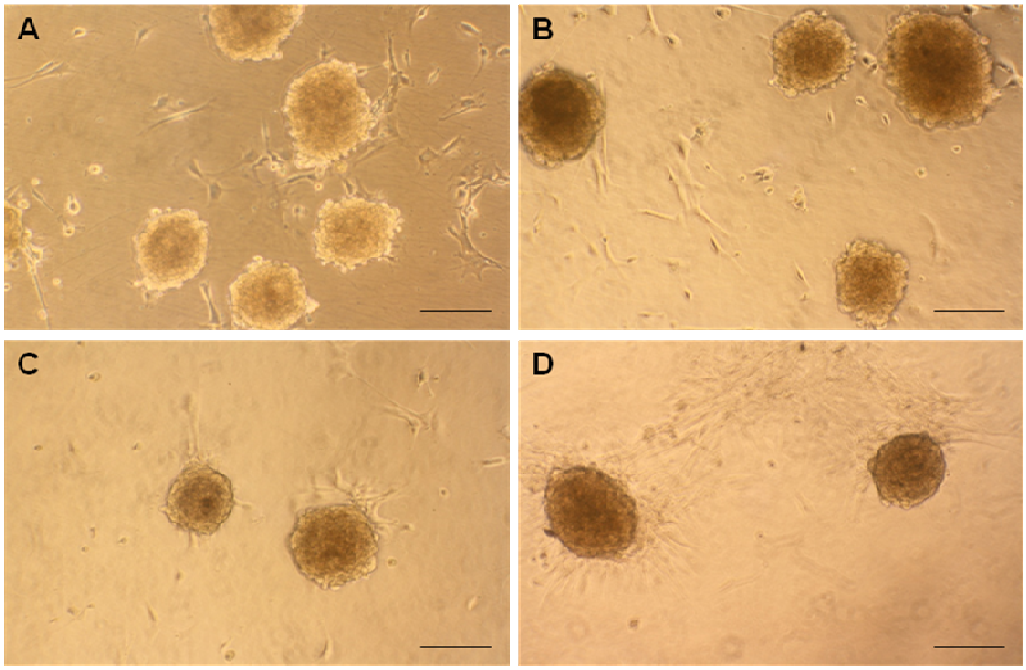

Figure 5.20 Representative photomicrographs of cardiospheres grown from wild-type and mdx mice at ages of 6 and 18 months (magnification x10). *(**A** - **D**) Isolated explant-derived cells were seeded onto poly-D-lysine-coated 24 well plates to form cardiospheres. Images were taken as follows: 6 month-old wild-type (A), 6 month-old mdx (B), 18 month-old wild-type (C), and 18 month-old mdx (D), showing similar pattern in morphology. Scale bars = 200 μm.*

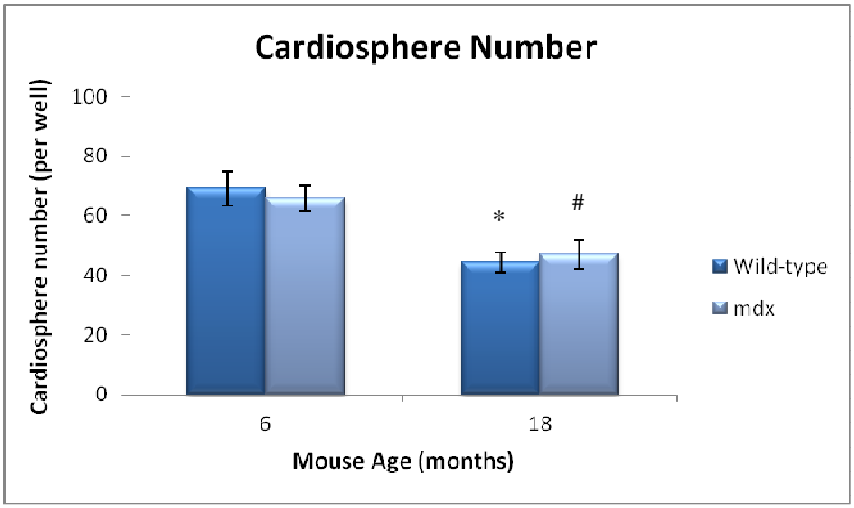

Figure 5.21 Number of cardiospheres from wild-type and mdx mice at 6 and 18 months. *Isolated explant-derived cells were seeded onto 24 well plates coated with fibronectin. The number of cardiospheres in each well was measured using a haemocytometer under a light microscope. Generally, no significant difference of cardiosphere number/well was found between wild-type and mdx mice at both ages of 6 month-old and 18 month-old. Data are presented as mean ± SEM. * $p < 0.05$ vs. 6 month-old wild-type; # $p < 0.05$ vs. 6 month-old mdx.*

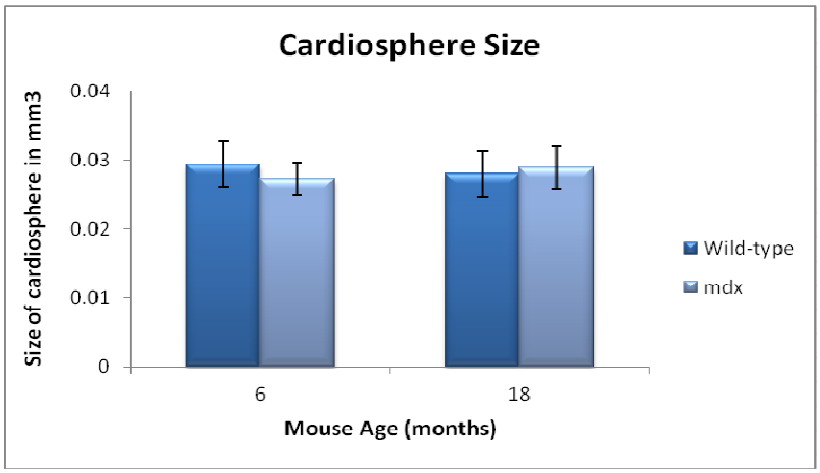

Figure 5.22 Size of cardiospheres derived from wild-type and mdx mice at 6 and 18 months. *Representative images of cardiospheres were taken and cardiosphere size was measured using ImageJ. The average size of cardiospheres from mdx mice showed no significant difference in comparison to that from wild-type mice, irrespective of age. Data are presented as mean ± SEM (n = 20).*

5.4.5.3 Cardiosphere-derived cells

In both young and old mouse groups, mdx mice revealed no significant difference in the yield of CDCs per mg heart tissue, when compared to wild-type mice (6 months $1.6 \pm 0.17 \times 10^4$ vs. $1.7 \pm 0.09 \times 10^4$ and 18 months $1.1 \pm 0.13 \times 10^4$ vs. $1.2 \pm 0.07 \times 10^4$; Figure 5.23). However, aged mice generated significantly lower numbers of CDCs than young mice, independent of mouse phenotype.

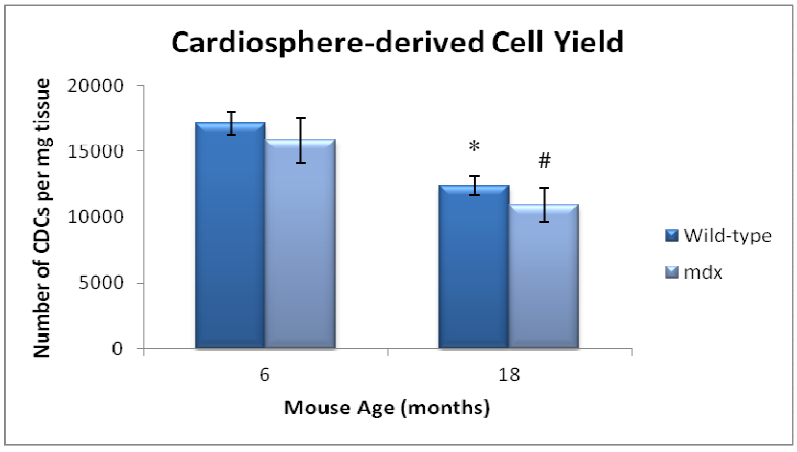

Figure 5.23 Yield of cardiosphere-derived cells isolated from wild-type and mdx mice at 6 and 18 months. *At passage 2, CDCs were isolated and counted. There was no significant difference of CDC yield per mg heart tissue between mdx and wild-type mice at either age of 6 months and 18 months. Data are presented as mean ± SEM. * $p < 0.05$ vs. 6 month-old wild-type; # $p < 0.05$ vs. 6 month-old mdx. Abbreviation: CDC = cardiosphere-derived cell.*

5.4.6 Characterization of cardiosphere-derived cells from wild-type and mdx mice

5.4.6.1 Phenotyping of CDCs using immunocytochemistry

As seen in cardiosphere-derived cells from wild-type mice, the expression of cardiac stem cell markers, c-kit and Sca-1, and mesenchymal cell marker, CD90 were detected in the CDC population from 6 and 18 month-old mdx mice (Figure 5.24).

5.4.6.2 Phenotype characterization of CDCs using flow cytometry

Flow cytometry confirmed the presence of c-kit, Sca-1, and CD90 expressing cells in the CDC population from mdx mice of both ages. Furthermore, the analysis of expression percentage showed no significant differences of c-kit, Sca-1 and CD90 between 6 month-old wild-type and mdx mice (11 ± 3 % vs. 10 ± 2 %; 72 ± 6 % vs. 77 ± 4 %; 57 ± 7 % vs. 46 ± 6 %, respectively; all p = NS; Figure 5.25). Likewise, no statistical differences were found between wild-type and mdx mice at the age of 18 months in the percentage of cells expressing c-kit (9 ± 2 % vs. 8 ± 2 %; p = NS), Sca-1 (62 ± 6 % vs. 58 ± 6 %; p = NS) and CD90 (66 ± 11 % vs. 50 ± 7 %; p = NS), respectively (Figure 5.26).

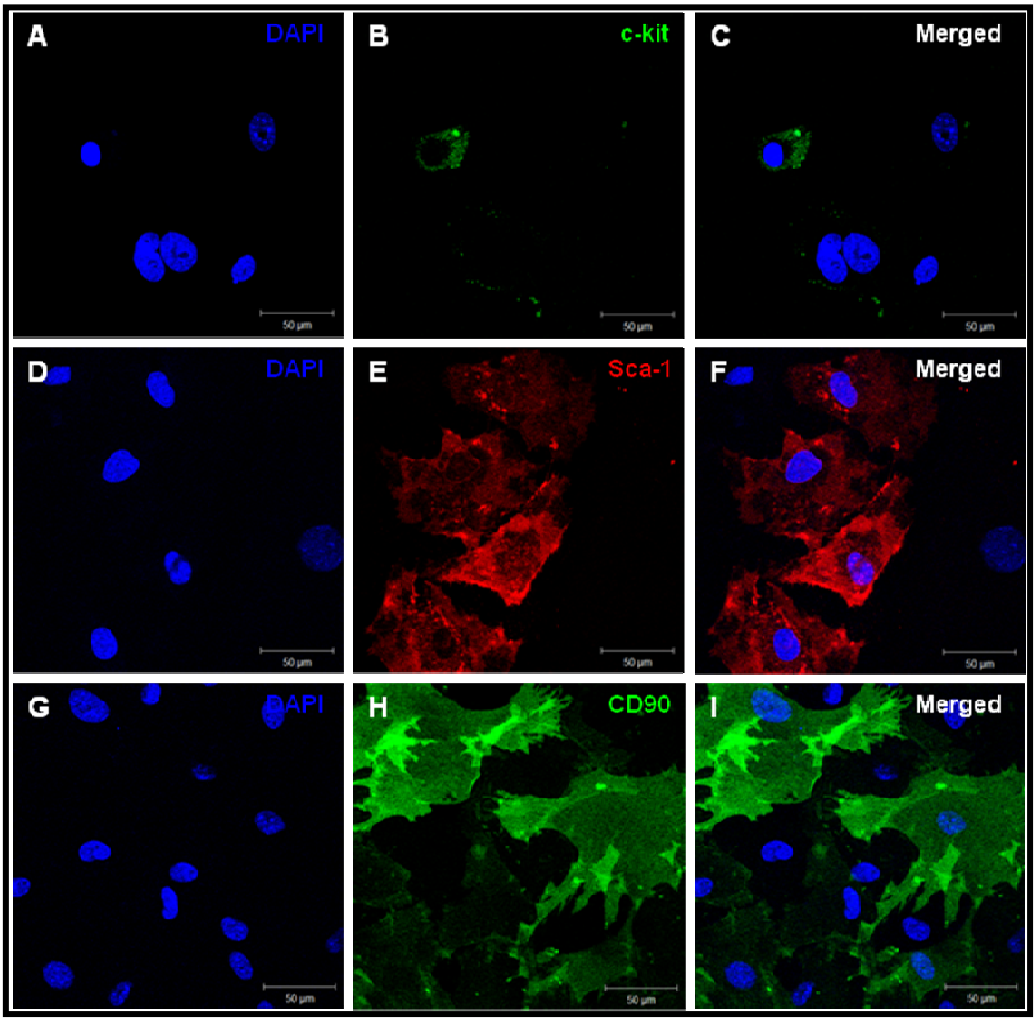

Figure 5.24 Immunophenotyping of cardiosphere-derived cells using immunocytochemistry. *Representative confocal images showed the localisation of positive cells in the CDC population from mdx mice, including cardiac stem cells – c-kit⁺ cells (green; upper panel) and Sca-1⁺ cells (red; middle panel), and mesenchymal stem cells – CD90⁺ cells (green; lower panel). This indicated that, like CDCs from wild-type mice, mdx-derived CDCs contained cardiac stem cells and mesenchymal cells. Nuclei were counterstained blue with DAPI. Scale bars = 50 μm. Abbreviations: CDC = cardiosphere-derived cell and DAPI = 4', 6-diamidino-2-phenylindole.*

A

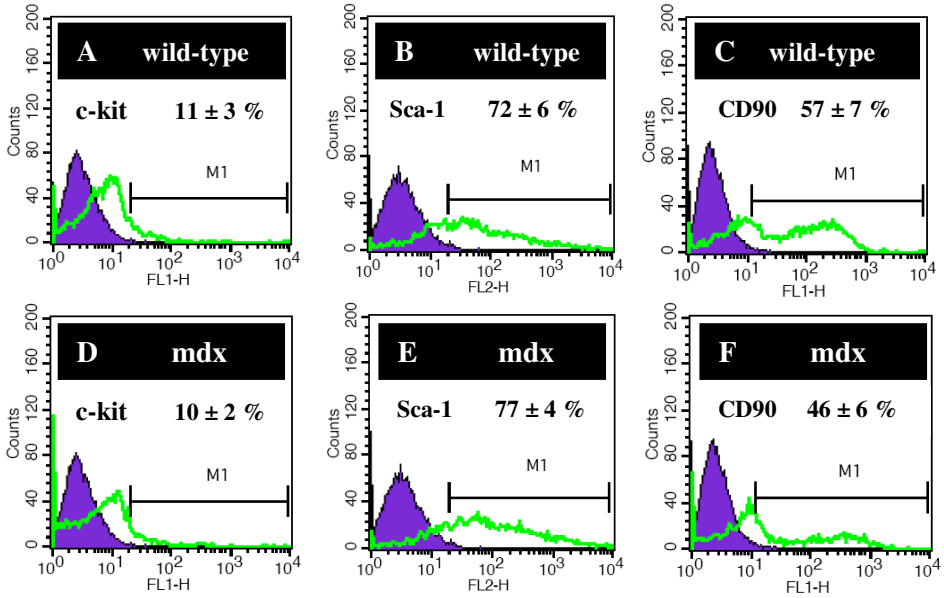

B

0

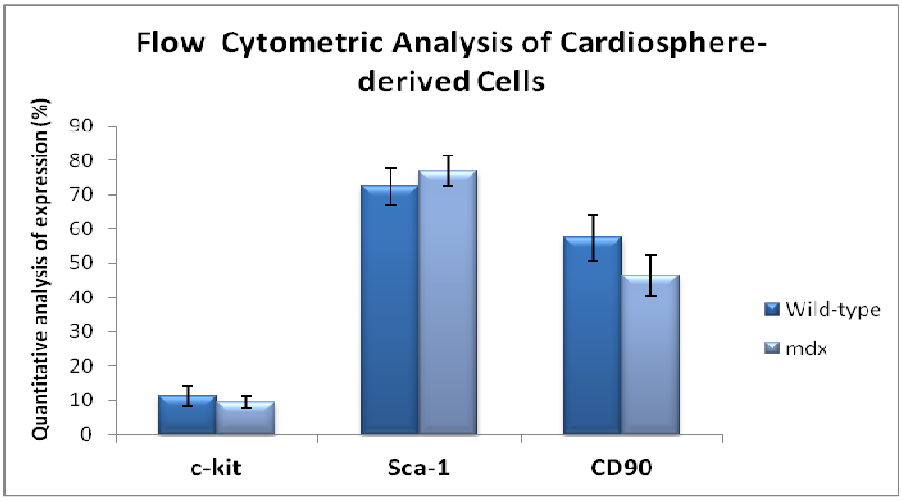

Figure 5.25 Flow cytometric analysis of cardiosphere-derived cells, isolated from 6 month-old wild-type and mdx mice. *(**A**) CDCs at passage 2 were stained for c-kit, Sca-1, and CD90 using flow cytometry. (**B**) There were no significant differences in percentages of cells expressing these proteins in CDCs between 6 month-old wild-type and mdx mice. Cells present in region M1 were defined as the positive population. Purple region: unstained cell control. Green line: corresponding stained samples. Data are presented as mean ± SEM. Abbreviation: CDC = cardiosphere-derived cell.*

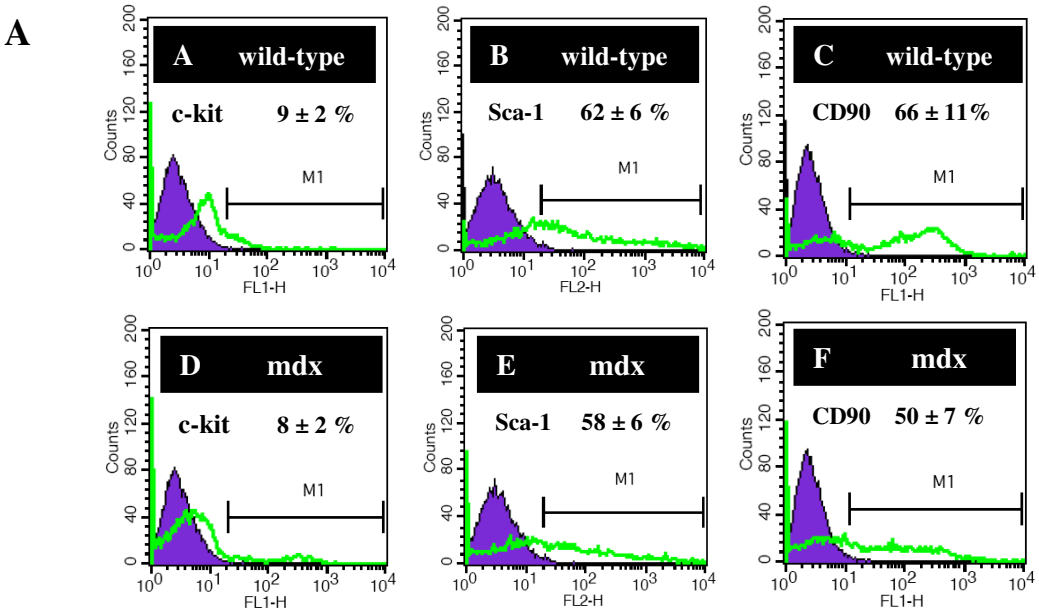

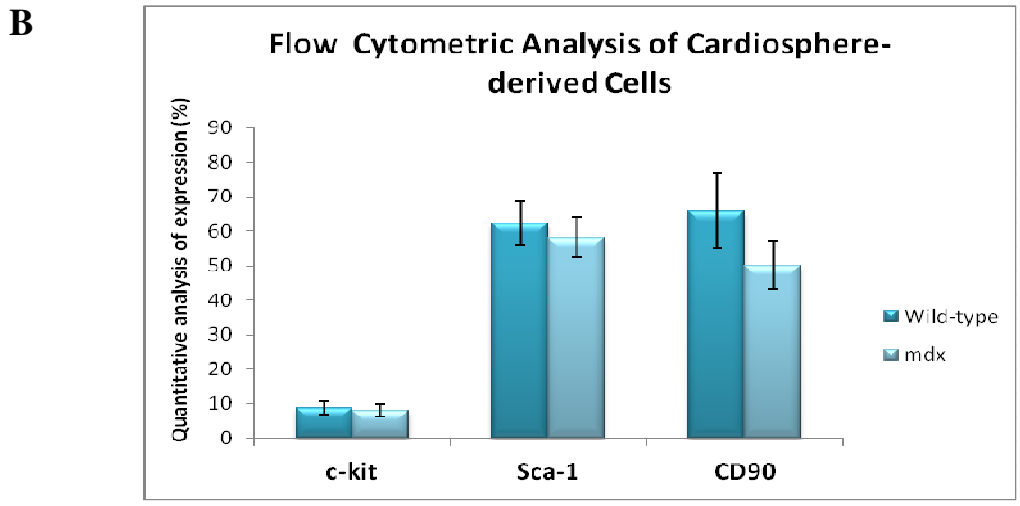

Figure 5.26 Flow cytometric analysis of cardiosphere-derived cells isolated from 18 month-old wild-type and mdx mice. *(**A**) Passage 2 CDCs were stained against c-kit, Sca-1, and CD90, for characterization using flow cytometry. (**B**) There were no significant differences in positive cells (c-kit⁺, Sca-1⁺ and CD90⁺) in the CDC populations between 18 month-old wild-type and mdx mice. Cells present in region M1 were defined as the positive population. Purple region: unstained cell control. Green line: corresponding stained samples. Data are presented as mean ± SEM. Abbreviation: CDC = cardiosphere-derived cell.*

5.4.7 *In vitro* property characterization of cardiac-derived stem cells from wild-type and mdx mice

5.4.7.1 Comparison of explant-derived cell migration capacity

As shown in Figure 5.27, explant-derived cells from mdx mice migrated out of heart explants to a similar extent as from EDCs from age-matched wild-type mice. Using ImageJ analysis software, the maximal migratory distances of EDCs from young and aged mdx mice were 0.7 ± 0.08 mm and 0.4 ± 0.04 mm, respectively, compared with aged-matched wild-type mice (0.7 ± 0.06 mm and 0.5 ± 0.05 mm, respectively) (Figure 5.28).

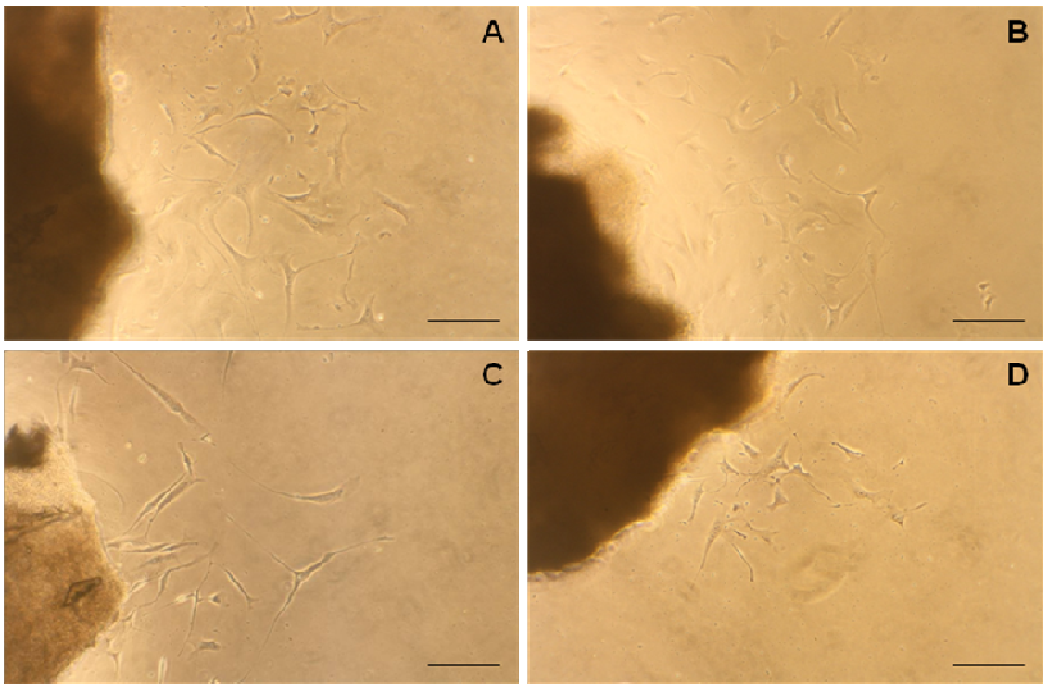

Figure 5.27 Representative photomicrographs of explant-derived cells migrating out of heart explants (magnification x10). *(**A** - **D**) Heart fragments were plated as explants on fibronectin-coated petri dishes. Microscopic images were taken 5 days post plating as follows: 6 month-old wild-type (A), 6 month-old mdx (B), 18 month-old wild-type (C), and 18 month-old mdx (D), showing EDCs migrating from explants. No obvious difference in maximal migration distance was noted between age-matched mdx and wild-type mice. Scale bars = 200 μm. Abbreviation: EDC = explant-derived cell.*

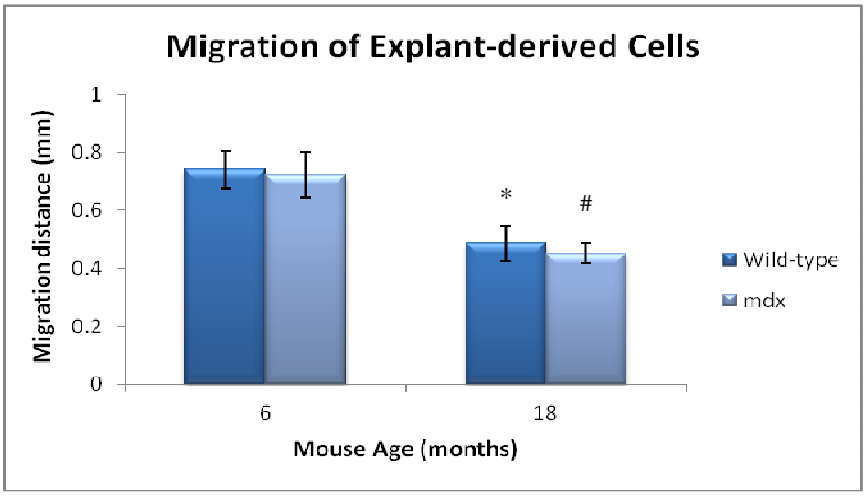

Figure 5.28 Comparison of explant-derived cell migration between wild-type and mdx mice at 6 and 18 months of age. *At day 5 following plating, the maximal distance of EDC migration was determined from randomly selected explants for each group using ImageJ. At both 6 and 18 months, mdx mice revealed no significant difference of migration capacity when compared to wild-type mice. Data are presented as mean ± SEM (n = 12). * p < 0.05 vs. 6 month-old wild-type; # p < 0.05 vs. 6 month-old mdx. Abbreviation: EDC = explant-derived cell.*

5.4.7.2 Comparison of cardiosphere-derived cell migration capacity

Overall, cardiosphere-derived cells from young mice migrated faster and further than CDCs from aged mice. However, there was no obvious difference of maximal migratory distance between CDCs from age-matched mdx and wild-type mice (Figure 5.29 and Figure 5.31). At 6 months of age, CDCs from mdx mice displayed a maximal migratory distance of 0.44 ± 0.03 mm at a given time (30 hours post cardiosphere seeding) relative to those from wild-type mice (0.43 ± 0.02 mm; p = NS; Figure 5.30). As for 18 month old mice, the maximal migratory distance of CDCs from mdx mice was 0.35 ± 0.03 mm compared to that of CDCs from wild-type mice at 0.35 ± 0.02 mm (p = NS; Figure 5.32).

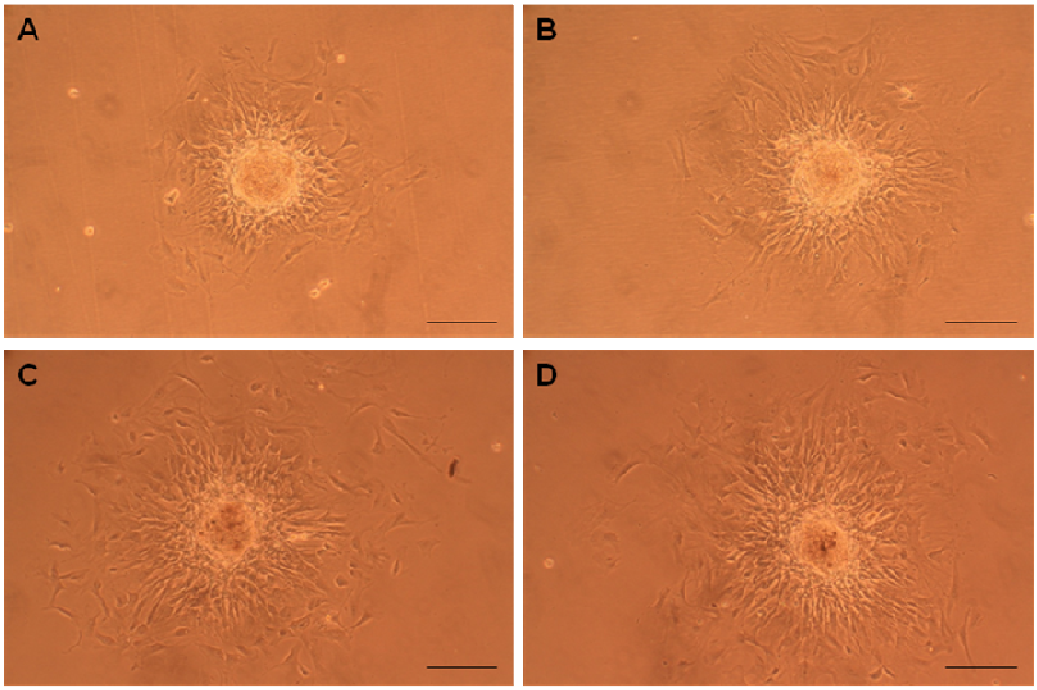

Figure 5.29 Representative photomicrographs of cardiosphere-derived cells migrating out of cardiospheres (magnification x10). *(**A** - **D**) Cardiospheres, from 6 month-old wild-type (A and C) and mdx mice (B and D), were grown on fibronectin-coated culture surface. The migration of CDCs was recorded at 18 hours (upper panel) and 30 hours (lower panel) after plating using a digital camera attached to a light microscope. In general, CDCs from wild-type and mdx mice migrated similarly. Scale bars = 200 μm. Abbreviation: CDC = cardiosphere-derived cell.*

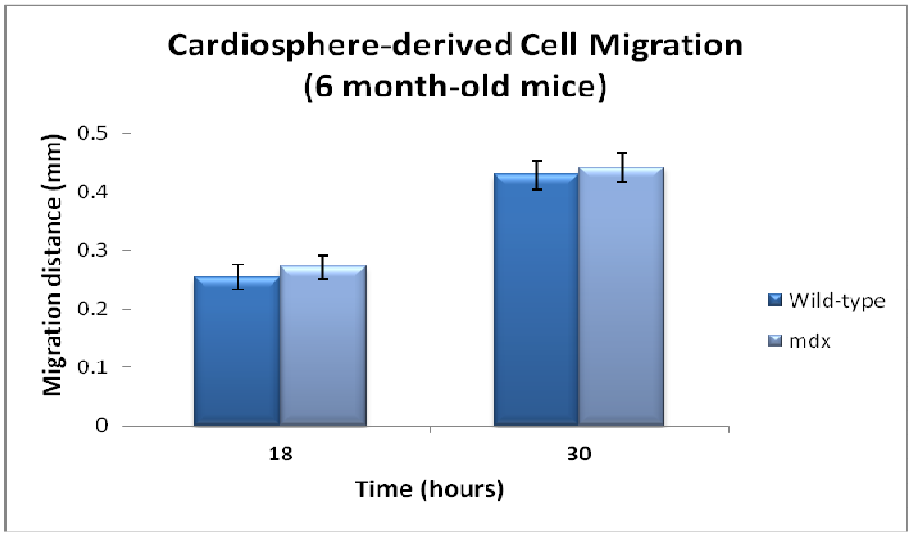

Figure 5.30 Comparison of cardiosphere-derived cell migration between wild-type and mdx mice at the age of 6 months. *No significant difference in maximal migration distance was found between 6 month-old control and mdx mice at 18 and 30 hours following plating Data are presented as mean ± SEM (n = 10). Abbreviation: CDC = cardiosphere-derived cell.*

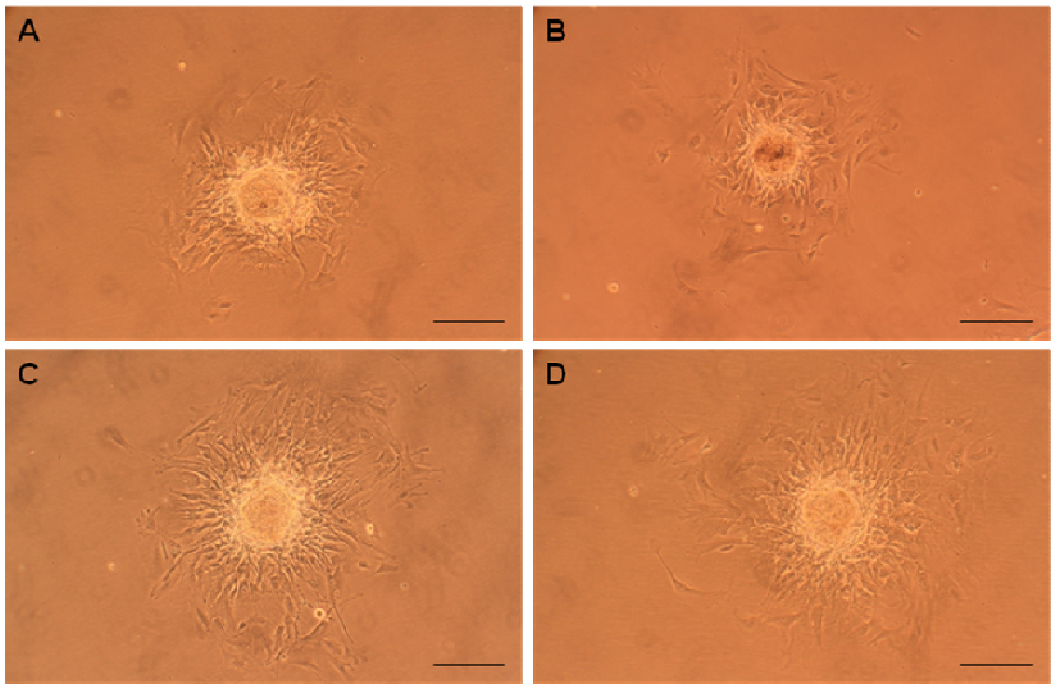

Figure 5.31 Representative photomicrographs of cardiosphere-derived cells migrating out of cardiospheres (magnification x10). *(**A** - **D**) Cardiospheres, from 18 month-old wild-type (A and C) and mdx mice (B and D), were grown on fibronectin-coated culture surface. The migration of CDCs was recorded at 18 hours (upper panel) and 30 hours (lower panel) after plating using a light microscope equipped with a digital camera. Generally, CDCs spread to a similar extent in wild-type and mdx mice. Scale bars = 200 µm. Abbreviation: CDC = cardiosphere-derived cell.*

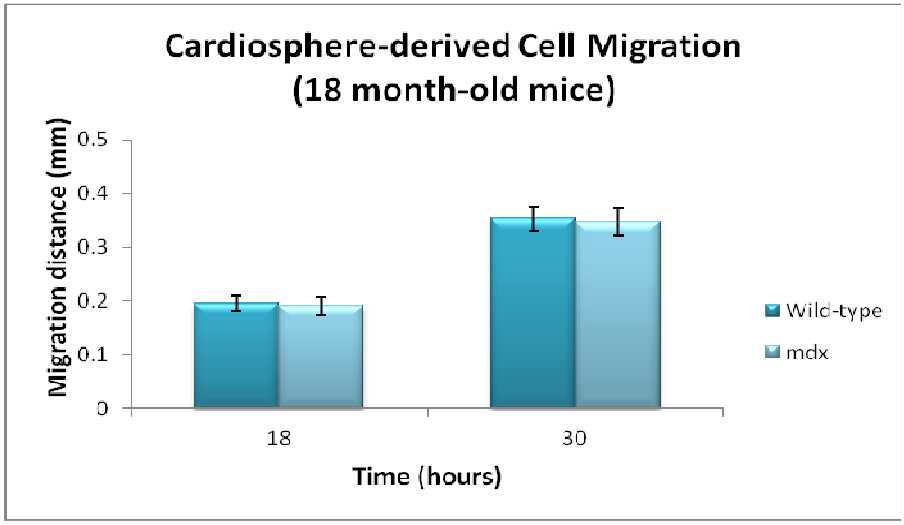

Figure 5.32 Comparison of cardiosphere-derived cell migration between wild-type and mdx mice at the age of 18 months. *There was no obvious difference of maximal migration distance from 18 month-old mdx mice compared to age-matched control mice at both time points of 18 and 30 hours post cardiosphere plating. Data are presented as mean ± SEM (n = 10). Abbreviation: CDC = cardiosphere-derived cell.*

5.4.7.3 Comparison of cardiosphere-derived cell clonogenic efficiency

There was no statistical difference in clonogenicity of cardiosphere-derived cells between age-matched wild-type and mdx mice. In 6 month-old mice, passage 2 CDCs of mdx mice exhibited a clonogenic efficiency of 44 ± 3 % in comparison to that of wild-type mice-derived CDCs (41 ± 2 %) (p = NS; Figure 5.33). For the age of 18 months, the clonogenic efficiency of CDCs from mdx mice was 31 ± 3 %, as compared to 33 ± 2 % of CDCs from wild-type mice (p = NS; Figure 5.33).

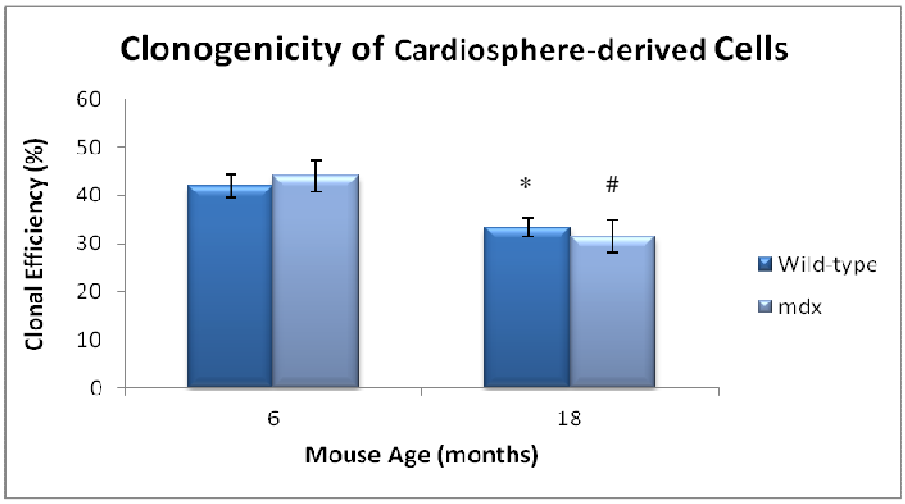

Figure 5.33 Comparison of clonogenicity of cardiosphere-derived cells between wild-type and mdx mice at ages of 6 and 18 months. *The clonogenic analysis showed no significant difference between CDCs from age-matched mdx and wild-type mice at both ages. Data are presented as mean ± SEM (n = 4). * p < 0.05 vs. 6 month-old wild-type; # p < 0.05 vs. 6 month-old mdx. Abbreviation: CDC = cardiosphere-derived cell.*

5.4.7.4 Comparison of cardiosphere-derived cell proliferation capacity

The number of cardiosphere-derived cells continuously increased in culture with time in 6 and 18 month-old mdx mice. As compared to CDCs from 6 month-old wild-type mice, age-matched mdx-derived CDCs did not show significant difference in proliferation rate at various time points (from day 1 to day 7) (Figure 5.34). Likewise, this was the case between 18 month-old mdx and wild-type mice (Figure 5.34).

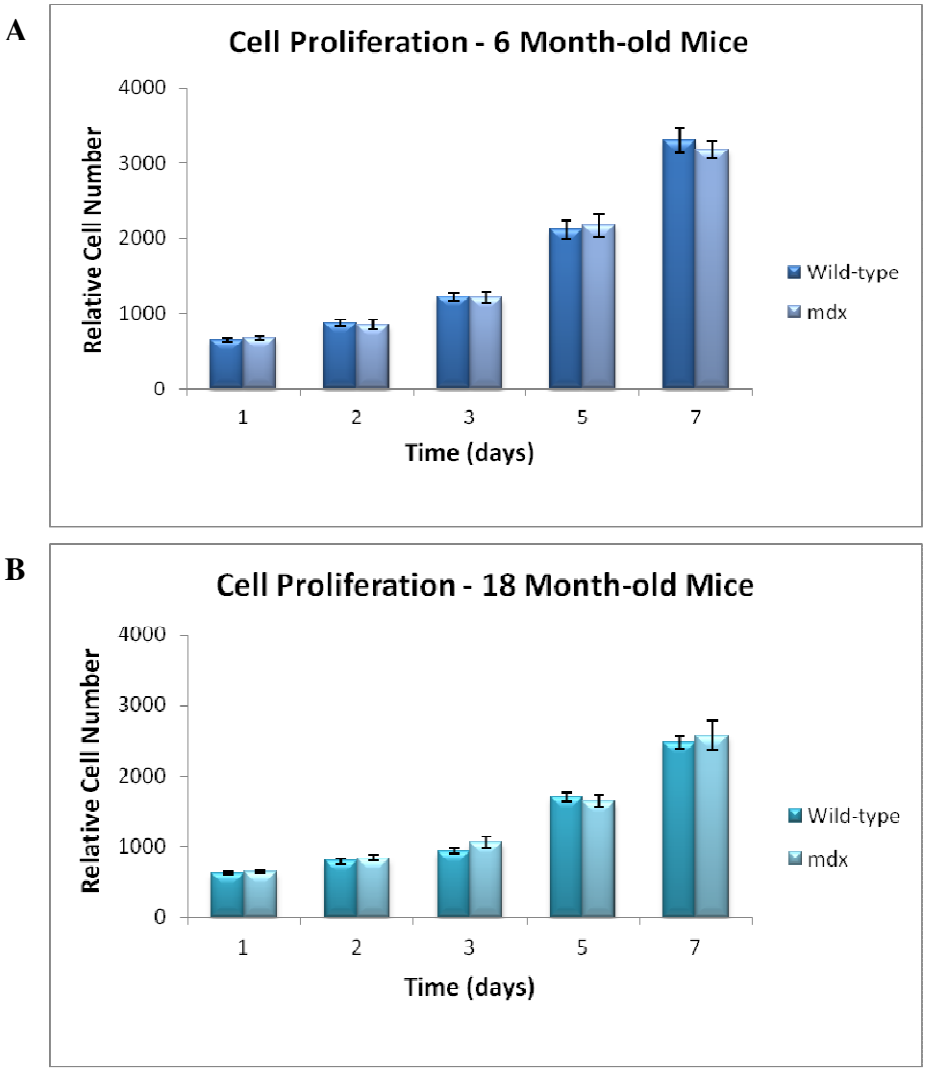

Figure 5.34 Proliferation of cardiosphere-derived cells grown from wild-type and mdx mice at 6 and 18 months of age. *Passage 2 CDCs were seeded onto 96 well plates pre-coated with fibronectin at a density of 500 cells per well. Relative fluorescence intensity was read using FLUOstar OPTIMA at day 0, day 1, day 2, day 3, day 5, and day 7. (**A**) Cell proliferation for 6 month-old mice. (**B**) Cell proliferation for 18 month-old mice. There was no significant difference in the cell number between CDCs from age-matched wild-type and mdx mice throughout the culture period of one week. Data are presented as mean ± SEM (n = 4). Abbreviation: CDC = cardiosphere-derived cell.*

5.5 Discussion

The study in this chapter was to test the hypothesis that the cardiac pathology in mdx mouse hearts reduced CSC number and impaired biological capabilities *in vitro*. For this purpose, the experiments were designed to investigate cardiac morphology and function in mdx mice using *in vivo* MRI and histology, isolate and expand mouse CDCs, and characterize mdx-derived CDCs for comparison with those from wild-type mice in terms of cell yield, migration, colony-forming and proliferation capacity.

Pathophysiology in dystrophin-deficient dilated cardiomyopathy

In cardiac muscle cells, as shown in Figure 5.35, dystrophin-associated protein complex (DAPC) at the sarcolemma (plasma membrane) consists of transmembrane, cytoplasmic and extracellular proteins, such as dystroglycan, sarcoglycan, and dystrophin [225, 227, 229, 350]. Dystrophin protein, a crucial part of DAPC, is located at the subsarcolemmal level in cardiomyocytes, which connects the intracellular actin cytoskeleton to the extracellular basal lamina *via* the DAPC [227].

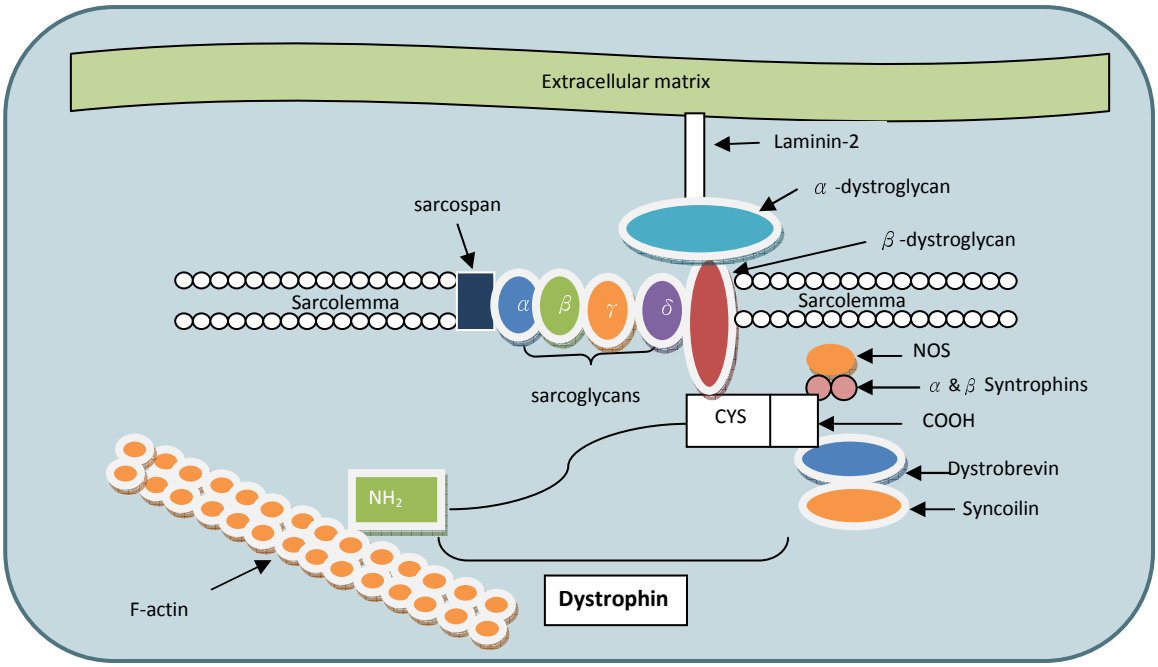

Figure 5.35 The dystrophin-associated protein complex (DAPC) in cardiac muscle. *The dystrophin acts as a bridge linking the intracellular cytoskeleton and the extracellular matrix via the DAPC [227].*

The major function of dystrophin is to stabilize the sarcolemma during repeated cycles of contraction and relaxation of muscle cells [229, 325]. Danialou and colleagues provided direct evidence that dystrophin acts to protect cardiomyocytes from mechanical stress and workload-induced damage caused by isoproterenol or temporary aortic occlusion [351]. Also, it has been suggested that this protein plays a role in the regulation of signal transduction through interaction with a number of membrane proteins [223, 225, 352].

In dystrophin-deficient hearts, the lack of dystrophin results in the loss of membrane integrity and increased susceptibility to damage from muscle contraction-induced stress, which in turn triggers a cascade of adverse downstream events, such as calcium overload and protein degradation, eventually leading to the death of cardiomyocytes [226]. Typically, the myocardial cell damage and death in Duchenne muscular dystrophy is limited to small areas scattered through the heart, referred to as microinfarcts [353]. Interestingly, this distribution pattern is different from myocardial infarction, in which the damaged area is infarcted artery-related. However, regardless of the aetiology, a series of inflammation-induced reactions occur following the death of cardiomyocyes within these necrotic lesions, with the resulting formation of fibrocollagenous scar tissues [31, 227]. In DMD, fibrotic scarring generally spares the atria [223, 354], likely due to the reduced mechanical stress in this region. As the disease progresses, the ventricles gradually stretch and enlarge, which causes chamber dilatation and wall thinning, leading to a reduction of contractility. Consequently, there is an impairment in cardiac function (dilated cardiomyopoathy) and ultimately irreversible hemodynamic decompensation (end-stage heart failure) [325].

Cardiac morphology and function of dystrophic hearts in mdx mice

There are a variety of imaging modalities employed in clinical and experimental studies. Echocardiography has traditionally been viewed as the standard tool to detect structural heart disease and to evaluate cardiac function. However, many features of DMD patients, including barrel-shaped chest, hyposcoliosis, and seated position (wheelchair-bound) make

echocardiographic examinations more challenging [223, 226]. As a result, cardiovascular MRI is increasingly being used in DMD patients to provide a sensitive and accurate non-invasive assessment of heart function as well as improved imaging of the right ventricle [226, 355]. In addition, cardiac MRI is able to identify the existence and degree of myocardial inflammation or fibrosis with the use of late gadolinium enhancement [341, 356, 357].

In the mdx mice, two-dimensional echocardiography has shown that left ventricle systolic function was normal at 2 months old and did not manifest dilated cardiomyopathy until 11 months old [329]. An MRI study by Zhang *et al.* found that the loss of dystrophin resulted in right ventricular dilatation with impaired function in 8 month-old mdx mice [330]. Recently, our group has detected early abnormalities of left ventricular function at 9 months and right ventricular function as early as 3 months in a serial study of mdx mice aged from 1 to 12 months using *in vivo* high-resolution MRI [341]. In the present investigation, as described by Zhang *et al.* and Stuckey *et al.* [330, 341], a right ventricular abnormality was found to precede left ventricular dysfunction, perhaps due to increased pressure load in the right ventricle, resulting from earlier onset of respiratory muscle weakness and pulmonary hypertension [358, 359]. In support of this mechanism, Crisp *et al.* reported that restoration of diaphragm function, irrespective of methods, can rescue cardiac function to a near normal level in mdx mice, as demonstrated by significant improvements in right ventricle EF at 6 months [340]. Furthermore, we imaged aged mdx mice of 18 months of age for follow up, and confirmed that ventricular dilatation and dysfunction progressively deteriorated in comparison to age-matched wild-type mice or young mdx mice. It should be noted that, to my knowledge, cardiac function has not previously been measured in mdx mice of this age. In addition, there were no localized hypokinesis or akinesis observed in the mdx mice, suggesting that dystrophic lesions are diffuse but not regional, which corresponds to the histopathology.

Dystrophic necrosis and fibrosis in the hearts of dystrophic mice

In the present study, immunofluorescence of wild-type and mdx mouse heart sections, stained against dystrophin, confirmed that the mdx mouse was dystrophin-deficient in the myocardium,

as shown by Zhang *et al.* [330]. Dispersed focal dystrophic changes (necrosis and fibrosis) were seen in right and left ventricles of mdx mouse hearts by H&E and picro-sirus red staining, while wild-type mouse hearts showed no necrosis. Necrotic lesions have been found in the hearts of mdx mice as early as 6 weeks [360], but the significant difference in the amount of fibrocollagenous tissues between control and mdx mice does not occur until 6 months of age [331, 341]. Interestingly, in a study of younger mdx mice (6 weeks old), Nakamura *et al.* demonstrated that regular treadmill-exercised mdx mice significantly developed dystrophic necrosis and fibrosis when compared to either exercised C57Bl/10 or non-exercised mdx mice [360].

Quinlan *et al.* reported that patchy fibrosis affects all regions of the left ventricle and the right ventricle to an approximately equal extent in 17 month-old mdx mice [329]. In contrast to their findings, our data show that the percentage of scar tissue in the right ventricle is significantly higher than that in the left ventricle ($p < 0.05$), but the degree of fibrotic change is similar in distinct left ventricular areas in the mdx mice at both ages of 6 and 18 months. This is in agreement with the present MRI results that impaired function of the right ventricle is more evident than that of the left ventricle in mdx mice at 6 months. Another investigation demonstrated that there was no significant difference in the distribution of fibrous scar tissues between superior and inferior regions of the left ventricle in the dystrophin-deficient mice aged from 3 to 18 months [331].

The extent of muscular fibrosis has been shown to be age-dependent in mdx skeletal muscles [342]. Likewise, a positive correlation between the degree of fibrosis and age in mdx heart muscle has seen shown using histology [329, 331]. Here, we found that cardiac fibrotic area accounts for 3% and 7% of myocardium in 6 and 18 month-old mdx mice, respectively. Van Erp *et al.* reported increased cardiac fibrosis from approximately 5% in 3 months, 8% in 6 months to 12% in 18 months of mdx mice [331]. In short, histopathology has revealed that interstitial myocardial fibrosis developed following dystrophic necrosis and inflammation over time, which was directly linked to cardiac dysfunction [329, 341].

Characterization of heart-derived cardiac stem cells from dystrophic mice

Here, it has been shown that CDCs can be generated from the atrial tissue from a mouse model of human DMD (mdx) at ages of 6 and 18 months. Similar to wild-type control mice, EDC, cardiosphere and CDC yield from old mdx mice was significantly less than that from young mdx mice. However, contrary to our hypothesis, there were no detectable differences in CDC number or characteristics between cells from mdx mice and wild type mice of either age.

Recently, Cassano *et al.* demonstrated that ventricle-derived cardiac progenitor cells (CPCs) from golden retriever muscular dystrophy (GRMD) dogs showed impaired self-renewal and cardiomyogenic differentiation *in vitro* and *in vivo* when compared to those from healthy dogs [336]. Based on the cardiac differentiation experiment, only terminally differentiated wild-type ventricular CPCs can express dystrophin, as documented by western blot analysis; in other words, CPCs do not express dystrophin until they become mature cardiomyocytes [336]. Additionally, iPSCs, derived from DMD patients, were differentiated into cardiomyocytes which could express dystrophin using either gene replacement or exon skipping [Dr C. Denning, FCVB conference presentation, 2012]. It may be presumed that dystrophin expression is not directly related to cardiac differentiation, or at least not indispensable during differentiation. This is generally in line with the observation that stem cells from embryos with a congenital defect in dystrophin protein expression can still develop into cardiovascular lineage cells, including cardiomyocytes, though they are dystrophin-deficient. Cassano *et al.* concluded that the differentiation of CPCs into cardiomyocytes is adversely affected by the pathological condition and not the lack of dystrophin [336].

Interestingly, as has been seen with studies in normal and dystrophic skeletal muscle, it was reported that skeletal myoblasts from adult dystrophic mice were capable of differentiating in culture and showed no appreciable differences compared with their normal counterparts [361]. Valentine *et al.* found no differences of cell morphology, growth, and differentiation in culture between cells from skeletal muscle of dystrophic and normal dogs [334]. Likewise, a recent study also showed that there were no obvious alterations to cell biology observed between

satellite cells isolated from wild-type or GRMD dystrophic dogs, as determined *in vitro* by proliferation capacity, clonogenicity, motility and expression of terminal differentiation proteins [335]. Thus, Berg *et al.* concluded that there was no major deficit in the regenerative function of *in vitro* satellite cells cultured from dystrophic muscle, even if the donor animals develop severe muscular dystrophy [335].

In the present work, surprisingly, there were no significant changes in the numbers of generated EDCs, cardiospheres and CDCs from dystrophic mdx mice compared with those from wild-type control mice. Heart-derived cells isolated from both mdx and wild-type mice did not show distinguishable alterations in morphology and size. We found no significant differences in the proportions of cardiac stem cell subpopulation (c-kit$^+$ or Sca-1$^+$) in CDCs between age-matched mdx and wild-type mice. In addition to morphologic and phenotypic similarities between the CDCs from both mouse type groups, again, the qualitative measures revealed that the biological characteristics of CDCs from mdx mice are comparable to those from wild-type animals at both young and old ages. Collectively, the results indicate no marked changes in stem cell properties between the two populations. There are several possible explanations for the finding. First, although there is an inflammatory response to the cell necrosis caused by contraction-induced stress, this may not result in the level of elevated ROS seen in ischemic heart damage. Second, the damage to the myocardium occurs gradually at locations throughout the heart, so the stem cell pool is able to keep up with repair due to self-renewal. Third, the CDCs were isolated from the atria, which have been reported to be the most abundant region of functionally competent CSCs [159, 267, 292]; these cells are maintained well in atria and are more resistant to the pathological environment. Additionally, the atria are generally spared from dystrophic changes relative to ventricles, thus minimizing the negative effect of pathology on atrial stem cells [223, 354]. Where CSCs are harvested from the left ventricle, it may be that the CSC reservoir would not be depleted as damage to left ventricle occurs slowly in disseminated small regions of myocardium. However, it is important to highlight that Cassano *et al.* compared cardiac progenitor cells grown from ventricles of healthy and GRMD dogs, which might explain the differences between results [336].

Study limitations

Although the data showed no distinguishable differences in culture yield and biological properties between CDCs from mdx and wild-type mice, there were a few limitations in terms of therapeutic potential for heart repair. Firstly, the ability of cardiomyogenic differentiation was not investigated from mdx-derived CDCs in the current work, which is directly linked to the regenerative capacity in the stem cell-based cardiac therapy. Secondly, due to the genetic defect of dystrophin expression in cells derived from mdx mice, differentiated cardiomyocytes would be dystrophin-deficient and vulnerable if no dystrophin gene replacement or mutation-specific modification was given. Undoubtedly, this is an important area of research in the development of autologous stem-based therapy using endogenous CSCs.

5.6 Conclusions

To sum up, the absence of dystrophin in the mdx mouse hearts was found to cause dystrophic lesions (necrosis, inflammation and fibrosis) in the myocardium, and fibrosis increased with advancing age. Cardiac fibrosis is related to ventricle chamber dilatation accompanied by abnormal systolic function (i.e., dilated cardiomyopathy), which resembles the pathological changes in patients with DMD. This confirms that the mdx mouse may act as a valuable model for cardiomyopathy research and therapy for DMD. Regardless of age, resident cardiac stem cells isolated from the dystrophic mouse hearts were comparable to those from age-matched wild-type mice in terms of expansion number, migratory distance, clonogenicity and proliferation, suggesting that CSCs might be a possible option of cell type to be explored for the management of cardiomyopathy and heart failure in DMD patients in conjunction with dystrophin replacement. In conclusion, cardiac-derived stem cells could be isolated and expanded from mdx mice and no detectable primary defects in CDCs cultured from mdx mice were found compared with wild-type mice.

Chapter 6

General discussion

General discussion

Endogenous cardiac stem cells (CSCs) represent an attractive and promising cell candidate for cardiac repair and regeneration due to their autologous origin, cardiac-committed fate, and ability to develop into three major myocardial lineages. Over the past few years, transplantation of CSCs has been shown to modulate the remodelling process, regenerate the damaged myocardium and improve heart function in animal models of myocardial infarction [286]. Recently, two phase I clinical studies, SCIPIO and CADUCEUS, using c-kit$^+$ CSCs and CDCs, respectively, confirmed early short-term safety and therapeutic efficacy (improvement in EF, reduced infarct size or increased viable myocardium) in patients with ischemic heart failure [79, 89]. Although great advances have been seen in this field, many relevant questions remain unanswered. The aim of the work described in this thesis was to investigate the feasability of myocardial tissue engineering as a novel therapeutic approach for HF by testing the hypotheses that the decellularization method (coronary detergent perfusion) could generate an accellular heart matrix with preservation of intact geometric architecture and nourishing vascular network but that chronological age of donor animals and myocardial pathology impair CSC expansion and characteristics.

Isolation, characterization, and function of cardiosphere-derived cells

The isolation of adult CSCs is either based on the stem cell surface antigen (i.e., c-kit or Sca-1) or *via* the formation of cardiospheres. In Chapter 3 and 4, adult cardiosphere-derived cells (CDCs) were isolated from rats and mice, grown and characterized *in vitro*. The culture of mouse CDCs was first established for this project in the lab. In contrast to antigenically-purified CSCs, CDCs are a heterogeneous population containing heart-derived stem cells expressing Oct3/4, Sox2, and c-kit or Sca-1, cardiac mesenchymal cells (CD90 and CD105), and early cardiac-committed cells (Nkx2.5), as shown here and by others [37].

Pure c-kit$^+$ or Sca-1$^+$ cardiac stem cells have been shown to be self-renewing, clonogenic and multipotent, giving rise to cardiac muscle, smooth muscle and endothelial cells [160, 183].

Likewise, cardiospheres and CDCs contain progenitor cells capable of self-renewal, clonal expansion and differentiation into cardiac lineages [158, 165]. Interestingly, Koninckx *et al.* suggested that c-kit$^+$ CSCs and CDCs probably share the same precursor in origin [362]. However, there seem to be two differences between both c-kit$^+$ CSC and CDC populations. First is the presence of mesenchymal stem cells (MSCs) in unsorted CDCs, which may be advantageous when used to improve heart function, as MSCs are known to secrete soluble paracrine factors, contributing to stimulation of tissue-specific stem cell differentiation, endogenous cardiomyogenesis and angiogenesis [363]. Second, CDCs consist of more than one CSC population including c-kit, MDR-1 (human), and Sca-1 (mice) or Sca-1-like (human) cells [165, 175, 184].

Based on most experimental studies, the number of newly formed cardiac myocytes from transplanted stem cells is too small to be proportional to the improvement observed in heart function [173]. This phenomenon could be attributable to the combination of poor cell engraftment and low cardiomyogenic potential *in vivo* following the introduction of stem cells into the injured myocardium [37]. Alternatively, the paracrine hypothesis is now widely believed to play a major role in the beneficial action of transplanted stem cells *via* the secretion of various cytokines and growth factors, such as VEGF, HGF and IGF-1 [50, 364, 365]. It has been reported that in human CDC populations, unselected mixed CDCs significantly improved heart function in comparison to c-kit-sorted CSCs, as determined by ejection fraction, when implanted into infarcted immunodeficient mice [294]. Furthermore, Chimenti *et al.* characterized potential actions of paracrine factors in human CDC transplantation and concluded that the contribution of the indirect effect rivals or exceeds that of direct myocardial regeneration [364]. In addition, Li *et al.* reported that human CDCs exhibited relatively high production of various growth factors, including angiopoietin-2, bFGF, HGF, SDF-1, IGF-1, and VEGF, and resulted in superior improvement of cardiac function compared with BM-MSCs, BM-MNCs and adipose tissue-derived MSCs [365]. Collectively, mesenchymal cells may synergize with c-kit$^+$ cells in the mixed CDC population to augment paracrine potency and thereby boost functional improvement [365].

Combination of stem cells and tissue/organ engineering for heart failure therapy

Currently, no available treatment has been able to restore the irreversibly injured heart, which has to involve the regeneration of lost myocardial cells, the recreation of a functional vascular network, and the return of the ventricle to its proper architecture [366]. However, the combination of cell therapy and tissue/organ engineering may offer unique advantages as a definitive therapy that could be used to treat advanced and terminal heart failure, irrespective of the underlying aetiology [122].

In Chapter 3, it was demonstrated for the first time that CDCs survived and proliferated for up to 7 weeks within engineered 3D porous alginate scaffolds and that CDC viability was improved within ECM protein-coated alginate constructs, which is a novel finding and could be considered to improve cell engraftment. Furthermore, the decellularized heart matrix scaffold can be generated by Langendorff coronary perfusion, leaving intact geometry, which was confirmed for the first time by high-resolution cine-MRI, and preserved perfusable vasculature shown by perfusion with Evan's blue dye. A novel approach for the differentiation of CDCs towards a cardiomyocyte phenotype in monolayer was adopted using 5-Aza or DMSO combined with ascorbic acid, though the differentiated cells may not have been fully mature. The differentiation of CDCs into endothelial and smooth muscle cells is also required for re-endothelialization of the vascular and lymphatic systems in the acellular extracellular matrix (ECM) scaffold. The fact that the CDC population is a heterogeneous mixture consisting of cardiac stem cells and mesenchymal stem cells, is a major strength here as CDC application may provide all cell types needed in the heart. It has been reported that differentiation of stem cells into mature cardiomyocytes was improved by the presence of mesenchymal cells (e.g., fibroblasts and endothelial cells), probably *via* paracrine actions and up-regulation of anti-apoptotic factors [84, 194]. Furthermore, the microenvironment associated with ECM is reported to direct stem cell differentiation [122]. Thus, it is plausible that the introduction of CDCs may repopulate the decellularized ECM scaffold and develop into all myocardial lineages in order to grow into a functional bioartificial heart. However, to reseed an acellular bioengineered matrix of a whole heart, it is imperative to grow sufficient cells *in vitro* to

provide adequate cell-to-cell interaction and achieve optimal engraftment, which would be a challenge when using an autologous cell source. Therefore, subsequent work in this thesis investigated the effect of age and of myocardial damage on the number and viability of expanded CDCs. Clearly, there is still much work to be done before translation to the clinical application; however this has moved a step further towards transplantation of an engineered new organ in the regenerative medicine field.

Location- and age-related alterations to yield and function of cardiosphere-derived cells

It is important to highlight that this present study was the first to use mouse CDCs for the investigation of effects of sampling location and chronological age on CSC characteristics (Chapter 4). The geographic distribution of cardiac stem cells may not be homogeneous within the heart, and cardiac niches may gather preferentially in specific anatomic regions [367]. Aging is an inevitable fact of life and may link to the biological state of tissue-specific stem cells [368]. These issues potentially interfere with cell acquisition in terms of clinically-relevant quantity and therapeutic potential. In agreement with previous studies focusing on c-kit$^+$ cells, atria were found to be the most abundant site of resident cardiac-derived stem cells.

CDCs were found to decline in yield and regenerative properties with increasing age. Aging is extremely complex and involves multiple mechanisms at various levels (i.e., molecular, cellular, organic and organismal) [385]. Although the exact interactions between senescence-related signalling pathways remain to be ascertained, theories have been proposed to explain the aging process, including theories of somatic mutation, mitochondrial DNA (mtDNA) mutation and telomere loss [385]. For example, with progressive shortening of telomeres to a critical length, cells eventually reach the limit of cellular division, known as the Hayflick limit, and enter a growth arrest state such that telomere attrition is the major cause of replicative senescence [384]. Furthermore, it was demonstrated that increased oxidative stress and inflammation, associated with DNA damage and impaired ATP production, further accelerate the telomere erosion rate [385, 386]. With time, telomere dysfunction leads to expression of apoptotic factors (e.g., p53), and positivity for cellular senescence markers (e.g., p16^{INK4a}) [295, 387], which exhaust CSCs

and impair CSC inherent traits in cardiac niches.

Collectively, a variety of intrinsic and extrinsic systems are involved in the regulation of stem cell number and biological performance, such as cell-to-ECM, telomere-telomerase, growth factor-receptor, and ROS-antioxidant defence systems [222, 318]. For instance, the IGF-1/IGF-1 receptor system preserves the pool of endogenous CSCs through enhancing telomerase activity and delaying senescence by activating the PI3K-Akt pathway [318]. It has been shown that the IGF-1/IGF-1 receptor axis exists in cardiac stem cells in very old animals [318, 369]. In this regard, preconditioning of cultured resident CSCs in old age by over-expressing telomerase or up-regulation of favourable growth factor signalling may improve the regenerative capabilities of survival, growth and differentiation *in vivo* following transplantation [221, 222, 324]. Furthermore, in our group, hypoxic culture as a preconditioning treatment not only significantly increased cell yield but also enhanced telomerase levels and secretion of paracrine factors (e.g., VEGF and EPO) in rat CDCs (Tan *et al*, in review). In short, further understanding of the interactions between CSC characteristics has significant clinical implications in the use of stem cells for cardiac therapy.

Characterization of cardiosphere-derived cells from dystrophic heart of mdx mice

In Chapter 5, histological analysis and *in vivo* high resolution MRI demonstrated cardiac fibrosis and dilated cardiomyopathy in older mdx mice. Cardiosphere-derived cells were isolated from the atria from mdx and wild-type mice and interestingly no significant differences in cell yield and biological characteristics, such as clonogenicity, migration and proliferation were found. This suggests that, where cardiac damage occurs slowly and progressively, as opposed to damage resulting from an acute ischaemic insult, it may be possible to grow a population of CSCs without detectable reduced potential from relatively unaffected areas (i.e., atria).

It has been suggested that CSCs can be cultured from failing human hearts, but pathological processes may influence the endogenous CSC pool function [370]. Importantly, Itzhaaki-Alfia

and colleagues demonstrated that human c-kit$^+$ CSCs can be isolated and expanded from the right atrium of most patients aged 50 to 75 years undergoing heart surgery, such as CABG, valve replacement and heart transplantation [267]. Furthermore, D'Amario *et al.* reported that c-kit$^+$ CSCs isolated from the diseased myocardium (RV septum apex or LV apical region) in patients with advanced heart failure were functionally competent, as measured by telomere length and telomerase level, indicating that autologous CSC therapy is realistic and can therefore be considered for use in the treatment of patients with severe heart failure [371].

Study limitations

Clinical applications using cardiac organ engineering with autologous stem cells face the limitation of scaling up sufficient cells *in vitro.* Although CDCs could be isolated and grown from old and diseased animals as shown here, characterization of long-term cultured CDCs following multiple passages was not conducted regarding karyotype (chromosomal stability), phenotype (stemness) and function (contractility after differentiation, calcium transients, regenerative potential).

Future directions

It is necessary to optimize methods to efficiently guide differentiation of CDCs into three major cardiac lineages (i.e., cardiac myocytes, endothelial and smooth muscle cells) *in vitro* using well-defined culture media supplemented with inducing chemical reagents or recombinant growth factors. Alternatively, another approach would be to differentiate CDCs cultured within alginate- or collagen-based scaffold with assistance from signals arising from cell-to-ECM interactions. It would be important to conduct cardiomyogenic differentiation on mdx-derived CDCs before and after restoration of dystrophin expression to determine whether dystrophin affects the phenotype of differentiated cells, and compare these with differentiated wild-type-derived CDCs in order to investigate the effect of pathology on differentiation potential.

Apart from age and environment, gender seems to play another relevant role in determining CSC quantity and growth [367, 368]. Myocardial tissue derived from female hearts yielded a

larger number of human c-kit$^+$ CSCs with sustained superior function [267, 322]. It would be valuable in clinical applications to understand the effect of gender on the CDC population.

In addition, to recellularize the decellularized ECM scaffold into a functional bioartificial organ, it is imperative to establish a suitable culture system resembling the *in vivo* physiological environment in terms of hemodynamic load and electro-mechanical coupling. During maturation, there are many fundamental and functional characterizations required. Undoubtedly, this is an ambitious and exciting goal, and requires a multidisciplinary team to work towards these achievements.

In short, a number of follow-up experiments should include: further optimization of *in vitro* cardiac lineage differentiation of CDCs to generate beating cardiomyocytes and measurement of calcium transients, optimisation of endothelial differentiation of CDCs, cardiomyocyte differentiation of mdx-derived CDCs following restoration of dystrophin, characterization of long-term cultured CDCs, hypoxic preconditioning of CDCs from old mice, and *in vivo* functional study of regenerative potential.

Conclusions

In summary, it is nearly 10 years since the identification of endogenous cardiac stem cells. Based on numerous experimental studies and recent clinical trials, there has been growing evidence showing that cardiac stem cells can be grown as autologous cells for cardiac therapy, as demonstrated by feasibility, safety and functional improvement. Importantly, regardless of age or disease, cardiac stem cells have been isolated and expanded from the diseased heart from most patients. Among various cardiac stem cells, cardiosphere-derived cells comprise mixed subpopulations and can give rise to major cardiac lineages. In addition, cardiosphere-derived cells are able to secrete a variety of cytokines and growth factors in support of paracrine actions. The work in this thesis has shown that CDCs can be expanded over many weeks within a 3D scaffold and that perfursion- decellularisation of the heart leaves a collagen scaffold with intact geometric architecture and vascular networks. CDCs can be isolated from mouse hearts as old

as 24 months, albeit in significantly reduced numbers, and from fibrotic hearts with reduced ventricular function. With rapid progress in stem cell biology and tissue/organ engineering, in spite of huge challenges, the combination of both approaches looks promising for treatment of patients with advanced heart failure.

References

1. World Health Organisation. The top 10 causes of death. 2008. Ref Type: Online source. http://www.who.int/mediacentre/factsheets/fs310/en/index.html (accessed on February 2, 2012).
2. Levy D, *et al*. Long-term trends in the incidence of any survival with heart failure. *N Engl J Med.* 2002; 347: 1397-1402.
3. Costanzo MR, et al. Characteristics of "Stage D" heart failure: insights from the Acute Decompensated Heart Failure 2008 National Registry Longitudinal Module (ADHERE LM). Am Heart J. 2008; 155(2): 339-47.
4. Bui AL, *et al*. Epidemiology and risk profile of heart failure. *Nat Rev Cardiol.* 2011; 8: 30-41.
5. Calvert MJ, *et al*. Evaluation of the management of heart failure in primary care. *Primary Practice.* 2009; 26: 145-153.
6. Roger VL, *et al.* Heart disease and stroke statistics--2011 update: a report from the American Heart Association. *Circulation.* 2011; 123: e18-e209.
7. Lloyd-Jones D, *et al*. Heart disease and stroke statistics--2010 update: a report from the American Heart Association. *Circulation.* 2010; 121: e46-215.
8. Norton C, *et al.* Epidemiology and cost of advanced heart failure. *Progress in Cardiovascular Disease.* 2011; 54: 78-85.
9. McMurray JJ. Systolic heart failure. *N Engl J Med.* 2010; 362: 228-238.
10. Dickstein K, *et al*. ESC guidelines for the diagnosis and treatment of acute and chronic heart failure 2008: the Task Force for the diagnosis and treatment of acute and chronic heart failure 2008 of the European Society of Cardiology: developed in collaboration with the Heart Failure Association of the ESC (HFA) and endorsed by the European Society of Intensive Care Medicine (ESICM). *Eur J Heart Fail.* 2008; 10: 933-989.
11. Hunt SA, *et al*. 2009 Focused update incorporated into the ACC/AHA 2005 guidelines for the diagnosis and management of heart failure in adults: a report of the American College of Cardiology Foundation/American Heart Association Task Force on practice guidelines: developed in collaboration with the International Society for Heart and Lung Transplantation. *Circulation.* 2009; 119(14): e391-479.
12. Cohn JN, *et al*. A randomized trial of the angiotensin-receptor blocker valsartan in chronic heart failure. *N Engl J Med.* 2001; 345: 1667-1675.
13. Granger CB, *et al*. Effects of candesartan in patients with chronic heart failure and reduced left ventricular systolic function intolerant to angiotensin-converting-enzyme inhibitors: the CHARM-Alternative trial. *Lancet.* 2003; 362: 772-776.
14. Pitt B, *et al,* The effect of spironolactone on morbidity and mortality in patients with severe heart failure. *N Engl J Med.*1999; 341: 709-717.
15. Ezekowitz JA, *et al.* Implantable cardioverter Defibrillators in primary and secondary prevention: a systematic review of randomized, controlled trials. *Ann Intern Med.* 2003; 138: 445-452.
16. McAlister FA, *et al.* Systematic review: cardiac resynchronization in patients with symptomatic heart failure. *Ann Intern Med.* 2004; 141: 381-390.
17. Bristow MR, *et al.* Cardiac-resynchronization therapy with or without an implantable defibrillator in advanced chronic heart failure. *N Engl J Med.* 2004; 350: 2140-2150.
18. Cleland JG, *et al*. The effect of cardiac resynchronization on morbidity and mortality in heart failure. *N Engl J Med.* 2005; 352: 1539-1549.
19. Bradley DJ, *et al.* Cardiac resynchronization and death from progressive heart failure: a meta-analysis of randomized controlled trials. *JAMA.* 2003; 289: 730-740.
20. McCarthy PM. Surgical therapies for post-myocardial infarction patients. *Am J Cardiol.* 2008; 102 [suppl]: 42G-46G.
21. Taylor DO, *et al.* Registry of the International Society for Heart and Lung Transplantation: twenty-fourth official adult heart transplant report-2007. *J Heart Lung Transplant*. 2007; 26: 769-781.
22. Popov AF, *et al.* Clinical experience with HeartWare left ventricular assist device in patients with end-stage heart failure. *Ann Thorac Surg.* 2012; 93(3): 810-815.

23. Iyer A, *et al.* Primary graft failure after heart transplantation. *Journal of Transplantation.* 2011; 2011: 1-9.
24. Russell SD, *et al.* Advanced heart failure: a call to action. *Congest Heart Fail.* 2008; 14: 316-321.
25. Stehlik J, *et al.* The Registry of the International Society for Heart and Lung Transplantation: twenty-seventh official adult heart transplant report--2010. *J Heart Lung Transplant.* 2010; 29(10): 1089-103.
26. Rose EA, *et al.* Long-term use of a left ventricular assist device for end-stage heart failure. *N Engl J Med.* 2001; 345: 1435-1443.
27. Caccamo M, *et al.* Current state of ventricular assist devices. *Curr Heart Fail Rep.* 2011; 8: 91-98.
28. Strueber M, *et al.* Multicenter evaluation of an intrapericardial left ventricular assist system. *J Am Coll Cardiol.* 2011; 57: 1375-1382.
29. Shah KB, *et al.* Evaluating heart failure after implantation of mechanical circulatory support devices. *Curr Heart Fail Rep.* 2012; 9: 65-74.
30. Lund LH, *et al.* Patient selection for left ventricular assist devices. *European Journal of Heart Failure.* 2010; 12: 434-443.
31. Murry CE, *et al.* Cell-based cardiac repair: reflections at the 10-year point. *Circulation.* 2005; 112(20): 3174-3183.
32. Wu KH, *et al.* Cellular therapy and myocardial tissue engineering: the role of adult stem and progenitor cells. *Eur J Cardiothorac Surg.* 2006; 30(5): 770-781.
33. Hou D, *et al.* Radiolabeled cell distribution after intramyocardial, intracoronary, and interstitial retrograde coronary venous delivery: implications for current clinical trials. *Circulation.* 2005; 112(9 Suppl): I150-156.
34. Wollert KC and Drexler H. Clinical applications of stem cells for the heart. *Circ Res.* 2005; 96(2): 151-163.
35. Gersh BJ, *et al.* Cardiac cell repair therapy: a clinical perspective. *Mayo Clin Proc.* 2009; 84(10): 876-892.
36. Terrovitis J, *et al.* Noninvasive quantification and optimization of acute cell retention by in vivo positron emission tomography after intramyocardial cardiac-derived stem cell delivery. *J Am Coll Cardiol.* 2009; 54(17): 1619-1626.
37. Malliaras K and Marban E. Cardiac cell therapy: where we've been, where we are, and where we should be headed. *Br Med Bull*. 2011; 98: 161-185.
38. Stamm C, *et al.* Cell therapy for heart disease: great expectations, as yet unmet. *Heart Lung Circ.* 2009; 18(4): 245-256.
39. Yau TM, *et al.* Increasing transplanted cell survival with cell-based angiogenic gene therapy. *Ann Thorac Surg.* 2005; 80(5): 1779-1786.
40. Zhang M, *et al.* Cardiomyocyte grafting for cardiac repair: graft cell death and anti-death strategies. *J Mol Cell Cardiol.* 2001; 33(5): 907-921.
41. Mangi AA, *et al.* Mesenchymal stem cells modified with Akt prevent remodeling and restore performance of infarcted hearts. *Nat Med.* 2003; 9(9): 1195-1201.
42. Li W. *et al.* Bcl-2 engineered MSCs inhibited apoptosis and improved heart function. *Stem Cells.* 2007; 25(8): 2118-2127.
43. Spyridopoulos I, *et al.* Statins enhance migratory capacity by upregulation of the telomere repeat-binding factor TRF2 in endothelial progenitor cells. *Circulation.* 2004; 110(19): 3136-3142.
44. Sasaki K, *et al.* Ex vivo pretreatment of bone marrow mononuclear cells with endothelial NO synthase enhancer AVE9488 enhances their functional activity for cell therapy. *Proc Natl Acad Sci U S A*. 2006; 103(39): 14537-14541.
45. Hu X, *et al.* Transplantation of hypoxia-preconditioned mesenchymal stem cells improves infarcted heart function via enhanced survival of implanted cells and angiogenesis. *J Thorac Cardiovasc Surg.* 2008; 135(4): 799-808.
46. Robey TE, *et al.* Systems approaches to preventing transplanted cell death in cardiac repair. *J Mol Cell Cardiol.* 2008; 45(4): 567-581.
47. Johnston PV, *et al.* Engraftment, differentiation, and functional benefits of autologous cardiosphere-derived cells in porcine ischemic cardiomyopathy. *Circulation.* 2009; 120(12): 1075-1083.

48. Jawad H, *et al.* Myocardial tissue engineering. *Br Med Bull.* 2008; 87: 31-47.
49. Vunjak-Novakovic G, *et al.* Challenges in cardiac tissue engineering. *Tissue Eng Part B Rev*. 2010; 16(2): 169-187.
50. Lovell MJ and Mathur A. Republished review: cardiac stem cell therapy: progress from the bench to bedside. *Postgrad Med J.* 2011; 87: 558-564.
51. Hatzistergos KE, *et al.* Bone Marrow Mesenchymal Stem Cells Stimulate Cardiac Stem Cell Proliferation and Differentiation. *Circ Res.* 2010; 107(7): 913-922.
52. Segers VF and Lee RT. Stem-cell therapy for cardiac disease. *Nature.* 2008; 451(7181): 937-942.
53. Martinez EC and Kofidis T. Myocardial tissue engineering: the quest for the ideal myocardial substitute. *Expert Rev Cardiovasc Ther.* 2009; 7(8): 921-928.
54. Akhyari P, *et al.* Myocardial tissue engineering: the extracellular matrix. *Eur J Cardiothorac Surg.* 2008; 34: 229-241.
55. Eschenhagen T, *et al.* Three-dimensional reconstitution of embryonic cardiomyocytes in a collagen matrix: a new heart muscle model system. *FASEB J.* 1997; 11(8): 683-694.
56. Zimmermann WH, *et al.* Three-dimensional engineered heart tissue from neonatal rat cardiac myocytes. *Biotechnol Bioeng.* 2000; 68(1): 106-114.
57. Leor J, *et al.* Bioengineered cardiac grafts: A new approach to repair the infarcted myocardium? *Circulation.* 2000; 102(19 Suppl 3): III56-61.
58. Courtman DW, *et al.* Development of a pericardial acellular matrix biomaterial: biochemical and mechanical effects of cell extraction. *J Biomed Mater Res.* 1994; 28(6): 655-666.
59. Grabow N, *et al.* Mechanical and structural properties of a novel hybrid heart valve scaffold for tissue engineering. *Artif Organs.* 2004; 28(11): 971-979.
60. Roy S, *et al.* Biomechanical properties of decellularized porcine common carotid arteries. *Am J Physiol Heart Circ Physiol.* 2005; 289(4): H1567-1576.
61. Tan M, *et al.* Repair of infarcted myocardium using mesenchymal stem cell seeded small intestinal submucosa in rabbits. *Biomaterials.* 2009; 30(19): 3234-3240.
62. Shimizu T, *et al.* Fabrication of pulsatile cardiac tissue grafts using a novel 3-dimensional cell sheet manipulation technique and temperature-responsive cell culture surfaces. Circ *Res.* 2002; 90(3): e40.
63. Masuda S, *et al.* Cell sheet engineering for heart tissue repair. *Adv Drug Deliv Rev.* 2008; 60(2): 277-285.
64. Miyahara Y, *et al.* Monolayered mesenchymal stem cells repair scarred myocardium after myocardial infarction. *Nat Med.* 2006; 12(4): 459-465.
65. Morritt AN, *et al.* Cardiac tissue engineering in an in vivo vascularized chamber. *Circulation.* 2007; 115(3): 353-360.
66. Nourse MB, *et al.* VEGF induces differentiation of functional endothelium from human embryonic stem cells: implications for tissue engineering. *Arterioscler Thromb Vasc Biol.* 2010; 30(1): 80-89.
67. Gerecht-Nir S, *et al.* Biophysical regulation during cardiac development and application to tissue engineering. *Int J Dev Biol.* 2006; 50(2-3): 233-243.
68. Yuasa S and Fukuda K. Cardiac regenerative medicine. *Circ J.* 2008; 72 Suppl A: A49-55.
69. Christman KL, *et al.* Injectable fibrin scaffold improves cell transplant survival, reduces infarct expansion, and induces neovasculature formation in ischemic myocardium. *J Am Coll Cardiol.* 2004; 44(3): 654-660.
70. Dai W, *et al.* Thickening of the infarcted wall by collagen injection improves left ventricular function in rats: a novel approach to preserve cardiac function after myocardial infarction. *J Am Coll Cardiol.* 2005; 46: 714-719.
71. Leor J, *et al.* Cells, scaffolds, and molecules for myocardial tissue engineering. *Pharmacol Ther.* 2005; 105(2): 151-163.
72. Davis ME, *et al.* Injectable self-assembling peptide nanofibers create intramyocardial microenvironments for endothelial cells. *Circulation.* 2005; 111(4): 442-450.
73. Kofidis T, *et al.* Novel injectable bioartificial tissue facilitates targeted, less invasive, large-scale tissue restoration on the beating heart after myocardial injury. *Circulation.* 2005; 112(9 Suppl): I173-177.
74. Leor J, *et al.* Intracoronary injection of in situ forming alginate hydrogel reverses left

ventricular remodeling after myocardial infarction in Swine. *J Am Coll Cardiol.* 2009; 54(11):1014-1023.
75. Buckberg GD. Basic science review: the helix and the heart. *J Thorac Cardiovasc Surg.* 2002; 124(5): 863-883.
76. Ott HC, *et al.* Perfusion-decellularized matrix: using nature's platform to engineer a bioartificial heart. *Nat Med.* 2008; 14(2): 213-221.
77. Dimmeler S and Zeiher AM. Cell therapy of acute myocardial infarction: open questions. *Cardiology.* 2009; 113(3): 155-160.
78. Hansson EM, *et al.* Regeneration next: toward heart stem cell therapeutics. *Cell Stem Cell.* 2009; 5(4): 364-377.
79. Bolli R *et al.* Cardiac stem cells in patients with ischemic cardiomyopathy (SCIPIO): initial results of a randomised phase 1 trial. *Lancet.* 2011; 378 (9806): 1847-1857.
80. Makkar RR, *et al.* Intracoronary cardiosphere-derived cells for heart regeneration after myocardial infarction (CADUCEUS): a prospective, randomised phase 1 trial. *Lancet.* 2012; 379 (9819): 895-904.
81. Breitbach M, *et al.* Potential risks of bone marrow cell transplantation into infarcted hearts. *Blood.* 2007; 110(4): 1362-1369.
82. Yoon YS, *et al.* Unexpected severe calcification after transplantation of bone marrow cells in acute myocardial infarction. *Circulation.* 2004; 109(25): 3154-3157.
83. Bradley A, *et al.* Formation of germ-line chimaeras from embryo-derived teratocarcinoma cell lines. *Nature.* 1984; 309(5965): 255-256.
84. Stubbs SL, *et al.* Toward Clinical Application of Stem Cells for Cardiac Regeneration. *Heart Lung Circ.* 2011; 20(3): 73-79.
85. Evans MJ and Kaufman MH. Establishment in culture of pluripotential cells from mouse embryos. *Nature.* 1981; 292(5819): 154-156.
86. Thomson JA, *et al.* Embryonic stem cell lines derived from human blastocysts. *Science.* 1998; 282(5391): 1145-1147.
87. Klug MG, *et al.* Genetically selected cardiomyocytes from differentiating embronic stem cells form stable intracardiac grafts. *J Clin Invest.* 1996; 98(1): 216-224.
88. Min JY, *et al.* Transplantation of embryonic stem cells improves cardiac function in postinfarcted rats. *J Appl Physiol.* 2002; 92(1): 288-296.
89. Yang Y, *et al.* VEGF enhances functional improvement of postinfarcted hearts by transplantation of ESC-differentiated cells. *J Appl Physiol.* 2002; 93(3): 1140-1151.
90. Laflamme MA, *et al.* Cardiomyocytes derived from human embryonic stem cells in pro-survival factors enhance function of infarcted rat hearts. *Nat Biotechnol.* 2007; 25(9): 1015-1024.
91. Boyle AJ, *et al.* Is stem cell therapy ready for patients? Stem cell therapy for cardiac repair. Ready for the next step. *Circulation.* 2006; 114(4): 339-352.
92. Schabort E, *et al.* Potential myogenic stem cell populations: sources, plasticity, and application for cardiac repair. *Stem Cells Dev.* 2009; 18(6): 813-830.
93. Li SC, *et al.* Stem cell engineering for treatment of heart diseases: potentials and challenges. *Cell Biol Int.* 2009; 33(3): 255-267.
94. Takahashi K and Yamanaka S. Induction of pluripotent stem cells from mouse embryonic and adult fibroblast cultures by defined factors. *Cell.* 2006; 126(4): 663-676.
95. Takahashi K, *et al.* Induction of pluripotent stem cells from adult human fibroblasts by defined factors. *Cell.* 2007; 131: 861-872.
96. Mauritz C, *et al.* Generation of functional murine cardiac myocytes from induced pluripotent stem cells. *Circulation.* 2008; 118(5): 507-517.
97. Pfannkuche K, *et al.* Cardiac myocytes derived from murine reprogrammed fibroblasts: intact hormonal regulation, cardiac ion channel expression and development of contractility. *Cell Physiol Biochem.* 2009; 24(1-2): 73-86.
98. Yu J, *et al.* Induced pluripotent stem cell lines derived from human somatic cells. *Science.* 2007; 318(5858): 1917-1920.
99. Nelson TJ *et al.* Repair of acute myocardial infarction by human stemness factors induced pluripotent stem cells. *Circulation.* 2009; 120(5): 408-416.
100. Zhang J, *et al.* Functional cardiomyocytes derived from human induced pluripotent stem cells. *Circ Res.* 2009; 104(4): e30-41.

101. Chin MH, *et al.* Induced pluripotent stem cells and embryonic stem cells are distinguished by gene expression signatures. *Cell Stem Cell.* 2009; 5(1): 111-123.
102. Okita K, *et al.* Generation of mouse induced pluripotent stem cells without viral vectors. *Science.* 2008; 322(5903): 949-953.
103. Kim D, *et al.* Generation of human induced pluripotent stem cells by direct delivery of reprogramming proteins. *Cell Stem Cell.* 2009; 4(6): 472-476.
104. Yu J, *et al.* Human induced pluripotent stem cells free of vector and transgene sequences. *Science.* 2009; 324(5928): 797-801.
105. Nakagawa M, *et al.* Generation of induced pluripotent stem cells without Myc from mouse and human fibroblasts. *Nat Biotechnol.* 2008; 26(1): 101-106.
106. Poulsom R, *et al.* Adult stem cell plasticity. *J Pathol.* 2002; 197(4): 441-456.
107. Wagers AJ and Weissman IL. Plasticity of adult stem cells. *Cell.* 2004; 116: 639-648.
108. Dowell JD, *et al.* Myocyte and myogenic stem cell transplantation in the heart. *Cardiovasc Res.* 2003; 58(2): 336-350.
109. Taylor DA, *et al.* Regenerating functional myocardium: improved performance after skeletal myoblast transplantation. *Nat Med.* 1998; 4(8): 929-933.
110. Jain M, *et al.* Cell therapy attenuates deleterious ventricular remodeling and improves cardiac performance after myocardial infarction. *Circulation.* 2001; 103(14): 1920-1927.
111. Ghostine S, *et al.* Long-term efficacy of myoblast transplantation on regional structure and function after myocardial infarction. *Circulation.* 2002; 106(12 Suppl 1): I131-136.
112. Tambara K, *et al.* Transplanted skeletal myoblasts can fully replace the infarcted myocardium when they survive in the host in large numbers. *Circulation.* 2003; 108 Suppl 1: II259-263.
113. Menasche P, *et al.* Myoblast transplantation for heart failure. *Lancet.* 2001; 357(9252): 279-280.
114. Menasche P, *et al.* The Myoblast Autologous Grafting in Ischemic Cardiomyopathy (MAGIC) trial: first randomized placebo-controlled study of myoblast transplantation. *Circulation.* 2008; 117(9): 1189-1200.
115. Duckers HJ, *et al.* Final results of a phase IIa, randomised, open-label trial to evaluate the percutaneous intramyocardial transplantation of autologous skeletal myoblasts in congestive heart failure patients: the SEISMIC trial. *EuroInternation.* 2011; 6: 805-812.
116. Menasche P, *et al.* Autologous skeletal myoblast transplantation for severe postinfarction left ventricular dysfunction. *J Am Coll Cardiol.* 2003; 41(7): 1078-1083.
117. Abkowitz JL, *et al.* Evidence that the number of hematopoietic stem cells per animal is conserved in mammals. *Blood.* 2002; 100(7): 2665-2667.
118. Strauer BE and Steinhoff G. 10 years of intracoronary and intramyocardial bone marrow stem cell therapy of the heart. *J Am Coll Cardiol.* 2011; 58: 1095-1104.
119. Amado LC, *et al.* Cardiac repair with intramyocardial injection of allogeneic mesenchymal stem cells after myocardial infarction. *Proc Natl Acad Sci U S A.* 2005; 102(32): 11474-11479.
120. Wu SM, *et al.* Origins and fates of cardiovascular progenitor cells. *Cell.* 2008; 132(4): 537-543.
121. Byun KH and Kim SW. Is stem cell-based therapy going on or out for cardiac disease? *Korean Circ J.* 2009; 39(3): 87-92.
122. Wu J, *et al.* Stem cells for cardiac regeneration by cell therapy and myocardial tissue engineering. *Adv Biochem Eng Biotechnol.* 2009; 114: 107-128.
123. Orlic D, *et al.* Bone marrow cells regenerate infarcted myocardium. *Nature.* 2001; 410(6829): 701-705.
124. Balsam LB, *et al.* Haematopoietic stem cells adopt mature haematopoietic fates in ischaemic myocardium. *Nature.* 2004; 428(6983): 668-673.
125. Murry CE, *et al.* Haematopoietic stem cells do not transdifferentiate into cardiac myocytes in myocardial infarcts. *Nature.* 2004; 428(6983): 664-668.
126. Dominici M, *et al.* Minimal criteria for defining multipotent mesenchymal stromal cells. The International Society for Cellular Therapy position statement. *Cytotherapy.* 2006; 8(4): 315-317.
127. Chamberlain G, *et al.* Concise review: mesenchymal stem cells: their phenotype, differentiation capacity, immunological features, and potential for homing. *Stem Cells.*

2007; 25: 2739-2749.
128. Tomita S, *et al.* Autologous transplantation of bone marrow cells improves damaged heart function. *Circulation.* 1999; 100(19 Suppl): II247-256.
129. Shake JG, *et al.* Mesenchymal stem cell implantation in a swine myocardial infarct model: engraftment and functional effects. *Ann Thorac Surg.* 2002; 73(6): 1919-1925; discussion 1926.
130. Makino S, *et al.* Cardiomyocytes can be generated from marrow stromal cells in vitro. *J Clin Invest.* 1999; 103(5): 697-705.
131. Toma C, *et al.* Human mesenchymal stem cells differentiate to a cardiomyocyte phenotype in the adult murine heart. *Circulation.* 2002; 105(1): 93-98.
132. Rangappa S, *et al.* Transformation of adult mesenchymal stem cells isolated from the fatty tissue into cardiomyocytes. *Ann Thorac Surg.* 2003; 75(3): 775-779.
133. Davani S, *et al.* Mesenchymal progenitor cells differentiate into an endothelial phenotype, enhance vascular density, and improve heart function in a rat cellular cardiomyoplasty model. *Circulation.* 2003; 108: II-253-II-258.
134. Silva GV, *et al.* Mesenchymal stem cells differentiate into an endothelial phenotype, enhance vascular density, and improve heart function in a canine chronic ischemia model. *Circulation.* 2005; 111: 150-156.
135. Chen SL, *et al.* Effect on left ventricular function of intracoronary transplantation of autologous bone marrow mesenchymal stem cell in patients with acute myocardial infarction. *Am J Cardiol.* 2004; 94(1): 92-95.
136. Abdel-Latif A, *et al.* Adult bone marrow-derived cells for cardiac repair: a systematic review and meta-analysis. *Arch Intern Med.* 2007; 167(10): 989-997.
137. Pijnappels DA, *et al.* Forced alignment of mesenchymal stem cells undergoing cardiomyogenic differentiation affects functional integration with cardiomyocyte cultures. *Circ Res.* 2008; 103(2): 167-176.
138. Peichev M, *et al.* Expression of VEGFR-2 and AC133 by circulating human CD34(+) cells identifies a population of functional endothelial precursors. *Blood.* 2000; 95: 952-958.
139. Smart N and Riley PR. The Stem Cell Movement. *Circ Res.* 2008; 102: 1155-1168.
140. Asahara T, *et al.* Isolation of putative progenitor endothelial cells for angiogenesis. *Science.* 1997; 275: 964-967.
141. Hristov M, *et al.* Endothelial progenitor cells: mobilization, differentiation, and homing. *Arterioscler Thromb Vasc Biol.* 2003; 23: 1185-1189.
142. Kalka C, *et al.* Transplantation of ex vivo expanded endothelial progenitor cells for therapeutic neovascularisation. *Proc Natl Acad Sci USA.* 2000; 97(7): 3422-3427.
143. Kawamoto A, *et al.* Therapeutic potential of *ex vivo* expanded endothelial progenitor cells for myocardial ischemia. *Circulation.* 2001; 103: 634-637.
144. Kocher AA, *et al.* Neovascularization of ischemic myocardium by human bone-marrow-derived angioblasts prevents cardiomyocyte apoptosis, reduces remodelling and improves cardiac function. *Nat Med.* 2001; 7(4): 430-436.
145. Badorff C, *et al.* Transdifferentiation of blood-derived human adult endothelial progenitor cells into functionally active cardiomyocytes. *Circulation.* 2003; 107(7): 1024-1032.
146. Yet ET, *et al.* Transdifferentiation of human peripheral blood CD34+-enriched cell population into cardiomyocytes, endothelial cells, and smooth muscle cells *in vivo*. *Circulation.* 2003; 108: 2070-2073.
147. Rubart M, *et al.* Cardiac regeneration: repopulating the heart. *Annu Rev Physiol.* 2006; 68: 29-49.
148. Young PP, *et al.* Biological properties of endothelial progenitor cells and their potential for cell therapy. *Prog Cardiovasc Dis.* 2007; 49: 421-429.
149. Codina M, *et al.* Current status of stem cell therapy in heart failure. *Curr Cardiol Rep.* 2010; 12(3):199-208.
150. Schachinger V, *et al.* Improved clinical outcome after intracoronary administration of bone-marrow-derived progenitor cells in acute myocardial infarction: final 1-year results of the REPAIR-AMI trial. *Eur Heart J.* 2006; 27(23):2775-2783.
151. Yousef M, *et al.* The BALANCE Study: clinical benefit and long-term outcome after intracoronary autologous bone marrow cell transplantation in patients with acute myocardial infarction. *J Am Coll Cardiol.* 2009; 53: 2262-2269.

152. Strauer BE, *et al.* The acute and long-term effects of intracoronary stem cell transplantation in 191 patients with chronic heARt failure: the STAR-heart study. *Eur J Heart Fail.* 2010; 12(7): 721-729.
153. Martin-Rendon E, *et al.* Autologous bone marrow stem cells to treat acute myocardial infarction: a systematic review. *European Heart Journal.* 2008; 29: 1807-1818.
154. Clifford DM, *et al.* Stem cell treatment for acute myocardial infarction. *Cochrane Database Syst Rev.* 2012; 2:CD006536.
155. Traverse JH, *et al.* A phase-II, randomized, double-blinded, placebo-controlled, pilot trial evaluating the safety and effect of administration of bone marrow mononuclear cells 2 to 3 weeks after acute myocardial infarction (Late TIME). *Tex Heart Inst J.* 2010; 37(4): 412-420.
156. Willerson JT, *et al.* Rationale and design for the intramyocardial injection of autologous bone marrow mononuclear cells for patients with chronic ischemic heart disease and left ventricular dysfunction trial (FOCUS). *Am Heart J.* 2010; 160(2): 215–223.
157. Mozid AM, *et al.* Stem cell therapy for heart disease. *Bri Med Bull.* 2011; 98: 143-159.
158. Messina E, *et al.* Isolation and expansion of adult cardiac stem cells from human and murine heart. *Circ Res.* 2004; 95(9): 911-921.
159. Urbanek K, *et al.* Stem cell niches in the adult mouse heart. *Proc Natl Acad Sci USA.* 2006; 103(24): 9226-9231.
160. Beltrami AP, *et al.* Adult cardiac stem cells are multipotent and support myocardial regeneration. *Cell.* 2003; 14(6): 763-776.
161. Carr CA, *et al.* Cardiosphere-derived cells improve function in the infarcted rat heart for at least 16 weeks – an MRI study. *PLoS ONE.* 2011; 6(11): e25669.
162. Linke A, *et al.* Stem cells in the dog heart are self-renewing, clonogenic, and multipotent and regenerate infarcted myocardium, improving cardiac function. *Proc Natl Acad Sci USA.*2005; 102: 8966-8971.
163. Ellison GM, *et al.* Endogenous cardiac stem cell activation by insulin-like growth factor-1/hepatocyte growth factor intracoronary injection fosters survival and regeneration of the infarcted pig heart. *J Am Coll Cardiol.* 2011; 58: 977-986.
164. Urbanek K, *et al.* Intense myocyte formation from cardiac stem cell in human cardiac hypertrophy. *Proc Natl Acad Sci USA.* 2003; 100(18): 10440-10445.
165. Smith RR, *et al.* Regenerative potential of cardiosphere-derived cells expanded from percutaneous endomyocardial biopsy specimens. *Circulation.* 2007; 115(7): 896-908.
166. Hsieh CH, *et al.* Evidence from a genetic fate-mapping study that stem cells refresh adult mammalian cardiomyocytes after injury. *Nat Med.* 2007; 13(8): 970-974.
167. Lyman SD and Jacobsen SE. c-kit ligand and Flt3 ligand: stem/progenitor cell factors with overlapping yet distinct activities. *Blood.* 1998; 91: 1101-1134.
168. Bearzi C, *et al.* Human cardiac stem cells. *Proc Natl Acad Sci U S A.* 2007; 104(35): 14068-14073.
169. Urbanek K, *et al.* Myocardial regeneration by activation of multipotent cardiac stem cells in ischemic heart failure. *Proc Natl Acad Sci USA.* 2005; 102(24): 8692-8697.
170. Fransioli J, *et al.* Evolution of the c-kit-positive cell response to pathological challenge in the myocardium. *Stem Cells.* 2008; 26: 1315-1324.
171. Torella D, *et al.* Growth-factor-mediated cardiac stem cell activation in myocardial regeneration. *Nat Clin Pract Cardiovasc Med.* 2007; 4 Suppl 1: S46-51.
172. Miyamoto S, *et al.* Characterization of Long-Term Cultured c-kit+ Cardiac Stem Cells Derived From Adult Rat Hearts. *Stem Cells and Development.* 2010; 19(1): 105-116.
173. Tang XL, *et al.* Intracoronary administration of cardiac progenitor cells alleviates left ventricular dysfunction in rats with a 30-day-old infarction. *Circulation.* 2010; 121: 293-305.
174. van de Rijn M, *et al.* Mouse hematopoietic stem-cell antigen Sca-1 is a member of the Ly-6 antigen family. *Proc Natl Acad Sci USA.* 1989; 86: 4634-4638.
175. Askura A, *et al.* Myogenic specification of side population cells in skeletal muscle. *J Cell Biol.* 2002; 159: 123-134.
176. Qu-Petersen Z, *et al.* Identification of a novel population of muscle stem cells in mice: Potential for muscle regeneration. *J Cell Biol.* 2002; 157: 851-864.
177. Gojo S, *et al.* In vivo cardiovasculogenesis by direct injection of isolated adult

mesenchymal stem cells. *Exp Cell Res.* 2003; 288(1): 51-59.
178. Vieira JM and Riley PR. Epicardium-derived cells: a new source of regenerative capacity. *Heart.* 2011; 97(1): 15-19.
179. Oh H, *et al.* Cardiac progenitor cells from adult myocardium: homing, differentiation, and fusion after infarction. *Proc Natl Acad Sci U S A.* 2003; 100(21): 12313-12318.
180. Matsuura K, *et al.* Adult cardiac Sca-1-positive cells differentiate into beating cardiomyocytes. *J Biol Chem.* 2004; 279: 11384-11391.
181. Wang X, *et al.* The role of the Sca-1+/CD31- cardiac progenitor cell population in postinfarction left ventricular remodelling. *Stem Cells.* 2006; 24: 1779-1788.
182. Tateishi K, *et al.* Clonally amplified cardiac stem cells are regulated by Sca-1 signaling for efficient cardiovascular regeneration. *J Cell Sci.* 2007; 120: 1791-1800.
183. Tang YL, *et al.* A novel two-step procedure to expand cardiac Sca-1+ cells clonally. *Biochem Biophys Res Commun.* 2007; 359: 877-883.
184. Smits AM, *et al.* Human cardiomyocyte progenitor cells differentiate into functional mature cardiomyocytes: an in vitro model for studying human cardiac physiology and pathophysiology. *Nat Protoc.* 2009; 4(2): 232-242.
185. Zhou S, *et al.* The ABC transporter Bcrp1/ABCG2 is expressed in a wide variety of stem cells and is a molecular determinant of the side-population phenotype. *Nat Med.* 2001; 7: 1028-1034.
186. Hierlihy AM, *et al.* The post-natal heart contains a myocardial stem cell population. *FEBS Lett.* 2002; 530: 239-243.
187. Yamahara K, *et al.* Heterogeneic nature of adult cardiac side population cells. *Biochem Biophys Res Commun.* 2008; 371: 615-620.
188. Martin CM, *et al.* Persistent expression of the ATP-binding cassette transporter, Abcg2, identifies cardiac SP cells in the developing and adult heart. *Dev Biol.* 2004; 265: 262-275.
189. Pfister O, *et al.* CD31- but not CD31+ cardiac side population cells exhibit functional cardiomyogenic differentiation. *Circ Res.* 2005; 97: 52-61.
190. Oyama T, *et al.* Cardiac side population cells have a potential to migrate and differentiate into cardiomyocytes in vitro and in vivo. *J Cell Biol.* 2007; 176: 329-341.
191. Liang SX, *et al.* Differentiation and migration of Sca-1+/CD31- cardiac side population cells in a murine myocardial ischemic model. *Int J Cardiol.* 2010; 138: 40-49.
192. Davis DR, *et al.* Validation of the cardiosphere method to culture cardiac progenitor cells from myocardial tissue. *PLoS ONE.* 2009; 4(9): e7195.
193. Marban E and Malliaras K. Boot camp for mesenchymal stem cells. *J Am Coll Cardiol.* 2010; 56(9):735-737.
194. Caspi O, *et al.* Tissue engineering of vascularized cardiac muscle from human embryonic stem cells. *Circ Res.* 2007; 100(2):263-272.
195. Lee ST, *et al.* Intramyocardial injection of autologous cardiosphere or cardiosphere-derived cells preserves function and minimizes adverse ventricular remodelling in pigs with heart failure post-myocardial infarction. *J Am Coll Cardiol.* 2011; 57: 455-465.
196. Laugwitz KL, *et al.* Postnatal isl1+ cardioblasts enter fully differentiated cardiomyocyte lineages. *Nature.* 2005; 433: 647-653.
197. Cai CL, *et al.* Isl1 identifies a cardiac progenitor population that proliferates prior to differentiation and contributes a majority of cells to the heart. *Dev Cell.* 2003; 5: 877-889.
198. Laugwitz KL, *et al.* Islet1 cardiovascular progenitors: a single source for heart lineages? *Development.* 2008; 135(2): 193-205.
199. Moretti A, *et al.* Multipotent embryonic isl1+ progenitor cells lead tocardiac, smooth muscle, and endothelial cell diversification. *Cell.* 2006; 127: 1151-1165.
200. Moretti A, *et al.* Biology of Isl1+ cardiac progenitor cells in development and disease. *Cell Mol Life Sci.* 2007; 64(6): 674-682.
201. Bollini S, *et al.* Resident cardiac progenitor cells: At the heart of regeneration. *J Mol Cell Cardiol.* 2011; 50: 296-303.
202. Smart N, *et al.* Thymosin beta4 induces adult epicardial progenitor mobilization and neovascularisation. *Nature.* 2007; 445: 177-182.
203. van TJ, *et al.* Epicardial cells of human adults can undergo an epithelial-to-mesenchymal transition and obtain characteristics of smooth muscle cells in vitro. Stem *Cells.* 2007; 25: 271-278.

204. Limana F, *et al.* Identification of myocardial and vascular precursor cells in human and mouse epicardium. *Circ Res.* 2007; 101: 1255-1265.
205. Cai CL, *et al.* A myocardial lineage derives from Tbx18 epicardial cells. *Nature.* 2008; 454: 104-108.
206. Zhou B, *et al.* Epicardial progenitors contribute to the cardiomyocyte lineage in the developing heart. *Nature.* 2008; 454: 109-113.
207. Tomanek RJ. Formation of the coronary vasculature during development. *Angiogenesis.* 2005; 8: 273-284.
208. Wessels A and Perez-Pomares JM. The epicardium and epicardially derived cells (EPDCs) as cardiac stem cells. *Anat Rec A Discov Mol Cell Evol Biol.* 2004; 276: 43-57.
209. Winter EM, *et al.* Preservation of left ventricular function and attenuation of remodelling after transplantation of human epicardium-derived cells into the infarcted mouse heart. *Circulation.* 2007; 116: 917-927.
210. Riley PR and Smart N. Thymosin beta4 induces epicardium-derived neovascularisation in the adult heart. *Biochem Soc Trans.* 2009; 37(Pt6): 1218-1220.
211. Smart N, *et al.* De novo cardiomyocytes from within the activated adult heart after injury. *Nature.* 2011; 474(7353): 640-644.
212. Rosamond W, *et al.* Heart disease and stroke statistics – 2007 update: a report from the American Heart Association Statistics Committee and Stroke Statistics Subcommittee. *Circulation.* 2007; 115(5): e69-e171.
213. Thijssen DH, *et al.* The role of endothelial progenitor and cardiac stem cells in the cardiovascular adaptations to age and exercise. *Front Biosci.* 2009; 14: 4685-702.
214. Vasa M, *et al.* Number and migratory activity of circulating endothelial progenitor cells inversely correlate with risk factors for coronary artery disease. *Circ Res.* 2001; 89: e1-7.
215. Werner N, *et al.* Circulating endothelial progenitor cells and cardiovascular outcomes. *N Engl J Med.* 2005; 353: 999-1007.
216. Kissel CK, *et al.* Selective functional exhaustion of hematopoietic progenitor cells in the bone marrow of patients with postinfarction heart failure. *J Am Coll Cardiol.* 2007; 49: 2341-2349.
217. Mayani H. Biological differences between neonatal and adult human hematopoietic stem/progenitor cells. *Stem Cells Dev.* 2010; 19(3): 285-98.
218. Nishino J, *et al.* Hmga2 promotes neural stem cell self-renewal in young but not old mice by reducing p16Ink4a and p19Arf expression. *Cell.* 2008; 135(2): 227-239.
219. Baerlocher GM, *et al.* Telomeres in hematopoietic stem cells. *Ann N Y Acad Sci.* 2003; 996: 44-48.
220. Fan M, *et al.* The effect of age on the efficacy of human mesenchymal stem cell transplantation after a myocardial infarction. *Rejuvenation Res.* 2010; 13(4): 429-438.
221. Ballard VL and Edelberg JM. Stem cells for cardiovascular repair - the challenges of the aging heart. *J Mol Cell Cardiol.* 2008; 45(4): 582-92.
222. Dimmeler S and Leri A. Aging and disease as modifiers of efficacy of cell therapy. *Circ Res.* 2008; 102: 1319-1330.
223. Romfh A and McNally EM. Cardiac assessment in Duchenne and Becker muscular dystrophies. *Curr Heart Fail Rep.* 2010; 7: 212-218.
224. Finsterer J and Stollberger C. The heart in human dystrophinopathies. *Cardiology.* 2003; 99: 1-19.
225. Fayssoil A, *et al.* Cardiomyopathy in Duchenne muscular dystrophy: pathogenesis and therapeutics. *Heart Fail Rev.* 2010; 15: 103-107.
226. Spurney CF. Cardiomyopathy of Duchenne muscular dystrophy: current understanding and future directions. *Muscle Nerve.* 2011; 44: 8-19.
227. Ameen V and Robson LG. Experimental models of Duchenne muscular dystrophy: relationship with cardiovascular disease. *The Open Cardiovascular Medicine Journal.* 2010; 4: 265-277.
228. Connuck DM, *et al.* Characteristics and outcomes of cardiomyopathy in children with Duchenne or Becker muscular dystrophy: a comparative study from the Pediatric Cardiomyopathy Registry. *Am Heart J.* 2008; 155: 998-1005.
229. Fairclough RJ. *et al.* Progress in therapy for Duchenne muscular dystrophy. *Exp Physiol.* 2011; 96(11): 1101-1113.

230. Koh GY, *et al.* Stable fetal cardiomyocyte grafts in the hearts of dystrophic mice and dogs. *J Clin Invest.* 1995; 96: 2034-2042.
231. Farini A, *et al.* Cell based therapy for Duchenne muscular dystrophy. *J Cell Physiol.* 2009; 221: 526-534.
232. Kang PB, *et al*. Inefficient dystrophin expression after cord blood transplantation in Duchenne muscular dystrophy. *Muscle Nerve.* 2010; 41: 746-750.
233. Winter J, *et al.* Development and validation of real-time quantitative reverse transcriptase-polymerase chain reaction for monitoring gene expression in cardiac myocytes in vitro. *Anal Biochem.* 1999; 270(1): 41-49.
234. Schmittgen TD and Zakrajsek BA. Effect of experiment treatment on housekeeping gene expression: validation by real-time, quantitative RT-PCR. *J Biochem Biophys Methods.* 2000; 46(1-2): 69-81.
235. Livak KJ and Schmittgen TD. Analysis of relative gene expression data using real-time quantitative PCR and the 2(-Delta Delta C(T)) method. *Methods.* 2001; 25(4): 402-408.
236. Tyler DJ, *et al.* Cine-MR imaging of the normal and infarcted rat heart using an 11.7 T vertical bore MR system. *J Cardiovasc Magn Reson.* 2006; 8: 327-333.
237. Taylor DA and Robertson MJ. The basics of cell therapy to treat cardiovascular disease: one cell dose not fit all. *Rev Esp Cardiol.* 2009; 62(9): 1032-1044.
238. Shachar M, *et al.* The effect of immobilized RGD peptide in alginate scaffolds on cardiac tissue engineering. *Acta Biomater.* 2011; 7(1): 152-162.
239. Sapir Y, *et al.* Integation of multiple cell-matrix interactions into alginate scaffolds for promoting cardiac tissue engineering. *Biomaterials.* 2011; 32(7): 1838-1847.
240. Zimmermann WH, *et al.* Engineered heart tissue grafts improve systolic and diastolic function in infarcted rat hearts. *Nat Med.* 2006; 12(4): 452-458.
241. Radisic M, *et al.* High density seeding of myocyte cells for tissue engineering. *Biotechnol Bioeng.* 2003; 82: 403-414.
242. Zhu Y, *et al.* Collagen–chitosan polymer as a scaffold for the proliferation of human adipose tissue-derived stem cells. *J Mater Sci: Mater Med.* 2009; 20: 799-808.
243. Li RK, *et al.* Survival and function of bioengineered cardiac grafts. *Circulation.* 1999; 100: II63-II69.
244. Chien KR, *et al* Cardiogenesis and the complex biology of regenerative cardiovascular medicine. *Science.* 2008; 322 (5907): 1494-1497.
245. Jawad H, *et al.* Myocardial tissue engineering: a review. *J Tissue Eng Regen Med.* 2007; 1: 327-342.
246. Schwarzkopf R, *et al.* Autospecies and post-myocardial infarction sera enhance the viability, proliferation, and maturation of 3D cardiac cell culture. *Tissue Engineering.* 2006; 12(12): 3467-3475.
247. Dar A, *et al.* Optimization of cardiac cell seeding and distribution in 3D porous alginate scaffolds. *Biotechnol Bioeng.* 2002; 80: 305-312.
248. Heng BC, *et al.* Strategies for directing the differentiation of stem cells into the cardiomyocyte lineage in vitro. *Cardiovasc Res.* 2004; 62(1): 34-42.
249. Lyon A and Harding S. The potential of cardiac stem cell therapy for heart failure. *Curr Opin Pharmacol.* 2007; 7(2): 164-170.
250. Stevens MM, et al. A rapid-curing alginate gel system: utility in periosteum-derived cartilage tissue engineering. *Biomaterials.* 2004; 25(5): 887-894.
251. Simpson NE, *et al.* The role of the CaCl2-guluronic acid interaction on alginate encapsulated betaTC3 cells. *Biomaterials.* 2004; 25(13): 2603-2610.
252. Wainwright JM, *et al.* Preparation of cardiac extracellular matrix from an intact porcine heart. *Tissue Eng Part C Methods.* 2010; 16(3): 525-532.
253. Petersen TH, *et al.* Tissue-engineered lings for in vivo implantation. *Science.* 2010; 329(5991): 538-541.
254. Ott HC, *et al.* Regeneration and orthotopic transplantation of a bioartificial lung. *Nat Med.* 2010; 16(8): 927-933.
255. Uygun BE, *et al.* Organ reengineering through development of a transplantable recellularized liver graft using decellularized liver matrix. *Nat Med.* 2010: 16(7): 814-820.
256. Shupe T, *et al.* Method for the decellularization of intact rat liver. *Organogenesis.* 2010: 6(2): 134-136.

257. Ross EA, *et al.* Embryonic stem cells proliferate and differentiate when seeded into kidney scaffolds. *J Am Soc Nephrol.* 2009; 20(11): 2338-2347.
258. Baptista PM, *et al.* Whole organ decellularization – a tool for bioscaffold fabrication and organ bioengineering. *Conf Proc IEEE Eng Med Biol Soc.* 2009; 2009: 6526-6529.
259. Macchiarini P, *et al.* Clinical transplantation of a tissue-engineered airway. *Lancet.* 2008; 372: 2023-2030.
260. Condorelli G, *et al.* Cardiomyocytes induce endothelial cells to trans-differentiate into cardiac muscle: implications for myocardial regeneration. *Proc Natl Acad Sci USA.* 2001; 98(19): 10733-10738.
261. Iijima Y, *et al.* Beating is necessary for transdifferentiation of skeletal muscle-derived cells into cardiomyocytes. *FASEB J.* 2003; 17(10): 1361-1363.
262. Chen K, *et al.* Extrinsic regulation of cardiomyocyte differentiation of embryonic stem cells. *J Cell Biochem.* 2008; 104(1): 119-128.
263. Xu C, *et al.* Characterization and enrichment of cardiomyocytes derived from human embryonic stem cells. *Circ Res.* 2002; 91(6): 501-508.
264. Fukuda K, *et al.* Use of adult marrow mesenchymal stem cells for regeneration of cardiomyocytes. *Bone Marrow Transplant.* 2003; 32(Suppl. 1): S25-7.
265. Hakuno D, *et al.* Bone marrow-derived regenerated cardiomyocytes (CMG Cells) express functional adrenergic and muscarinic receptors. *Circulation.* 2002; 105(3): 380-386.
266. Rangappa S, *et al.* Cardiomyocyte-mediated contact programs human mesenchymal stem cells to express cardiogenic phenotype. *J Thorac Cardiovasc Surg.* 2003; 126: 124-132.
267. Itzhaki-Alfia A, *et al.* Patient characteristics and cell source determine the number of isolated human cardiac progenitor cells. *Circulation.* 2009; 120: 2559-2566.
268. Choi SC, *et al.* 5-azacytidine induces cardiac differentiation of P19 embryonic stem cells. *Exp Mol Med.* 2004; 36(6): 515-523.
269. Ventura C, *et al.* Opioid peptide gene expression primes cardiogenesis in embryonal pluripotent stem cells. *Circ Res.* 2000; 87: 189-194.
270. Skerjanc IS, *et al.* Myocyte enhancer factor 2C and Nkx 2-5 up-regulate each other's expression and initiate cardiomyogenesis in P19 cells. *J Biol Chem.* 1998; 273: 34904-34910.
271. Naito AT, *et al.* Phosphatidylinositol 3-kinase-Akt pathway plays a critical role in early cardiomyogenesis by regulating canonical Wnt signalling. *Circ Res.* 2005; 97: 144-151.
272. Takahashi T, *et al.* Ascorbic acid enhances differentiation of embryonic stem cells into cardiacmyocytes. *Circulation.* 2003; 107: 1912-1916.
273. Florini JR, *et al.* Hormones, growth factors, and myogenic differentiation. *Annu Rev Physiol.* 1991; 53: 201-216.
274. Sekiguchi M, *et al.* Establishment and characterization of a human neuroblastoma cell line in tissue culture. *Jpn J Exp Med.* 1979; 49: 67-83.
275. Passier R, *et al.* Increased cardiomyocyte differentiation from human embryonic stem cells in serum-free cultures. *Stem Cells*. 2005; 23: 772-780.
276. Sachinidis A, *et al.* Identification of platelet-derived growth factor-BB as cardiogenesis-inducing factor in mouse embryonic stem cells under serum-free conditions. *Cell Physiol Biochem.* 2003; 13: 423-429.
277. Yoon BS, *et al.* Enhanced differentiation of human embryonic stem cells into cardiomyocytes by combining hanging drop culture and 5-azacytidine treatment. *Differentiation.* 2006; 74: 149-159.
278. Sachinidis A, *et al.* Cardiac specific differentiation of mouse embryonic stem cells. *Cardiovasc Res.* 2003; 58(2): 278-91.
279. Evans SM, *et al.* Myocardial lineage development. *Circ Res.* 2010; 107: 1428-1444.
280. Wang Y, *et al.* Enhancement of cardiomyocyte differentiation from human embryonic stem cells. *Sci China Life Sci.* 2010; 53(5): 581-589.
281. Leri A, *et al.* Cardiac stem cells and mechanisms of myocardial regeneration. *Physiol Rev.* 2005; 85(4): 1373-1416.
282. Cheng W, *et al.* Stretch-induced programmed myocyte cell death. *J Clin Invest.* 1995; 96: 2247-2259.
283. Sadoshima J, *et al.* The cellular and molecular response of cardiac myocytes to mechanical stress. *Annu Rev Physiol.* 1997; 59: 551-571.

284. Leri A, *et al.* Stretch-mediated release of angiotensin II induces myocyte apoptosis by activating p53 that enhances the local RAS and decreases the Bcl-2 to Bax protein ratio in the cell. *J Clin Invest.* 1998; 101: 1326-1342.
285. Estes BT, *et al.* Mechanical signals as regulators of stem cell fate. *Curr Top Dev Biol.* 2004; 60: 91-126.
286. Leri A, *et al.* Myocardial regeneration and stem cell repair. *Curr Probl Cardiol.* 2008; 33: 91-153.
287. Hill JM, *et al.* Circulating endothelial progenitor cells, vascular function, and cardiovascular risk. *N Engl J Med.* 2003; 348(7): 593-600.
288. Scheubel RJ, *et al.* Age-dependent depression in circulating endothelial progenitor cells in patients undergoing coronary artery bypass grafting. *J Am Coll Cardiol.* 2003; 42(12): 2073-2080.
289. Asumda FZ and Chase PB. Age-related changes in rat bone-marrow mesenchymal stem cell plasticity. *BMC Cell Biol.* 2011; 12: 44.
290. Davies M, *et al.* Prevalence of left-ventricular systolic dysfunction and heart failure in the Echocardiographic Heart of England Screening study: a population based study. *Lancet.* 2001; 358: 439-444.
291. Li Z, *et al.* Imaging survival and function of transplanted cardiac resident stem cells. *J Am Coll Cardiol.* 2009; 53: 1229-1240.
292. Mishra R, *et al.* Characterization and functionality of cardiac progenitor cells in congenital heart patients. *Circulation.* 2011; 123: 364-373.
293. Gambini E, *et al.* C-kit+ cardiac progenitors exhibit mesenchymal markers and preferential cardiovascular commitment. *Cardiovasc Res.* 2011; 89(2): 362-373.
294. Smith RR, *et al.* Unselected human cardiosphere-derived cells are functionally superior to c-kit- or CD90-purified cardiosphere-derivedc cells. *Circulation.* 2008; 118: S_420. Abstract.
295. Anversa P, *et al.* Life and death of cardiac stem cells. A paradigm shift in cardiac biology. *Circulation.* 2006; 113: 1451-1463.
296. Shenje LT, *et al.* Lineage tracing of cardiac explant derived cells. *PLoS ONE.* 2008; 3: e1929.
297. Andersen DC, *et al.* Murine "carrdiospheres" are not a source of stem cells with cardiomyogenic potential. *Stem Cells.* 2009; 27: 1571-1581.
298. Davis DR, *et al.* Human cardiospheres are a source of stem cells with cardiomyogenic potential. *Stem Cells.* 2010; 28: 903-904.
299. Seeger FH, *et al.* Cell isolation procedures matter: a comparison of different isolation protocols of bone marrow mononuclear cells used for cell therapy in patients with acute myocardial infarction. *Eur Heart J.* 2007; 28: 766-772.
300. Li L and Xie T. Stem cell niche: structure and function. *Annu Rev Cell Dev Biol.* 2005; 21: 605-631.
301. Fuchs E, *et al.* Socializing with the neighbors: stem cells and their niche. *Cell.* 2004; 116(6): 769-778.
302. Cotsarelis G, *et al.* Label-retaining cells reside in the bulge area of pilosebaceous unit: implications for follicular stem cells, hair cycle, and skin carcinogenesis. *Cell.* 1990; 61: 1329-37.
303. Potten CS, *et al.* Intestinal stem cells protect their genome by selective segregation of template DNA strands. *J Cell Sci*. 2002; 115: 2381-88.
304. Davis DR, *et al.* Isolation and expansion of functionally-competent cardiac progenitor cells directly from heart biopsies. *J Mol Cell Cardiol.* 2010; 49: 312-321.
305. Zhu Y, *et al.* Collagen–chitosan polymer as a scaffold for the proliferation of human adipose tissue-derived stem cells. *J Mater Sci: Mater Med.* 2009; 20: 799-808.
306. Duan YG, *et al.* Expression patterns of age-related molecule c-kit, HIWI and vimentin in the rat testis and epididymis. *Zhonghua Nan Ke Xue.* 2007; 13(11): 992-996.
307. Belluardo N, *et al.* Nicotine-induced fibroblast growth factor-2 restores the age-related decline of precursor cell proliferation in the subventricular zone of rat brain. *Brain Res.* 2008; 1193: 12-24.
308. Hudon-David F, *et al.* Thy-1 expression by cardiac fibroblasts: lack of association with myofibroblast contractile markers. *J Mol Cell Cardiol.* 2007; 42(5): 991-1000.

309. Halfon S, *et al.* Markers Distinguishing Mesenchymal Stem Cells from Fibroblasts Are Downregulated with Passaging. *Stem Cells and Development.* 2011; 20(1): 53-66.
310. Covas DT, *et al.* Multipotent mesenchymal stromal cells obtained from diverse human tissues share functional properties and gene-expression profile with CD146þ perivascular cells and fibroblasts. *Exp Hematol.* 2008; 36: 642-654.
311. Haudek SB, *et al.* Monocytic Fibroblast Precursors Mediate Fibrosis in Angiotensin-II-induced Cardiac Hypertrophy. *J Mol Cell Cardiol.* 2010; 49(3): 499-507.
312. Flores I, *et al.* Effects of telomerase and telomere length on epidermal stem cell behaviour. *Science.* 2005; 309: 1253-1256.
313. Allsopp RC, *et al.* Telomere shortening accompanies increased cell cycle activity during serial transplantation of hematopoietic stem cells. *J Exp Med.* 2001; 193: 917-924.
314. Samper E, *et al.* Long-term repopulating ability of telomerase-deficient murine hematopoietic stem cells. *Blood.* 2002; 99: 2767-2775.
315. Karagiannides I, *et al.* Altered expression of C/EBP family members results in decreased adipogenesis with aging. *Am J Physiol Regul Integr Comp Physiol.* 2001; 280: R1772-R1780.
316. Zheng H, *et al.* Impact of aging on rat bone marrow-derived stem cell chondrogenesis. *J Gerontol A Biol Sci Med Sci.* 2007; 62: 136-148.
317. Alt EU, *et al.* Aging alters tissue resident mesenchymal stem cell properties. *Stem Cell Res.* 2012; 8(2): 215-225.
318. Torella D, *et al.* Cardiac stem cell and myocyte aging, heart failure, and insulin-like growth factor-1 overexpression. *Circ Res.* 2004; 94: 514-524.
319. Blackburn EH. Structure and function of telomere. *Nature.* 1991; 350(6319): 569-573.
320. Leri A, *et al.* Telomerase expression and activity are coupled with myocyte proliferation and preservation of telomeric length in the failing heart. *Proc Natl Acad Sci USA.* 2001; 98: 8626-8631.
321. Chimenti I, *et al.* Senescence and death of primitive cells and myocytes leads to premature cardiac aging and heart failure. *Circ Res.* 2003; 93: 604-613.
322. Kajstura J, *et al.* Myocyte turnover in the aging human heart. *Circ Res.* 2010: 107: 1374-1386.
323. Blasco MA. Telomere length, stem cells and aging. *Nat Chem Biol.* 2007; 3(10): 640-649.
324. Capogrossi MC. Cardiac stem cells fail with aging. A new mechanism for the age-dependent decline in cardiac function. *Circ Res.* 2004; 94: 411-413.
325. Kaspar RW, *et al.* Current understanding and management of dilated cardiomyopathy in Duchene and Becker muscular dystrophy. *J Am Acad Nurse Pract.* 2009; 21: 241-249.
326. Yasuma F, *et al.* A new lease on life for patients with Duchenne muscular dystrophy in Japan. *Am J Med.* 2004; 117: 363.
327. Baxter P. Treatment of the heart in Duchenne muscular dystrophy. *Dev Med Child Neurol.* 2006; 48: 163.
328. Toussaint M, *et al.* Diurnal ventilation *via* mouthpiece: survival in end-stage Duchenne patients. *Eur Repair J.* 2006; 28: 549-555.
329. Quinlan JG, *et al.* Evolution of the mdx mouse cardiomyopathy: physiological and morphological findings. *Neuromuscul Disord.* 2004; 14: 491-496.
330. Zhang W, *et al.* Abnormal cardiac morphology, function and energy metabolism in the dystrophic mdx mouse: An MRI and MRS study. *J Mol Cell Cardiol.* 2008; 45: 754-760.
331. Van Erp C. *et al.* Timeline of cardiac dystrophy in 3–18-month-old MDX mice. *Muscle Nerve.* 2010; 42: 504-513.
332. Gaschen L, *et al.* Cardiomyopathy in dystrophin-deficient hypertrophic feline muscular dystrophy. *J Vet Intern Med.* 1999; 13: 346-356.
333. Gaschen F, *et al.* Changes of skeletal muscle in young dystrophin-deficient cats: a morphological and morphometric study. *Acta Neuropathol.* 2001; 101: 591-600.
334. Valentine BA, *et al.* In vitro characteristics of normal and dystrophic skeletal muscle from dogs. *Am J Vet Res.* 1991; 52: 104-107.
335. Berg Z, *et al.* Muscle satellite cells from GRMD dystrophic dogs are not phenotypically distinguishable from wild type satellite cells in ex vivo culture. *Neuromuscul Discord.* 2011; 21(4): 282-290.
336. Cassano M, *et al.* Alteration of cardiac progenitor cell potency in GRMD dogs. *Cell*

Transplant. 2012.
337. Sicinski P, *et al.* The molecular basis of muscular dystrophy in the mdx mouse: a point mutation. *Science.* 1989; 244: 1578-1580.
338. Bia BL, *et al.* Decreased myocardial nNOS, increased iNOS and abnormal ECGs in mouse models of Duchenne muscular dystrophy. *J Mol Cell Cardiol.* 1999; 31: 1857-1862.
339. Merrick D, *et al.* Muscular dystrophy begins early in embryonic development deriving from stem cell loss and disrupted skeletal muscle formation. *Dis Model Mech.* 2009; 2(7-8): 374-88.
340. Crisp A, et al. Diaphragm rescue alone prevents heart dysfunction in dystrophic mice. *Hum Mol Genet.* 2011; 20: 413-421.
341. Stuckey DJ, *et al. In vivo* MRI Characterization of Progressive Cardiac Dysfunction in the mdx Mouse Model of Muscular Dystrophy. *PLoS ONE.* 2012; 7(1): e28569.
342. Chamberlain JS. *et al.* Dystrophin-deficient mdx mice display a reduced life span and are susceptible to spontaneous rhabdomyosarcoma. *FASEB J.* 2007; 21: 2195-2204.
343. Torrente Y, *et al.* Autologous transplantation of muscle-derived CD133+ stem cells in Duchenne muscle patients. *Cell Transplantation.* 2007; 16: 563-577.
344. Yue Y, *et al.* Microdystrophin gene therapy of cardiomyopathy restores dystrophin-glycoprotein complex and improves sarcolemma integrity in the mdx mouse heart. *Circulation.* 2003; 108: 1626-1632.
345. Lu QL, *et al.* Systemic delivery of antisense oligoribonucleotide restores dystrophin expression in body-wide skeletal muscles. *ProcNatl Acad Sci USA.* 2005; 102: 198-203.
346. Yin H, *et al.* Functional rescue of dystrophin-deficient mdx mice by a chimeric peptide-PMO. *Mol Ther.* 2010; 18(10): 1822-1829.
347. Tinsley JM, *et al.* Amelioration of the dystrophic phenotype of mdx mice using a truncated utrophin transgene. *Nature.* 1996; 384: 349-353.
348. Mattei E, *et al.* Utrophin up-regulation by an artificial transcription factor in transgenic mice. *PLoS ONE.* 2007; 2: e774.
349. Townsend D, *et al.* Emergent dilated cardiomyopathy caused by targeted repair of dystrophic skeletal muscle. *Mol Ther.* 2008; 16(5): 832-835.
350. Blake DJ and Martin-Rendon E. Intermediate Filaments and the Function of the Dystrophin–Protein Complex. *TCM.* 2002; 12(5): 224-228.
351. Danialou G, *et al.* Dystrophin-deficient cardiomyocytes are abnormally vulnerable to mechanical stress-induced contractile failure and injury. *FASEB J.* 2001; 15: 1655-1657.
352. Lapidos KA, *et al.* The dystrophin glycoprotein complex: signalling strength and integrity for the sarcolemma. *Circ Res.* 2004; 94(8): 1023-1031.
353. Ramaciotti C, *et al.* Myocardial cell damage in Duchenne muscular dystrophy. *Pediatr Cardiol.* 2003; 24: 503-506.
354. Frankel KA and Rosser RJ. The pathology of the heart in progressive muscular dystrophy: epimyocardial fibrosis. *Hum Pathol.* 1976; 7: 375-386.
355. Puchalski MD, *et al.* Late gadolinium enhancement: precursor to cardiomyopathy in Duchenne muscular dystrophy? *Int J Cardiovasc Imaging.* 2009; 25: 57-63.
356. Guillaume MD, et al. Delayed enhancement cardiac magnetic resonance imaging in a patient with Duchenne muscular dystrophy. *Tex Heart Inst J.* 2008; 35: 367–368.
357. Barison A, *et al.* Cardiac magnetic resonance imaging and management of dilated cardiomyopathy in a Duchenne muscular dystrophy manifesting carrier. *J Neurol.* 2009; 256: 283–284.
358. Smith PE, *et al.* Practical problems in the respiratory care of patients with muscular dystrophy. *N Engl J Med.* 1987; 316: 1197-1205.
359. Melacini P, *et al.* Cardiac and respiratory involvement in advanced stage Duchenne muscular dystrophy. *Neuromuscul Disord.* 1996; 6: 367-376.
360. Nakamura A, *et al.* Progression of dystrophic features and activation of mitogen-activated proein kinases and calcineurin by physical exercise, in hearts of mdx mice. *Fed Eur Biochem Soc Lett.* 2002; 520: 18-24.
361. Cossu G, *et al.* In vitro differentiation of satellite cells isolated from normal and dystrophic mammalian muscles. A comparison with embryonic myogenic cells. *Cell Differ.* 1980; 9(6): 357-68.
362. Koninckx R, *et al.* Mesenchymal stem cells or cardiac progenitors for cardiac repair? A

comparative study. *Cell Mol Life Sci.* 2010; 68(12): 2141-2156.
363. Williams A and Hare JM. Mesenchymal stem cells. Biology, pathophysiology, translational findings, and therapeutic implications for cardiac disease. *Circ Res.* 2011; 109: 923-940.
364. Chimenti I, *et al.* Relative roles of direct regeneration versus paracrine effects of human cardiosphere-derived cells transplanted into infarcted mice. *Circ Res.* 2010; 106: 971-980.
365. Li TS, *et al.* Direct Comparison of Different Stem Cell Types and Subpopulations Reveals Superior Paracrine Potency and Myocardial Repair Efficacy With Cardiosphere-Derived Cells. *J Am Coll Cardiol.* 2012; 59: 942-953.
366. Mazo M, *et al.* Stem Cell Therapy for Chronic Myocardial Infarction. *J Cardiovasc Trans Res.* 2010; 3(2): 79–88.
367. Leri A, *et al.* Human Cardiac Stem Cells: The Heart of a Truth. *Circulation.* 2009; 120: 2515-2518.
368. Porrello E and Olson EN. Building a new heart from old parts. Stem cell turnover in the aging heart. *Circ Res.* 2010; 107: 1292-1294.
369. Gonzalez A, *et al.* Activation of cardiac progenitor cells reverses the failing heart senescent phenotype and prolongs lifespan. *Circ Res.* 2008; 102: 597-606.
370. Cesselli D, *et al.* Age and pathology impair cardiac stem ells. *Circulation.* 2009; 120: S595. Abstract.
371. D'Amario D, *et al.* Functionally competent cardiac stem cells can be isolated from endomyocardial biopsies of patients with advanced cardiomyopathy. *Circ Res.* 2011; 108: 857-861.
372. Schneider JE, *et al.* Fast, high-resolution in vivo cine magnetic resonance imaging in normal and failing mouse hearts on a vertical 11.7 Y system. *J Magn Reson Imaging.* 2003; 18: 691-701.
373. Cawthon RM. Telomere measurement by quantitative PCR. *Nucleic Acids Res.* 2002; 30(10): e47.
374. O'Callaghan NJ and Fenech M. A quantitative PCR method for measuring absolute telomere length. Biol Proced Online. 13:3.
375. Claycomb WC, *et al.* HL-1 cells: A cardiac muscle cell line that contracts and retains phenotype characteristics of the adult cardiomyocyte. *Proc Natl Acad Sci USA.* 1998; 95: 2979-2984.
376. White SM, *et al.* Cardiac physiology at the cellular level: use of cultured HL-1 cardiomyocytes for studies of cardiac muscle cell structure and function. *Am J Physiol Heart Circ Physiol* 2004; 286: H823-H829.
377. Zhang J, *et al.* Differentiation induction of cardiac c-kit positive cells from rat heart into sinus node-like cells by 5-azacytidine. *Tissue and Cell* 2010;
378. Burry RW. Specificity controls for immunocytochemical methods. *The Journal of Histochemistry & Cytochemistry* 2000; 48(2): 163-165.
379. Zaruba M. *et al*. Cardiomyogenic potential of c-kit+ expressing cells derived from neonatal and adult mouse hearts. *Circulation* 2010; 121: 1992-2000.
380. Fox KF, *et al.* Coronary artery disease are the cause of incident heart failure in the population. *Eur Heart J* 2001; 22: 228-236.
381. Towbin JA and Bowles NE. The failing heart. *Nature* 2002; 415: 227-233.
382. Ott HC and Taylor DA. From cardiac repair to cardiac regeneration – ready to translate? *Expert Opin Biol Ther* 2006; 6(9): 867-878.
383. Stuckey DJ. *et al.* Cine-MRI versus two-dimensional echocardiography to measure in vivo left ventricular function in rat heart. *NMR Biomed* 2008; 21(7): 765-772.
384. Aubert G and Lansdorp PM. Telomeres and aging. *Physiol Rev* 2008; 88: 557-579.
385. Kirkwood Thomas BL.Understanding the odd scienceof aging. *Cell* 2005; 120: 437-447.
386. De Meyer T, *et al.* Studying telomeres in a longitudinal population basd study. *Front Biosci* 2008; 13: 2960-2970.
387. Alt EU *et al,* Aging alters tissue resident mesenchymal stem cell properties. *Stem Cell Research* 2012; 8: 215-225.
388. Li SH, *et al.* Tracking cardiac engraftment and distribution of implanted bone marrow cells: comparing intra-aortic, intravenous, and intramyocardial delivery. *J Thorac Cardiovasc Surg* 2009; 137: 1225-1233.
389. Dawn B, *et al*. Cardiac repair with adult bone marrow-derived cells: the clinical evidence.

Antioxidants & Redox Signaling 2009; 11(8): 1865-1882.

Appendix

Table 1 Composition of complete explant medium (CEM)

Complete Explant Medium (CEM)	Concentration	Manufacturer
Iscove's Modified Dulbecco's Medium (IMDM)	79% (v/v)	Invitrogen
Foetal Bovine Serum (FBS)	20% (v/v)	Biosera
Penicillin Streptomycin Glutamine (PSG) (10000 Units/ml penicillin, 10000 μg/ml streptomycin, and 29.2 mg/ml L-glutamine in 0.85% saline)	1% (v/v)	Invitrogen
2-mercaptoethanol	0.1 mM	Sigma

Table 2.1 Composition of cardiosphere growth medium (CGM)

Cardiosphere Growth Medium (CGM)	Concentration	Manufacturer
Iscove's Modified Dulbecco's Medium (IMDM)	28% (v/v)	Invitrogen
Dulbecco's Modified Eagles's Medium (DMEM)/F-12	65% (v/v)	Invitrogen
Foetal Bovine Serum (FBS)	7% (v/v)	Biosera
Penicillin Streptomycin Glutamine (PSG)	1% (v/v)	Invitrogen
2-mercaptoethanol	0.1 mM	Sigma
Growth factors (described below)	-	-

Table 2.2 Growth factors in cardiosphere growth medium (CGM)

Growth Factor	Concentration	Manufacturer
B27	2% (v/v)	Invitrogen
Recombinant Human Cardiotrophin-1	25 ng/mL	Peprotech
Recombinant Human Epidermal Growth Factor (EGF)	10 ng/mL	Peprotech
Recombinant Human Fibroblast Growth Factor, basic (bFGF)	20 μg/mL	Promega
Thrombin from human plasma	5 units	Sigma

Table 3 Composition of incubation buffer for flow cytometry

Incubation Buffer	**Concentration**	**Manufacturer**
Dulbecco's Phosphate Buffered Saline (DPBS)	99% (v/v)	Sigma
Bovine Serum Albumin (BSA)	1% (w/v)	Sigma
Ethylenediaminetetraacetic Acid (EDTA)	2 μM	Sigma
Penicillin/Streptomycin	1% (v/v)	Invitrogen

Table 4 Composition of basal differentiation medium (BDM)

Basal Differentiaiton Medium (BDM)	**Concentration**	**Manufacturer**
Iscove's Modified Dulbecco's Medium (IMDM)	47% (v/v)	Invitrogen
Dulbecco's Modified Eagles's Medium (DMEM)/F-12	47% (v/v)	Invitrogen
Foetal Bovine Serum (FBS)	2% (v/v)	Invitrogen
Penicillin/Streptomycin	2% (v/v)	Invitrogen
Insulin-Selenium-Transferrin solution (IST) (1 mg/ml insulin, 0.55 mg/ml transferrin, and 67 ng/ml sodium selenite)	1% (v/v)	Invitrogen
Non-Essential Amino Acid	1% (v/v)	Sigma

Table 5 List of primers used in quantitative real-time PCR

Primer	Gene name	Forward primer 5' to 3'	Reverse primer 5' to 3'	Gene accession number	Manufacturer
cTnI	Cardiac troponin I	ACGTGGAAGCA AAAGTCACC	CCTTCTTCACCT GCTTGAGG	NM_144730	Sigma
cTnT	Troponin T type 2 (cardiac)	CGTATTCGCAA TGAACGAGA	CTGTTCTCCTCC TCCTCACG	NM_012676	Sigma
MLC2v	Myosin light chain 2v	GGCACCATCAA AAAGCAATTC	TCTTGATCTCCT CCTGGGAAAA	NM_012605.2	Sigma
TERT	Telomerase reverse transcriptase	AGTGGTGAACT TCCCTGTGG	CAACCGCAAGA CTGACAAGA	NM_053423	Eurofins MWG Operon
GAPDH	Glyceraldehyde-3-phosphate dehydrogenase	GGGTGTGAACC ACGAGAAAT	ACTGTGGTCAT GAGCCCTTC	NM_017008	Sigma
Tel	Telomere	GGTTTTTGAGG GTGAGGGTGAG GGTGAGGGTGA GGGT	TCCCGACTATCC CTATCCCTATCC CTATCCCTATCC CTA	Sequence from published paper [373]	Eurofins MWG Operon
36B4	Acidic ribosomal phosphoprotein	ACTGGTCTAGG ACCCGAGAAG	TCAATGGTGCC TCTGGAGATT	Sequence from published paper [374]	Eurofins MWG Operon

Table 6 Primer efficiency

Primer / Gene	Correlation coefficient (R^2)	Primer efficiency, $E = (\exp^{-1/m} - 1) \times 100\%$
GADPH (housekeeping gene)	0.99	99%
cTnI	0.90	93%
cTnT	0.98	98%
MLC2v	0.95	102%
TERT	1.00	91%
Telomere	0.98	96%
36B4	0.95	110%

Table 7 Advantages and disadvantages of various stem cell types for cardiac repair

Cell Type	ESC	SM	BMC	CSC	iPSC
Proliferative Capacity	Yes	Yes	Yes	Yes	Yes
Cardiomyogenic Differentiation	Yes	No	Controversial	Yes	Yes
Arrhythmia	ND	Yes	No	ND	ND
Ethical Problem	Yes	No	No	No	No
Immune Response	Yes	No	No	No	No
Tumor Formation	Yes	No	No*	No	ND
Results in Clinical Trial	No	Mixed	Mixed	Positive §	No

*ESC = embryonic stem cell; SM = skeletal myoblast; BMC = bone marrow-derived cell; CSC = resident cardiac stem cell; iPSC = induced pluripotent stem cell; ND = not determined. * It has been reported that bone formation and substantial intramyocardial calcification in infarcted hearts occurred after delivery of bone marrow cells in animal models [81, 82]. § So far, there are two phase I clinical trials reporting that resident cardiac stem cells (c-kit+ cells or cardiosphere-derived cells) exerted beneficial effects when transplanted post infarction in ischemic heart disease patients [79, 80].*

.